Imperial College
London

Modelling the weathering process of stored liquefied natural gas (LNG)

by

Calogero Migliore Cappello

Imperial College of London
Department of Earth Science and Engineering

A thesis submitted for the degree of

Doctor of Philosophy

April 2016

DECLARATION OF ORIGINALITY

'I, **Calogero Migliore Cappello**, declare that this thesis **'Modelling the weathering process of stored liquefied natural gas (LNG)'** is my own work. Any information from other publication and sources have been duly acknowledge and clearly referenced at the point of use, and also fully described in the reference sections of this thesis'.

COPYRIGHT DECLARATION

Calogero Migliore Cappello
December 2015

ACKNOWLEDGEMENTS

First of all I'd like to express my sincere appreciation and gratitude to Prof. Velisa Vesovic for being my PhD supervisor, and for giving me the opportunity to carry out this research. His guidance, continuous feedback and flexibility were very valuable for the successful completion of this work.

My sincere thanks also go to Repsol, S. A. for their support and assistance, and for making possible for me to undertake this program.

I´d like to express my appreciation towards my friends at Imperial College London who have made my time there not only a memorable, but also an enjoyable experience. I would also like to thank my close colleagues at Repsol for their continuous support and encouragement.

Calogero Migliore Cappello
London, England

DEDICATION

I dedicate this work to my parents to whom I am in debt for everything that I have achieved in my life. To my wife Laura for her love, extraordinary patience and encouragement to accomplish this remarkable achievement; and to my daughters Maria Laura and Daniela Alessandra for filling with joy my present and shaping my future.

Rino

ABSTRACT

Weathering occurs in stored liquefied natural gas (LNG) due to the removal of the boil-off gas (BOG) from the LNG container and results in the remaining LNG being richer in heavier components.

A model has been developed to predict stored LNG weathering in containment tanks, typically used in regasification. The model integrates a vapour-liquid equilibrium model, and a realistic heat transfer model. It provides a number of advances on previously developed models: (*i*) heat ingress is calculated based on outside temperature and LNG composition, allowing for daily/seasonal variations; (*ii*) boil-off-ratio is not an input; (*iii*) LNG density is estimated using an experimentally based correlation. The model was validated using real industry data and the agreement obtained in predicting overall composition, density and amount vaporized was within industry requirements.

Two modelling approaches have been developed: (*i*) assuming thermodynamic equilibrium between vapour and liquid; and (*ii*) assuming heat exchange between the two phases. Both models were run in a predictive mode to assess the BOG under different scenarios.

One of the main results of this work is that the BOG generation is 25% less when considering the non-equilibrium approach, which will have a significant impact on industry where simple equilibrium models are used. In the initial stages of weathering nitrogen content of LNG has a marked effect on BOG generation. Even 0.5% mol of nitrogen leads to nearly 7% BOG decrease, making the initial BOG unmarketable. That is a result of preferential evaporation of nitrogen and increase in the direct differential molar latent heat. In the final stages of weathering the heavier hydrocarbons govern the BOG dynamics, which becomes a strong function of initial composition and the LNG remaining in the tank.

TABLE OF CONTENTS

Page Nº

LIST OF FIGURES

Page Nº

LIST OF TABLES

Page Nº

EXTERNAL PUBLICATIONS

[1] Migliore, C., Tubilleja, C., Vesovic V. (2015) Weathering prediction model for stored liquefied natural gas (LNG). *Journal of Natural Gas Science and Engineering*, 26, 570-580, ISSN: 1875-5100.

Paper selected as Editor's Choice of authors' research by Elsevier (Sept. 2015).

[2] Migliore C., Tubilleja C., Vesovic V. (2015) Weathering prediction model for stored liquefied natural gas (LNG). Presented at the LNG Programme Committee Meeting of the European Gas Research Group (GERG), 25th September 2015, Stockholm, Sweden.

NOMENCLATURE

Roman letters

a *Helmholtz free energy (J/mol)*

a^o *Helmholtz free energy ideal gas mixture behaviour (J/mol)*

a^r *Helmholtz free energy residual gas mixture behaviour (J/mol)*

A *Area (m^2)*

A_o *External heat transfer area (m^2)*

A_i *Internal heat transfer area (m^2)*

A_m *Mean heat transfer area (m^2)*

B *Boil-off gas, BOG (mol)*

C *Polytropic constant (dimensionless)*

C_p *Specific heat (J/mol K)*

d *Mass density (kg/m^3)*

D *Diameter (m)*

D_o *Tank external diameter (m)*

D_i *Tank internal diameter (m)*

e *Equivalent insulation thickness (m)*

f *Fugacity (Pa)*

F *View factor (dimensionless)*

g *gravity (m/s^2)*

g *Molar Gibbs free energy (J/mol)*

g^o *Molar Gibbs free energy at reference state (J/mol)*

G *Gibbs free energy (J)*

Gr *Grashof number (dimensionless)*

h *Heat transfer convection coefficient (W/m^{2}K)*

h *Specific enthalpy (J/mol)*

h_i *Internal convection heat transfer coefficient (W/m^{2}K)*

h_l *Tank liquid height (m)*

h_o *External convection heat transfer coefficient (W/m^{2}K)*

h^{id} *Molar ideal enthalpy (J/mol)*

H *Enthalpy (J)*

H^o *Enthalpy at reference state (J)*

iter *Maximum number of iterations (dimensionless)*

k *Thermal conductivity (W/m K)*

K *Vapour-liquid equilibrium constant (dimensionless)*

l *Length (m)*

L *Latent heat (J/mol)*

L_f *Liquid fraction (dimensionless)*

m *Mass (kg)*

MW *Molecular weight (g/mol)*

M *Total moles (mol)*

n *number of constituent species in a mixture (dimensionless)*

Nu *Nusselt number (dimensionless)*

P *Pressure (Pa)*

P_c *Critical pressure (Pa)*

P_{pc} *Pseudo critical pressure (Pa)*

P_r *Reduced Pressure (dimensionless)*

P_T *LNG tank pressure (Pa)*

P_v *Vapour pressure (Pa)*

Pr *Prandtl number (dimensionless)*

q *Heat flux (W/m^2)*

Q *Heat (J)*

Q_{roof} *Heat ingress from the tank roof (J)*

Q_{slab} *Heat ingress from the tank slab (J)*

R *Gas constant (8.3145 J/mol K)*

Ra *Rayleigh number (dimensionless)*

s *Specific entropy (J/mol K)*

s^o *Specific entropy at reference state (J/mol K)*

S *Entropy (J/K)*

t *time (s)*

t_s *time step (s)*

tol *Convergence tolerance (dimensionless)*

T *Temperature (K)*

T_{air} *Ambient air temperature (K)*

T_c *Critical temperature (K)*

T_f *Film temperature (K)*

T_{LNG} *LNG temperature (K)*

T_{pc} *Pseudo critical temperature (K)*

T_r *Reduced pressure (dimensionless)*

T_w *Temperature of the wall (K)*

U *Internal energy (J)*

U *Overall heat transfer coefficient (W/m^2K)*

V *Volume (m^3)*

V^* *Characteristic volume (l/mol)*

V_L *LNG volume (m^3)*

V_s *Saturated liquid volume (l/mol)*

W *Work (J)*

x_i *Mol fraction of component i in liquid phase water free basis (dimensionless)*

y_i *Mol fraction of component i in gas phase water free basis (dimensionless)*

z *Height (m)*

z_i *Mol fraction global composition of component i water free basis (dimensionless)*

Z *Compressibility factor (dimensionless)*

Greek letters

α *Thermal diffusivity (m^2/s)*

α *Helmholtz Free Energy expressed as dimensionless variable (dimensionless)*

β *Thermal expansion coefficient (K^{-1})*

δ *Reduced density (dimensionless)*

ε *Emissivity (dimensionless)*

μ *Dynamic viscosity (kg/m s)*

μ *Chemical potential (J/mol)*

ρ *molar density ($kmol/m^3$)*

σ *Stefan-Boltzmann constant ($5.6704.10^{-8}$ W/m^2K^4)*

τ *inverse reduced temperature (dimensionless)*

ν *Kinematic viscosity (m^2/s)*

v *Molar volume (l/mol)*

v' *Corrected molar volume (l/mol)*

ϕ *Fugacity coefficient (dimensionless)*

ω *Acentric factor (dimensionless)*

Subscripts

atm *Atmospheric (referred to atmospheric pressure)*

B *Vapour generated from flashing liquid*

c *Combustion*

C *Condensed*

dry *Dry area (referred to heat transfer area)*

f *Formation*

F *Feed*

i, j *Any component*

iso *isothermal (referred to isothermal weathering model)*

L, l *Liquid*

n *Number*

ori *origin (referred to a number of moles at origin at the initial stage of weathering)*

p *Products*

r *Reactants*

ref *Reference state*

shv *superheated vapour (referred to superheated vapour weathering model)*

T *Total*

V, v *Vapour*

vap *Vapour*

wet *Wet area (referred to heat transfer area)*

0, 1 *Two time positions*

Superscripts

L, l *Liquid phase*

V, v *Vapour phase*

Acronyms

API *American Petroleum Institute*

BOG *Boil-off gas*

BOR *Boil-off rate*

CBOG *Cargo BOG (weight percentage of BOG generated to initial cargo load)*

EBO *Enthalpy basis offset*

EOS *Equation of state*

GIIGNL *International Group of Liquefied Natural Gas Importers*

HHV *High Heating Value*

IGT *Institute of Gas Technology*

LNG *Liquefied Natural Gas*

MTA *Million tons per annum (referred to LNG production capacity)*

NBS *National Bureau of Standards, US*

ORV *Open rack vaporizer*

SCV *Submerged combustion vaporizer*

VLE *Vapour-liquid equilibrium*

WI *Wobbe Index*

1 INTRODUCTION

1.1 PREAMBLE

As part of resolving the energy challenges faced by our society, it is recognized that the high demand for energy has to be balanced against the need to mitigate ever increasing carbon dioxide emissions, without compromising in the long term energy security. In this context natural gas is seen by many as a good vehicle to ensure an orderly transition from the fossil-fuel driven economy to one driven by renewable energy [1].

Natural gas is the fastest growing form of energy in the world. Currently the global consumption is 3.4 Tm^3/a [2] and the share of natural gas in the global energy mix is around 20%, with forecasts indicating that the demand for natural gas by 2035 is expected to be 50% higher than today [1].

Natural gas is a more environmental friendly energy source compared to oil and coal. It is increasingly being utilised for power generation, and is already extensively used for industrial and household consumption, as well as for the production of advanced petrochemical derivatives. Those facts describe the importance and perspectives of natural gas as a future major energy commodity, holding the promise of being the energy source of the 21st century.

The development of the natural gas industry has been very much influenced by the physical characteristics of natural gas. Oil, being a liquid at ambient temperature, can be contained and transported relatively easily using simple and less expensive technologies; natural gas transport/storage is more complex and generally more expensive because of its physical nature, which requires high pressures and/or very low temperatures.

Getting gas to the market has always been challenging and has prevented the development of many natural gas fields. Most natural gas industry developments have thus been based on indigenous resources. Natural gas was traded initially based on transmission through pipelines between neighbouring countries. It was only with the success of the transport trials as Liquefied Natural Gas (LNG) in the 1960s that long distance trade between non-bordering countries was established.

Transportation is a major aspect of the natural gas industry to ensure the supply of product to users. The main objective of a natural gas supply system is to produce gas from an underground field, move it to a processing facility where the gas is processed to an acceptable quality and then deliver to customers where it is used for an economic purpose. This cannot happen without there being a continuous physical link between the producing field and the consumer of the gas. This is referred to as the Gas Supply Chain concept [3].

Currently there exist two chains in the natural gas industry. One scheme involves a conventional arrangement in which natural gas is transmitted all the way from the field to the consumer facility in high pressure pipelines. The other one is the LNG scheme, which involves the liquefaction of the gas, its transportation in bulk carriers, the regasification at the point of delivery and the transportation to the final users also through high pressure pipelines. The choice on which scheme to use depends primarily on the distance, but also on the location of the natural gas field and issues concerning the security of supply.

Production of LNG involves cooling the treated natural gas to approximately -160 ºC at atmospheric pressure. At these conditions natural gas occupies 1/600th of its standard volume which has important implications for the transported energy content per unit volume. The fact that natural gas can be liquefied in commercial quantities has made possible the development of the LNG chain, thus increasing the availability and versatility of natural gas. Figure 1.1 below shows the structure of the LNG supply chain [3].

Figure 1.1 LNG supply chain structure [3].

The LNG usage is expanding rapidly and a number of industrial sectors are also utilizing it in its own right, without regasification to natural gas. For instance, it is increasingly being used as fuel in marine transport [4] and in heavy-duty road vehicles [5].

The increase in demand translates to increasing trade in LNG. Gas supplied via LNG is growing by 4.3% per annum, more than twice as fast as total trade. As a result, it is expected that LNG will overtake the pipeline as the dominant form of traded gas by 2035 [6]. Figure 1.2 shows the outlook of the share of global gas consumption by 2035 [6].

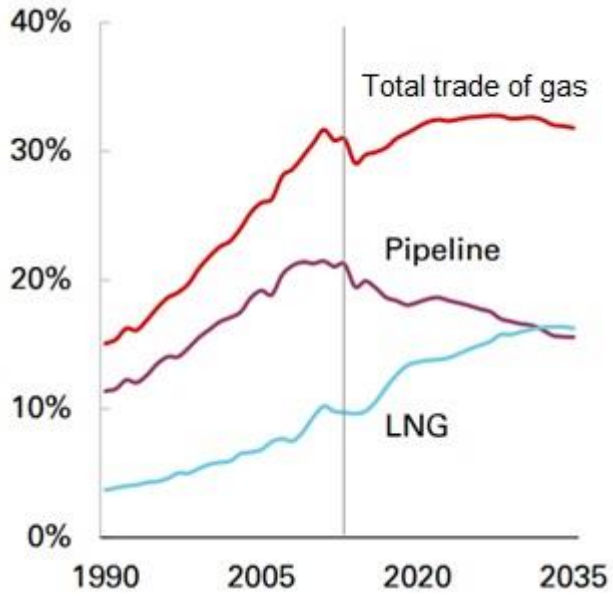

Figure 1.2 Share of global gas consumption outlook by 2035 [6].

The projected figures show that the LNG market is preparing for a significant growth with a number of new projects adding 0.62 Gm^3/d (22 Bcf/d[1]) by 2020. Overall, the LNG supply is expected to grow by 1.36 Gm^3/d (48 Bcf/d) by 2035, with Australia and the US each contributing around a third of that increase, 0.45 Gm^3/d (16 Bcf/d) and 0.4 Gm^3/d (14 Bcf/d) respectively. African LNG supply, led by East Africa, also increases significantly adding around 0.34 Gm^3/d (12 Bcf/d). Qatar, which has the largest market share today, is to be overtaken by Australia (24% share of the market by 2035),

[1] Bcf/d stands for billion cubic feet per day and is equivalent to 10^9 ft^3/d.

Africa (21%), and the US (18%) by 2035. Asia, the largest destination for LNG, remains above 70% share in the global LNG demand by 2035, with China becoming the second largest LNG importer with 0.34 Gm^3/d (12 Bcf/d), just behind Japan with 0.37 Gm^3/d (13 Bcf/d). Europe's share of global LNG imports rises from 16% to 19% between 2013 and 2035, with an additional 0.28 Gm^3/d (10 Bcf/d) of LNG consumption [6]. Figure 1.3 shows the outlook of the global LNG supply and demand by 2035 [6].

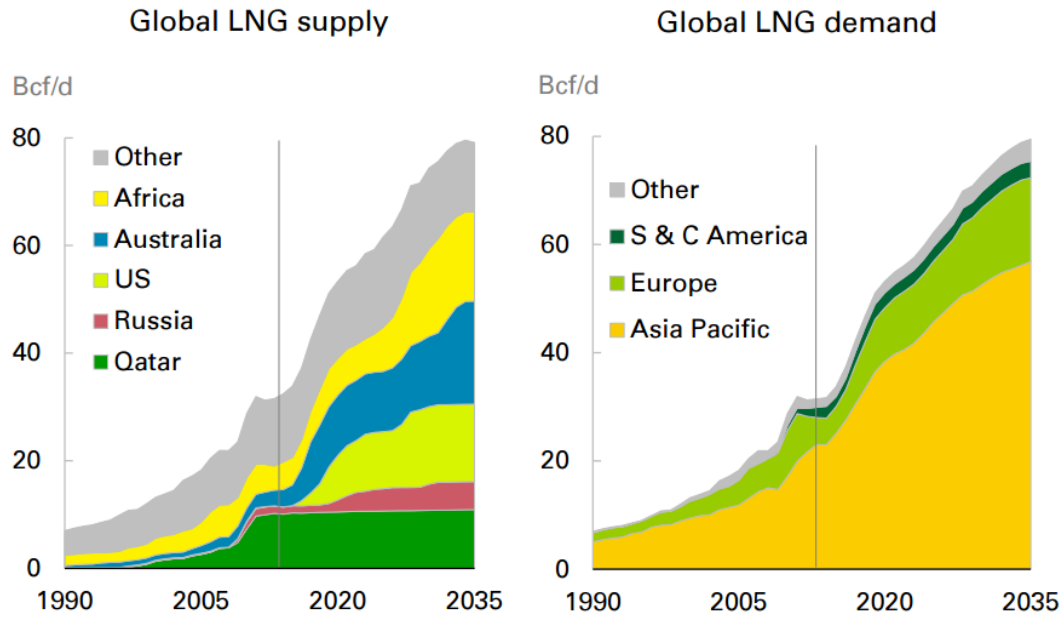

Figure 1.3 Global LNG supply and demand outlook by 2035 [6].

The LNG is transported from the production facilities to the regasification terminals by special marine carriers. Figure 1.4 shows a sketch of the two basic ship design concepts used by the LNG industry, (*a*) Self-supporting Tanks and (*b*) Integral Membrane [7].

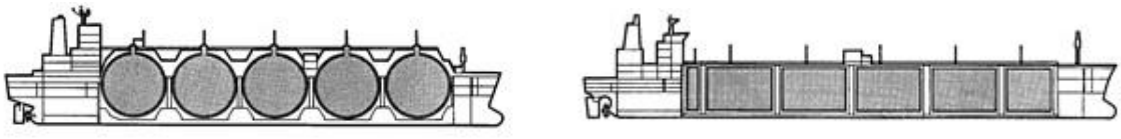

(*a*) (*b*)

Figure 1.4 LNG ships: (*a*) Self-supporting tanks; (*b*) Integral membrane [7].

At the regasification terminal, LNG is stored in highly insulated storage tanks at pressures slightly above atmospheric and temperatures corresponding to its bubble point (~ -160 ºC).

Due to the heat in-leak into the storage tank from the surroundings some of the LNG will vaporize, resulting in the increase of the overall tank pressure. In order to avoid over-pressurization of the tank the boil-off gas (BOG) produced is continuously removed by BOG compressors at the rate at which the LNG vaporizes, thus maintaining constant pressure inside the tank. Figure 1.5 represents a schematic diagram of an LNG storage tank, showing the heat in-leak from different sources (bottom, roof and lateral walls).

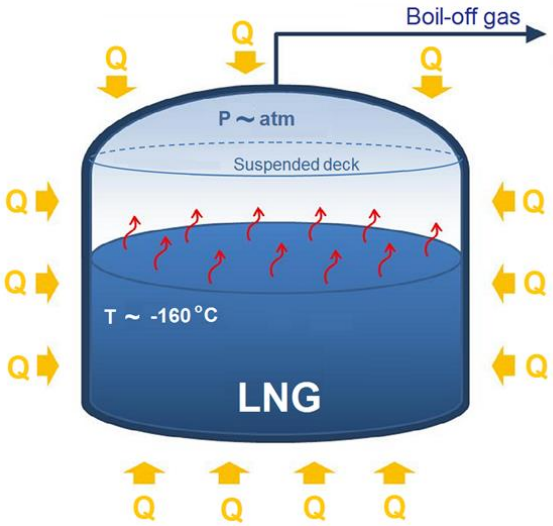

Figure 1.5 LNG storage tank heat in-leak from different sources.

Since commercial LNG is a mixture rich in methane that also contains nitrogen, ethane, propane and traces of heavier alkanes, as LNG evaporates the more volatile components (methane and nitrogen) will vaporize preferentially and the remaining LNG will get richer in the heavier components (ethane, propane, etc.). This process not only takes the system to a new stage in thermodynamic equilibrium, but also leads to changes in the thermophysical properties of both coexisting phases, liquid (LNG) and vapour. Over time, the composition of LNG will change and that will influence not only its thermodynamic properties, in particular the boiling temperature and latent heat, but also its quality properties, such as the heating value. The process of preferential vaporization of stored LNG is known in the industry as “weathering”, and can be summarized as the progressive alteration of thermophysical properties of stored LNG through vaporization, due to the heat ingress from the surroundings.

Weathering prediction of stored LNG is of particular significance for the LNG industry, especially in LNG shipping and in the operation of regasification facilities. In LNG shipping, it helps to anticipate the allocation of LNG cargoes and to set up in advance the operation of the receiving terminal. In the regasification terminal an accurate estimation of the weathering effect on the received LNG, allows to plan in advance operating procedures to ensure the suitability of the delivered natural gas in terms of its properties and heating value.

In regasification facilities, weathering has been traditionally a minor problem in base load[2] terminals, compared to peak-shaving[3] installations; however, today's combined effect of sudden fluctuations in regional gas price and seasonality, is producing an increase in the storage time in regasification terminals, and thus demanding the accurate prediction of the thermophysical properties of stored LNG as a function of time. In this regard, the accurate prediction of LNG weathering becomes an important task in long term LNG storage planning. It allows for not only optimizing normal terminal operations, but also evaluating the compatibility of the stored LNG with the supplied gas system and final users.

Furthermore, if LNG has undergone a substantial weathering in a storage tank its boiling temperature and density will increase as a consequence of it being richer in heavier components. This condition leads to a layering effect caused by density differences that may give rise to a rollover hazard. The rollover phenomenon occurs when the lighter components preferentially evaporate from the surface, the heavier fractions that remain form a dense layer at the top of the storage tank trapping the less dense layer below. As the LNG stock continues to warm the layers at the bottom get less dense, and at a certain stage the situation becomes unstable, resulting that the dense layer at the top rolling over to the bottom causing lighter fractions to rise to the top with a heavy release of vapour [8]. Within the history of the LNG industry, a major LNG rollover event was registered in La Spezia LNG regasification terminal in Italy, in 1971. In that case, about 2,000 tons of LNG

[2] Base load is the rate of production below which demand is not expected to fall during a given period of time.

[3] A peak-shaving installation is a facility used to store surplus natural gas to meet demand requirements during peak consumption periods (typically in winter).

vapour discharged from the tank safety valves and vents over a period of few hours, damaging the roof of the storage tank [9].

LNG weathering prediction is also important in LNG supply planning. If a new batch of LNG is introduced in the storage tank, which will by necessity be lighter and cooler, then a number of undesirable events, involving stratification, sudden vapour release and the possibility of rollover can take place, which can put in risk normal operations.

For stored LNG, the amount and quality of produced BOG depends on the initial composition, the insulation of the LNG tank and primarily on the time elapsed since the tank was filled. In LNG shipping, the liquid stock in a LNG carrier remains almost constant during the trip from the production facility to the receiving terminal. The longest trips are of the order of 20 days during which 2-3% of the total volume of the transported LNG evaporates. The usual approach, to predict LNG weathering during marine transport, is to assume the constant boil-off rate (BOR), where BOR is defined as the ratio of volume in liquid terms, of LNG that has evaporated in one day relative to the initial LNG volume in the tank. The BOR figure used in industry for LNG carriers depends on carrier size. For smaller and older ships a BOR of 0.15% tends to be used [10], whilst for the latest LNG tankers with an average capacity of 170,000 m^3 the BOR is nearer to 0.1%.

The prediction of weathering in above-ground LNG storage tanks such as those typically used in regasification terminals, the situation is somewhat different. A constant BOR tends to be assumed based on the value adopted during the design stage when a maximum BOR value is specified, usually around 0.05% [11], and the tank insulation is designed accordingly. However, that assumption is not accurate when used in the estimation of the LNG weathering, as BOR changes with the LNG stock. Furthermore, the impact of the aforementioned assumption and simplification on the accuracy of BOR predictions is not well understood.

The rigorous modelling of the LNG weathering phenomenon can make a significant contribution to industry and science. Such a model development will enable the industry to better understand the operation of an LNG storage tank under dynamic conditions. Additionally can provide a tool that can be used in managing LNG regasification

operations, checking, and if required improving, the accuracy of current estimation methods used by the industry. To science, accurate modelling of LNG weathering will contribute in the understanding of the thermal and evaporation behaviour of stored LNG, as well as to increase the knowledge of LNG quality evolution as function of time under storage conditions.

1.2 AIM AND OBJECTIVE

The objective of this research project is to develop a rigorous model to describe the LNG weathering phenomena, based on first principles, aiming to predict the vaporization rate and the compositional variation over time of LNG stored in a full containment above ground tank, due to the effect of heat in-leak from the surroundings and vapour release to control tank pressure.

Two modelling developments are considered in this research, the equilibrium and non-equilibrium thermodynamic approach. The dynamics and evaporation behaviour of stored LNG under both equilibrium approaches are assessed and compared as part of this research project.

1.3 SCOPE OF STUDY

To properly account for the weathering phenomena taking place inside the LNG tank, the composition of the vapour and liquid phases needs to be calculated as a function of time. This requires solving both the vapour-liquid equilibrium (VLE) and heat transfer processes developing in the LNG tank. Therefore, the LNG weathering model developed in this research integrates: (*i*) a rigorous LNG VLE model, and (*ii*) a realistic heat transfer model, into a combined model to predict the compositional variation of the stored LNG over time. The aim of the aforementioned integration is to develop a self-sufficient model that predicts the LNG weathering, without knowing upfront the BOG generation rate, which is determined by the actual heat entering into the stored LNG. In this respect, the model must take into account the actual variation of the heat ingress into the tank with time, owing to the change in the temperature difference between the surroundings and the weathered LNG.

Additionally, the heat transfer model should have the option to separate the influence of the heat influx from the surroundings into the vapour and liquid spaces of the tank. Within this approach, the heat contribution from the vapour (which will heat up much faster due to its lower specific heat) to the liquid can be taken into account, under non-equilibrium thermodynamic conditions.

The model takes advantage of the advances reported in previously published work, however removing a number of constraints that exist in the reported studies [12-19], namely: (*i*) heat ingress is calculated based on the outside temperature and LNG composition, that allows for daily or seasonal variations; (*ii*) BOR is not an input parameter, but is calculated as part of the weathering simulation, and (*iii*) the LNG density is estimated using an accurate experimentally based correlation, thus replacing the need for the estimate based on equation of state (EOS) that for two parameter cubic EOS requires an empirical correction.

The model developed in this research has been tested and validated using real industry data, and thereafter run in a predictive mode to explore the sensitivity and evaporation behaviour of stored LNG to different weathering scenarios.

1.4 THESIS OUTLINE

This thesis is organized into a total of seven chapters.

Chapter 1 introduces and describes the subject matter of this research project, which forms the background of this thesis. The motivation for the research is explained and different aspects of LNG market development, including some issues concerning future supply, are also discussed. The objectives are specified and the scope of work is also described within this chapter.

Chapter 2 focuses on presenting the relevant literature review for this research. Topics in this chapter include an overview of the LNG supply chain, with a brief description of the elements involved within it. Relevant previous works on LNG weathering and stored LNG thermodynamic behaviour are reviewed and their major findings are highlighted.

Chapter 3 focuses on the theoretical background of the thesis, including phase equilibria, thermophysical properties calculation, and heat transfer.

Chapter 4 explains the development of the LNG weathering model and the calculation procedure involved to determine the thermophysical properties of the liquid and vapour phases within the LNG storage tank.

Chapter 5 explains the LNG weathering model testing and verification procedure. The weathering prediction results from both modelling approaches are compared against measured data and results from previous published studies.

Chapter 6 presents the results of the assessments performed in a predictive mode for the different LNG weathering scenarios analysed using both modelling approaches.

Chapter 7 provides the summary and conclusions of the major findings of this research project and suggestions for future work.

1.5 REFERENCES

[1] International Energy Agency (2011) *World Energy Outlook: Are we entering a golden age of gas?*. Special report, Paris.

[2] BP Statistical Review of World Energy (2015). BP plc., London.

[3] Migliore, C. (2013) Natural Gas Conditioning and Processing. In: Riazi, M. R., Eser, S., Agrawal, S. S., Peña Díez, J. L. (eds.) *Petroleum Refining and Natural Gas Processing*. ASTM International, USA, pp. 249-286.

[4] Lowell, D., Wang, H., Lutsey, N. (2013) *Assessment of the fuel cycle impact of liquefied natural gas as used in international shipping*. The International Council on Clean Transportation (ICCT), White paper, USA.

[5] Rosenstiel, D. P. von. (2014) *LNG in Germany: Liquefied Natural Gas and Renewable Methane in Heavy-Duty Road Transport*. German Energy Agency (DENA), Berlin.

[6] BP Energy Outlook 2035 (2015). BP plc., London, UK.

[7] Peebles, M. (1992) *Natural Gas Fundamentals*. Shell International Gas Limited, London, UK.

[8] Nasr, G. G., Connor, N. E. (2014) *Natural Gas Engineering and Safety Challenges*. Springer, UK.

[9] Arjomandnia, P., Tade, M. O., Pareek, V., May, E. F. (2013) Analysis of available data from liquefied natural gas rollover incidents to determine critical stability ratios. *AIChE Journal*, 60 (1), 362–374.

[10] Colson, D., Haquin, N., Malochet, M. (2012) Reduction of boil-off generation in cargo tanks of liquid natural gas carriers - Recent developments of Gaztransport & Technigaz (GTT) cargo containment systems, *25th World Gas Conference, June 2012, Kuala Lumpur, Malaysia*. International Gas Union (IGU), paper Nº 452.00.

[11] Yang, Y., Kim, J., Seo, H., Lee, K., Yoon, I. (2006) Development of the world's largest above-ground full containment LNG storage tank, Korea Gas Corporation, *23rd World Gas Conference, June 2006, Amsterdam, Netherlands*. International Gas Union (IGU).

[12] Kountz, K. J. (1999) *Weathering of LNG in on-board storage tanks*. Institute of Gas Technology (IGT), USA, project report 32034-02.

[13] Dimopoulos, G. G., Frangopoulos, C. A. (2008) A dynamic model for liquefied natural gas evaporation during marine transportation. *International Journal of Thermodynamics*, 11 (3), 123−131.

[14] Miana, M., Del Hoyo, R., Rodrigálvarez, V., Valdés, J. R., Llorens, R. (2010) Calculation models for prediction of liquefied natural gas (LNG) ageing during ship transportation. *Applied Energy*, 87 (5), 1687–1700.

[15] Adom, E., Islam, S. Z., Ji, X. (2010) Modelling of boil-off gas in LNG tanks: A case study. *International Journal of Engineering and Technology*, 2 (4), 292-296.

[16] Pellegrini, L. A., Moioli, S., Brignoli, F., Bellini, C. (2014) LNG Technology: The weathering in above-ground storage tanks. *Industrial and Engineering Chemistry*, 53 (10), 3931–3937.

[17] Shah, J. M., Aarts, J. J. (1974) Effect of weathering of LNG in storage tanks. *Advances in Cryogenics Engineering*, 19, 253-260.

[18] Aspelund, A., Gjovag, G. A., Neksa, P., Kolsaker K. (2006) LNG-chain, a calculation tool for natural gas quality in small scale LNG distribution chains. *Proceedings of the 21st International Cryogenic Engineering Conference, 17-21 July 2006, Prague, Czech Republic*. CR06-133.

[19] Hasan, M. M. F., Zheng, A. M., Karimi, I. A. (2009) Minimizing boil-off losses in liquefied natural gas transportation. *Industrial Engineering and Chemistry Research*, 48, 9571–9580

2 LITERATURE REVIEW

This chapter focuses on the relevant literature review related to the main subject of this research work, the modelling of stored LNG weathering. Pertinent details on the modelling approach and performance of the previous developments are presented and their limitations discussed. Relevant studies involving LNG vaporization are also reviewed and discussed, with their major findings highlighted.

Due to its importance with the research theme of this thesis, this chapter also includes an overview of the LNG supply chain, with a brief description of the main elements involved in it.

The structure of the chapter is organized that the description of the LNG supply chain is presented first, and the review of the relevant work studies come afterwards.

2.1 THE LNG SUPPLY CHAIN

The need to transport gas long distances across oceans led to the development of the international LNG trade. The first shipment of LNG was made on a trial basis in 1959 between the US and the UK by the "Methane Pioneer" ship. The world's first LNG commercial-scale project to ship LNG from Algeria to the UK was inaugurated in 1964 [1]. Since then, LNG trade has grown steadily and taking up an increasing proportion of the international natural gas trade.

As described in Figure 1.1 the LNG supply chain comprises gas production, liquefaction of the gas, its transportation in bulk carriers, the regasification at the point of delivery and the transportation to the final users through high pressure pipelines.

The key elements of the LNG supply chain are liquefaction, LNG shipping and regasification. The following sections describe in more detail those three elements of the LNG supply chain.

2.2 NATURAL GAS LIQUEFACTION

The process for the liquefaction of natural gas is essentially the same as that used in modern domestic refrigerators, but on a massive scale. A refrigerant gas is compressed,

cooled, condensed, and let down in pressure through a valve that reduces its temperature by the Joule-Thomson effect. The refrigerant gas is then used to cool the feed gas (natural gas). The temperature of the feed gas is eventually reduced to approximately -160 °C, the temperature at which methane, the main constituent of natural gas, liquefies.

Gas pre-treatment and natural gas liquids (NGL) recovery are normally included within the liquefaction facility. Natural gas taken from the field contains undesirable pollutants like hydrogen sulphide (H_2S) and carbon dioxide (CO_2). These impurities substances are absorbed and removed from natural gas usually using an amine base acid gas removal unit.

In the NGL recovery stage, constituents of the natural gas (methane, ethane, and propane) are typically recovered to be used as refrigerants either individually or as a mixture within the liquefaction process. LPG and condensate may be also recovered as by-products within the liquefaction process.

Figure 2.1 shows the process stages involved within a natural gas liquefaction plant [2].

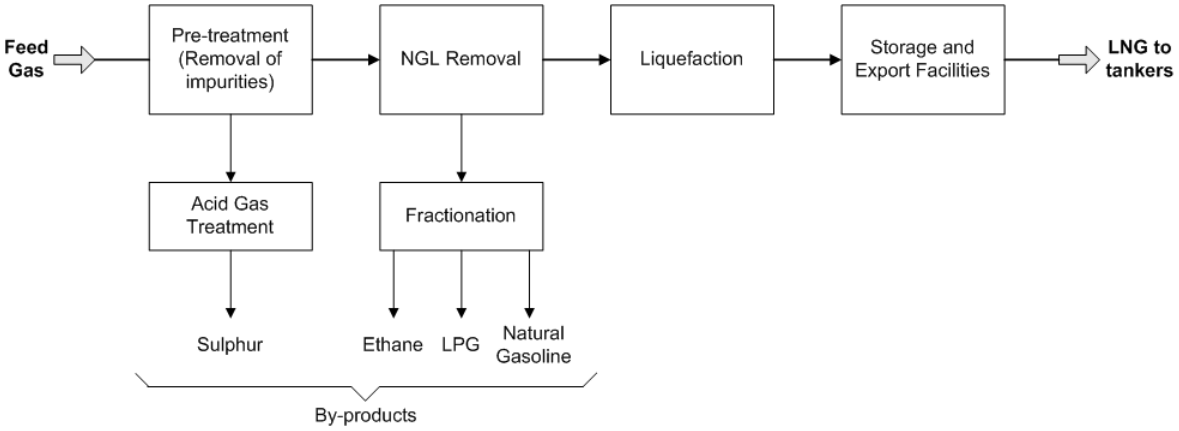

Figure 2.1 Process stages typically involved in a liquefaction plant [2].

There are three main liquefaction processes used for LNG base load plants. These processes include: (*i*) the pure-component cascade, (*ii*) the mixed-refrigerant cycle, and (*iii*) the propane-precooled mixed-refrigerant cycle.

2.2.1 THE PURE-COMPONENT CASCADE PROCESS

The pure-component cascade process consists of three refrigeration cycles using three separate refrigerants. Typically, propane, ethylene and methane are used in the cooling cycles to provide cooling at progressively lower temperatures. The term cascade derives from the transfer of heat from the colder stages to the warmer stages of the process.

Figure 2.2 shows a simplified diagram of the cascade process [3].

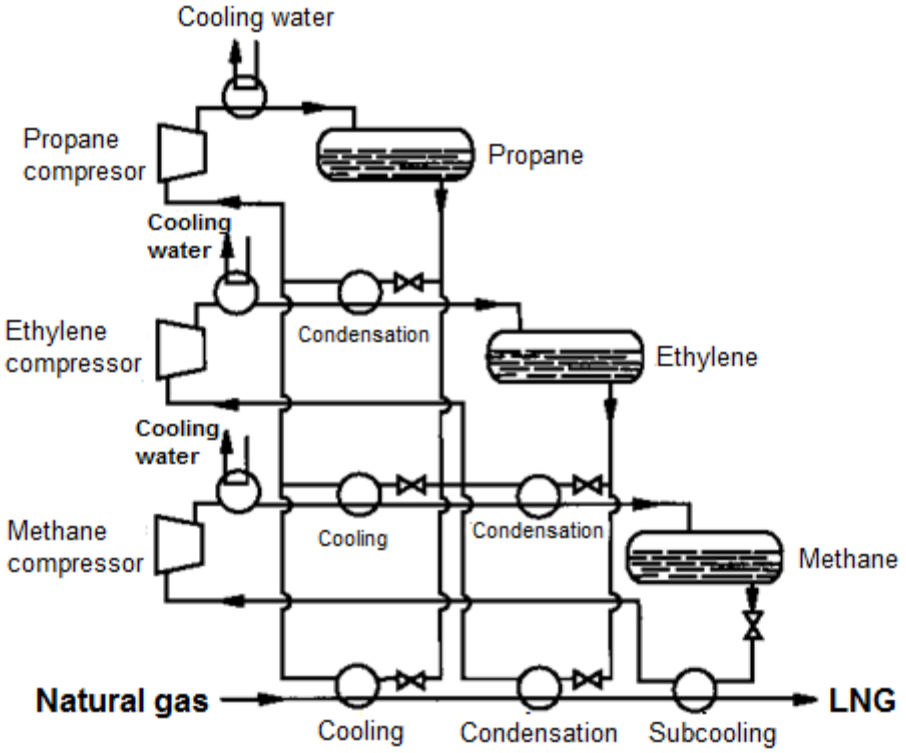

Figure 2.2 Simplified diagram of the cascade process [3].

In the first cycle, the propane refrigerant is condensed at high pressure by using either cooling water or air. Then the pressure of the liquid propane is let down through the expansion valve, and it can vaporise at a lower temperature by condensing the ethylene of the second cycle, as well as cooling the natural gas down to -30 ^{o}C, all in a series of evaporators. Finally, the propane vapours are recompressed to the initial high pressure at which they can be condensed at ambient temperature. The ethylene and methane

refrigeration cycle work on the same pattern. Ethylene is condensed under pressure by the propane of cycle one and, once depressured, vaporises by cooling the natural gas down to about -100 ^{o}C. In the last cycle, methane is condensed by the ethylene and after pressure let down, is vaporised by cooling the natural gas to its complete atmospheric liquefaction temperature of about -160 ^{o}C [3].

The pure refrigerant cascade process is more efficient than other LNG processes; however, the disadvantage is that the capital and maintenance costs are high, owing the multiplicity of compressors, evaporators and complex refrigerant piping [4].

2.2.2 THE SINGLE MIXED-REFRIGERANT CYCLE

The single mixed refrigerant cycle process retains the principle of the classical cascade but reduces capital and maintenance costs, as well as providing a simpler operation.

Developed by Air Products and Chemicals Inc. (APCI) the process uses a single multi-component refrigerant but employs several refrigeration steps. There is only one base load LNG application in use at Marsa El-Brega in Libya [2]. APCI has subsequently superseded the process by the propane pre-cooled mixed refrigerant process described in the next section.

Figure 2.3 shows a simplified diagram of the APCI single mixed-refrigerant cycle process [2].

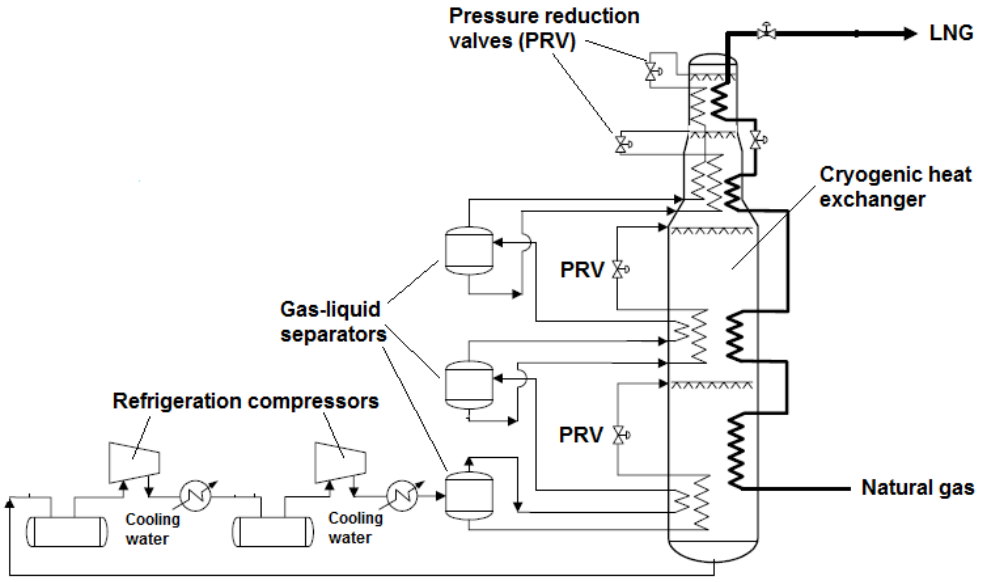

Figure 2.3 Simplified diagram of the APCI mixed-refrigerant cycle process [2].

Whereas with pure refrigerants a series of separate cycles are involved, with a mixed refrigerant, consisting of methane, ethane, propane and butane with a small amount of nitrogen, condensation and evaporation take place in only one cycle over a wide temperature range down to around -160 ^{o}C. After compression, the mixed refrigerant is partially condensed against cooling water and sent to a gas liquid separator. The liquid and vapour are distributed over the tubes in the main heat exchanger and are condensed completely. After pressure reduction, gradual evaporation provides refrigeration to liquefy the natural gas. The process is much simpler than the cascade process; however, power consumption is substantially greater [3].

2.2.3 THE PROPANE-PRECOOLED MIXED-REFRIGERANT CYCLE

The precooled mixed refrigerant process is a combination of the pure refrigerant cascade and the mixed refrigerant processes.

Figure 2.4 shows a simplified diagram of the pre-cooled mixed refrigerant process [2].

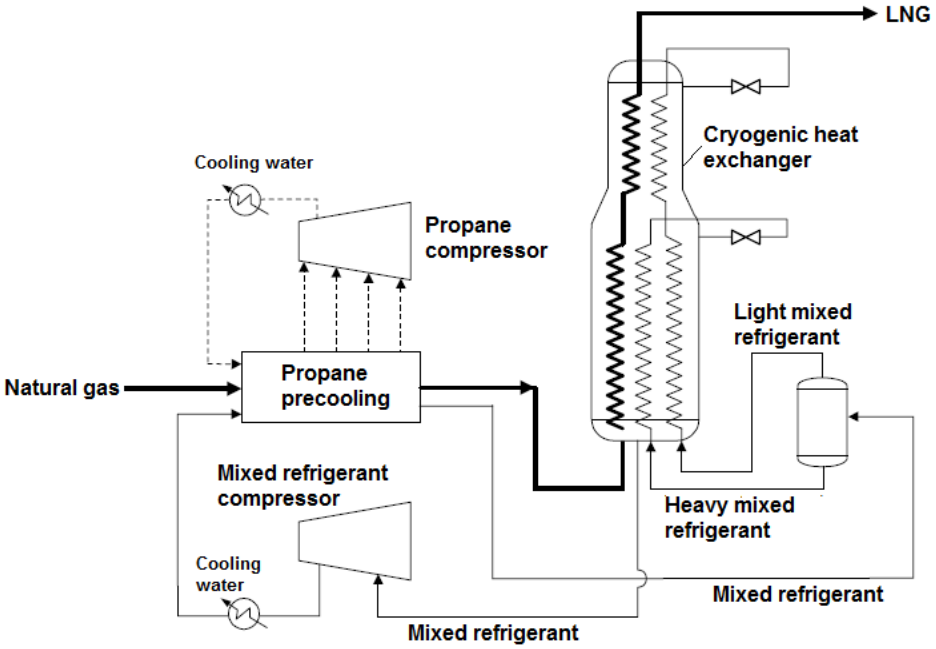

Figure 2.4 Simplified diagram of the pre-cooled mixed refrigerant process [2].

Propane is first condensed by cooling water and then with heat exchangers in three stages, cooling the feed gas stream and the mixed refrigerant to about -30 ^{o}C. After compression, the mixed refrigerant stream is also first cooled by water and then by propane. The mixed refrigerant is APCI proprietary multi-component refrigerant (MCR), which is a combination of methane, ethane, propane and nitrogen. At this stage, and before the MCR is fed into the cryogenic heat exchanger, it is separated into two fractions, the light MCR and the heavy MCR. Natural gas, already cooled to around -30 ^{o}C, is fed into the bottom of the cryogenic heat exchanger with both MCR fractions and distributed through spirally-wound tube bundles. The heavy MCR fraction leaves the top of the lower part of the heat exchanger and, after pressure reduction, is separated into vapour and liquid at a temperature of about -110 ^{o}C. They are then reintroduced into the shell of the heat exchanger. The liquid is sprayed over the tube bundles whilst the vapour mixes with the vapour and liquid flowing downwards from the shell of the upper bundle. In the top part of the heat exchanger, the light MCR fractions and natural gas are cooled to around -160 ^{o}C by spraying light MCR after pressure reduction over the remaining bundles. At

this point the natural gas is liquefied and fed to storage. Low pressure MCR vapours are collected at the bottom of the heat exchanger, compressed and recycled [2].

Propane-precooled mixed-refrigerant technology is the most-used liquefaction process in LNG plants, accounting for near 90% of the liquefaction trains currently on-stream.

2.3 LNG SHIPPING

LNG is transported by special carriers from the production facilities to regasification terminals. Since the first LNG shipment was made on a trial basis in 1959 between the US and the UK, over the years the development of containment systems for LNG ships has been along two basic design concepts [3]:

i. Self-supporting tanks

ii. Integral membrane

Those designs consist basically of either (i) self-supporting LNG tanks within the hull or (ii) use the hull as an integral tank and as a support for the insulation membranes.

Individual cargo capacities of the current LNG fleet range from 125,000 m^3 to 266,000 m^3. One important design characteristic of the ship cargo operations, irrespective of the type of containment system employed, is to do with the management of the boil-off gas produced during transportation. As LNG is carried at, or very nearly at, its boiling point at atmospheric pressure, the heat added to the cargo from the ambient air and sea water causes part of the cargo to evaporate. Therefore, the use of the generated boil-off as fuel is the standard practice in almost all LNG ships today, as on-board re-liquefaction facilities are complex and expensive in capital and operating cost.

As shipping distance increases, transport costs play a significant role in project economics. As discussed earlier, the longest trips are of the order of 20 days, during which 2-3% of the total volume of the transported LNG evaporates. To address this challenge a new generation of high capacity LNG ships have been developed, the Q-Max (capacity: 266,000 m^3). The economy of scale achieved by increasing the size of this new vessel design, and the incorporation of slow-speed diesel engines and on-board re-liquefaction

have helped to reduce the capital cost of the initial investment, as fewer ships are needed to transport larger LNG volumes, reducing the operating costs [5].

Figures 2.5 and 2.6 [2] respectively show the diagrams of the self-supporting and integral membrane ship tank designs.

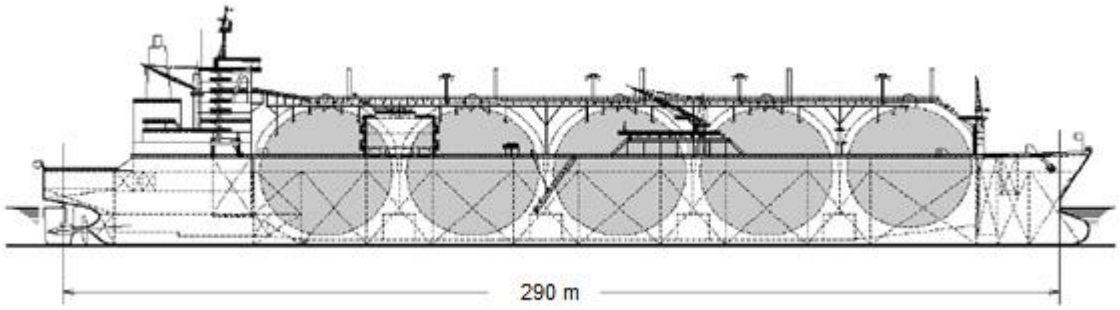

Figure 2.5 Moss type ship with spherical self-supporting tanks [2].

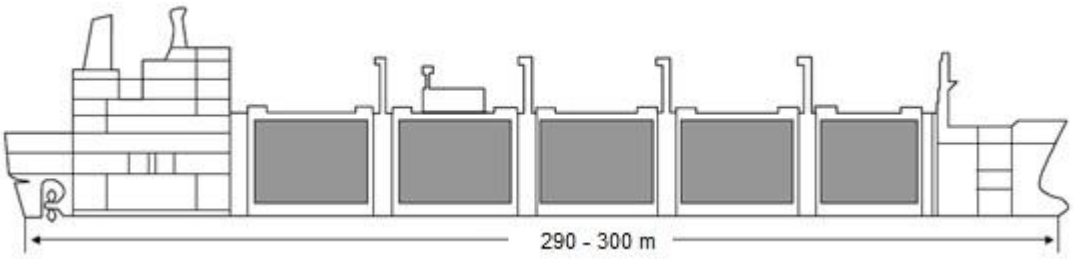

Figure 2.6 Gaz Transport Technigaz ship with integral membrane tanks [2].

2.4 LNG REGASIFICATION

Regasification terminals, also referred as import terminals, take charge of receiving the LNG carriers, storing the LNG and vaporizing it according to user demand. They are intended to provide the necessary infrastructure to link the natural gas producers to the final markets.

Figure 2.7 shows a diagram of an LNG regasification terminal based on the submerged combustion vaporizer (SCV) [6].

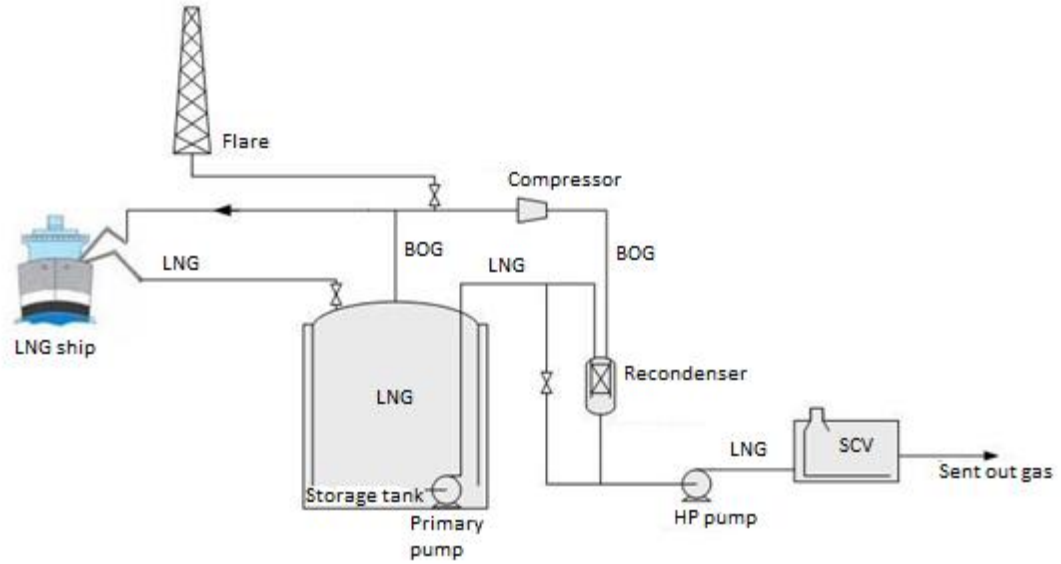

Figure 2.7 Diagram of an SCV LNG regasification terminal [6].

The LNG is offloaded from the LNG carrier and stored in insulated tanks. As gas is demanded by the end users, a liquid stream from the tanks is pumped out by the primary pumps. It can be sent either to the recondenser, when the terminal has this piece of equipment for vapour handling, or directly to the high pressure (HP) pumps (also known as secondary pumps), when there is no recondenser. The liquid stream from the secondary pumps is vaporized in the vaporizers. The amount of energy required for the phase change depends on the composition of the LNG and the final temperature required. Before being delivered to the market, natural gas must be metered for billing purposes and odorized for safety reasons, if injected into the grid.

There exists several vaporization systems whose main difference is the heat source used to vaporize the LNG. The most used are the following [6]:

i. Sea water as heating medium

ii. Combustion gas heating

Two systems are commonly used, the Open Rack Vaporizer (ORV) and Submerged Combustion Vaporizers (SCV).

The ORV consists of a group of panels formed by finned tubes with the LNG flowing upwards through them (refer to Figure 2.8). A film of seawater flows downwards outside the tubes, absorbing the cold from the LNG and returning to the sea few degrees colder. The heat used is essentially free, although capital and operating costs related to pumping and piping seawater should be taken into account. The use of such vaporizers is not advisable when seawater temperature is lower than 5 °C [6].

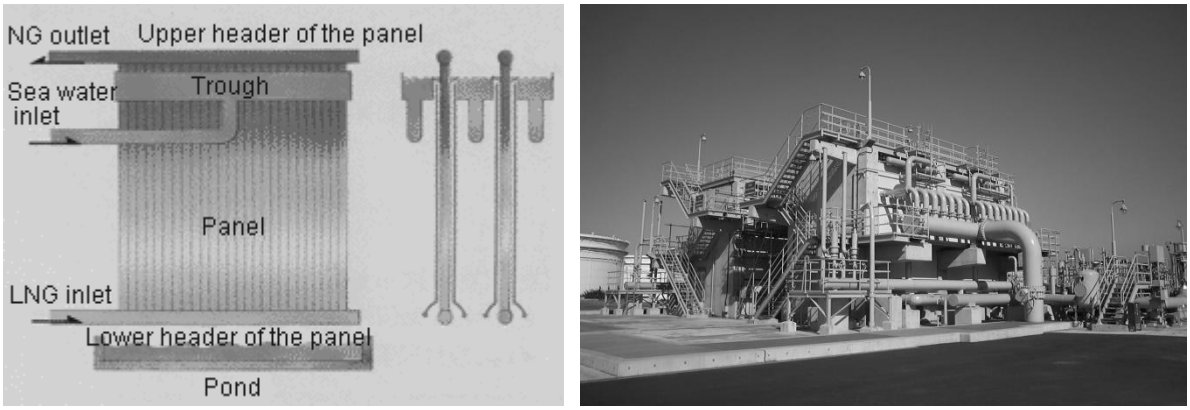

Figure 2.8 Open rack LNG vaporizer [6].

The SCV consists of a warm water bath with a bundle of tubes immersed in it. The LNG flows through the tubes, requiring the burning of a certain percentage of the send-out gas for its vaporization. The hot gases from the combustion are bubbled through the water, heating up the bath. The hot water, hence, acts as an intermediate fluid between the hot gases and the LNG (refer to Figure 2.9) [6].

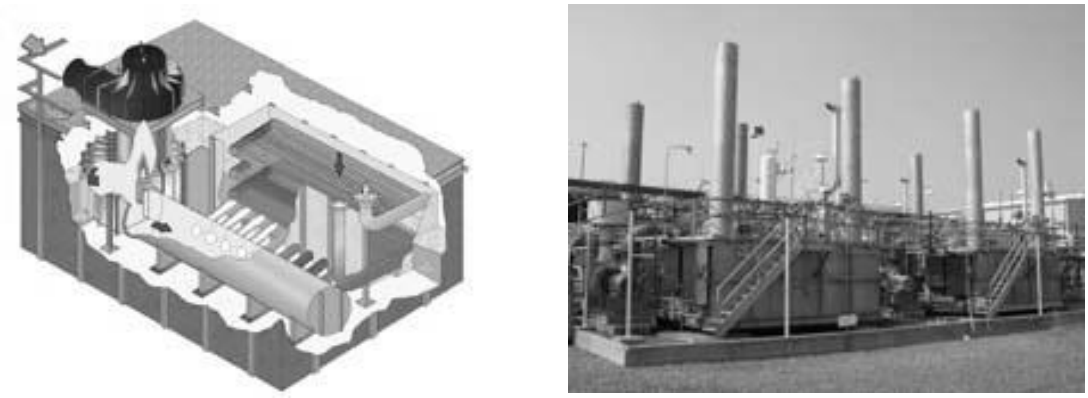

Figure 2.9 LNG submerged combustion vaporizer [6].

Another important part of the LNG import terminal process is the vapour handling system. BOG is continuously produced inside the storage tanks due to external heat input. In order to maintain the internal pressure at a constant level, the generated BOG must be processed. During the offloading of an LNG carrier, larger quantities of vapour are also produced mainly due to energy input from the unloading pumps of the LNG ship and also from heat in-leak in the transfer line. There is also a significant amount of vapour generated due to the displacement produced in the tanks. Part of this vapour is returned to the tanker but the rest must be also processed. There are two approaches for BOG processing: (*i*) compression up to the discharge pressure and send-out to gas users, used in terminals without recondenser; and (*ii*) compression up to the primary pump discharge pressure and transfer to the recondenser where it is reliquefied by direct contact with sub-cooled LNG.

In regasification plants special attention needs to be taken to LNG stratification and rollover. Terminals receive LNG from different locations, and therefore with different compositions and densities, which can cause stratification. As mentioned earlier, if one of the upper layers has a density higher than the lower ones, a rapid mixing between layers, known as rollover, can happen [7-8]. This would lead to a huge amount of BOG generation, which the plant may not be able to process. In order to prevent this phenomenon, terminals have lines to circulate LNG between tanks and use different filling

procedures, bottom filling and upper filling, to cope with density differences between stored LNG and unloaded LNG.

2.5 LNG STORAGE

The objective of the LNG storage tank at both production plant and receiving terminal is to act as a buffer within the LNG supply chain. Hence, the processing facility is free to operate independently of any variability from production, shipping and gas user demand.

LNG is stored in highly insulated tanks at temperatures of about -160 °C and pressures slightly above atmosphere, at its bubble point. Due to the heat in-leak BOG is continuously produced in the tank, which is mainly composed by nitrogen and methane with only small quantities of ethane and heavier compounds. The pressure in the tank is controlled by the BOG compressors that continuously remove the BOG to avoid tank to overpressure.

The BOG generation depends on the liquid stock, therefore the BOG flow rate will change as the liquid level does inside the tank. The BOG generation also depends on the heat transfer acting on the stored LNG, comprising heat transfer through the lateral wall, roof and bottom (constant heat coming in from the bottom thermal slab, using an electrical heating element to prevent ground freezing).

As the BOG is removed from the tank, the content of lighter compounds in the LNG is reduced and the relevant properties of the LNG over time change. The released vapour is a dry gas composed mainly by nitrogen and methane, with only small quantities of ethane and heavier compounds. As a result, the content of the higher boiling point compounds remaining in the LNG increases producing a direct effect in the gas quality, in particular heating value and Wobbe index. This process of compositional change of the LNG is called weathering.

The LNG industry uses two measures of quality for natural gas, namely Higher Heating Value (HHV) and Wobbe index (WI), to ascertain the suitability of natural gas in different markets. Both are measures of energy content; and whilst HHV is equivalent to heat of combustion, the WI is an indicator of the interchangeability of fuel gases, giving a measure

of the relative heat input into a burner at a fixed gas pressure [7]. The relationship between the two is as follows:

$$WI = \frac{HHV}{\sqrt{\rho/\rho_{ref}}} \tag{2.1}$$

where ρ is the density of LNG mixture in the gaseous state, and ρ_{ref}, the reference density, is taken as the density of air at standard conditions. HHV and WI are later described in Chapter 3.

The main aspects related to storage within an LNG facility are the selected containment technology and total storage capacity.

With regards to containment technology, LNG storage tanks are divided into three main categories: underground, in-ground and above ground storage tanks. Figure 2.10 shows the three LNG storage tank categories, as used by the LNG industry [6].

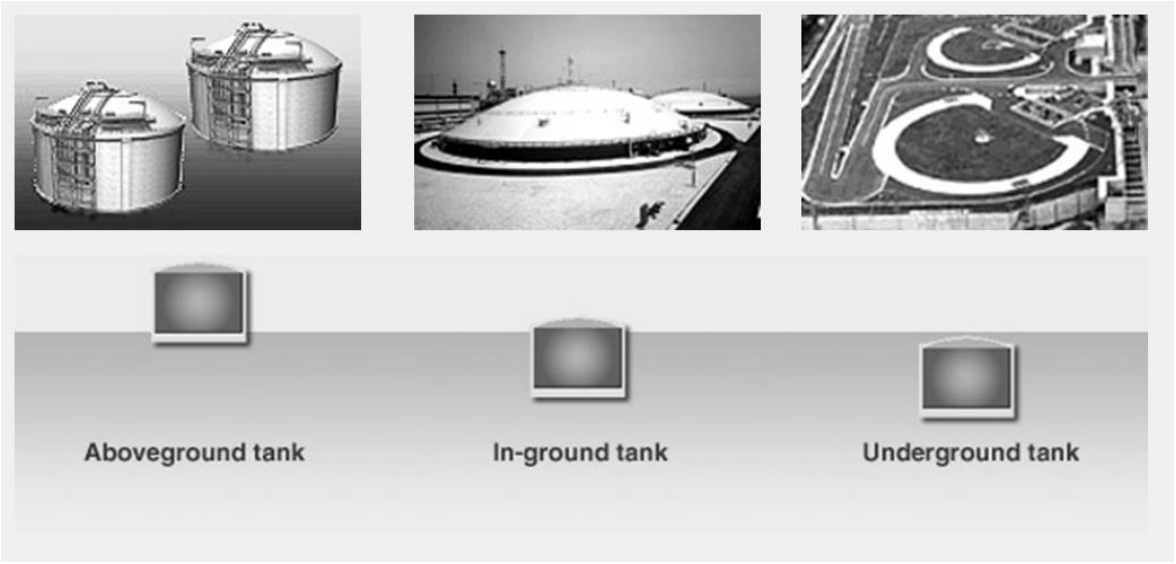

Figure 2.10 LNG storage tanks categories [6].

The above ground or self-supporting LNG storage tank is the technology mostly used by the industry. The technology can be subdivided according to its structural details [7] as follows:

i. Single containment tank (SCT)

ii. Double containment tank (DCT)

iii. Full containment tank (FCT)

The trend over the years, as shown in Figure 2.11, has been to evolve from single containment, through double containment, to full containment, due to the increase in safety and reduced plot space [6]. The full containment type is spreadly used in LNG receiving terminals. In liquefaction plants however, the containment technology used is more project specific.

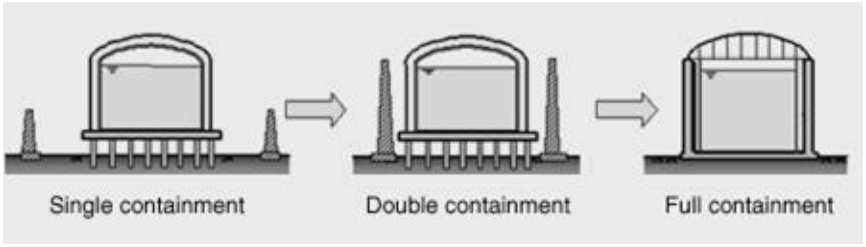

Figure 2.11 Above ground LNG storage technology evolution [6].

The following sections describe each of the above ground LNG storage tank technologies, according to their structural details.

2.5.1 SINGLE CONTAINMENT TANK (SCT)

The above ground single containment LNG storage tank consists of a suitable cryogenic metal (9% nickel steel) inner container designed to hold the LNG, a carbon steel outer supporting tank, and a steel roof. The inner tank is surrounded by insulation to control the heat in-leak through the tank wall. The outer tank is not designed to meet the low temperature ductility requirements to contain the LNG in the event of an inner tank leak.

In case of the inner tank rupture, a secondary mean of LNG containment is generally provided such as an earthen safety dike, able to contain the 110% of the total tank volume capacity [9]. The downside of this type of storage tanks is the requirement for a large tank farm area, as the required space taken by the earthen dike significantly adds to the total land usage.

Figure 2.12 shows a scheme of the single containment LNG storage tank [7].

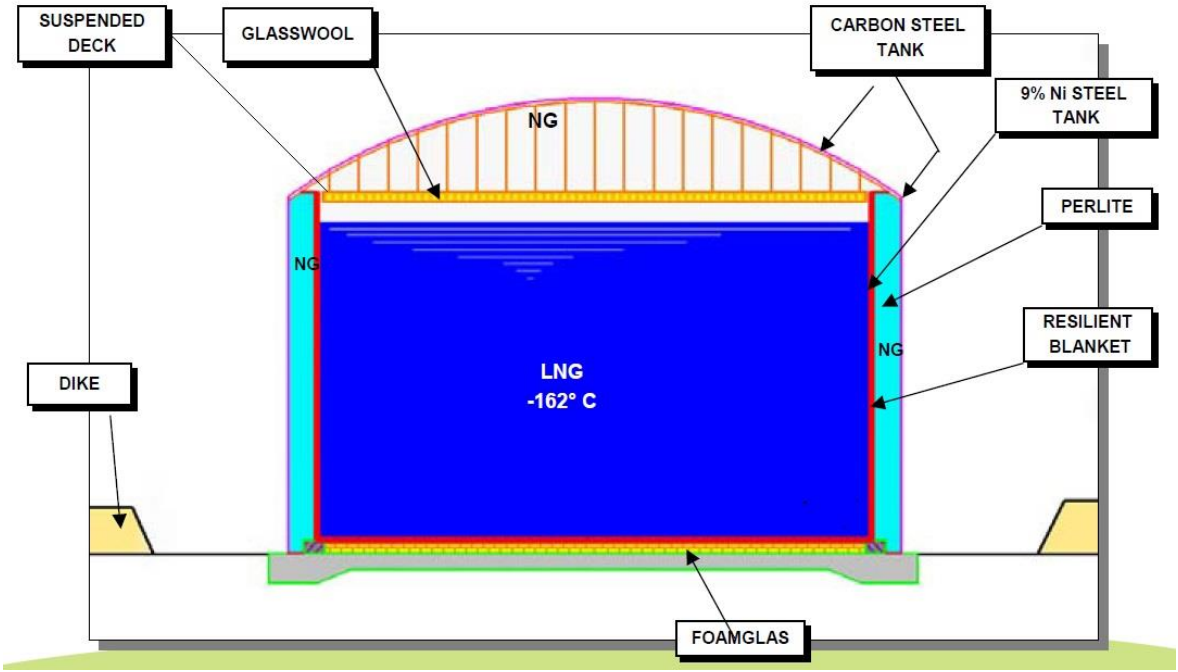

Figure 2.12 Scheme of the single containment LNG storage tank [7].

2.5.2 DOUBLE CONTAINMENT TANK (DCT)

The double containment LNG storage tank is basically a single containment tank, surrounded by a close-in reinforced open top concrete outer container to hold any potential LNG leak from the inner tank, but not to contain any vapour released during the spill.

Like the SCT, the DCT consists of a suitable cryogenic metal inner container (9% nickel steel) designed to hold the LNG, a carbon steel outer supporting tank, and a steel roof. Insulation surrounds the inner tank to control heat in-leak through the tank wall.

In addition to the outer carbon steel wall, the DCT design also includes a concrete outer container which functions as a secondary mean of LNG containment. The outer container is a reinforced concrete cylinder surrounding the outer carbon steel tank shell and is designed to contain the full tank volume plus an additional safety margin.

Figure 2.13 shows a scheme of the double containment LNG storage tank [7].

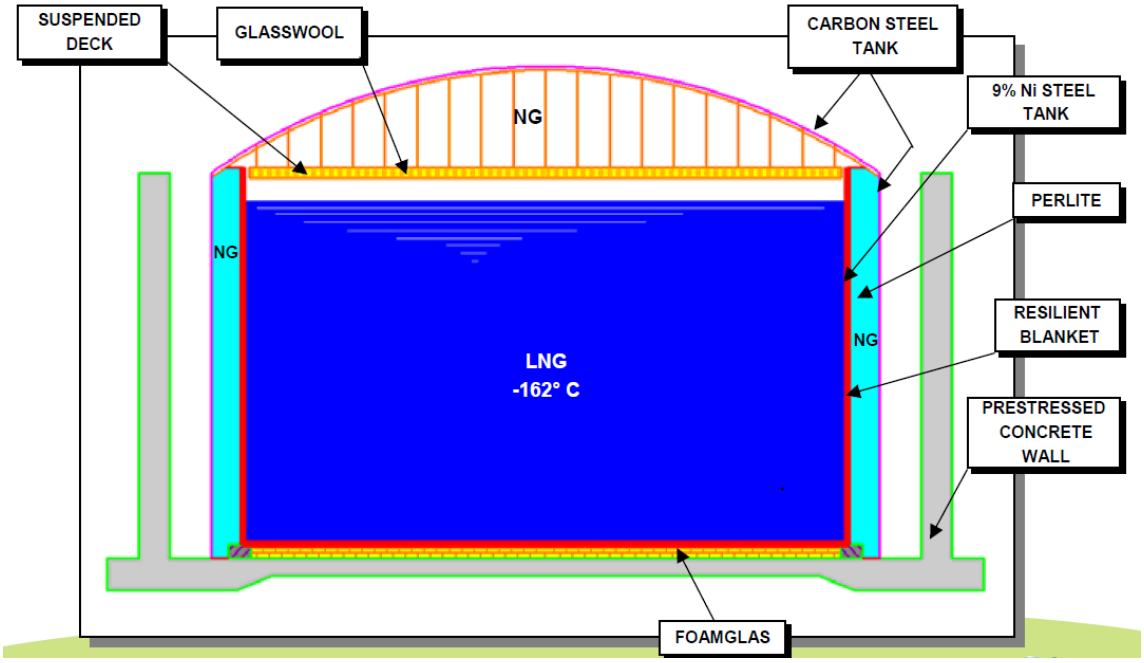

Figure 2.13 Scheme of the double containment LNG storage tank [7].

2.5.3 FULL CONTAINMENT TANK (FCT)

Similarly to the SCT and DCT, the full containment LNG storage tank consists of a suitable cryogenic metal liner container (9% nickel steel) designed to hold the LNG, with a reinforced concrete outer tank, and a reinforced concrete roof. The outer concrete tank is also designed to contain the LNG in the event of an inner tank leak or rupture. Insulation surrounds the inner tank to control heat in-leak through the tank wall. Different types of insulation are used in different parts of the tank. Typically, the annular space between the inner and outer tanks is filled with loose perlite. In addition, a resilient blanket, such as fibreglass material, is installed on the outside of the inner tank. The blanket provides

resiliency of the perlite. The reinforced concrete roof is lined with carbon steel, with the liner also functioning as framework for the concrete.

Heat in-leak from the roof of the tank is limited by installing insulation on the suspended deck (directly suspended from the roof). There is no insulation immediately beneath the roof, and the vapour space between the suspended deck and the tank roof is close to ambient temperature. For the bottom insulation most of the LNG tanks use cellular glass (foam glass).

Figure 2.14 shows a scheme of the full containment LNG storage tank [7].

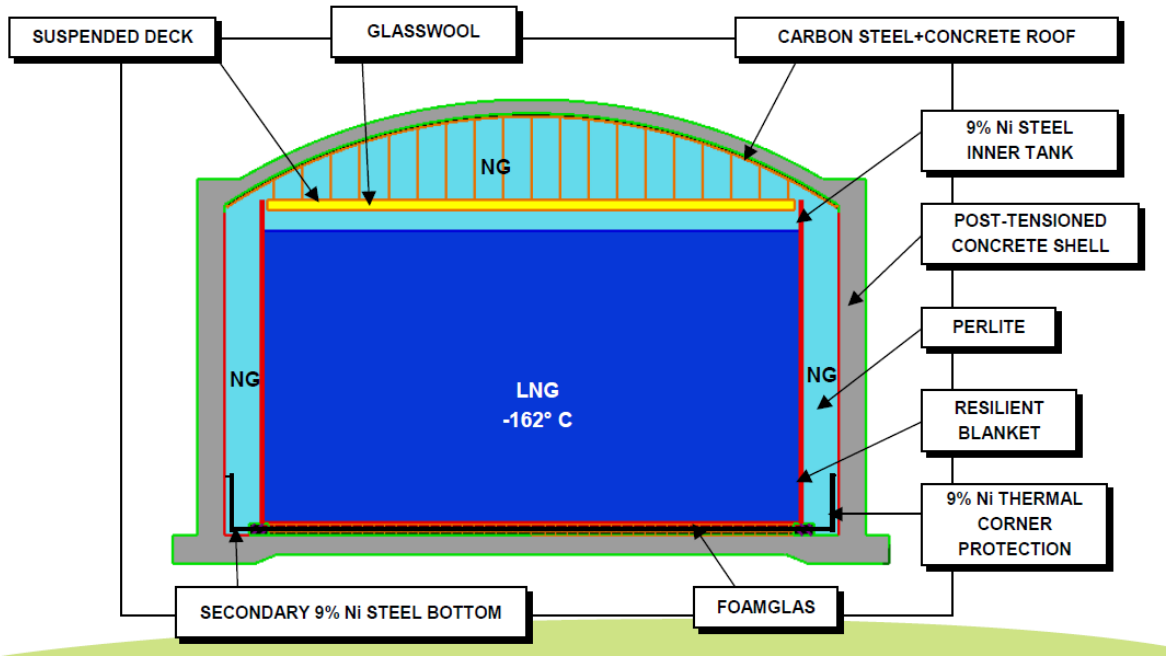

Figure 2.14 Scheme of the full containment LNG storage tank [7].

With regards to storage capacity, one approach is to set it in terms of days of LNG production in liquefaction facilities or gas send out delivered volume in regasification terminals. In liquefaction plants, the storage capacity usually ranges from 5 to 8 days of production capacity. However, in regasification terminals, storage capacity depends more on demand shapes, and typically runs from 10 to 20 days of terminal gas send out capacity.

As LNG tanks are very reliable equipment, larger tanks are preferred over multiple smaller tanks. Since the first LNG tank constructed in Canvey Island UK in 1957 [6], the size has

significantly increased over the years. Currently, the largest above-ground tank has a storage volume of 190,000 m^3, whilst the largest in-ground tank has a storage capacity of 200,000 m^3 [6]. Most of the new developments favour above-ground tanks and aim for even larger capacities, up to 300,000 m^3. The main advantages for larger tanks are the economy of scale and footprint. Moreover, the construction schedule, which is commonly in the critical path of LNG project execution, is not increased as the tank becomes larger [6].

2.6 LNG STORAGE TANK THERMAL CONDITIONING PRIOR TO INITIAL FILLING

After the commissioning[4] procedure is finalised, and prior to operating at normal conditions, the LNG storage tank is progressively cooled down to cryogenic temperature before the initial filling with LNG. Since the introduction of a cold liquid such as LNG in a warm tank container can produce large thermal stresses in the vessel plates, direct cooling by a cryogenic liquid is avoided. In this respect, during the start up stage, the tank is thermally conditioned in a stepwise approach to ensure a safe and reliable shift from mechanical completion to the operation state.

The start up procedure of an LNG storage tank is carried out in two steps:

- Purging and dry out
- Pre-cooling and tank cool-down

The following sections describe in more detail each of the above steps for the start up of an above ground LNG storage tank.

2.6.1 PURGING AND DRY OUT

The LNG storage tank is initially filled with air, once its construction is finalised. Nitrogen gas is used to displace the air from the tank. Air needs to be purged and replaced with nitrogen to ensure the oxygen concentration remains below the explosive limit when the methane gas is added as part of the cooling down procedure.

[4] Commissioning refers to the integrated application of a set of engineering techniques and procedures, for inspection and system testing from mechanical completion up to start up.

In parallel with the air displacement process, drying out of the tank is also carried out, as the presence of moisture in the storage tank may result in solid deposits during the cool-down process. In this respect, it is mandatory to reduce the moisture to a level at which there is no adverse influence to the tank mechanical integrity.

The purging set up, to push the air out of the tank, consists of arranging the piping system to have different inlet and outlet, in order to introduce nitrogen on one side and remove the displaced oxygen-nitrogen mixture from an outlet point. The purging process thus operates in a continuous mode [10]. An effective way to proceed is to introduce the purge gas via the bottom filling line at low pressure. This slowly displaces the total volume of air in the tank with little mixing. Air purging is complete once the reading measurement of oxygen concentration inside the tank is below the marginal explosive range of methane [11].

In regard to the drying out process, the progression is carried out by monitoring the water dew point of the gas mixture inside the tank. Moisture is partially removed during the nitrogen purging process, and is completely eliminated from the system early in the next step, during methane gas introduction [10].

2.6.2 PRE-COOLING AND TANK COOL-DOWN

Substitution to methane gas follows the air purging. This is usually done with cold gas from a berthed LNG carrier. Cold gas initially flows from the ship vapour space through the vapour return line to the LNG tank. From the LNG tank, the displaced gas mixture, nitrogen-methane, is routed to the vent stack via the BOG header [11]. This pre-cooling phase using cold gas circulation removes a substantial quantity of heat from the tank. After nitrogen is displaced from the inner tank the cooling down process continues by using LNG.

The LNG flow from ship is introduced and sprayed into the storage tank through the cool-down ring. The LNG flow rate is monitored and adequately controlled to prevent vacuum from occurring by too rapid cooling of the vapour space in the inner tank. During the cool-down process a constant positive pressure is maintained inside the tank by venting to the flare stack via the vapour header [11].

The LNG flowrate is progressively increased to maintain the cool-down rate of the tank uniform. Once the inner tank bottom reachs approximately -160 ºC, LNG begins to build up. The process is completed when a minimum liquid level is established in the tank bottom. At this point the tank is considered cooled down; therefore, the LNG introduction into the tank may be continued via the normal loading procedure, top or bottom filling [11].

In this work we have not modelled the operation of the storage tank during the thermal conditioning period and have only examined the weathering during the normal operations.

2.7 REVIEW OF RELEVANT WORK DONE IN LNG WEATHERING

As discussed previously, LNG weathering is the progressive alteration of the main variables of stored LNG as the effect of vaporization, due to the heat ingress from the surroundings.

This section presents the literature review related to the main subject of this research, LNG weathering. Due to similarities and its relevance to the research theme the review also includes work performed on modelling the blowdown of pressurised vessels containing hydrocarbons.

LNG vaporization work especially that carried out in LNG vaporization on water following an LNG spill, has also been reviewed. This is a subject that is receiving special attention in recent years, as the LNG industry is demanding a better quantification, and eventually a reduction, of the risk associated to an accidental spillage of LNG during LNG shipping, as well as during loading and unloading shipping operations.

Finally, the influence of LNG weathering is also discussed. In this regard, selected work on Rapid Phase Transition (RPT) has been reviewed, as it is an area where LNG weathering could play an important role.

2.7.1 LNG WEATHERING LITERATURE REVIEW

The review of the work carried out to date shows that LNG weathering is a rarely studied phenomenon, with a small number of publications available in the literature.

The BOR of stored LNG was initially studied in the early stages of the LNG industry (1960s) by Churchill [12] in 1962 and Neill *et al.* [13] in 1968, who focused on the influence of insulation and radiative cooling of the vapour exposed section of the tank wall on BOR, assuming steady-state and without taking compositional variation of LNG into account.

Churchill [12] presented analytical solutions for a small prototype LNG tank, to calculate wall temperatures and heat leak rates in the vapour space. Although Churchill's analytical solutions were easy to apply, the correspondence with the measured wall temperature in the prototype tank was only fair.

Following Churchill's work, Neill *et al*. [13] sought to develop a technique to calculate BOG rates and vapour space wall temperatures. Neill *et al.* [13] were able to present a calculation technique to estimate BOG rates and tank wall temperatures by using the storage tank design parameters and conventional heat transfer calculations, but the testing and validation of the method was very limited. Thus, the reliability of the method for accurate predictions of BOG rates and tank wall temperatures, was uncertain. The applicability of the method to extend the calculation to other tank configurations than the one (prototype) used in the research reported by the authors was another unknown.

In 1974, Shah and Aarts [14] proposed a first mathematical model to describe LNG weathering, based on analysis similar to that of Neill *et al*. [13], but including a simple thermodynamic model that made use of experimentally deduced thermodynamic properties. The model was developed for LNG stored in above ground tanks and shipped LNG. The modelling approach assumed a constant BOR of 0.05% for LNG stored in above ground tanks and 0.25% for shipped LNG (considering a 125,000 m^3 LNG ship). The latter being nearly twice the current recommended value [15]. The BOG was estimated by knowing the heat flow entering into the tank, which is assumed constant during the weathering process. For shipped LNG Shah and Aarts [14] were able to predict volume and temperature evolution, as well as heating value of the weathered LNG, with 1% or less variations. No reference, however, was given for variations on weathered LNG in above ground tanks. Although the Shah and Aarts [14] model was not able to predict the

composition of the weathered LNG, it is recognised that it was a very good tool, back in the 1970s, to predict volume and quality of received LNG, following a cargo voyage from the LNG production facility to the regasification terminal.

It is important to highlight that empirical evidence (based on operational data) shows that the boil-off rate (BOR) for LNG stored in above ground tanks is below 0.05 % v/v (considering fully loaded tank), and 0.15 % v/v for shipped LNG. Both BOR factors are for normal use by the LNG industry today for gross and quick estimates. In the case of above ground storage tanks that simplification leads to an inaccurate prediction of the resulting LNG composition, as BOG flowrate is a function of the liquid stock.

In 1999 Kountz [16], at the Institute of Gas Technology (IGT), conducted an experimental test program to measure LNG weathering in on-board storage tanks. The test program was aimed at vehicles utilizing LNG as fuel. The experimental set up measured the evolution of composition, mass and average bulk temperature of stored LNG in a pressurized container under controlled constant heat inflow, of six (6) different LNG compositions. Kountz [16] experimented with relatively high nitrogen content LNG mixtures, up to 6.2% on a molar basis. As part of the project Kountz [16] developed a non-disclosed physical model that demonstrated reasonable agreement with the measured data. Figure 2.15 [16] shows the predicted vs. measured LNG composition values over time of one of the experiments, using an unweathered LNG mixture with 4.4% mol of nitrogen (actual composition is 87.8% mol of methane, 6.8% mol of ethane, 1.0% mol propane and 4.4% mol nitrogen).

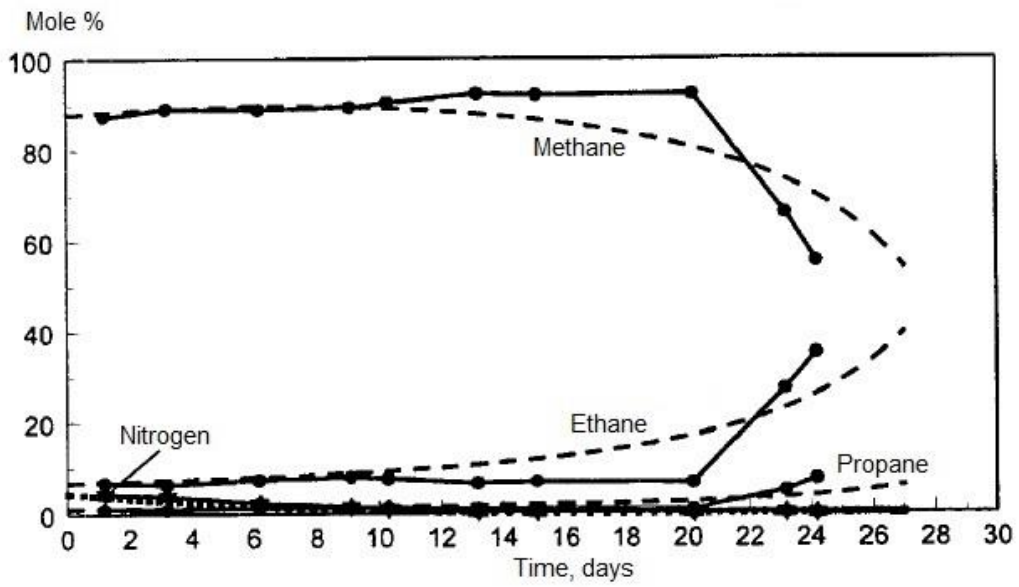

Figure 2.15 Predicted vs. measured LNG composition Kountz weathering model [16].
(-●-Experiment; - - - Model)

Figure 2.15 [16] shows that Kountz's [16] model suitably reproduces the weathering compositional behaviour inside the tank.

Aspelund *et al.* [17] have also developed an in-house physical LNG weathering model, geared towards applications to small-scale LNG chains. Aspelund and co-workers [17] developed their model by recreating the weathering tests results of two LNG mixtures used by Kountz [16]. The validation of the model using the experimental data obtained by Kountz [14] was reported by Aspelund *et al.* [17] indicating good agreement.

LNG weathering has been mainly studied in LNG shipping, to predict the LNG composition and properties at the receiving terminal. Recently works of Dimopoulos and Frangopolous [18], Hasan *et. al.* [19] and Miana *et. al.* [20] provide independent studies of the phenomena.

Dimopoulos and Frangopolous [18] in 2008 developed a model, based on treating LNG as an ideal mixture and constant heat ingress into the stored LNG, to study the BOG and compositional variation during a typical sea-voyage. In particular, the model was used to examine natural and forced BOG during a hypothetical 25 day journey and the effect that

would have on the composition and the heating value of the resulting BOG. Dimopoulos and Frangopolous [18] concluded that the handling of the BOG during the LNG vessel operation and the assessment of its thermodynamic properties are key issues in the technical and economic evaluation of the energy system of LNG vessels.

Hasan *et al.* [19] in 2009 conducted a study on boil-off gas generation for LNG transportation aiming to minimise the boil-off gas losses in LNG shipping. Hasan *et al.* [19] built a process simulation using Aspen HYSYS, and Soave-Redlich-Kwong (SRK) for VLE, to model the journey of an LNG tanker from an export terminal to an import terminal. The model assumes the LNG is thermodynamic equilibrium during the voyage, and considers a variable heat input into the LNG owing the LNG temperature increase due to the preferential evaporation of lighter components. They estimated the BOG generation of the LNG tanker for a variety of conditions and different voyages scenarios.

Hasan *et al.* [19] found that nitrogen content in LNG can be adjusted to minimize BOG losses, since BOG decreases (nonlinearly) as LNG nitrogen content increases. As a part of their study, the BOG generation behaviour of two LNG mixtures, rich and lean, was compared against the LNG nitrogen content. The rich LNG containing around 80% mol methane and nitrogen content ranging from 0% mol up to 3% mol, the remaining being a mixture of heavier compounds between ethane, propane and butane. The lean LNG case containing around 90% mol methane and nitrogen content ranging also from 0% mol up to 3% mol, but the remaining being ethane only. Figure 2.16 shows the BOG generation vs. LNG nitrogen content graph [19], where the BOG generation is expressed as CBOG, which is the weight percentage of BOG generated to initial cargo load.

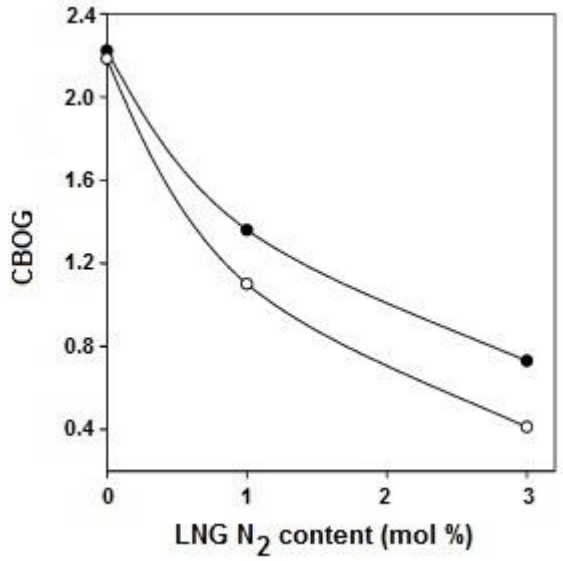

Figure 2.16 CBOG vs. LNG N_2 content - Hasan's study [19].
(CBOG is the weight percentage of BOG generated to initial cargo load)
(-●- Lean LNG; -○- Rich LNG)

From Figure 2.16 it is observed that BOG generation decreases more sharply with nitrogen content for rich LNG than lean LNG. Note that although more nitrogen in the LNG seems to be good to reduce BOG generation, it does decrease the heating value in the LNG [19]. However, it should be possible to optimize nitrogen content in LNG shipping to produce less BOG during the laden[5] and ballast[6] voyages. Therefore, nitrogen content design in stored LNG is an interesting and non intuitive problem that deserves some attention. The effect of N_2 content in LNG to stored LNG weathering and BOG generation is examined as part of the scope of this research project, and is presented in the weathering simulations results chapter (Chapter 6) of this thesis.

It is not possible to make a judgement on the modelling approach taken by Hasan *et al.* [19] in their study, as the paper does not provide enough information on how the BOG generation is mathematically described. However, Hasan *et al.* [19] model approach is tested in Section 5.3.2 (Chapter 5) of this thesis, by comparing the results of their BOG

[5] The trip from the LNG production facility to the receiving terminal is called laden voyage.
[6] The return trip from the receiving terminal to the LNG production facility is called ballast voyage.

generation estimates, to those obtained by the weathering model developed in this research project.

Miana *et al.* [20] in 2010 developed two models, the physical model and intelligent model (i-model), with the aim of predicting the composition and properties evolution over time of shipped LNG. The development of the physical model is based on a material balance, constrained with the assumption of constant boil-off rate (BOR) generation during the trip. The second model is based on neural networks, to account for the non linearities derived from the specific characteristics of each ship, the LNG quality and to provide the link between the origin and destination ports. Molar composition, temperature and volume at the receiving terminal are then calculated based on historical data. If no historical data is available to train the neural network one reverts to the physical model presented by the authors [20].

With regard to the physical model Miana *et al.* [20] assume the LNG mixture is in thermodynamic equilibrium during the entire voyage. The prediction of LNG weathering is carried out in two sequential calculation blocks by means of an iterative method. In the first block the thermodynamic equilibrium is solved; thereafter, the second block calculates the number of LNG moles evaporated by solving the material balance in the LNG tank taking into account the BOR, which is an input data. The moles of vapour leaving the storage tank are calculated considering the total tank volume being fully occupied by the liquid and vapour. The model is run for a finite time interval until the voyage duration is reached.

The thermodynamic equilibrium is solved by the Rachford-Rice [21] equation:

$$x_i = \frac{z_i}{1+\frac{M_V}{M_F}(K_i-1)} \tag{2.2}$$

where x_i is the component mole fraction in the LNG, z_i is the overall component mole fraction of the system (liquid and vapour), M_V is the number of moles of vapour, M_F is the total number of moles in the system (liquid and vapour), and K_i is the equilibrium constant. Subscript *i* denotes each component within the mixture. Rachford-Rice [21] equation for flash calculations is further discussed in Chapter 3.

The material balance to calculate the vapour moles leaving the tank, within a time period from $t = t_0$ to $t = t_1$, is written as follows:

$$B_{t_1} = M_{\mathrm{V},t_0} - \rho_{\mathrm{V},t_1} V + \frac{\rho_{\mathrm{V},t_1}}{\rho_{\mathrm{L},t_1}} M_{\mathrm{L},t_0} + \left(1 - \frac{\rho_{\mathrm{V},t_1}}{\rho_{\mathrm{L},t_1}}\right) \frac{BOR}{48} M_{\mathrm{L},ori} \qquad (2.3)$$

where in addition to quantities defined above, B is the boil-off gas leaving the tank system, M_{L} is the number of moles in the liquid, V is the tank volume and ρ_{L} and ρ_{V} are the liquid and vapour density, respectively. The subscripts ori and t_0 refer to initial quantities and at time t_0, respectively. BOR is the boil-off rate in volume fraction basis defined as the volume ratio of evaporated LNG in one day to initial LNG volume.

Miana *et al.* [20] tested both models using selected registers from historical cargo measurements received in an actual regasification terminal. Miana *et al.* [20] carried out an accuracy study over the following selected variables: methane molar fraction, LNG high heating value (HHV), LNG Wobbe Index (WI) and LNG density. Figure 2.17 and 2.18 respectively show the deviation graphs for the physical and intelligent models, for the assessed cargoes, for each of the selected variables under study. Both graphs also include the acceptable deviation limit used in their paper for each variable assessed.

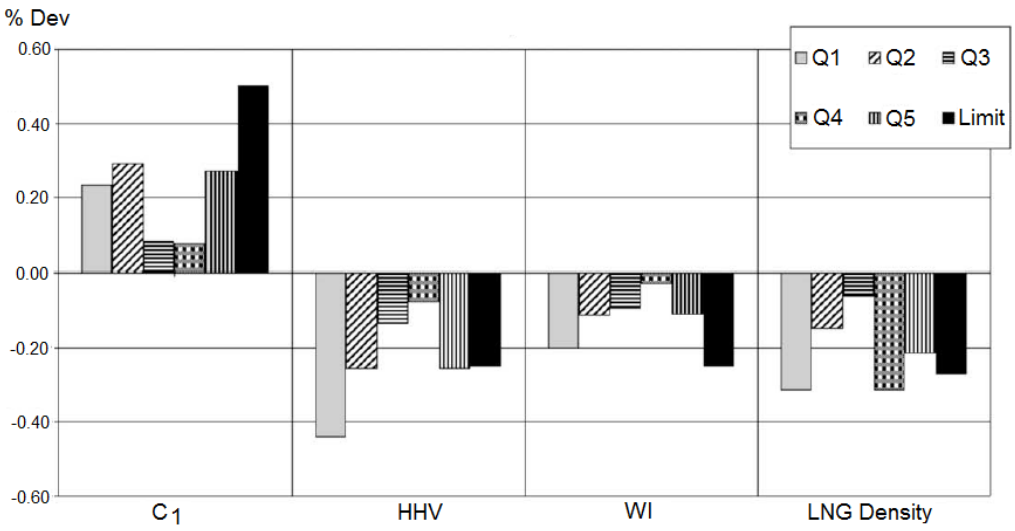

Figure 2.17 Physical model deviation [20].
(*Qn*: cargo number)

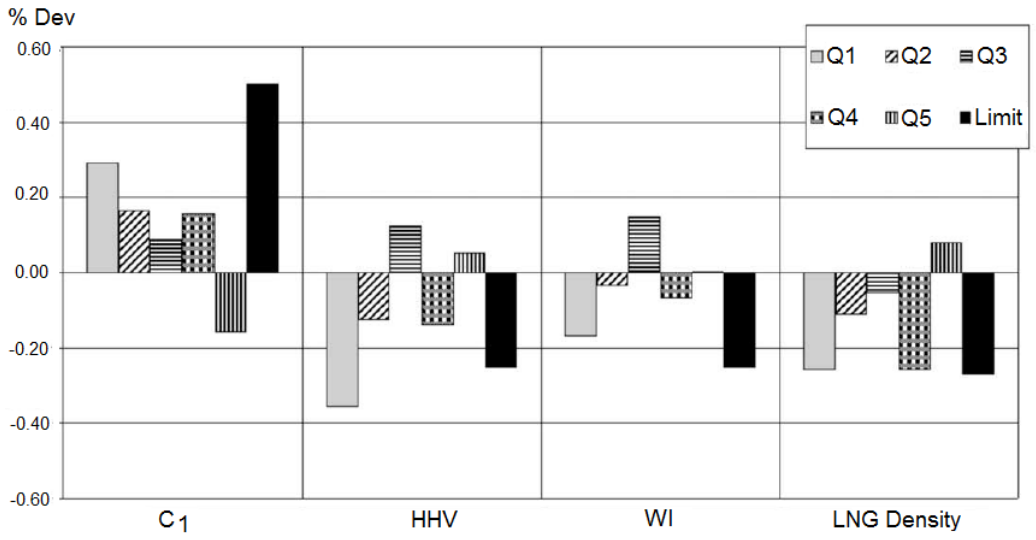

Figure 2.18 i-model deviation [20].
(*Qn*: cargo number)

Miana *et al.* [20] calculated the deviation percentage, *% Dev*, using the following equation:

$$\%\, Dev = \frac{x_{msd} - x_{mod}}{x_{msd}} x100 \qquad (2.4)$$

where x_{msd} is the measured variable and x_{mod} is the value predicted by the model.

From Figures 2.17 and 2.18 one can observe that both models produce in most of the cases (cargoes) accurate predictions for each variable assessed. The i-model however, consistently gives better results than the physical model overall, excluding few exceptions.

The constant BOR weathering prediction approach taken by Miana *et al.* [20] in their physical model is a simple one; it does not account for instance for variations due to LNG inventory. The BOR generation depends on the liquid stock. In this respect, it is important to highlight that the liquid volume in a LNG carrier remains almost constant during the trip; hence, the assumption of constant BOR to predict weathering by Miana *et al.* [20] is valid (although not rigorous) as long as it is applied in LNG shipping.

For LNG stored in above ground tanks the assumption of constant BOR is not applicable, as the liquid volume changes in time, particularly in long term LNG storage operations. BOR also changes with composition, as discussed earlier in the review of Hasan *et al.* [19] work with nitrogen enriched LNG mixtures. In this respect, the integration of the heat

transfer model considered in this research to simulate LNG weathering is a more rigorous approach to follow, as it does account for variations in BOR due to changes in the liquid stock, and as a result of variations in the LNG composition. Moreover, modelling the heat transfer as a part of the weathering calculation accounts for variable heat input into the LNG, owing the LNG temperature increase due to the preferential evaporation of lighter components.

Adom *et al*. [22] and Pellegrini *et al*. [23] have recently investigated boil-off from LNG storage tanks. Adom *et al*. [22] in 2010 developed a weathering model for LNG stored in above ground storage tanks. They analysed the impact of the heat in-leak in the BOG generated for different tank sizes and different commercial LNG mixtures. Neither the compositional evolution of the weathered LNG nor the BOG was analysed. The model was developed following the assumptions that the system was in VLE, and temperature and density of LNG were constant during the vaporization process. Although Adom and co-workers [22] were able to evaluate the dependence of the BOG generated for different tank sizes and LNG mixtures, the prediction capabilities of the model are limited since LNG temperature and density change in time as LNG gets weathered.

Of special interest to current research is the work of Pellegrini *et al*. [23] in 2014 that have developed a weathering model for LNG stored in above-ground tanks based on mass and energy balance, but without the assumption of constant BOR. The model considers thermodynamic equilibrium for the stored LNG, ideal mixture for enthalpy of vapour and liquid, and uses the SRK equation of state (EOS) for phase equilibria and density calculation, with Peneloux correction for liquid density. Same as for Shah and Aarts [14], the BOG is estimated by knowing the heat flow entering into the tank, which is assumed constant during the weathering process. The model was validated using the data of Kountz [16] and data quoted by Miana *et al.* [20].

The equation proposed by Pellegrini *et al.* [23] to model stored LNG weathering is written as follows:

$$\dot{B} = \frac{\dot{Q}_{in}}{\frac{\left(\sum x_i c_{p,i}^{l}\right)\left[\sum x_i\left(x_i\frac{\partial K_i}{\partial x_i}+K_i\right)(K_i-1)\right]+\frac{dP}{dt}\Sigma\left(x_i\frac{\partial K_i}{\partial P}\right)}{\Sigma\left(x_i\frac{\partial K_i}{\partial T}\right)}+\sum\left(K_i x_i \Delta H_{vap}\right)} \quad (2.5)$$

Equation (2.5) correlates the number of moles evaporated to the heat rate input into the storage tank, within a period of time. The denominator expression in the right hand side of the equation has two terms. The first term represents the contribution of sensible heat to weathering, which is very small compared to the second term that represents the contribution of latent heat.

Pellegrini *et al*. [23], using one of the experimental datasets from Kountz [16], run their model to compare the prediction of the BOG generation rate considering a constant heat rate into the LNG storage tank to that assuming constant BOR, throughout the weathering process.

Table 2.1 and Figure 2.19 respectively show the experimental input data and results [23], of the BOG generation prediction comparison performed by Pellegrini *et al*. [23].

Table 2.1 Data used for the BOG generation prediction comparison [23].

Tank operating pressure, *P*	770 kPa (7.7 bar)
Heat rate, $\dot{Q}$	14.64 W
Initial tank filling	81.42 %
Time duration of the experiment	21 days
Boil-off rate, BOR	4.0% v/v (day^{-1})
Composition (mol fraction)	
Methane	0.919
Ethane	0.068
Propane	0.013

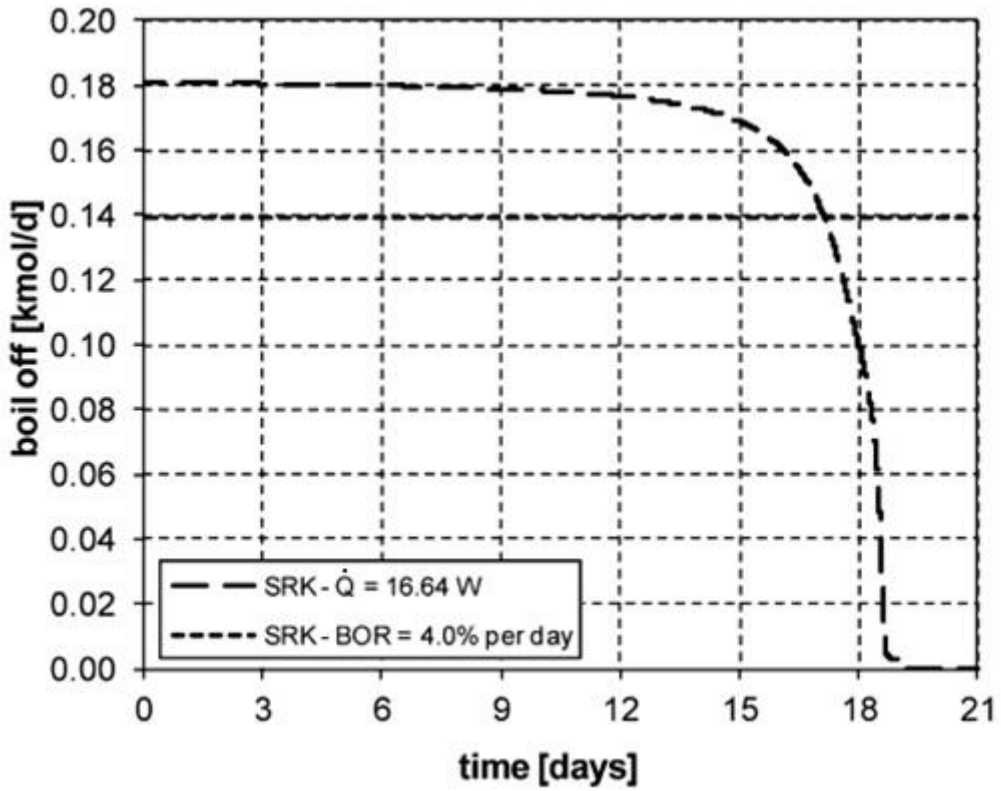

Figure 2.19 BOG rate comparison Pellegrini's model [23].
(— — Constant heat rate input: 16.64 W; ····· Constant BOR: 4% v/v per day)

From Figure 2.19 one can observe that BOR can be assumed constant in the first half of the weathering period, when considering constant heat rate input into the LNG; after 11 days the evolution of the vapour generation rate of the system is nonlinear. Additionally, the assumption of constant BOR underestimates the BOG generation rate by 22% in the first half of the weathering period. In this respect, as the estimated boil-off is higher in that initial stage, the predicted composition of the weathered LNG is heavier, and the corresponding equilibrium temperature higher.

Pellegrini *et al*. [23] model is limited in terms of its applicability to conditions where both the surrounding temperature and the LNG boiling temperature do not show large temporal variation. When applied to real cases, the constant heat rate approach might be acceptable to model weathering in the short run, but is limited in predicting weathering for long term LNG storage. As discussed earlier, the heat entering into the tank varies in time owing to the change in the temperature difference between the surrounding and the stored

(weathered) LNG. This is due to the increase in the equilibrium temperature inside the tank, as the LNG gets richer in heavier compounds.

2.7.2 BLOWDOWN OF PRESSURISED VESSELS CONTAINING HYDROCARBONS

Rapid depressurisation or blowdown refers to a time-dependent discharge of a pressurised vessel. In the oil and gas industry blowdown is a common way of reducing the failure risk of pressurised process vessels in an emergency situation.

A consequence of blowdown is the dramatic drop in the fluid temperature, due to the auto-refrigeration effect resulting as the system is depressurised; plus the massive heat transfer effect between the fluid and the vessel wall, leading to a reduction of the wall temperature [24,25]. This effect is more significant if the vessel is depressurised whilst not being under a fire attack.

Blowdown is a hazardous operation, the pressure and thermal stresses to which the vessel is exposed during the depressurisation process may lead to a number of consequences, such as vessel failure and the potential escalation from accidental release of hydrocarbon [24].

The main aspect that has to be addressed in the development of a pressurised vessel blowdown model is the description of the physical phenomena governing the fluid behaviour inside the vessel, to estimate the final temperature reached by the fluid that further determines the minimum temperature at which the vessel wall is exposed. The minimum wall temperature reached during the blowdown process is a key variable in vessel design, as that is the value used for the selection of its construction material. This is very important, as if the wall temperature falls below the ductile-brittle transition temperature of the constituent material there is a risk for the vessel wall to rupture. Therefore, being too conservative may result in predicting unrealistically low fluid and vessel wall temperatures, which leads to incremental equipment safety margins and pricey designs. The optimum vessel design then needs a correct and reliable prediction of the minimum fluid and wall temperatures that can be reached during the blowdown process [26].

The description of the physical processes occurring during the blowdown of a hydrocarbon pressurised vessel involves some similarities to that of LNG weathering phenomenon, such as modelling the boiling of a hydrocarbon and the heat transfer effects into a vessel containing a two-phase hydrocarbon mixture. There are however notable differences that should be taken into account, they are the rapidity of the blowdown process, and the sudden decrease of the system pressure that causes a rapid change of the thermodynamic state inside the vessel and an important drop of the fluid temperature.

A number of simple methods commonly used in the oil and gas industry for blowdown modelling assume that the fluid in the vessel is homogeneous and in thermodynamic equilibrium. This means that, in the case of a multiphase hydrocarbon mixture, the fluid is treated as a mixture with average properties with a single vessel wall temperature calculated [25,26]. Traditionally, depressurisation systems have been designed in accordance to standards API-520 [27,28] and API-521 [29], which have in the past implied that the depressurisation system should be capable of reducing the system pressure to 800 kPa or to 50% of the system design pressure, whichever is lower within the next 15 minutes; so that stress rupture of the vessel is not an immediate concern. Fire depressurization models typically use the same models as for normal depressurization, but apply an extremal heat flux entering into the system [27].

The expansion that takes place during depressurization can be assumed to be isentropic, isenthalpic, or somewhere in between. The selection of the thermodynamic path is often arbitrary and is usually selected considering an expansion efficiency to predict the temperature drop used for design. Typically an efficiency of 50% is selected to avoid extremely low temperatures [26].

There is experimental evidence that the assumption of thermodynamic equilibrium is not deemed appropriate, since several two-phase vessels depressurization tests indicate the existence of a temperature gradient and independent temperature evolution between both phases [30]. Due to the greater heat transfer between the liquid phase and the wall, the wall in contact with the liquid is subject to more cooling than the wall in contact with the gas,

during the blowdown. Hence, the vessel should be designed for a lower temperature than if it was supposed to contain vapour only.

In this respect, Haque *et al.* [30] in 1992 developed a rigorous mathematical model named BLOWDOWN, for multicomponent systems, including free water, accounting for non-equilibrium condition between the constituent phases inside the vessel. The model was able to predict system pressure and fluid phases temperatures and compositions, all as function of time. All heat transfer acting on the vessel is taken into account, except for the one exchanged between the vapour and liquid phases, albeit the temperature difference between the two. Haque *et al.* [30] limited the model to ambient conditions surroundings, so the blowdown under a fire situation was not considered. The model was validated by comparison to experimental data from full–scale vessel tests.

The mathematical algorithm developed by Haque *et al*. [30] to solve the blowdown process assumes the vessel is divided in three zones; one for each of the phases eventually present inside. Zone 1 for gas, which includes gaseous hydrocarbon and vaporized water; zone 2 for liquid hydrocarbon; and zone 3 for free water.

Figure 2.20 shows a schematic diagram of the pressured vessel with the BLOWDOWN modelling approach.

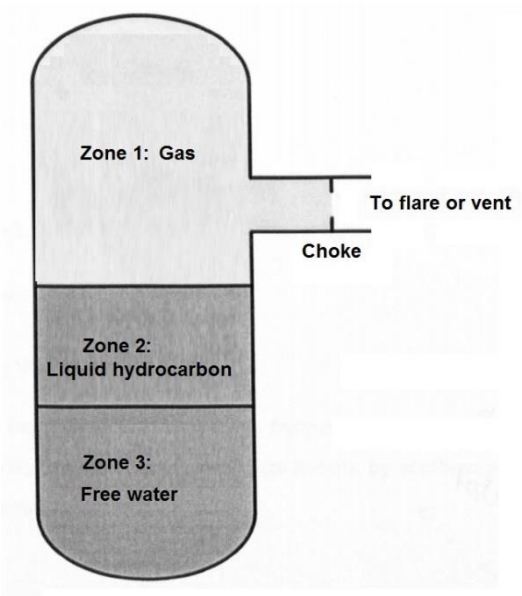

Figure 2.20 Vessel diagram showing BLOWDOWN modelling approach [30].

The model is run in an iterative approach and the entire continuous depressurisation process is approximated by a series of discrete pressure steps. The authors claim that the discrete pressure steps approach is computationally more efficient and more convenient solution-wise, since the calculations are based on a state variable such as pressure rather than a thermodynamically irrelevant variable such as time. Pressure is assumed to be spatially uniform within the vessel, whilst temperature and composition are assumed to be spatially uniform in each phase zone in which the vessel is divided to.

The approach taken by Haque *et al.* [30] to describe the blowdown process is to assume that the fluid expands polytropically followed by the heat transfer from the adjacent vessel wall, for each pressure step. Haque *et al*. [30] applied the same thermodynamic trajectory to all phases present in the vessel. The polytropic expansion then follows the expression:

$$T\frac{dS}{dT} = C \tag{2.6}$$

where T is the fluid temperature, S is the fluid entropy and C is the polytropic constant.

Equation (2.6) is solved by assuming a linear relationship between heat and temperature over a given pressure increment during blowdown. The heat Q being transferred to the fluid is then given by:

$$Q = \int_1^2 T dS = C(T_2 - T_1) \tag{2.7}$$

where the integral limits and subscripts 1 and 2 are the initial and final states of the system.

Based on the first law of thermodynamics, the work W is defined by:

$$W = (H_2 - H_1) - Q \tag{2.8}$$

where H is the fluid enthalpy.

Eq. (2.7) is solved as follows:

$$Q = \frac{(S_2 - S_1)(T_2 - T_1)}{\ln\left(\frac{T_2}{T_1}\right)} \tag{2.9}$$

Rearranging eq. (2.9), the entropy at the final state is written as:

$$S_2 = S_1 + \frac{Q \ln\left(\frac{T_2}{T_1}\right)}{(T_2 - T_1)} \tag{2.10}$$

From eq. (2.10) the entropy at the final state can be calculated by knowing the initial conditions (pressure, temperature and entropy), the final pressure and the polytropic constant. The fluid temperature is then calculated by performing a flash calculation at the final pressure and entropy.

Haque *et al*. [30] considered convection heat transfer between each fluid phase and the adjacent vessel wall. For zone 1 (gas) either natural or forced convection are assumed depending on the conditions. Natural convection usually dominates over forced convection, as at high pressures gas density and hence density differences that drive natural convection are large, whilst viscosities, which retard natural convection, are low, owing that they are not significantly affected by pressure. For zone 2 (liquid) nucleate and film boiling heat transfer are considered that involves higher heat transfer coefficients compared to zone 1. In the case of zone 3 (water), natural convection is considered. Standard correlations are used to determine the heat transfer coefficients for each of the individual zones (phases) [30].

With regard to the heat transfer between the vessel wall and the surroundings, Haque *et al*. [30] considered to be either by natural or forced convection depending on the nature of the surroundings. Normally, the mechanism is by natural convection if the wind speed is low, for instance when the vessel is sheltered within an enclosed module in an offshore platform; otherwise the heat transfer is by forced convection. In either case, standard correlations are used to determine the heat transfer coefficient in each zone of the vessel wall to the surroundings [30].

Thermodynamic and transport properties for the BLOWDOWN model are calculated using PREPROP, which is an in-house computer software developed to calculate the thermophysical properties of multi-component mixtures, by an extended principle of corresponding states [31]. Haque *et al*. [30] justified the choice (of the extended principle

of corresponding states) over the well known cubic equations of states (EOS) due to the more accurate representation of phase equilibrium, enthalpy and density; whilst the EOS claimed to be much less successful in predicting the last two properties. However, Haque *et al*. [30] pointed out that solving the extended principle of corresponding states is more computationally demanding compared to solving EOS.

The BLOWDOWN model has been tested by comparing with a significant amount of experimental data, including testing at elevated pressures of up to 15,000 kPa, showing very good agreement. Actually, after its release in 1992 the BLOWDOWN model has been used as an engineering tool by many oil and gas companies for the simulation of future and existing depressurisation systems. Applications have included a large number of individual vessels on offshore platforms and also accident investigation [32].

Figure 2.21 shows the comparison between the measured and BLOWDOWN predicted values of a selected experiment, for the fluid phases bulk temperature variations with time during a blowdown process [32]. The bulk liquid temperature was not measured in the test; nevertheless, the predicted value by the BLOWDOWN model is shown. The experimental set up used was a vertical vessel filled with a fluid composition of 85.5 % mole methane, 4.5 % mole ethane and 10 % mole propane.

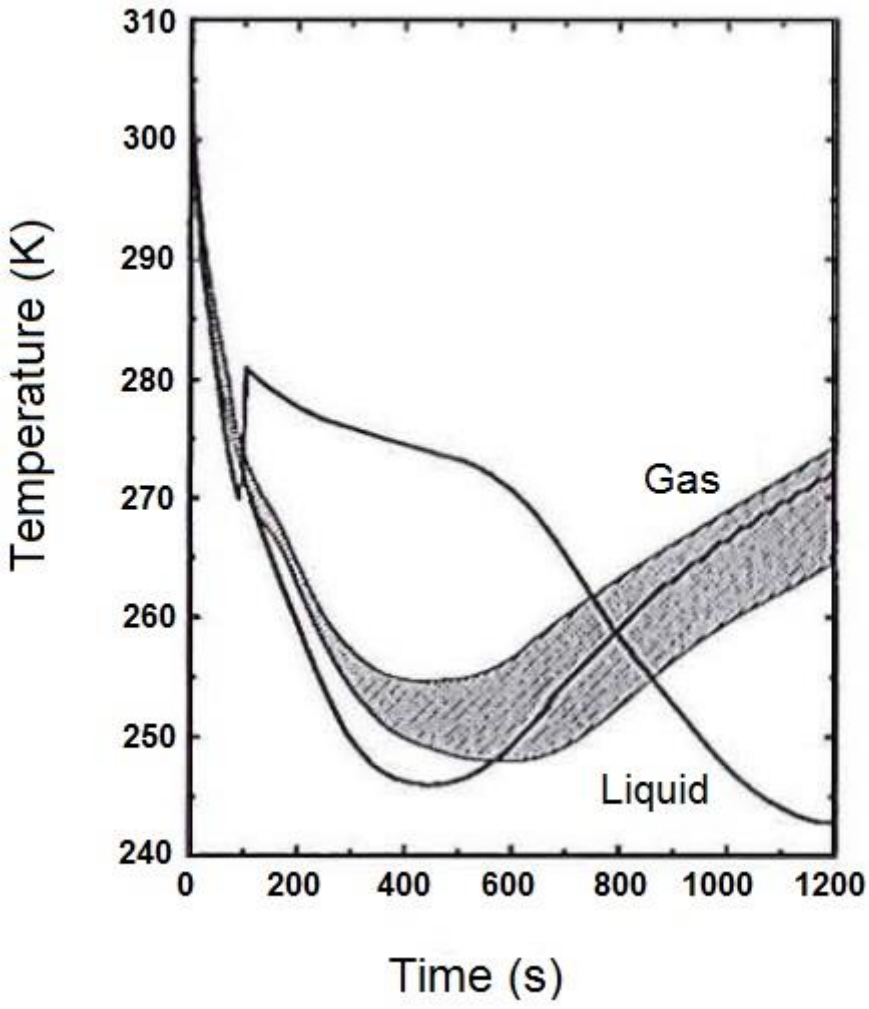

Figure 2.21 Bulk *T* of fluid phases vs. time BLOWDOWN model [32].
(Shaded region spans bulk gas temperature experimental measurements.
Solid lines are BLOWDOWN model predicted values)

From Figure 2.21 one can observe that there is very good agreement between the experimental measurements and the predicted values by the BLOWDOWN model. In particular, the minimum bulk gas temperature is predicted to within 4 K.

Whilst the BLOWDOWN is a sophisticated model, its main limitation is the use of the extended principle of corresponding states for estimating the thermophysical properties, which not only makes running the simulation computationally demanding, but also introduces accuracy uncertainties and potential consistency problems, as in practice the use of cubic EOS is nearly universal for hydrocarbon process modelling [25]. Although it is

important to mention that commonly used cubic equations of state fail to predict reliable values of volumetric properties, therefore its effect is unknown on the performance of the blowdown simulation. Nevertheless, the BLOWDOWN model remains as a very comprehensive mathematical method to simulate the depressurisation of process vessels.

In 1994 Overa *et al.* [26] developed the SPLIT FLUID blowdown model that accounts for the non-equilibrium condition between the vapour and liquid phases. Unlike the BLODOWN model, the SPLIT FLUID model divides the vessel during the blowdown process into two zones, vapour and liquid, consequently no free water is considered. The vapour phase, comprising the original vapour and the evaporated portion from the boiling liquid; and the liquid phase, comprising the original liquid and the condensed portion from the cooling vapour.

As the BLOWDOWN model, the SPLIT FLUID model is able to handle multicomponent systems, except for the presence of free water, and can predict system pressure and fluid phases temperatures and compositions, all as function of time. Overa *et al*. [26] applied different thermodynamic trajectories to liquid and vapour phases. In contrast to the BLOWDOWN model, the heat exchange between the vapour and liquid phases inside the tank is taken into account as part of the blowdown simulation. Moreover, the model can be used to simulate blowdown under a fire situation.

For the liquid zone, the model calculates the temperature from a pressure-enthalpy flash equation performed at vessel pressure. The enthalpy change of the liquid phase during a given time interval is assumed to be due to heat transfer effects only; hence, work done by the liquid owing the expansion is ignored. Nucleate and film boiling heat transfer is considered between the wetted wall surface and the liquid phase, with the boiling heat transfer coefficient determined experimentally [26].

The specific enthalpy equation for the liquid, within a time period from $t = t_0$ to $t = t_1$, is given by:

$$h_{\mathrm{L},t_1} = \frac{M_{\mathrm{L}}}{M_{\mathrm{L}}+M_{\mathrm{C}}}\left(h_{\mathrm{L},t_0} - \frac{(\dot{Q}_{\mathrm{L}}-\dot{Q}_{\mathrm{L-V}})t_s}{M_{\mathrm{L}}}\right) + \frac{M_{\mathrm{C}}}{M_{\mathrm{L}}+M_{\mathrm{C}}} h_{\mathrm{L-C},t_1} \qquad (2.11)$$

where h_L is the specific enthalpy of the liquid, M_L are the number of moles in the liquid phase, M_C are the number of moles of condensed vapour, $\dot{Q}_L$ is the heat transfer rate between liquid and vessel, $\dot{Q}_{L-V}$ is the heat transfer rate between the liquid and vapour phases, $h_{L\text{-}C}$ is the specific enthalpy of the condensed vapour, and t_s is the finite time interval. The equation is solved by the finite time difference method.

The flash calculation gives the new equilibrium liquid and vapour quantities at the calculated temperature. Liquid properties are determined at the calculated temperature. The liquid level is updated to reflect changes in equilibrium and specific volume [26].

For the vapour zone, the vapour temperature, T_V, and vessel pressure, P, are determined from a second law of thermodynamics analysis, by performing a volume-entropy flash. The vapour volume is fixed, as both the vessel and liquid volumes are known. The model considers natural or forced convection depending on the conditions between vessel wall and vapour by employing standard correlations.

The specific entropy equation for the vapour, within a time period from $t = t_0$ to $t = t_1$, is given by:

$$s_{V,t_1} = \frac{M_V}{M_V + M_B}\left(s_{V,t_0} - \frac{\frac{(\dot{Q}_V + \dot{Q}_{L-V})t_s}{T_V}}{M_V}\right) + \frac{M_B}{M_V + M_B} s_{B,t_1} \qquad (2.12)$$

where s_V is the specific entropy of the vapour, M_B are the number of moles of vaporized liquid, s_B is the specific enthalpy of the vaporized liquid.

The liquid condensed from the equilibrium calculation, M_C, is added to the liquid within the vessel. Vapour composition is updated taking into account the vapour generated, M_B.

With regard to the heat transfer between the vessel wall and the surroundings, Haque *et al*. [30] considered to be either by natural or forced convection depending on the nature of the surroundings. In both cases standard correlations are used to determine the heat transfer coefficient.

As discussed earlier, Overa *et al*. [26] also takes into account the heat exchange between vapour and liquid, as both phases are at different temperature, and assume natural

convection as the heat transfer mechanism between the two. In this respect Overa *et al*. [26] use a standard correlation to determine the appropriate convection heat transfer coefficient at the interface. The assumption is adopted for both cases, warm liquid and cold vapour, and vice versa.

The vapour-liquid interface heat transfer rate $\dot{Q}_{\mathrm{L-V}}$ is given by:

$$\dot{Q}_{\mathrm{L-V}} = hA(T_{\mathrm{L}} - T_{\mathrm{V}}) \tag{2.13}$$

where A is the interfacial area between liquid and vapour phases; h is the convection heat transfer coefficient; T_{L} is the temperature of the liquid phase; and T_{V} is the temperature of the vapour phase. The thermophysical properties are predicted by using an in-house process simulator.

The SPLIT FLUID model was validated against experimental data from a depressurising small vessel containing a hydrocarbon gas and unstabilised oil. The model was tested up to a maximum pressure of 2,100 kPa.

Figure 2.22 shows the comparison between the experimental and SPLIT FLUID model predicted values for phase temperatures [26].

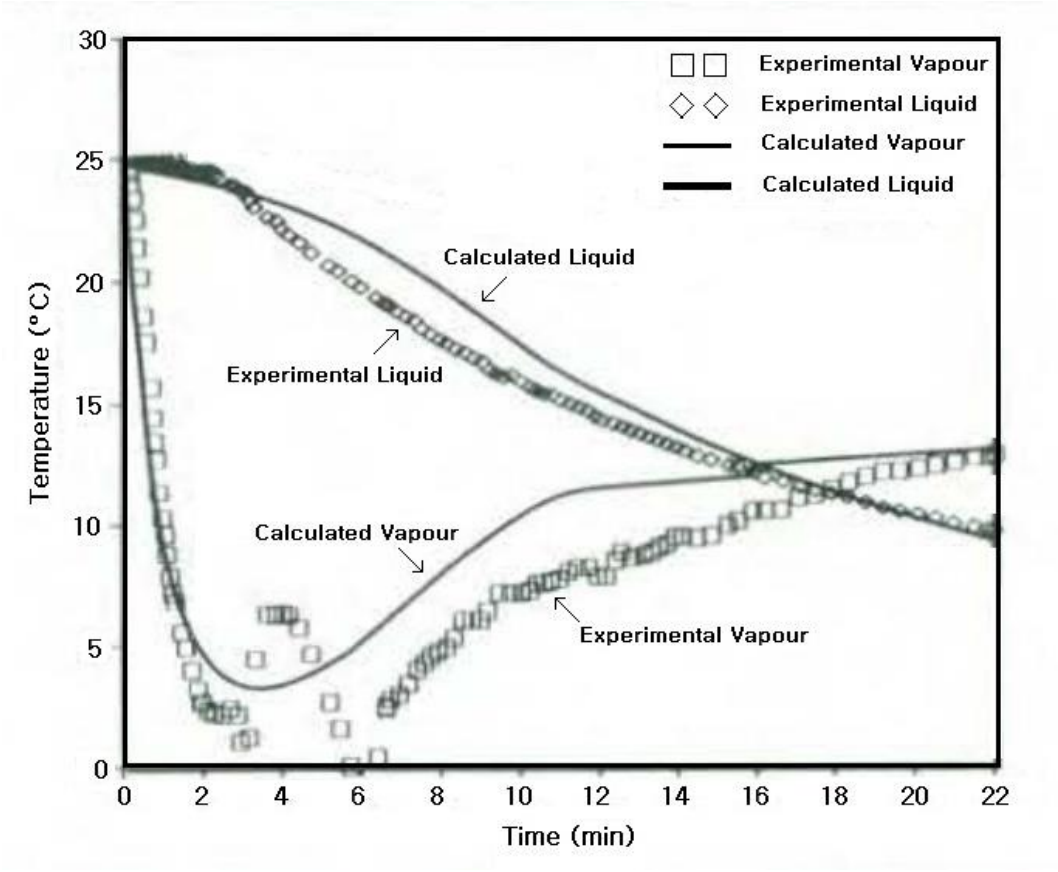

Figure 2.22 Bulk temperature of fluid phases vs. time SPLIT FLUID model [26].
(□ Experimental vapour; ◊ Experimental liquid;
— Calculated vapour; ▬ Calculated liquid)

The SPLIT FLUID model demonstrated fair agreement with experimental values being capable of predicting the fluid phases temperatures within 4 ºC, which is an acceptable accuracy for engineering purposes [26].

Although the SPLIT FLUID is a simple blowdown model for multicomponent systems it has not been tested at high pressures, above 2,100 kPa. The need to experimentally determine the heat transfer coefficient between the wetted wall and the liquid phase limits the predictive capability of the model. The effects of this assumption on the predictions of temperature and pressure during blowdown, especially at high pressures, are unknown [26].

In 1999 Mahgerefteh and Wong [24] developed an ambient conditions surroundings blowdown model named BLOWSIM, capable to simulate two-phase (vapour and liquid)

hydrocarbon mixtures, accounting for the non-equilibrium effects between phases. The model is limited to ambient conditions surroundings, so the blowdown under a fire situation is not considered. Mahgerefteh *et al*. [33] later extended (2002) the BLOWSIM model including the option to simulate the blowdown process under fire attack situations.

The BLOWSIM model output includes the variations with time of the system pressure, fluid phases temperatures and compositions. Similar to BLOWDOWN, the algorithm in the BLOWSIM model is solved by discrete pressure steps. Heat exchange between the vapour and liquid phases is not taken into account within the BLOWSIM model scope.

The BLOWSIM model divides the fluid in the vessel during blowdown into two zones. Zone 1 comprising the sub-cooled vapour and condensed vapour, whereas zone 2 represents the liquid or condensed vapour from zone 1.

Figure 2.23 shows a schematic diagram of the pressured vessel with the BLOWSIM modelling approach.

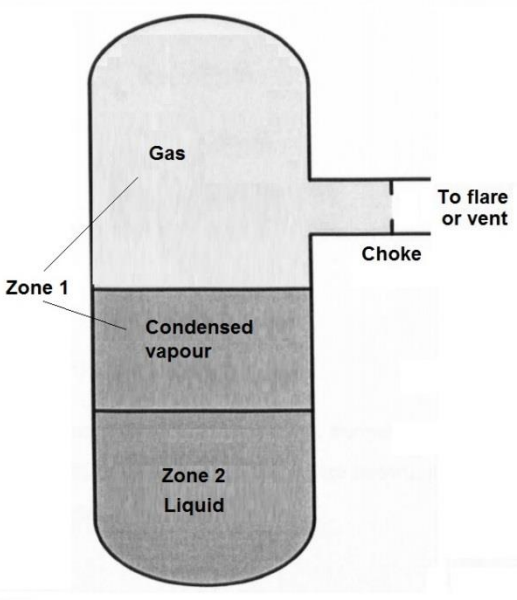

Figure 2.23 Vessel diagram showing BLOWSIM modelling approach [24].

Mahgerefteh and Wong [24] propose a different thermodynamic trajectory for each vessel zone to describe the blowdown process and therefore to determine the final vapour and liquid temperatures. Similar to the BLOWDOWN model, the effect of non-isentropic

expansion of each fluid phase inside the vessel during blowdown is accounted for by assuming polytropic expansion in which both heat and work are transferred [24].

For zone 1 Mahgerefteh and Wong [24] assume a reversible expansion of the fluid. In this respect, they apply the second law of thermodynamics which relates entropy to heat. Thereafter the first law of thermodynamics is solved for the work done by the fluid to get the liquid temperature.

Based on the second law of thermodynamics, assuming that the amount of heat transferred to each fluid phase during a given small time interval is infinitesimal, so that the fluid temperature remains unchanged. The specific entropy in zone 1 for a vessel containing a two-phase mixture is given by the following expression,

$$s_2 = \frac{T_2\left[s_{\mathrm{V},1}M_{\mathrm{V},1}+s_{\mathrm{B},2}M_{\mathrm{B},2}\right]+Q_2}{T_2\left(M_{\mathrm{V},1}+M_{\mathrm{B},2}\right)} \tag{2.14}$$

Whilst for a vessel containing vapour only it reads,

$$s_2 = s_1 + \frac{Q_2}{T_2 M_{\mathrm{F},1}} \tag{2.15}$$

where Q is the total heat transfer to zone 1. Subscripts 1 and 2 are respectively the initial and final states of the system.

The specific entropy in zone 2 for a two-phase mixture is given by the following expression [24]:

$$s_2 = \frac{T_2\left[s_{\mathrm{L},1}M_{\mathrm{L},1}+s_{\mathrm{C},1}M_{\mathrm{C},1}\right]+Q_2}{T_2\left(M_{\mathrm{L},1}+M_{\mathrm{C},1}\right)} \tag{2.16}$$

where subscripts 1 and 2 are respectively the initial and final states of the system.

Mahgerefteh and Wong [24] assume that during the blowdown process natural convection dominates forced convection in zone 1, induced by the discharging material in the vapour space, and selected the Churchill and Chu's correlation [34] to determine the heat transfer coefficient between the vessel wall and the vapour. For zone 2, Mahgerefteh and

Wong [24] assume that heat transfer is by nucleate boiling, since the differences in wall and liquid temperature are expected to be small due to the very high heat transfer rates.

For the thermodynamic and phase properties predictions BLOWSIM have the option to use three cubic EOS, which include Soave-Redlich-Kwong (SRK), Peng-Robinson (PR) and Twu-Coon-Cunningham (TCC). The latter has been specifically used to address the drawbacks of SRK and PR EOS in predicting liquid densities and vapour pressures at low temperatures as well as those for hydrocarbons with acentric factors above 0.5.

The BLOWSIM model has been validated against published experimental data and the predicted values of the BLOWDOWN model [24]. The validation results demonstrated that there is good agreement between experimental and predicted values for bulk liquid and vapour temperatures.

Figure 2.24 and 2.25 respectively show the vapour and liquid bulk temperature predictions [24].

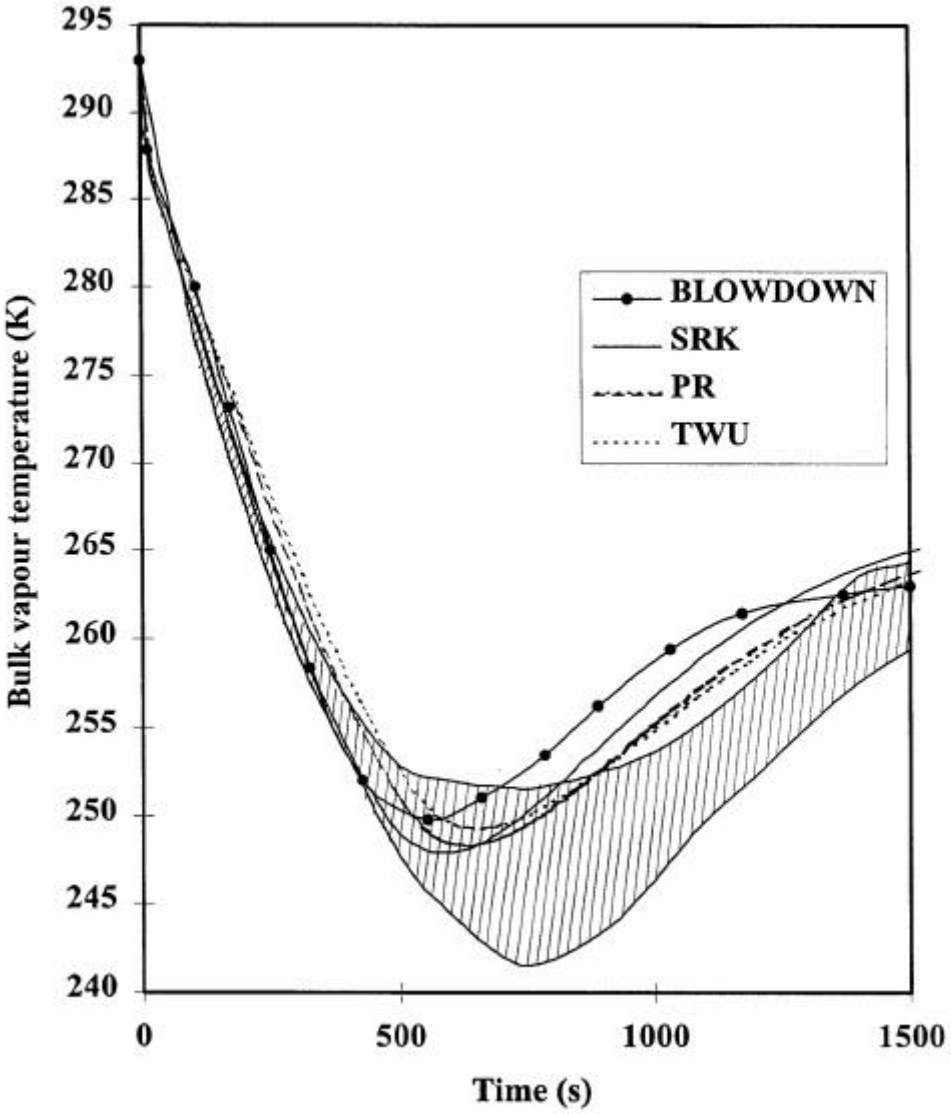

Figure 2.24 Bulk vapour temperature vs. time BLOWSIM model [24].
(Shaded region spans bulk vapour temperature experimental measurements)
(-●- BLOWDOWN; — SRK; ---- PR; ····· TWU)

From Figure 2.24 one can observe that in all three EOS cases the BLOWSIM model produces relatively accurate predictions of field data throughout the blowdown process. Assuming a minimum measured average bulk vapour temperature of 247 K, BLOWSIM predicts that temperature to 2 K approximately.

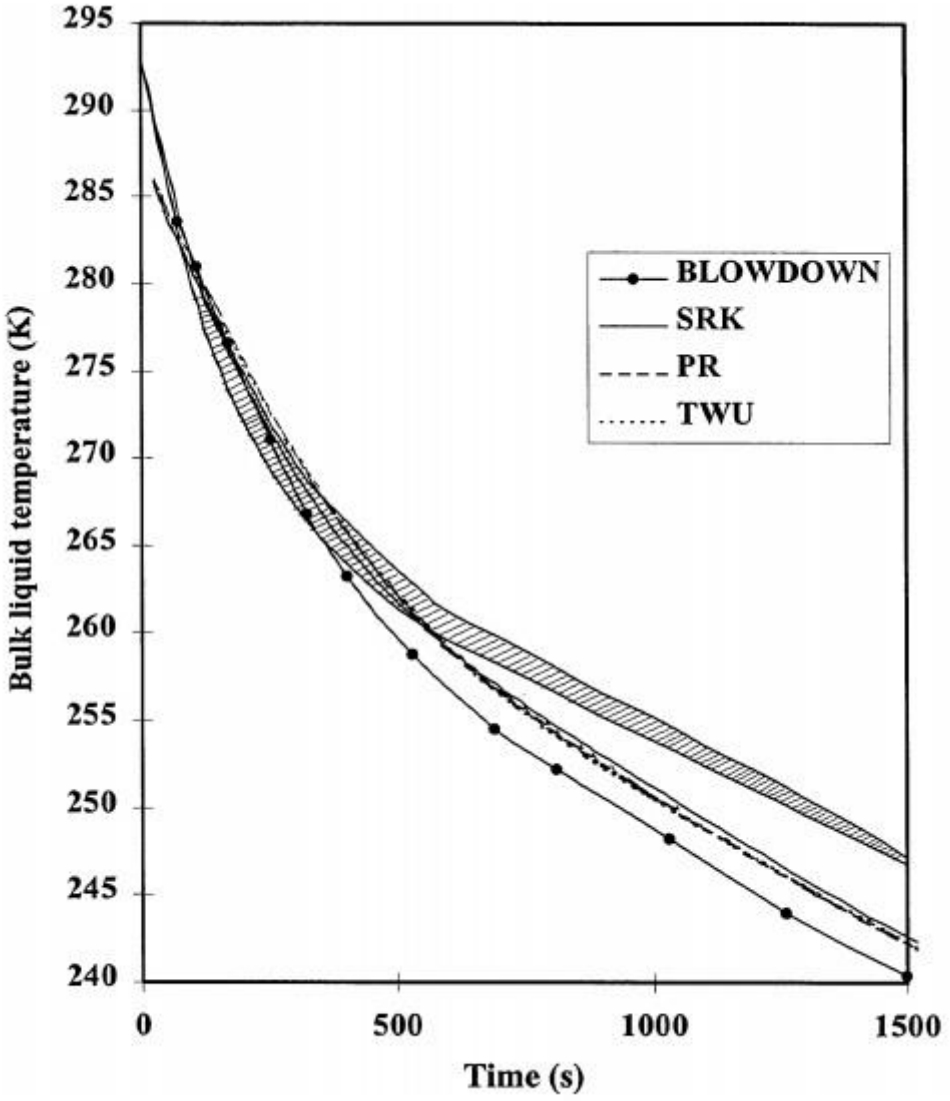

Figure 2.25 Bulk liquid temperature vs. time BLOWSIM model [24].
(Shaded region spans bulk vapour temperature experimental measurements)
(-●- BLOWDOWN; ― SRK; ---- PR; ····· TWU)

From Figure 2.25 one can observe that at the initial stage of depressurisation, up to 600 seconds, there is very good agreement between the experimental measurements and the predicted values by the BLOWSIM model for the three EOS. For the rest of the depressurisation period the agreement is within 5 K.

BLOWSIM is a very robust model for simulating blowdown of pressurised vessels containing multi-component hydrocarbon mixtures, including the ones under a fire attack.

The validation of BLOWSIM [24] based on three EOS lead to similar accuracies to those obtained by BLOWDOWN's predictions, showing that EOS are an efficient mean to estimate thermophysical properties and VLE data required by blowdown modelling of hydrocarbons, thus eliminating the potential consistency problem introduced by the use of the extended principle of corresponding states by the BLOWDOWN model. Nonetheless, as in the BLOWDOWN model, the computational run time associated to BLOWSIM model is still rather long [25].

The rigorous approach taken by Haque *et al.* [30], Overa *et al.* [26] and Mahgerefteh and Wong [24] in blowdown simulation where the vapour and liquid phases follow different thermodynamic trajectories confirms to be a better modelling solution of the phenomenon, compared to treating the fluid inside the vessel as homogeneous and in thermodynamic equilibrium. Moreover, dividing the vessel system in zones along with the phases present within shows to be a convenient heat transfer distribution scheme to separate the heat influx influence into the vapour and liquid spaces of the vessel, and a suitably calculation method to predict the individual temperature evolution of the vapour and liquid phases during the depressurization process. Due to its similar grounds, that approach can be extended to the modelling of stored LNG weathering.

2.7.3 LNG VAPORIZATION ON WATER FOLLOWING AN LNG SPILL

The LNG industry is aware that the projected increase in LNG trading and the amount of LNG transported will inevitably increase the risk of accidental spillage. Hence, there is a renewed pressure to improve the quantification of risk associated with LNG transport and loading operations. Although the track record of LNG industry is very good, the regulators remain unconvinced, demanding that safety precautions can be put in place to reduce the risk of accidental LNG spills, especially since on average the new LNG ships carry loads above 100,000 tons. In that respect, significant work has been carried out in LNG vaporization following an LNG spill in water. Of particular relevance are the studies developed by Valencia-Chavez [35], Boe [36], and Conrado and Vesovic [23].

Valencia-Chavez [35] in 1979 conducted a series of experimental tests to study the influence of the chemical composition on the boiling rates of LNG spilled on water. The

experimental set-up initially examined the boiling phenomena of pure cryogenic liquids such as methane, ethane, propane and nitrogen, and thereafter investigated with commercial LNG mixtures. Valencia-Chavez [35] reported that the vaporization rate of LNG was considerably different to that of pure components. It was concluded that the addition of ethane and propane to methane, significantly changes the boiling process on water by increasing the vaporization rate in the early stages of the boiling.

Boe [36] in 1998 carried out experimental tests at laboratory scale using pure methane, as well as binary mixtures of liquefied methane-ethane and methane-propane, boiling on water. Although the experimental set-up was similar to that used by Valencia-Chavez [35], Boe's testing programme [36] covered a higher initial water temperature ranging 25 - 40 ºC, as compared to 11 - 24 ºC used by Valencia-Chavez [35]. Boe [36] found that the addition of ethane or propane introduces significant differences in the boiling behaviour, increasing the BOG rate of the cryogen in the early stage of the boiling compared to pure methane, thus confirming the results obtained by Valencia-Chavez [35] 20 years earlier.

An important reference is the study developed by Conrado and Vesovic [37] in 2000, concerning LNG vaporization on water following an LNG spill. Conrado and Vesovic [37] developed a model to examine the importance of the chemical composition on the vaporization rate of LNG spilled on water surfaces, by comparing the vaporization rates of LNG and pure methane. They found that the vaporisation rate of an LNG mixture is markedly different to that of pure methane, and the behaviour can be attributed primarily to the contributions of the direct and indirect component of the total differential isobaric latent heat during the boiling process. For LNG as the liquid mixture gets rich in heavier compounds (weathered), due to the more volatile compounds vaporizing preferentially, the total differential isobaric latent heat increases rapidly leading to a large decrease in the vaporisation of LNG, especially at the later stages of the spill, when compared to pure methane.

Figure 2.26 shows one of the results obtained by Conrado and Vesovic [37] illustrating the vaporization rate of methane and LNG following a spill in water.

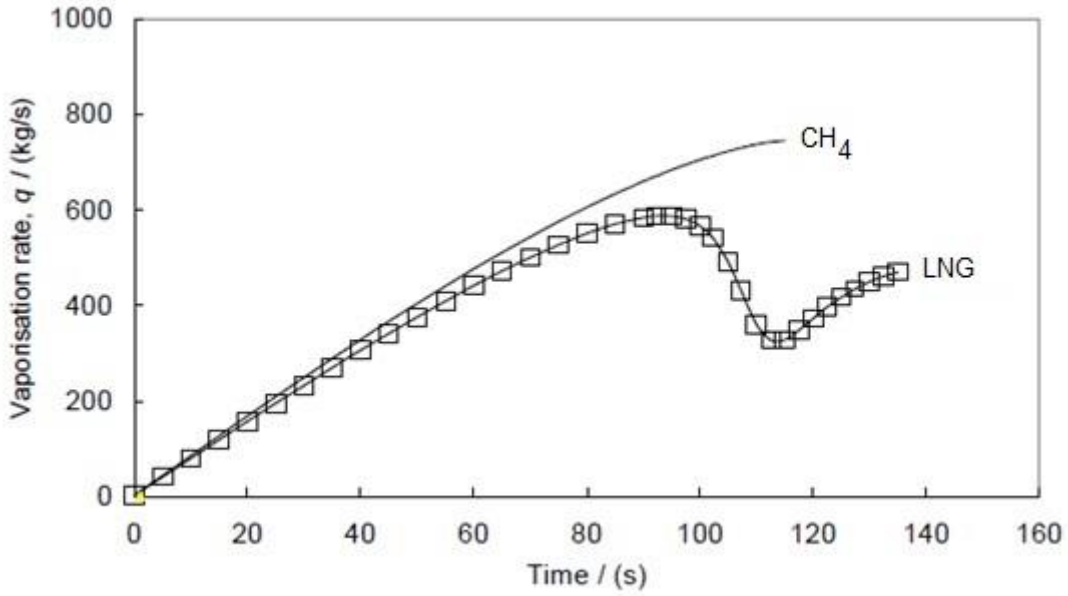

Figure 2.26 Methane and LNG vaporization rate vs. time [37].
(--- CH_4; -□- LNG)

Furthermore, the boiling process does not take place at a constant temperature, but follows the phase envelope. Thus, it is not possible to assume that the thermophysical properties of a cryogen are constant over the vaporization process, as is often considered for a pure liquid.

Conrado and Vesovic [37] concluded that it is essential both, from a scientific and industrial perspective, to ascertain the importance of a full thermophysical formulation of the problem to the rate of vaporisation of LNG on unconfined water surfaces. This is because treating an LNG spill as a pure methane spill, results in underestimation of the total spillage time of the order of 10-15%, will result in overestimation of the vaporisation rates in the latter stages of the spill and qualitatively wrong dynamics [37].

2.7.4 INFLUENCE OF LNG WEATHERING IN RAPID PHASE TRANSITION (RPT)

Experimental work has demonstrated that LNG weathering plays a role in the event of an LNG spill in water, and specifically the resulting Rapid Phase Transition (RPT).

The mixing of LNG with water following an LNG accidental spillage can also lead to RPT of LNG. The RPT occurs when a drop of cold liquid in contact with the hot liquid is heated

to its superheat limit, at which point the cold liquid undergoes homogeneous nucleation and vaporizes nearly almost instantaneously [38]. Two types of RPT situations are identified during an LNG spill: (*i*) early-stage RPT, as a result of the initial impact and mixing of LNG and water. This leads to the generation of a shock wave both in air and water; (*ii*) delayed RPT as a result of LNG weathering. Both types of RPT can also result in the ejection of high velocity water jets and the presence of LNG aerosol in the air [38].

The LNG industry classifies RPT as a hazard, as it can lead to structural damage to LNG ships, as well as to LNG operations offshore, such as Floating LNG installations. In this respect, significant experimental and modelling work has been carried out in recent years to better quantify the risk associated to a RPT event. As RPT involves vaporization of LNG and somehow LNG weathering, selected work on the RPT theme has also been reviewed due to its relevance to the subject of this PhD research.

An interesting study from Enger and Hartman [39] back in 1972 concluded that only mixtures with less than 40% of methane can undergo RPT. Hence, according to that, no commercial LNG as used by the industry today would initially undergo RPT. However, once LNG spills, preferential vaporization of methane will take place. As LNG weathers in the later stages of the spill it can reach the compositions where RPT will be possible. Experiments on small spills confirmed this possibility and RPT events have been observed for ethane-rich LNG mixtures [38].

Again in 1972, Burgess *et al*. [40] carried out a test where LNG was discharged continuously onto water, in a different experimental setting. The RPT event was a moderate explosion which happened five minutes after the spillage started indicating that most likely the RPT occurred due to the weathering of LNG and the decrease in methane content. Following that test, further experimental tests were carried out but the only reliable results were obtained for propane spills on water [41].

Delayed RPTs were also observed in one of the ESSO tests by Feldbauer *et al*. [42] also reported in 1972. The first one started 17 seconds after the spill and was followed by a few smaller ones in the next 15 seconds.

Experimental work performed by Reid [43] in 1983 showed that weathered LNG did produce RPT, but the experimental results were neither reproducible nor very reliable.

More recently, in 2007, Koopman and Ermak [44], reported that in the COYOTE-5 test[7] a large RPT occurred after 101 seconds. The RPT event resulted in increasing ethane concentration in the cloud from 20% to about 35% by volume, and increasing the lower flammability limit (LFL) by 30%. The cloud ignited approximately 30 seconds later showing the occurrence of RPT late in the spill due to the LNG weathering, and suggested that, in the right circumstances, RPT can pose an additional hazard [38].

2.8 CHAPTER SUMMARY

On the basis of the literature reviewed in this chapter the following conclusions can be extracted:

- The literature review of the different LNG weathering models developed so far shows that LNG weathering prediction is usually based on the assumption of constant BOG generation rate. Since the amount of BOG produced depends on the LNG stocked in a given container, that assumption might be acceptable for short term weathering. However, the assumption is not valid for the estimation of long term LNG weathering in storage tanks, as BOR changes as LNG evaporates from the tank.
- The impact of the aforementioned simplification on the accuracy of BOR estimate is not well understood. Rigorous prediction of LNG weathering could make a significant contribution in operating LNG regasification terminals, as enables to optimize normal operation, as well as to capture upside opportunities in LNG storage management. Having a rigorous weathering model also provides a useful tool that can be used to check, and if required improve, the accuracy of current estimation methods used by industry.

[7] COYOTE were a series of experimental tests programme on LNG spill dispersion, vapour burn, and rapid-phase-transition, run by the Lawrence Livermore National Laboratory (LLNL) and the Naval Weapons Center (NWC) in the US.

- Accurate prediction of LNG weathering is key for the thermodynamic assessment of weathered LNG, which allows optimizing normal operation of LNG facilities and ensures the gas specification suitability to the destination market.
- The rigorous approach taken by Haque *et al*. [30], Overa *et al*. [26] and Mahgerefteh and Wong [24] in blowdown simulation where vapour and liquid phases do not follow thermodynamic equilibrium confirms to be a better modelling solution compared to conventional engineering practice, allowing the specification of minimum design temperatures to be higher for a gas filled vessel and lower for liquid and two phase vessels.
- Due to its similarities, the previous conclusion can be extended to stored LNG weathering simulation. The accurate modelling of LNG weathering demands then the appropriate definition of the thermodynamic trajectory followed by the LNG mixture throughout the weathering process.
- Dividing the containing vessel in zones consistent with the phases present within shows to be a convenient heat transfer distribution scheme to separate the heat influx influence into the vapour and liquid spaces of the vessel, and a suitably calculation method to predict the individual temperature evolution of the vapour and liquid phases during the depressurization process. This approach is to be also extended to simulate the weathering of stored LNG.
- LNG weathering plays a part following an LNG spill in water. Experimental work has demonstrated the occurrence of RPT late in the spill due to LNG weathering,

In this PhD research project a more accurate approach to predict LNG weathering is developed, aiming to predict the vaporization rate and the compositional variation of the LNG stored in a full containment above-ground tank, due to the effects of heat ingress and BOG release. The model integrates the combined effect of the thermodynamic and transport phenomena occurring inside the tank, such as vapour-liquid equilibrium and heat transfer. The model builds on the previously published work, but removes a number of constraints that exist in the reported models [14,16-20,22-23], namely: (*i*) heat ingress is calculated based on the outside temperature and LNG composition, that allows for daily or

seasonal variations; (*ii*) BOR is not an input parameter, but is calculated as part of the simulations, and (*iii*) the LNG density is estimated using an accurate experimentally based correlation, thus replacing the need for the estimate based on EOS that for two parameter cubic EOS requires an empirical correction.

The following chapter reviews the thermodynamic and heat transfer equations used to describe the LNG behaviour under storage conditions to predict weathering.

2.9 REFERENCES

[1] Migliore, C. (2003) *Design and Economic Analysis of the Hydrate Technologies for Transportation and Storage of Natural Gas*. MSc Dissertation. University of Salford.

[2] Process Evaluation/Research Planning (PERP) program report (2004). *Advances in LNG Technology*. NEXANT ChemSystems, New York.

[3] Peebles, M. (1992) *Natural Gas Fundamentals*. Shell International Gas Limited, London, United Kingdom

[4] Manning, F. S., Thompson, R. E. (1991) *Oilfield Processing of Petroleum, Volume 1: Natural Gas*. PennWell Publishing Company. Tulsa, USA.

[5] Ibrahim, I., Harrigan, F. (2012) Qatar's economy: Past, present and future. *QScience Connect, Qatar Foundation Academic Journal*, 2012, 9.

[6] Migliore, C. (2013) Natural Gas Conditioning and Processing. In: Riazi, M. R., Eser, S., Agrawal, S. S., Peña Díez, J. L. (eds.) *Petroleum Refining and Natural Gas Processing*. ASTM International, USA, pp. 249-286.

[7] Nasr G. G., Connor N. E. (2014) *Natural Gas Engineering and Safety Challenges*, Springer, UK.

[8] Arjomandnia P., Tade M. O., Pareek V., May E. F. (2013) Analysis of available data from liquefied natural gas rollover incidents to determine critical stability ratios. *AIChE Journal*, 60 (1), 362–374.

[9] Sedlaczek, R. (2008) *Boil-Off in large and small-scale LNG chains*. Diploma Thesis. Norwegian University of Science and Technology (NTNU), Trondheim

[10] Morise, T., Shirakawa, Y., Meguro, T. (2007). Applying optimum commissioning technology of LNG receiving terminals, *15th International Conference and Exhibition on Liquefied Natural Gas (LNG 15)*, International Gas Union (IGU), poster PO-48.

[11] Operations supervisor, LNG regasification facility. (Personal communication, 17th September 2015).

[12] Churchill, S. W. (1962) Heat leakage and wall temperature profiles for above-ground low-temperature storage tanks. *Chemical Engineering Progress Symposium Series*, 58 (11), 55-60

[13] Neill, D. T., Hashemi, H. T., Sliepcevich, C. M. (1968) Boil-off rates and wall temperatures in above ground LNG storage tanks. *Chemical Engineering Progress Symposium Series*, 64 (87), 111−119

[14] Shah, J. M., Aarts, J.J. (1974) Effect of weathering of LNG in storage tanks. *Advances in Cryogenics Engineering*, 19, 253-260.

[15] Colson, D., Haquin, N., Malochet, M. (2012) Reduction of boil-off generation in cargo tanks of liquid natural gas carriers - Recent developments of Gaztransport & Technigaz (GTT) cargo containment systems, *25th World Gas Conference, June 2012, Kuala Lumpur, Malaysia*. International Gas Union (IGU), paper Nº 452.00.

[16] Kountz K. J. (1999) *Weathering of LNG in on-board storage tanks*. Institute of Gas Technology (IGT), US, project report 32034-02.

[17] Aspelund A., Gjovag G. A., Neksa P., Kolsaker K. (2006) LNG-chain, a calculation tool for natural gas quality in small scale LNG distribution chains. *Proceedings of the 21st International Cryogenic Engineering Conference, 17-21 July 2006, Prague, Czech Republic*. CR06-133.

[18] Dimopoulos, G. G., Frangopoulos C. A. (2008) A dynamic model for liquefied natural gas evaporation during marine transportation. *International Journal of Thermodynamics*, 11 (3), 123−131.

[19] Hasan, M. M. F., Zheng, A. M., Karimi, I. A. (2009) Minimizing boil-off losses in liquefied natural gas transportation. *Industrial Engineering and Chemistry Research*, 48, 9571–9580

[20] Miana, M., Del Hoyo, R., Rodrigálvarez, V., Valdés, J. R., Llorens, R. (2010) Calculation models for prediction of liquefied natural gas (LNG) ageing during ship transportation. *Applied Energy*, 87 (5), 1687–1700.

[21] Seader, J. D., Henley, E. J. (2010) *Separation Process Principles*, *2nd edition*. USA, John Wiley & Sons Inc.

[22] Adom, E., Islam S. Z., Ji X. (2010) Modelling of boil-off gas in LNG tanks: A case study. *International Journal of Engineering and Technology*, 2 (4), 292-296.

[23] Pellegrini, L. A., Moioli, S., Brignoli, F., Bellini, C. (2014) LNG Technology: The weathering in above-ground storage tanks. *Industrial and Engineering Chemistry*, 53 (10), 3931–3937.

[24] Mahgerefteh, H., Wong, S. M. A. (1999). A numerical blowdown simulation incorporating cubic equations of state. *Computers and Chemical Engineering*, 23 (9), 1309-1317

[25] Wong, S. M. A. (1998) *Development of a mathematical model for blowdown of vessels containing multi-component hydrocarbon mixtures*. PhD Thesis. University College London.

[26] Overa, S. J., Stange, E., Salater, P. (1993). Determination of temperatures and flare rates during depressurization and fire, *Proceedings of 72nd Gas Processors Association Annual Convention*, 15-16 March, San Antonio, TX, USA, pp. 235-247.

[27] American Petroleum Institute. (2014). *Sizing, selection, and installation of pressure-relieving devices, 9th edition*. API Standard 520. Part I - Sizing and selection. API publishing services. Washington, D.C. USA.

[28] American Petroleum Institute. (2015). *Sizing, selection, and installation of pressure-relieving devices, 6th edition*. API Standard 520. Part II - Installation. Washington, D.C. USA.

[29] American Petroleum Institute. (2014). *Pressure-relieving and depressuring Systems, 6th edition*. API Standard 521. Washington, D.C. USA.

[30] Haque, M. A., Richardson, S. M., Saville, G. (1992). Blowdown of pressure vessels. I. Computer model. *Process Safety and Environmental Protection*, 70, 3-9.

[31] Rowlinson, J. S., Watson, I. D. (1969). The prediction of the thermodynamic properties of fluids and fluid mixtures – I. The principle of corresponding states and its extensions. *Chemical Engineering Science*, 24 (10), 1565–1574.

[32] Haque, M. A., Richardson, S. M., Saville, G., Chamberlain, G., Shirvill, L. (1992). Blowdown of pressure vessels. II. Experimental validation of computer model and case studies. *Process Safety and Environmental Protection*, 70, 10-17.

[33] Mahgerefteh, H., Gboyega B., Falope, O., Oke, Adeyemi O. (2002). Modeling blowdown of cylindrical vessels under fire attack. *AIChE Journal*, 48 (2), 401-41.

[34] Incropera, F. P., De Witt, D. P. (1996) *Fundamentals of heat and mass transfer, 4th edition*. USA, John Wiley & Sons Inc.

[35] Valencia-Chavez, J., Reid, R. (1979) The effect of composition on the boiling rates of liquefied natural gas for confined spills on water. *International Journal of Heat and Mass Transfer*, 22, 831–838.

[36] Boe, R. (1998). Pool boiling of hydrocarbon mixtures on water. *International Journal of Heat and Mass Transfer*, 41, 1003-1011

[37] Conrado, C., Vesovic, V. (2000) The influence of chemical composition on vaporisation of LNG and LPG on unconfined water surfaces. *Chemical Engineering Science*, 55, 4549−4562

[38] Vesovic, V. (2012) *Rapid Phase Transition and its relevance to Floating LNG Facilities*. Imperial College London, Technical Report.

[39] Enger, T., Hartman, D. E. (1972) Rapid Phase Transformations during LNG Spillage on Water, *3rd International Conference on LNG, LNG 3,Washington, D.C.*

[40] Burgess, D. S., Biordi, J., Murphy, J. (1972) *Hazards of Spillage of LNG into Water*. U.S. Bureau of Mines, PMSRC Report No. 4177.

[41] Zubairu, A. (2011) *Modelling LNG spill on water – The heat transfer aspects*. PhD Thesis. Imperial College of London.

[42] Feldbauer, G. F., Heigel, J. J., McQueen, W., Whipp, R. H., May, W. G. (1972), *Spills of LNG on Water*. Esso Research and Engineering Co., Report Nº EE61E-72.

[43] Reid, R. C., (1983) Rapid Phase Transitions from liquid to vapour. *Advances in Chemical Engineering*, 12, 105-208.

[44] Koopman, R. P., Ermak, D. L. (2007). Lessons learned from LNG safety research. *Journal of Hazardous Materials*, 140 (3), 412-428.

3 THEORETICAL BACKGROUND

In this chapter certain thermodynamic and heat transfer relations that are fundamental to predict stored LNG behaviour are discussed and reviewed. These form the foundation for all the methods and calculations used for the development and testing of the LNG weathering model in the remaining chapters of this thesis.

3.1 PHASE EQUILIBRIA

As the LNG tank is a closed system, predicting the VLE of stored LNG demands assessing the coexistence of both vapour and liquid phases inside the storage system.

For closed systems, as stated in the first law of thermodynamics, the change of system internal energy *U* is due to the transfer of heat *Q* and work *W* across its boundaries when considering no changes in the kinetic and potential energy [1]:

$$\Delta U = Q - W \tag{3.1}$$

If the system undergoes an ideal but unreal reversible process, the combined first and second laws of thermodynamics states [1]:

$$dU = TdS - PdV \tag{3.2}$$

where *S* is the system entropy and *V* the volume.

If the process is irreversible the above equation (3.2) is rewritten as follows:

$$dU < TdS - PdV \tag{3.3}$$

Considering all real processes are irreversible eq. (3.3) states that for a process at constant *S* and *V*, *U* tends to decrease as the equilibrium state is approached.

The Gibbs free energy, *G*, is another important property to describe VLE and is defined as follows [1]:

$$G = H - TS \tag{3.4}$$

where *H* is the system enthalpy and is defined as follows [1]:

$$H = U + PV \tag{3.5}$$

Substituting eq. (3.5) in eq. (3.4), and then in eq. (3.3), one obtains:

$$dG \leq -SdT + VdP \tag{3.6}$$

The above equation states that at constant *T* and *P*, the Gibbs free energy tends to decrease in real processes, and remains constant in a reversible process. With the equilibrium state being the ultimate condition of any real process, then the system Gibbs free energy turns out to be minimum [1]. That is:

$$(\partial G)_{T,P} = 0 \tag{3.7}$$

For a system containing an *n* number of constituent species (mixtures) such as the LNG, the fundamental equation of chemical thermodynamics in terms of Gibbs energy is written as follows [1]:

$$dG = -SdT + VdP + \sum_i^n \left(\frac{\partial G}{\partial n_i}\right)_{T,P,n_{j\neq i}} dn_i \qquad i=1,\ldots, n \tag{3.8}$$

The partial derivative of molar Gibbs energy is called the chemical potential μ_i, and is defined as follows:

$$\mu_i = \left(\frac{\partial G}{\partial n_i}\right)_{T,P,n_{j\neq i}} \tag{3.9}$$

The chemical potential reflects the change in free energy when the number of particles of one of the species changes, as each chemical species has its own chemical potential. As discussed before, at equilibrium the free energy is at its minimum for the system (eq. 3.7). It follows that the sum of chemical potentials is also zero therefore, at constant temperature and pressure conditions the general requirement of equilibrium, eq. (3.8), leads to the following equation:

$$(\partial G)_{T,P} = \sum_i^n \mu_i \, dn_i = 0 \tag{3.10}$$

The equality in eq. (3.10) becomes a convenient calculation tool if Gibbs free energy can be related to measurable properties. That can be achieved by expressing the Gibbs free

energy in terms of auxiliary thermodynamic functions, such as fugacity. The following section describes how VLE can be described by the fugacity property, *f*.

3.1.1 FUGACITY

Rewriting eq. (3.6) based in molar properties for a pure substance, one gets:

$$dg = -sdT + vdP \tag{3.11}$$

where *g*, *s* and *v*, are respectively the molar Gibbs free energy, molar entropy and molar volume.

At constant temperature eq. (3.11) reduces to:

$$\left(\frac{\partial g}{\partial P}\right)_T = v \tag{3.12}$$

this leads to a simple expression for an ideal gas, relating pressure to volume as follows [1]:

$$Pv = RT \tag{3.13}$$

that is:

$$\left(\frac{\partial g}{\partial P}\right)_T = \frac{RT}{P} \tag{3.14}$$

where *R* is the universal gas constant.

Ideal gas is a hypothetical concept, but it is a useful tool to explain the more complex real gas behaviour. Conceptually, an ideal gas is a gas in which the molecules occupy negligible volume; there are no interactions between them and collisions are purely elastic, implying no energy loss.

Integrating equation (3.14) at constant temperature, one gets [1]:

$$g - g^o = RT \ln \frac{P}{P^o} \tag{3.15}$$

Where the g^o and P^o are the respective values of Gibbs free energy and pressure, at the reference state.

Equation (3.15) is a simple relation to calculate the change of the Gibbs free energy of a pure ideal gas, when its pressure changes from the reference state pressure value P^o to pressure P, at constant temperature T.

Substituting pressure by fugacity, f, equation (3.15) can be used to describe the change of Gibbs free energy of a pure real gas. Eq. (3.15) is then rewritten as follows:

$$g - g^o = RT \ln \frac{f}{f^o} \tag{3.16}$$

Fugacity is a conceptual term used to relate the deviation of Gibbs free energy, and other basic thermodynamic properties, of a pure real gas from those of an ideal gas. It has pressure units, and is one way to correct for non-ideal behaviour. Consequently, for ideal gas the fugacity is equal to its pressure, and the fugacity of each component in a multicomponent system is equal to its partial pressure.

The ratio fugacity to pressure is called the fugacity coefficient ϕ. The fugacity coefficient in a multicomponent system is defined as follows [1]:

$$\phi_i = f_i/(P y_i) \tag{3.17}$$

where y_i is the mol fraction of component i in the gas mixture.

To relate fugacity to measurable quantities one can start with the following thermodynamic expression [1]:

$$\ln \phi_i = \frac{1}{RT} \int_V^\infty \left[\left(\frac{\partial P}{\partial M_i} \right)_{T,V} - \frac{RT}{V} \right] dV - \ln Z; \quad i=1,\ldots, n \tag{3.18}$$

where M_i is the number of moles of component i, V is the total volume, and Z is the compressibility factor of the gas mixture defined as follows:

$$Z = \frac{PV}{MRT} \tag{3.19}$$

where:

$$M = \sum M_i \tag{3.20}$$

Substituting eq. (3.20) and (3.19) into (3.18), and after some rearrangement, the fugacity coefficient for a component *i* in a multicomponent gas mixture is written as:

$$\ln \phi_i = (Z - 1) + \frac{1}{RT}\int_{\infty}^{V}\left[\frac{RT}{v} - P\right] dV - \ln Z \tag{3.21}$$

where v is the molar volume.

3.1.2 FLASH CALCULATION - RACHFORD-RICE EQUATION

Flash calculations are used for processes where vapour-liquid equilibrium, VLE, is involved.

Consider a flash separator where a feed stream M_F of a number of components is separated into a vapour M_V and liquid M_L products, as shown in Figure 3.1, where the composition of the feed stream is defined by z_i, whilst the composition of liquid and vapour streams are defined by x_i and y_i, respectively. M_F, M_V and M_L are the feed, vapour and liquid moles, respectively.

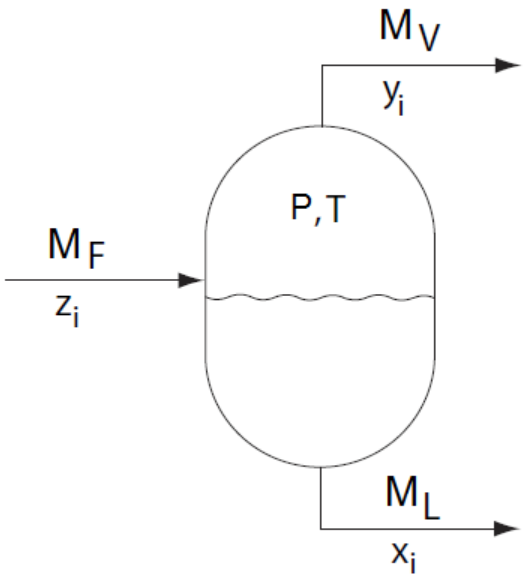

Figure 3.1 Flash separator diagram.

The material balance for each component is written as follows:

$$M_F z_i = M_L x_i + M_V y_i \quad (3.22)$$

The equilibrium constant K_i is defined as the ratio of mol fraction of component i in the vapour phase y_i, to that in the liquid phase x_i [2]:

$$K_i = \frac{y_i}{x_i} \quad (3.23)$$

Equation (3.23) can be rewritten as follows:

$$y_i = K_i x_i \quad (3.24)$$

The relations $\sum_i x_i = 1$ and $\sum_i y_i = 1$, for the liquid and vapour compositions respectively, are also valid for the flash separator.

Substituting eq. (3.24) into eq. (3.22) and solving for (x_i):

$$x_i = \frac{M_F z_i}{(M_L + M_V K_i)} \quad (3.25)$$

From the global material balance the liquid stream M_L is defined as follows:

$$M_L = M_F - M_V \quad (3.26)$$

Substituting eq. (3.26) into eq. (3.25) and rearranging, one gets:

$$x_i = \frac{z_i}{1 + \frac{M_V}{M_F}(K_i - 1)} \quad (3.27)$$

Eq. (3.27) cannot be used to directly calculate x_i, as the ratio M_V/M_F is unknown. One way to find the M_V/M_F is to use eq. (3.23), or, alternatively, eq. (3.24).

A better approach however, is by using the combination of equations (3.23) and (3.24), as follows:

$$\sum_i (y_i - x_i) = 0 \quad (3.28)$$

Substituting equations (3.22) and (3.27) in (3.28), and after some rearrangement, the resulting equation is the so-called Rachford-Rice flash equation [2], and is written as follows:

$$\sum_i \frac{z_i(K_i-1)}{1+\frac{M_V}{M_F}(K_i-1)} = 0 \tag{3.29}$$

The Rachford-Rice flash equation is a monotonic function in M_V/M_F, and is therefore an equation that can easily be solved numerically. The physical solution must satisfy:

$$0 \leq \frac{M_V}{M_F} \leq 1 \tag{3.30}$$

Solving phase equilibrium is an iterative process. When the ideal approach is assumed the equilibrium constant K_i depends on temperature only. Therefore, for given temperature the equilibrium constant K_i is known and the Rachford-Rice equation (3.29) can be solved iteratively for M_V/M_F.

For the non-ideal cases, K_i depends also on x_i and y_i, so the numerical approach to solve the Rachford-Rice flash equation is to include an additional outer iteration loop for K_i.

The evaluation of the equilibrium constant considering the ideal and non-ideal approach is discussed in the following section.

3.1.3 EQUILIBRIUM CONSTANTS

An equivalent set of VLE condition is derived by the use of fugacity of the species, which is directly related to Gibbs free energy. The equilibrium state can be described by the equality of fugacities of each component between phases, as follows [1]:

$$f_i^L = f_i^V; \qquad i=1,\ldots, n \tag{3.31}$$

where f_i^L and f_i^V are the fugacities for liquid and vapour, respectively.

Equation (3.31) can be written as follows [1]:

$$f_i^{\mathrm{L}} = x_i \phi_i^{\mathrm{L}} P = \ y_i \phi_i^{\mathrm{V}} P = f_i^{\mathrm{V}} \tag{3.32}$$

where ϕ_i^{L} and ϕ_i^{V} are the fugacity coefficients for liquid and vapour respectively and P is the total pressure of the multicomponent system.

From equation (3.32) the equilibrium constant K_i can be written as the ratio of fugacity coefficients of both phases, namely:

$$K_i = \frac{y_i}{x_i} = \frac{\phi_i^{\mathrm{L}}}{\phi_i^{\mathrm{V}}} \tag{3.33}$$

A general approach to determine the equilibrium constants in a multicomponent system is by the component ratio of the fugacity coefficients.

Two approaches exist to describe VLE, and hence to calculate the equilibrium constant K_i, assuming ideal and non-ideal behaviour. When ideal behaviour of the phases is assumed, eq. (3.33) can be simplified using the Dalton and Raoult laws [3]. The resulting equation is:

$$x_i P v_i = \ y_i P \tag{3.34}$$

Hence K_i can be calculated as follows:

$$K_i = \frac{y_i}{x_i} = \frac{P v_i}{P} \tag{3.35}$$

where Pv_i is the vapour pressure of the pure component.

Within the non-ideal approach the component fugacity coefficients in equation (3.33) are calculated using an equation of state (EOS). EOS and the theoretical background behind it are discussed later in Section 3.1.5.

3.1.4 VAPOUR PRESSURE

Assuming vapour-liquid equilibrium of a pure component, from first law of thermodynamics the vapour pressure P_v is then governed by:

$$\frac{dP_v}{dT} = \frac{\Delta H_{vap}}{T(v_2 - v_1)} = \frac{PL}{T^2 R} \tag{3.36}$$

where L is the molar latent heat.

The equation (3.36) is known as the Clasius-Clapeyron equation [3]. Most vapour-pressure correlation equations develop from the integration of eq. (3.36).

Antoine [3] proposed a simple modification of eq. (3.36) that has been widely used to calculate the vapour pressure P_v of pure components, producing satisfactory results over a limited temperature range. The Antoine equation is written as follows [3]:

$$\log P_v = A - \frac{B}{T+C} \tag{3.37}$$

where A, B and C are the component specific constants of the Antoine equation. A, B and C, constants are tabulated for a number of compounds [4].

The Antoine equation is a suitable equation to describe vapour-pressure behaviour over small temperature ranges, but cannot be used to describe the full saturated vapour pressure curve from the triple point to the critical point. A more accurate approach is to use multiple parameter sets for single components. A low-pressure parameter set can be used to describe the vapour pressure curve up to the normal boiling point, and another set of parameters can be used for the range from the normal boiling point to the critical point.

3.1.5 EQUATION OF STATE

The equation of state (EOS) is the mathematical representation that links pressure P, volume V, and temperature T for any fluid and can be expressed as [1]:

$$f(P, V, T) = 0 \tag{3.38}$$

One of the simplest equations of state is the Ideal Gas Law, which is defined as follows [1]:

$$PV = MRT \tag{3.39}$$

where P and T are respectively the absolute pressure and temperature of the gas, M is the number of moles, V is the volume occupied by the gas, and R is the universal gas constant.

Although the Ideal Gas Equation is approximately accurate at low pressures and supercritical temperatures, it becomes increasingly inaccurate at higher pressures and lower temperatures, and fails to predict condensation from gas to liquid.

Real gases deviate from ideal behaviour as molecules occupy a finite volume, intermolecular forces are exerted between molecules and molecular collisions are never perfectly elastic. In that respect, in 1873 van der Waals (vdW) improved the ideal gas equation by introducing his semi-empirical equation, considering attractive and repulsive forces between molecules. The van der Waals equation is written as follows [1]:

$$\left(P + \frac{a}{v^2}\right)(v - b) = RT \tag{3.40}$$

where *a* and *b* are empirical constants, representing the attractive and repulsive parameters respectively. Terms *a* and *b* are substance specific constants calculated from critical properties, as follows:

$$a = \frac{27}{64}\left(\frac{R^2 T_c^2}{P_c}\right) \tag{3.41}$$

$$b = \frac{1}{8}\left(\frac{RT_c}{P_c}\right) \tag{3.42}$$

The van der Waals equation is one form of a cubic equation of state, as it is cubic when written in terms of molecular volume. Following eq. (3.40) in its cubic form [1]:

$$v^3 - \left(b + \frac{RT}{P}\right)v^2 + \left(\frac{a}{P}\right)v - \frac{ab}{P} = 0 \tag{3.43}$$

The van der Waals equation is not very accurate in modelling the behaviour of dense fluids; however, it has set the basis for many concepts used to correlate fluid properties.

In 1949, Redlich and Kwong [5] introduced their EOS by modifying the attractive term of the vdW equation (3.40) as follows:

$$\left(P + \frac{a}{T^{0.5} v(v+b)}\right)(v - b) = RT \tag{3.44}$$

Where the *a* and *b* parameters are calculated as follows:

$$a = 0.42748 \left(\frac{R^2 T_c^{2.5}}{P_c}\right) \tag{3.45}$$

$$b = 0.08664 \left(\frac{RT_c}{P_c}\right) \tag{3.46}$$

Equation (3.44), whilst being superior to the van der Waals EOS, it has a poor performance when it comes to model liquid phase, hence it cannot be used to accurately calculate vapour–liquid equilibria.

In 1972, Soave [6] replaced the $T^{0.5}$ term of the Redlich-Kwong equation (3.44) with a general function α involving the temperature and acentric factor as:

$$\alpha = [1 + m(1 - T_r^{0.5})]^2 \tag{3.47}$$

where m and T_r are defined as [6]:

$$m = 0.37464 + 1.54226\omega - 0.26992\omega^2 \tag{3.48}$$

$$T_r = \frac{T}{T_c} \tag{3.49}$$

where ω and T_c are the acentric factor and critical temperature, respectively.

The modified equation is known as the Soave-Redlich-Kwong (SRK) equation [6]:

$$\left(P + \frac{a\alpha}{v(v+b)}\right)(v - b) = RT \tag{3.50}$$

where parameter b is calculated by eq. (3.46) and a is defined as follows [6]:

$$a = 0.42748 \left(\frac{R^2 T_c^2}{P_c}\right) \tag{3.51}$$

The α function was formulated to fit the vapour pressure data of hydrocarbons, thus the equation performs fairly well for these substances.

In 1976, Peng-Robinson (PR) [7] introduced their EOS by modifying the attractive term to improve the liquid density calculation in comparison with SRK.

The Peng-Robinson EOS (PR-EOS) is defined as follows [7]:

$$\left(P + \frac{a\alpha}{v^2+2vb-b^2}\right)(v-b) = RT \tag{3.52}$$

where the effective parameters *a* and *b* are defined as follows [7]:

$$a = 0.45724\frac{R^2T_c^2}{P_c} \tag{3.53}$$

$$b = 0.07780\frac{RT_c}{P_c} \tag{3.54}$$

Peng-Robinson used a similar approach to the one proposed by Soave for α, eq. (3.47), but correlated *m* using vapour-pressure data from normal boiling point to the critical point. The parameter *m* is then defined as follows [7]:

$$m = 0.37464 + 1.54226\omega - 0.26992\omega^2 \tag{3.55}$$

The coefficients in eq. (3.55) were obtained by fitting PR-EOS to reproduce the vapour pressure of the first ten alkanes.

Written in its cubic version, using *Z*, the PR-EOS is expressed as follows [7]:

$$Z^3 - (1-B)Z^2 + (A - 3B^2 - 2B)Z - (AB - B^2 - B^3) = 0 \tag{3.56}$$

where:

$$A = 0.45724\frac{\alpha P_r}{T_r^2} = a\frac{\alpha P}{R^2T^2} \tag{3.57}$$

$$B = 0.07780\frac{P_r}{T_r} = b\frac{P}{RT} \tag{3.58}$$

Since its publication, the PR-EOS has become one of the reference methods of use within the oil and gas industry; there is plenty of evidence that it is a good EOS for phase equilibrium calculation of reservoir fluids.

Whilst solving the cubic version of the EOS, as eq. (3.56), is an algebraic equation of third order, three different roots for molar volume and compressibility factor are provided [7]. In that respect, if one considers a pure component at pressure P_1 and temperature lower than critical (within the two phase region), the cubic EOS yields three real roots for molar volume v or compressibility factor *Z*, as shown in Figure 3.2 [1]. The highest value, v_1 or

Z_1, corresponds to that of vapour phase, whereas the lowest value, v_3 or Z_3, corresponds to that of liquid phase. The value in between, within the two phase conditions, v_2 or Z_2, has no physical significance.

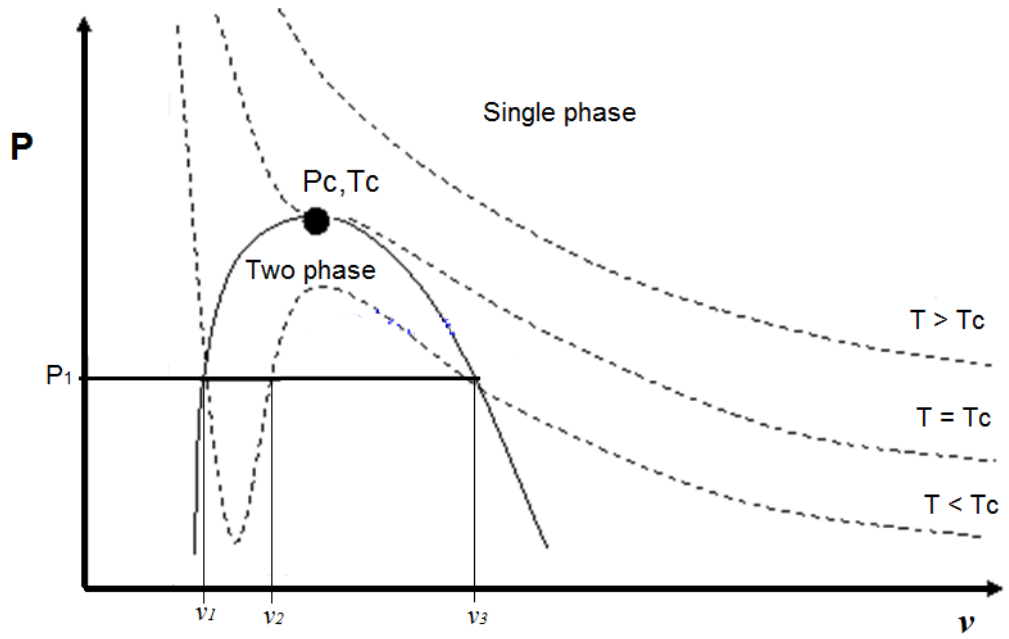

Figure 3.2 Multiple roots in cubic EOS [1].

Near the critical region, the cubic EOS such as defined in eq. (3.56) yields one single root for each phase. When at a selected temperature-pressure conditions cubic EOS gives one real root only, it is expected that the root is the correct solution for the phase under consideration. Since the vapour-liquid equilibrium calculation is an iterative process, and is the composition of one or both phases unknown upfront, the EOS parameters and the initial estimated composition for a phase may provide a wrong single root, due to the function characteristics as shown in Figure 3.3 [1].

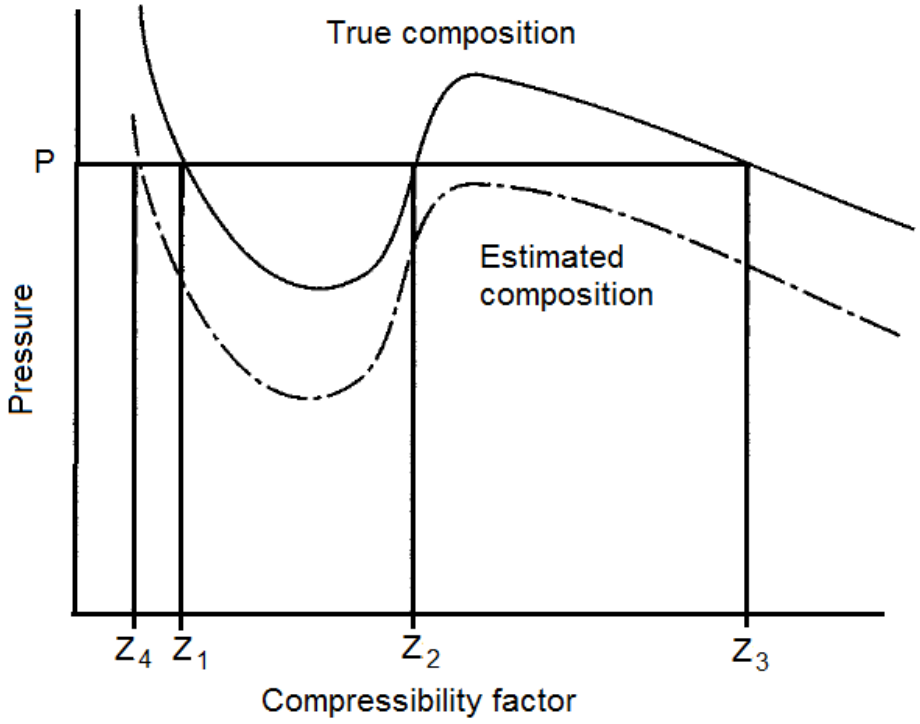

Figure 3.3 Improper root selection near the critical region [1].

Close to the critical region, both roots may well be liquid-like or vapour-like which may correct themselves during further iterations, thus interfering in the iterative process by adjusting roots and having an adverse effect on the convergence [1].

Recently, the European Gas Research Group (GERG) has developed a new equation of state for natural gas, and similar mixtures, named the GERG-2008 [8], which is an improved version of the original GERG-2004 EOS, presented in 2004.

The GERG-2008 EOS [8] is based on 21 natural gas components including methane, ethane, propane, n-butane, isobutane, n-pentane, isopentane, n-hexane, n-heptane, n-octane, n-nonane, n-decane, nitrogen, hydrogen, oxygen carbon dioxide, carbon monoxide, water, hydrogen sulphide, helium, and argon, covering the entire composition range, gas and liquid phase, supercritical region, and vapour–liquid equilibrium states for mixtures of those components.

The GERG-2008 EOS is explicit in the Helmholtz Free Energy *a*, as a function of density, temperature and composition, and is written as follows [8]:

$$a(\rho, T, x) = a^o(\rho, T, x) + a^r(\rho, T, x) \quad (3.59)$$

where a^o and a^r is the free energy representing the ideal gas and residual mixtures behaviour respectively. The normal range of validity of GERG-2008 includes temperatures from 90 K to 450 K and pressures up to 35 MPa.

The Helmholtz free energy is usually used in its dimensionless form, thus eq. (3.59) becomes:

$$\alpha(\delta, \tau, x) = \alpha^o(\delta, \tau, x) + \alpha^r(\delta, \tau, x) \quad (3.60)$$

where α is the Helmholtz Free Energy expressed as follows [8]:

$$\alpha = \frac{a}{RT} \quad (3.61)$$

δ is the reduced density and τ is the inverse reduced temperature. Both are defined as follows [8]:

$$\delta = \frac{\rho}{\rho_c} \quad (3.62)$$

$$\tau = \frac{T_c}{T} \quad (3.63)$$

The dimensionless free energy representing the ideal gas mixture is given by [8]:

$$\alpha^o(\delta, \tau, x) = \sum_i x_i[\alpha_i^o(\delta, \tau) + \ln x_i] \quad (3.64)$$

Where α_i^o is the dimensionless form of Helmholtz free energy of the pure component *i* and x_i is the mol fraction of component *i.*

The dimensionless free energy representing the residual part of eq. (3.60) is defined as [8]:

$$\alpha^r(\delta, \tau, x) = \sum_i x_i \alpha_i^r(\delta, \tau) + \Delta\alpha^r(\delta, \tau, x) \quad (3.65)$$

where α_i^r is the residual part of the reduced Helmholtz free energy of pure component *i*, and $\Delta\alpha^r$ is the departure function developed for various binary mixtures. The reducing functions and the departure function are developed based on experimental data, allowing

for a suitable predictive description of multi-component mixtures over a wide range of compositions, fluid regions, temperatures and pressures.

The tests run to the GERG-2008 EOS [8] since its introduction in 2012, have demonstrated a better performance compared to cubic EOS in the description of natural gas phase behaviour, showing lower deviations from experimental values. Higher deviations, though, are observed for nitrogen-containing mixtures. Furthermore, the presence of carbon dioxide has a pronounced effect on increasing saturated liquid density, whilst the presence of nitrogen has a more profound impact on bubble-point pressure [9].

Aimed at the development of the LNG weathering model under this research project, the PR-EOS has been selected as the equation of state of choice to describe phase equilibrium and predict most of the associated thermodynamic and physical properties. The PR-EOS is a reasonable choice due to its prediction power, and as it has long demonstrated to be a suitable method to describe hydrocarbon fluid behaviour mixtures over a wide range of temperatures and pressures. Although the GERG 2008 equation could also be a good option for the development of the LNG weathering model, as it has been developed specifically for natural gas, at the time the selection was made for this research project, the equation was not tested enough to be considered as a reliable candidate.

3.1.6 MIXING RULES

Equations of state are basically developed for pure components, but extended to multicomponent systems by employing mixing rules. The mixing rules are applied to describe the intermolecular forces between the components forming the mixture. The van der Waals mixing rules are the most extensively used modelling tool to describe vapour-liquid equilibrium of hydrocarbon mixtures.

According to the van der Waals mixing rules the extension of PR-EOS, eq. (3.52), to mixtures, requires the replacement of a and b parameters, by the composition dependent parameters a_m and b_m, calculated by the following expressions [1]:

$$a_m = \sum_i \sum_j x_i \, x_j a_{ij} \tag{3.66}$$

$$b_m = \sum_i x_i b_i \tag{3.67}$$

where a_{ij} is defined as [1]:

$$a_{ij} = \left(1 - k_{ij}\right)\sqrt{a_i\alpha_i \cdot a_j\alpha_j} \tag{3.68}$$

where a_i, a_j ($i \neq j$) and b_i for each of the species making the mixture are calculated from their critical temperature and pressure using equations (3.53) and (3.54) respectively [3]. The k_{ij} is the binary interaction coefficient [1].

Equation of state and mixing rules can be used to calculate phase enthalpies and fugacity coefficients.

With regards to phase enthalpy (molar basis), this can be related to PVT properties by means of residual enthalpy, as follows [10]:

$$\frac{h-h^{id}}{RT} = Z - 1 + \frac{1}{RT}\int_{\infty}^{v}\left[T\left(\frac{\partial P}{\partial T}\right)_v - P\right]dv \tag{3.69}$$

where h^{id} is the ideal gas enthalpy given by:

$$h^{id} = \sum_i x_i\, h_i^{id} \tag{3.70}$$

Substituting PR-EOS, eq. (3.52), into the right hand side of eq. (3.69) [11]:

$$\frac{h-h^{id}}{RT} = Z - 1 - \frac{1}{2\sqrt{2}bRT}\left(a - T\frac{da}{dT}\right)\ln\left(\frac{v+\left(1+\sqrt{2}\right)b}{v+\left(1-\sqrt{2}\right)b}\right) \tag{3.71}$$

The molar enthalpy for each phase can be calculated at a given temperature and density from the knowledge of PR-EOS parameters *a*, *b* and the value of compressibility factor *Z*.

The ideal gas enthalpies of each species to get h^{id} in eq. (3.70) can be calculated from a thermodynamic database such as REFPROP [4].

The fugacity coefficient for vapour and liquid can be also calculated by substituting PR-EOS, eq. (3.52), into the right hand side of eq. (3.21), and by means of vdW mixing rules:

$$\ln \phi_i^{\mathrm{V}} = -\ln(Z^{\mathrm{V}} - B) + \frac{b_i}{b_m}(Z^{\mathrm{V}} - 1) - \frac{a_m}{b_m RT 2\sqrt{2}}\left(\frac{2\sum_j a_{ij} y_j}{a_m} - \frac{b_i}{b_m}\right) - \ln \frac{Z^{\mathrm{V}} + B\left(1+\sqrt{2}\right)}{Z^{\mathrm{V}} + B\left(1-\sqrt{2}\right)} \quad (3.72)$$

$$\ln \phi_i^{\mathrm{L}} = -\ln(Z^{\mathrm{L}} - B) + \frac{b_i}{b_m}(Z^{\mathrm{L}} - 1) - \frac{a_m}{b_m RT 2\sqrt{2}}\left(\frac{2\sum_j a_{ij} x_j}{a_m} - \frac{b_i}{b_m}\right) - \ln \frac{Z^{\mathrm{L}} + B\left(1+\sqrt{2}\right)}{Z^{\mathrm{L}} + B\left(1-\sqrt{2}\right)} \quad (3.73)$$

where:

$$B = b_m \frac{P}{RT} \quad (3.74)$$

Compressibility factors can be calculated by solving the PR-EOS cubic equation (3.56). The equation is solved twice to get the compressibility factors for vapour Z^{V} and liquid Z^{L}:

- Once considering the vapour phase composition y_i for A and B calculation, then producing Z^{V}
- Once considering the liquid phase composition x_i for A and B calculation, then producing Z^{L}

Appendix I provides the details of the solution method of the PR-EOS cubic equation to calculate the compressibility factors Z^{V} and Z^{L}.

Equations (3.72) and (3.73) enable the calculation of the fugacity coefficients analytically. Furthermore, the same approach is used to calculate the vapour-liquid equilibrium constants K_i using equation (3.33).

3.2 THERMOPHYSICAL PROPERTIES CALCULATION

The principles of thermodynamics find very wide application in correlating and predicting the properties of hydrocarbons. In this regard, the properties of greatest interest when studying stored LNG behaviour are the liquid density, specific heat of gas and liquid, latent heat, and heating value.

The following sections describe how to correlate each of the above properties when analysing vapour-liquid equilibrium of stored LNG.

3.2.1 LIQUID DENSITY CALCULATION

The Peng-Robinson equation could also be used to estimate liquid density. Although it is well-known that any two parameter cubic EOS, which uses critical temperature and pressure to calculate parameters *a* and *b*, fails to describe volumetric behaviour. As *a* and *b* are fixed by using *Tc* and *Pc*, then the equation will invariably produce an incorrect value for the critical volume. Therefore, the phase envelope will follow the dew point line accurately, as PR-EOS was developed by using the vapour pressure, although it will underestimate the bubble point curve in terms of volume.

To correct for this deficiency, an empirical approach based on the volume shift concept [1] can be taken to calculate liquid density. The concept proposed is to shift the predicted molar volume by a constant term, adjusting by a corrected molar volume v', as follows:

$$v' = v - \sum_i c_i x_i \tag{3.75}$$

The volume translation parameter *c* for SRK is calculated by the Peneloux correlation [1], which is also applicable to any cubic EOS. The Peneloux correlation for the volume translation parameter is written as follows:

$$c = 0.40768(0.29441 - Z_R)\frac{RT_c}{P_c} \tag{3.76}$$

Where Z_R is the Rackett compressibility factor [3] that can be calculated as follows:

$$Z_R = 0.29056 - 0.08775\ \omega \tag{3.77}$$

Although the use of cubic EOS with the corrected volume is a standard practice to estimate the reservoir fluid density in the oil and gas industry, in this research project the revised Klosek-McKinley method [12] was selected as it was specifically developed for estimating the density of LNG. It is a reliable and accurate method that is frequently used for custody transfer purposes and is the recommended option by the Groupe International des Importateurs de Gaz Naturel Liquéfié – Paris, GIIGNL (International Group of Liquefied Natural Gas Importers). It is valid over the compositions and boiling temperatures of

interest to LNG industry and has a claimed uncertainty of ±0.1%, providing either the nitrogen or butane content does not exceed 4%.

The application of the revised Klosek-McKinley method only requires knowing the LNG temperature and composition.

Table 3.1 shows the limits of the revised Klosek-McKinley method on composition and temperature.

Table 3.1 Limits of the revised Klosek-McKinley method [12].

CH_4	>	60% mol
$iC_4 + nC_4$	<	4% mol
$iC_5 + nC_5$	<	2% mol
N_2	<	4% mol
T	<	115 K

The method is based on an empirical correlation of the molar volume of the mixture in the thermodynamic state of the LNG considered.

The molar density of LNG is calculated as follows:

$$\rho_L = \frac{1}{v} \tag{3.78}$$

where ρ_L is the molar density of LNG and v the molar volume of the mixture.

The molar volume *v* is calculated as follows [12]:

$$v = \sum v_i x_i - \left[k_1 + (k_2 - k_1)\left(\frac{x_{N_2}}{0.0425}\right)\right] x_{CH_4} \tag{3.79}$$

where k_1 and k_2 are correction factors dependent on the temperature.

To get the mass density, ρ_L from eq. (3.78) is multiplied by the molecular weight of the mixture *MW*, which is calculated as follows:

$$MW = \sum MW_i \, x_i \qquad (3.80)$$

Table 3.2 [12] gives the molar volume in *l/mol* for CH_4 to C_5 and N_2, and for temperatures ranging from 106 K to 118 K. Tables 3.3 and 3.4 [12] give the volume correction factors, k_1 and k_2 (in l/mol), for various molecular weights and temperatures varying from 105 K to 135 K.

Table 3.2 Component molar volumes – revised Klosek-McKinley [12].

Component	Molar volume *v*, l/mol						
	118 K	**116 K**	**114 K**	**112 K**	**110 K**	**108 K**	**106 K**
CH_4	0.038817	0.038536	0.038262	0.037995	0.037735	0.037481	0.037234
C_2H_6	0.048356	0.048184	0.048014	0.047845	0.047678	0.047512	0.047348
C_3H_8	0.062939	0.062756	0.062574	0.062392	0.062212	0.062033	0.061855
iC_4H_{10}	0.078844	0.078640	0.078438	0.078236	0.078035	0.077836	0.077637
nC_4H_{10}	0.077344	0.077150	0.076957	0.076765	0.076574	0.076384	0.076194
iC_5H_{12}	0.092251	0.092032	0.091814	0.091596	0.091379	0.091163	0.090948
nC_5H_{12}	0.092095	0.091884	0.091673	0.091462	0.091252	0.091042	0.090833
N_2	0.050885	0.049179	0.047602	0.046231	0.045031	0.043963	0.043002

Table 3.3 Volume correction factor, $k_1.10^3$ – revised Klosek-McKinley [12].

MW mixture g/mol	Volume reduction, l/mol						
	105 K	**110 K**	**115 K**	**120 K**	**125 K**	**130 K**	**135 K**
16	-0.007	-0.008	-0.009	-0.010	-0.013	-0.015	-0.017
17	0.165	0.180	0.220	0.250	0.295	0.345	0.400
18	0.340	0.375	0.440	0.500	0.590	0.700	0.825
19	0.475	0.535	0.610	0.695	0.795	0.920	1.060
20	0.635	0.725	0.810	0.920	1.035	1.200	1.390
21	0.735	0.835	0.945	1.055	1.210	1.370	1.590
22	0.840	0.950	1.065	1.205	1.385	1.555	1.800
23	0.920	1.055	1.180	1.330	1.525	1.715	1.950
24	1.045	1.155	1.280	1.450	1.640	1.860	2.105
25	1.120	1.245	1.380	1.550	1.750	1.990	2.272

Table 3.4 Volume correction factor, $k_2.10^3$ – revised Klosek-McKinley [12].

MW mixture g/mol	Volume reduction, l/mol						
	105 K	110 K	115 K	120 K	125 K	130 K	135 K
16	-0.010	-0.015	-0.024	-0.032	-0.043	-0.058	-0.075
17	0.240	0.320	0.410	0.600	0.710	0.950	1.300
18	0.420	0.590	0.720	0.910	1.130	1.460	2.000
19	0.610	0.770	0.950	1.230	1.480	1.920	2.400
20	0.750	0.920	1.150	1.430	1.730	2.200	2.600
21	0.910	1.070	1.220	1.630	1.980	2.420	3.000
22	1.050	1.220	1.300	1.850	2.230	2.680	3.400
23	1.190	1.370	1.450	2.080	2.480	3.000	3.770
24	1.330	1.520	1.650	2.300	2.750	3.320	3.990
25	1.450	1.710	2.000	2.450	2.900	3.520	4.230

3.2.2 SPECIFIC HEAT

One of the basic thermodynamic quantities is specific heat, defined as the amount of heat required to raise the temperature of a unit mass of a substance by one unit. It is an intensive property of a substance.

Experimentally, the measurement of the isobaric specific heat C_p of a fluid can be performed by supplying heat to a sample placed into a rigid container (calorimeter) at constant pressure, and measuring the resulting temperature increase. In this respect, specific heat at constant pressure is defined as follows [10]:

$$dQ = C_p dT \tag{3.81}$$

Eq. (3.81) in terms of enthalpy is written as follows:

$$dH = C_p dT \tag{3.82}$$

By rearranging eq. (3.82), C_p can be defined as:

$$C_p = \left(\frac{\partial H}{\partial T}\right)_P \tag{3.83}$$

From eq. (3.83), one can evaluate C_p by differentiating the molar enthalpy; however, the value might not be accurate enough. Hence, for the development of the weathering model under this research project C_p is obtained from a REFPROP database [4], to ensure the values used are derived more accurately.

3.2.3 DIRECT AND INDIRECT LATENT HEAT

The latent heat *L* or enthalpy of vaporization represents the energy needed for vaporization to occur, as it involves overcoming most of the intermolecular attractions in the liquid.

The enthalpy of vaporization ΔH_{vap} of a pure substance is the heat needed to make a phase change of one mol of liquid to form one mol of gas, under equilibrium conditions of constant temperature and pressure [13]. It is the difference between the enthalpy of the saturated vapour and that of the saturated liquid at the same temperature.

As discussed earlier, from Clausius-Clapeyron equation, eq. (3.36), the latent heat *L* can be related to measured variables *P*, *v* and *T*, as follows:

$$\frac{dP}{dT} = \frac{PL}{T^2 R} = \frac{L}{T(v_2 - v_1)} \tag{3.84}$$

For binary (and multicomponent) systems the calculation is more complex due to the fact that the isobaric evaporation is combined with a temperature increase, as a result of the lighter component being preferentially evaporated and the remaining liquid getting richer in the heavier component following the phase envelope. For mixtures that are undergoing isobaric phase change one needs to distinguish between the overall and differential latent heat. The former is simply the difference between the molar or specific enthalpy of the vapour and liquid phase at equilibrium and corresponds to the amount of heat necessary to evaporate the whole mixture. The latter corresponds to the amount of heat necessary to evaporate an infinitesimal amount of liquid mixture under isobaric conditions. As the liquid phase gets progressively richer in the heavier component, its boiling temperature increases and it is customary to separate the differential latent heat in two (2) terms, the direct and indirect latent heat [13-15].

The contribution of the direct differential latent heat is due to a change in entropy during isobaric evaporation between a mol of liquid and a mol of vapour in equilibrium with it. For instance, for a binary mixture is given by [13]:

$$L_{direct} = \frac{M^{\mathrm{l}}\left(\frac{\partial x_1}{\partial T}\right)_{p,b} T\left[y_1\left(s_1^{\mathrm{v}} - s_1^{\mathrm{l}}\right) + y_2\left(s_2^{\mathrm{v}} - s_2^{\mathrm{l}}\right)\right] + M^{\mathrm{v}}\left(\frac{\partial y_1}{\partial T}\right)_{p,d} T\left[x_1\left(s_1^{\mathrm{v}} - s_1^{\mathrm{l}}\right) + x_2\left(s_2^{\mathrm{v}} - s_2^{\mathrm{l}}\right)\right]}{M^{\mathrm{l}}\left(\frac{\partial x_1}{\partial T}\right)_{p,b} + M^{\mathrm{v}}\left(\frac{\partial y_1}{\partial T}\right)_{p,d}} \tag{3.85}$$

where s and M are the partial molar entropy and number of moles, respectively, of the given phase; y and x are the mol fractions in the vapour and liquid phases respectively; subscripts 1 and 2 indicate components of the binary mixture, whilst superscripts v and l indicate vapour and liquid phase respectively. The partial derivatives $(\partial x_1/\partial T)_{P,b}$ and $(\partial y_1/\partial T)_{P,d}$ are used to denote the displacement along the bubble-point line and dew-point line respectively.

The indirect differential latent heat is due to the change in temperature which accompanies the isobaric evaporation. For a binary mixture it is given by [13]:

$$L_{indirect} = \frac{(x_1 - y_1)(M^{l} C_p^{l} + M^{v} C_p^{v})}{M^{l}(\frac{\partial x_1}{\partial T})_{p,b} + M^{v}(\frac{\partial y_1}{\partial T})_{p,d}} \tag{3.86}$$

where C_p^{v} and C_p^{l} are the isobaric molar specific heat of the vapour and liquid phase respectively.

Although the indirect latent heat is rather small for mixtures with components of similar volatilities, as the relative volatility between components increases the contribution of the indirect differential latent heat to the total, differential latent heat becomes important and cannot be neglected.

3.2.4 HEATING VALUE

The heating value or standard enthalpy of combustion is defined as the enthalpy difference between the combustion reactants and that of its products in the vapour phase [16], at temperature of 298.15 K and pressure of 0.1 MPa and is given by the following relation:

$$\Delta H_c^o = \Delta H_p^o - \Delta H_r^o \tag{3.87}$$

where ΔH_c^o is the standard enthalpy of combustion, ΔH_p^o is the standard enthalpy of the combustion products, and ΔH_r^o is the standard enthalpy of the reactants.

The heating value of natural gas is the heat liberated (enthalpy of combustion) by the complete combustion of a unit of fuel with oxygen at standard[8] conditions. The products of combustion are H_2O and CO_2. When water remains as vapour the energy recovered is the net heating value, usually called Lower Heating Value (LHV). When the water product is liquid, the recovered energy by its condensation is added to the lower heating value to give the gross heating value, usually called Higher Heating Value (HHV).

The heating value is usually measured with a bomb calorimeter. It may also be calculated as the difference between the standard enthalpy of formation ΔH_f^o of the products and reactants, as there is a direct relation between the standard enthalpy of combustion and the standard enthalpy of formation.

The higher heating value HHV is a prime characteristic of a natural gas, often a quality factor in commercial transactions. The HHV of a gas mixture can be calculated from the following composition dependent expression:

$$HHV = \sum y_i HHV_i \tag{3.88}$$

where HHV_i is the higher calorific value of each of the pure compounds contained in the gas mixture, being zero for non-hydrocarbon species.

3.2.5 WOBBE INDEX

The wobbe index (WI) or wobbe number gives a measure of the relative heat input into a burner at a fixed gas pressure of any fuel gas [16]. As indicated before, WI is defined as:

$$WI = \frac{HHV}{\sqrt{\rho/\rho_{ref}}} \tag{3.89}$$

The WI is the combination of the heat input and the flow of gas into a burner. The heat input is directly proportional to the heating value (HHV), and the flow of gas into a burner is inversely proportional to the square root of the relative density of gas. Where ρ is the

[8] Standard conditions: T= 15.5 ºC and P= 0.1 MPa

density of LNG mixture in the gaseous state, and ρ_{ref}, the reference density, is taken as the density of air at standard conditions.

The WI is a measure of the burning character of a natural gas. WI is important for the calculation of the amount of air to be drawn into a simple burner, such as those used in typical domestic appliances. Raising the WI will increase the CO production, as the amount of air remains the same in the burner whilst the requirement for complete combustion increases. Conversely, a reduction in the WI will lead to a loss of heat service and flame instability.

The WI, together with the impurity levels, defines the suitability of a natural gas for a particular market, and more specifically to a particular appliance.

3.3 HEAT TRANSFER

Heat leakage into the LNG storage tanks is the main factor that causes BOG generation. The heat leakage entering into the LNG storage tank is determined by its structure. Of the various types of LNG storage tanks available, the full containment above-ground type (refer to Figure 2.14 in Chapter 2) is selected as the main structure LNG storage tank studied under this research project. That is because the full containment above-ground tank is the most common LNG storage containment employed worldwide by the industry, due to the increase in safety and reduced plot space [16].

The heat ingress into the storage tank comprises heat transfer through the lateral wall, roof and bottom slab. In industrial storage tanks, the tank bottom slab is maintained at constant temperature using an electrical heating element and temperature sensors, to prevent ground freezing. Hence, in the development of the weathering model the heat transfer through the bottom of the tank is assumed to be constant and independent of the temperature of the surroundings.

To predict the amount of heat entering into the stored LNG, and furthermore to solve the energy balance to estimate weathering, a thermal analysis of the LNG storage tank is required. The well-defined geometry of an above-ground LNG tank and the accurate availability of thermal properties of the insulation and wall section materials, allow a

rigorous estimation of the heat in-leak rate into the LNG. For a partially filled tank, the problem of predicting the heat in-leak rate and wall temperature as a function of liquid level depend on the relative contributions of the different modes of the heat transfer to the liquid, such as convection, radiation and wall conduction. Within this approach, the fundamental heat transfer relations to calculate the heat leakage, which are computed for each side of the tank, are reviewed in the following sections.

3.3.1 FREE CONVECTION HEAT TRANSFER

Convection is the transfer of heat from one place to another by the movement of fluids. It occurs when an object is immersed in a fluid which is at a different temperature; in this situation the heat exchange is between the fluid and the object. The heat exchange produced is due to buoyancy forces caused by density gradients developed in the body of the fluid.

The convection heat flow rate is defined by the following equation [17]:

$$\dot{Q} = h\, A\, \Delta T \tag{3.90}$$

then,

$$\dot{Q} = h\, A\, (T_{\mathrm{w}} - T) \tag{3.91}$$

where $\dot{Q}$ is the heat rate transferred between the exposed surface A of the wall and the fluid; h is the convection coefficient; T_w is the temperature of the wall; and T is the temperature of the free moving fluid.

Free convection originates when warmer (lighter) fluid moves upward the object, whilst the cooler (heavier) fluid moves downward. Within this process, the heat exchanged between the object wall and fluid is affected by fluid dynamics, whether the fluid motion regime involved is laminar or turbulent. The free convection mechanism then is strongly dependent on both, the fluid flow pattern and temperature distribution in the vicinity of the object wall.

Figure 3.4 [17] shows a scheme of the fluid velocity and temperature profiles, within the boundary layer, of a free convective heat transfer process.

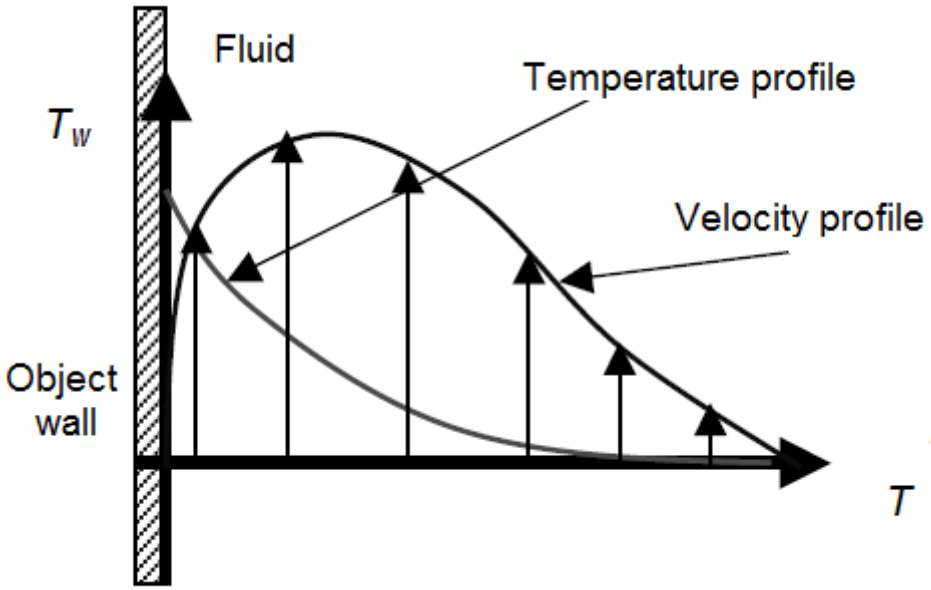

Figure 3.4 Velocity and T profiles within the boundary layer [18].

In the boundary layer, due to viscosity, the fluid in the immediate vicinity of the wall does not move relative to wall, producing the velocity to increase from zero to a maximum and then back to zero again, where the constant fluid temperature (room temperature) is reached. Within the same distance the temperature decreases from the wall temperature to the room temperature [17].

Next to the wall, due to fluid being stationary, the heat transfer is by thermal conduction only; the actual convection mechanism is only active away from the wall. That is why convection as heat transfer mechanism is a difficult phenomenon to describe with a high level of accuracy.

The calculation of an average convection heat transfer coefficient is an approximate approach, but it has been demonstrated to be suitable in most of practical applications [17]. The next section describes the expressions used to calculate the heat transfer coefficient, when free convection is present.

3.3.2 CONVECTION COEFFICIENT CALCULATION

In the LNG tank the effect of convection between the outer face and the environment, as well as in the inside wall, for the LNG (wet) and vapour (dry) sides, should be considered. In this respect, the external free convection heat transfer coefficient h_o, and the internal heat transfer coefficient h_i of the liquid (LNG) and gas are related by an expression in the form of the dimensionless numbers Nusselt *Nu* and Rayleigh *Ra* [17], as follows:

$$Nu = \frac{h\,l}{k} = C\ Ra^n \tag{3.92}$$

where l and k are the characteristic length and thermal conductivity respectively. The characteristic length is usually defined as the ratio of the volume of the body, to its surface area. C and n are coefficients depending on the free convection regime. Typically C = 0.59 and n = 0.25 for laminar flow; whilst C = 0.13 and n = 0.33 for turbulent flow. The convection regime is based on Rayleigh number, with $Ra < 10^9$ for laminar flow, and $Ra > 10^9$ for turbulent flow.

The Nusselt number is the ratio of the convective to the conductive heat transfer across the same surface. The conductive component is measured under the same conditions as the convective but considering (a hypothetically) motionless fluid. A Nusselt number near one means that convection and conduction are of similar magnitude, which is characteristic of laminar regime. A larger Nusselt number corresponds to more active convection, with turbulent regime typically in the order of 100–1,000 range [17].

The Rayleigh number is defined as the product of the Grashof, *Gr*, and Prandtl, *Pr*, numbers as follows [17]:

$$Ra = Gr\ Pr \tag{3.93}$$

The Grashof and Prandtl numbers are dimensionless parameters used in the correlation of natural convection heat transfer at a solid surface immersed in a fluid.

The significance of the Grashof number is that it represents the ratio between the buoyancy forces due to spatial variation in fluid density (caused by temperature differences) are the restraining forces due to the viscosity of the fluid [17].

The Grashof number *Gr* is given by the following expression [18]:

$$Gr = \frac{l^3 g\, \rho^2 \beta\, (T_w - T)}{\mu^2} \tag{3.94}$$

where l is the characteristic length, g is gravity, ρ is the density of the fluid, β is the thermal expansion coefficient, μ is the dynamic viscosity, υ is the kinematic viscosity, T_w is the temperature of the wall and T is the temperature of the fluid.

The kinematic viscosity υ is given by:

$$\upsilon = \frac{\mu}{\rho} \tag{3.95}$$

Substituting eq. (3.95) into eq. (3.94):

$$Gr = \frac{l^3 g\, \beta\, (T_w - T)}{\upsilon^2} \tag{3.96}$$

The Prandtl number represents the fluid state and is defined as the ratio of diffusion of momentum to diffusion of heat in a fluid. $Pr < 1$ means thermal diffusivity dominates; whilst $Pr > 1$ means momentum diffusivity dominates [17].

The Prandtl number *Pr* is given by the ratio of two transport properties, the kinematic viscosity ν, and the thermal diffusivity α [17], as follows:

$$Pr = \frac{\upsilon}{\alpha} \tag{3.97}$$

The thermal diffusivity α is given by [17]:

$$\alpha = \frac{k}{\rho C_p} \tag{3.98}$$

where C_p is the fluid specific heat.

The product between *Gr* and *Pr* numbers gives the *Ra* number, as expressed by eq. (3.93), which describes whether the natural convection boundary layer is laminar or turbulent. For a vertical surface for example the transition from laminar to turbulent regime takes place when $Ra \approx 10^9$ [17]. When the Rayleigh number indicates laminar regime, the heat transfer is primarily in the form of conduction; when it indicates turbulent regime, the heat transfer is primarily in the form of convection.

All fluid characteristics can be calculated at the film temperature T_f, which is a good and reasonable approximation to the temperature within the convection boundary layer. The film temperature is defined as the arithmetic mean temperature of the wall T_w and the fluid temperature T:

$$T_f = \frac{T_w + T}{2} \tag{3.99}$$

3.3.3 CONDUCTION HEAT TRANSFER

By Fourier's law the magnitude of the heat flux q is proportional to the negative temperature gradient across the stationary medium. This is summarized in the following equation [18]:

$$q = -k\nabla T \tag{3.100}$$

where k is the thermal conductivity.

Applied to one dimension, the Fourier's law equation (3.100) develops to:

$$q = -k\frac{\partial T}{\partial x} \tag{3.101}$$

Integrating eq. (3.101) through a defined cross-sectional area A, one gets the integral form of the Fourier equation:

$$\int_1^2 q\, dx = -\int_1^2 k\frac{\partial T}{\partial x} dx \tag{3.102}$$

Positions 1 and 2 (integral limits) define the boundaries of the stationary medium.

Equation (3.102) when integrated in one dimension for a homogeneous material geometry, and along its thickness Δx, gives the heat flow rate as [18]:

$$\frac{\Delta Q}{\Delta t} = kA\frac{(T_1 - T_2)}{\Delta x} \tag{3.103}$$

where T_1 and T_2 are the temperatures at the two boundaries of the material, and Δt is the time interval.

In LNG weathering conduction heat transfer is particularly important in order to calculate the heat leakage along the storage tank walls. The following section describes the calculation set up to estimate the heat ingress through the LNG tank walls considering external convection, conduction and internal convection to the LNG.

3.3.4 HEAT INGRESS THROUGH TANK LATERAL WALLS

The heat input rate $\dot{Q}$ through the tank lateral walls depends on the temperature of the surrounding air and the liquid level inside the tank. As the heat transfer from the surrounding air to the inside of the tank is by combination of conduction and convection, the expression for $\dot{Q}$ is written as follows [18]:

$$\dot{Q} = U\ A\ \Delta T \tag{3.104}$$

Considering the wet and dry sections of the tank, eq. (3.104) becomes:

$$\dot{Q} = (U_{wet}A_{wet})(T_{air} - T_{LNG}) + \left(U_{dry}A_{dry}\right)(T_{air} - T_{BOG}) \tag{3.105}$$

where U is the overall heat transfer coefficient, U_{wet} is the overall wet LNG heat transfer coefficient, U_{dry} is the overall dry BOG heat transfer coefficient, A is the heat transfer area, A_{wet} is the wet heat transfer area, A_{dry} is the dry heat transfer area, T_{air} is the air outside temperature, T_{LNG} is the LNG temperature and T_{BOG} is the BOG temperature.

In general, three (3) layers are clearly defined in the lateral wall section of an above-ground LNG storage tank. The materials comprising the three layers from the inner section are: the resilient blanket, expanded perlite and concrete. Figure 3.5 illustrates the

schematic of the wall section of a typical above-ground LNG storage tank, where the three layers with different diameters are shown.

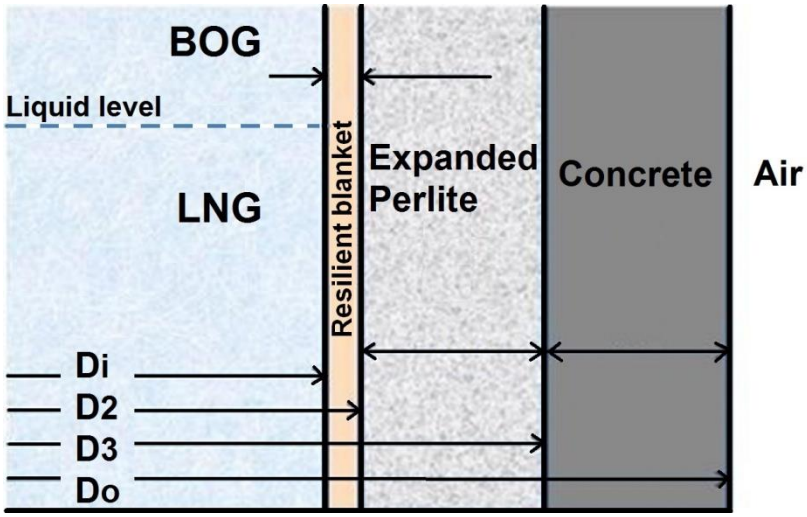

Figure 3.5 Above-ground LNG storage tank wall section

The expression for the overall heat transfer coefficient *U* follows the function below:

$$U_j = f\left(h_o, h_{ij}, D_o, D_i, k\right) \tag{3.106}$$

where subscript *j* refers to the wet (LNG) and dry (BOG) sections of the inner tank lateral wall, h_o is the external convection heat transfer coefficient, h_i is the internal convection heat transfer coefficient, D_o is the tank external diameter, D_i is the tank internal diameter, and *k* is the wall layer material thermal conductivity.

To calculate the overall heat transfer coefficient *U*, as the combined heat transfer processes acting through the tank lateral wall is considered: convection from the surrounding air to the outside wall, conduction through the three layered insulated wall and internal convection to the inside of the storage tank. It is assumed that the metal wall offers only a very small resistance to transfer of heat and its thermal conductivity is neglected. The expression for *U*, based on the external area, is defined as follows [18]:

$$\frac{1}{U_j} = \frac{1}{h_{\mathrm{o}}} + \frac{A_{\mathrm{o}}}{A_{\mathrm{i}} h_{\mathrm{i}j}} + \sum_{i=1}^{3} \frac{A_{\mathrm{o}}}{A_{mi}} \frac{e_i}{k_i} \tag{3.107}$$

where the summation index *i* denotes the different layer sections of the tank wall, A_o is the external heat transfer area, A_i is the internal heat transfer area, A_m is the mean heat transfer area, and *e* is the equivalent insulation thickness.

The mean heat transfer area A_m is defined as:

$$A_m = \pi \, D_{eq} \, l \tag{3.108}$$

where D_{eq} is the equivalent diameter, and *l* is the length of the heat transfer area.

The equivalent diameter D_{eq} is defined as:

$$D_{eq} = \frac{D_o - D_i}{\ln(D_o/D_i)} \tag{3.109}$$

Using D_{eq}, eq. (3.107) can be rewritten as:

$$\frac{1}{U_j} = \frac{1}{h_o} + \frac{D_o}{D_i h_{ij}} + \sum_{i=1}^{3} \frac{D_o}{D_{eq,i}} \frac{e_i}{k_i} \tag{3.110}$$

where D_o and D_i are respectively the external and internal diameters, and h_o and h_{ij} are respectively the external and internal convection heat transfer coefficients (*j* to denote wet and dry sections of the inner tank lateral wall).

3.3.5 RADIATION HEAT TRANSFER

Thermal radiation is a form of heat transfer based on electromagnetic waves energy exchange. All bodies with temperature above absolute zero emit energy by a process of electromagnetic radiation. The intensity of the radiation energy flux depends upon the temperature of the body and the nature of its surface. Thermal radiation propagates through vacuum or any transparent medium, solid or fluid [18].

The rate of net radiant energy transfer $\dot{Q}$ is described by the Stefan-Boltzmann law, which is defined as follows [18]:

$$\dot{Q} = \varepsilon \sigma A (T^4 - T_s^4) \tag{3.111}$$

where ε is the emissivity of the radiating surface, σ is the Stefan-Boltzmann constant ($5.6704.10^{-8}$ W/m^2 K^4), A is the radiating area, T is the temperature of the radiating object and T_s is the temperature of the surroundings. From eq. (3.111) it is observed that objects at lower temperatures emit less energy, as the energy emission varies with the fourth power of the absolute temperature.

The emissivity of the surface of a material is its effectiveness in emitting energy as thermal radiation. Quantitatively, emissivity is the ratio of thermal radiation from a surface to the radiation from an ideal black body[9] surface at the same temperature, as given by the Stefan–Boltzmann law, with the ratio varying from 0 to 1. In other words, real materials emit energy at a fraction of black-body energy levels, thus, by definition, a black body in thermal equilibrium has an emissivity of 1.

Radiant heat rate exchange can be described by assuming two (2) thermally black objects, *a* and *b*, where a heated object *a* radiates only to the other object *b*. All heat leaving object *a* arrives to object *b*, and all heat leaving object *b* arrives to object *a*. Therefore, the net heat rate $\dot{Q}$ exchanged from object *a* to object *b* is the difference between the heat from *a* to *b*, $\dot{Q}_{ab}$, and the heat from *b* to *a*, $\dot{Q}_{ba}$. Hence, the net radiation heat transfer between the two objects can be written as follows [18]:

$$\dot{Q} = A_1\sigma(T_a^4) - A_1\sigma(T_b^4) = A_1\sigma(T_a^4 - T_b^4) \tag{3.112}$$

where A_1 is the surface area of object *a*.

If for instance, there are other objects within the visualization field of object *a*, then a view factor is included in eq. (3.112):

$$q = \frac{\dot{Q}}{A_1} = \sigma F_{a-b}(T_a^4 - T_b^4) \tag{3.113}$$

where $F_{a\text{-}b}$ is the fraction of energy leaving object *a* that is intercepted by object *b*.

[9] A black body is an idealized physical body that absorbs all incident electromagnetic radiation, regardless of the frequency or angle of incidence

Radiation heat transfer plays also a part in the thermal analysis of an above ground LNG storage tank, in particular into the portion of the tank above the liquid level, in other words within the vapour phase, with the radiant heat exchanged between the inner face of tank walls and the liquid (LNG) surface [19]. The radiant heat rate exchanged is then written as follows:

$$q = \varepsilon\sigma F(T_w^4 - T_{\mathrm{L}}^4) \tag{3.114}$$

where T_w is the tank wall temperature and T_{L} is the LNG temperature.

Although radiation heat transfer plays a role when analysing heat transfer in an above ground LNG tank, Jeon *et al*. [20] have proven that its contribution can be neglected from the heat balance, when predicting the temperature distribution within the vapour phase. That is in the equilibrium condition or steady state the heat rate can be accounted as the heat penetrating into the vapour phase by conduction.

3.4 REFERENCES

[1] Danesh, A. (1998) *PVT and phase behaviour of petroleum reservoir fluids*. The Netherlands, Elsevier Science.

[2] Seader, J. D., Henley, E. J. (2010) *Separation process principles, 2nd edition*. USA, John Wiley & Sons Inc.

[3] Poling, B., Prausnitz, J., O'Connell J. (2007) *The properties of gases and liquids, 5th edition*. McGraw-Hill.

[4] Lemmon, E. W., Huber, M. L., McLinden, M. O. (2013) NIST standard reference database 23. *Reference fluid thermodynamic and transport properties REFPROP*, Version 9.1. Gaithersburg, National Institute of Standards and Technology (NIST).

[5] Redlich, O., Kwong, J. N. S. (1949) On the thermodynamics of solutions. V. An equation of state. Fugacities of gaseous solutions. *Chemical Reviews*, 44 (1), 233–244

[6] Soave, G. (1972) Equilibrium constants from a modified Redlich−Kwong equation of state. *Chemical Engineering Science*, 27, 1197−1203

[7] Peng, D. Y., Robinson, D. B. (1976) A new two-constant equation of state. *industrial and engineering chemistry fundamentals*, 15 (1), 59–64

[8] Kunz, O., Wagner, W. (2012) The GERG-2008 wide-range Equation of state for natural gases and other mixtures: An expansion of GERG-2004. *Journal of Chemical and Engineering Data*, 57 (11), 3032–309

[9] Ajetunmobi, T. (2010) *LNG Phase behaviour*. MSc thesis. Imperial College of London.

[10] Vidal, J. (2003) *Thermodynamics – Applications in chemical engineering and the petroleum industry*. Paris, Institut Française du Pétrole Publications, Editions Technip.

[11] Albrigh, L. F. (2009) *Albright's chemical engineering handbook.* Boca Raton, CRC Press, Taylor & Francis Group,

[12] Groupe International des Importateurs de Gaz Naturel Liquéfié – GIIGNL (2010) *LNG custody transfer handbook, 3rd edition*, Paris

[13] Bett, K. E., Rowlinson, J. S., Saville, G. (1975) *Thermodynamics for chemical engineers*. USA, the MIT press.

[14] Strickland-Constable, R. F. (1951) Two-Phase equilibrium in binary and ternary systems. VII. Calculation of latent heats and some other similar properties. *Proceedings of The Royal Society A*, 8 October 1951. London.

[15] Conrado, C., Vesovic, V. (2000) The influence of chemical composition on vaporisation of LNG and LPG on unconfined water surfaces. *Chemical Engineering Science*, 55, 4549−4562

[16] Migliore, C. (2013) Natural gas conditioning and processing. In: Riazi, M. R., Eser, S., Agrawal, S. S., Peña Díez, J. L. (eds.) *Petroleum refining and natural gas processing*. ASTM International, USA, pp. 249-286.

[17] Favre-Marinet, M., Tardu, S. (2009) *Convective heat transfer, solved problems*. ISTE Ltd. and John Wiley & Sons, Inc. UK

[18] Lienhard IV, J. H., Lienhard V, J. H. (2008) *A heat transfer textbook, 3rd edition*. Cambridge, Phlogiston Press.

[19] Neill, D. T., Hashemi, H. T., Sliepcevich, C. M. (1968) Boil-off rates and wall temperatures in above ground LNG storage tanks. *Chemical Engineering Progress Symposium Series*, 64 (87), 111−119

[20] Jeon, S., Jin, B., Kim, Y. (2007) Consistent thermal analysis procedure of LNG storage tank. *Structural Engineering and Mechanics*, 25 (4), 445-466.

4 LNG WEATHERING MODEL DEVELOPMENT

4.1 OVERVIEW

As defined in the previous sections, LNG weathering is the progressive alteration of thermophysical properties of stored LNG through vaporization, due to the heat ingress from the surroundings. The weathering process takes place as heat ingresses into the LNG storage tank (control volume); it produces the vaporization of the lighter components of the LNG, then changing the VLE inside the tank.

The following sections describe the mathematical analysis and the calculation procedure to predict stored LNG weathering as a function of time, based on mass and energy balance and thermodynamic equilibrium.

4.2 ENERGY BALANCE

Assume that a system such as the LNG storage tank, with an initial amount liquid and vapour, is initially (at $t= t_0$) in thermodynamic equilibrium. After some time has passed ($t= t_1$), the system undergoes an isobaric change as a result of heat input Q_{in}. At the end of the period the system is in a new thermodynamic equilibrium state, but now with a lower number of moles, as part of the vaporized product, B, has been released from the system. That process is represented in Figure 4.1 showing the VLE change inside an LNG tank, as heat ingresses into the stored LNG within a time period from $t= t_0$ to $t= t_1$.

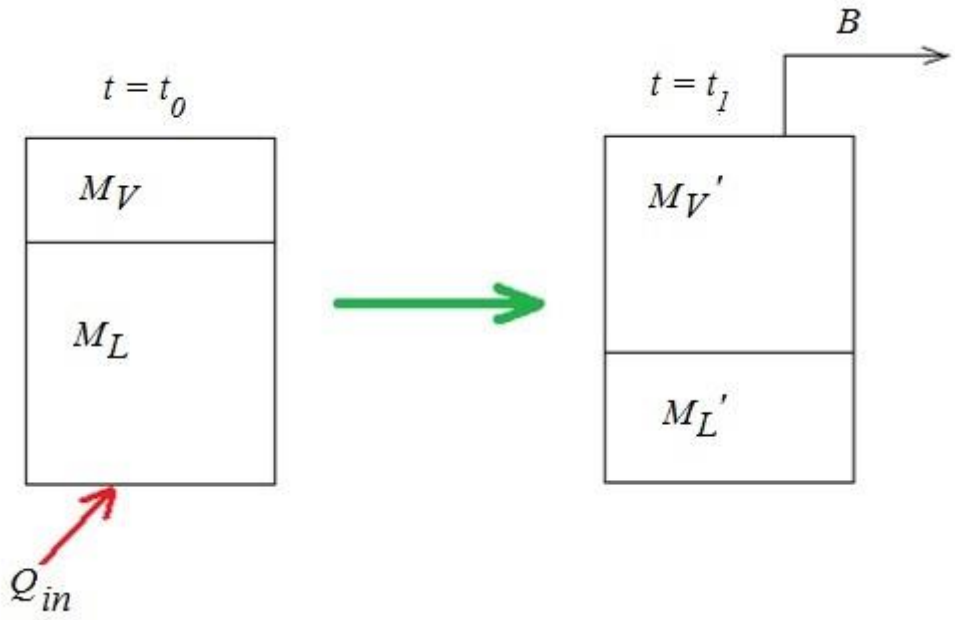

Figure 4.1 Scheme of VLE change inside an LNG tank from $t = t_0$ to $t = t_1$

M_L and M_V in Figure 4.1 are the mol quantities of the liquid and vapour phases respectively.

The energy balance over the storage tank that links the amount of heat entering the tank per unit of time, $\dot{Q}_{in}$, to the rate of vapour removal, dB/dt, can be expressed by the following differential equation:

$$\dot{Q}_{in} = \frac{dH_V}{dt} + \frac{dH_L}{dt} + \frac{dB}{dt} h_V \qquad (4.1)$$

where H_V is the vapour enthalpy, H_L is the liquid (LNG) enthalpy and h_V is the vapour specific enthalpy.

The rate of vapour removal can be obtained from the mass balance, as follows:

$$-\dot{B} \equiv -\frac{dB}{dt} = \frac{d(\rho_L V_L)}{dt} + \frac{d(\rho_V V_V)}{dt} \qquad (4.2)$$

where ρ_L is the liquid mass density, ρ_V is the vapour mass density, V_L is the liquid (LNG) volume, V_V is the vapour volume and B is the mass of boil-off gas (BOG).

Rewriting eq. (4.2):

$$-\frac{dB}{dt} = V_{\mathrm{L}}\frac{d\rho_{\mathrm{L}}}{dt} + \rho_{\mathrm{L}}\frac{dV_{\mathrm{L}}}{dt} + V_{\mathrm{V}}\frac{d\rho_{\mathrm{V}}}{dt} + \rho_{\mathrm{V}}\frac{dV_{\mathrm{V}}}{dt} \tag{4.3}$$

The tank volume *V* is defined as:

$$V = V_{\mathrm{L}} + V_{\mathrm{V}} = constant \tag{4.4}$$

Taking into account that tank volume is constant, one gets:

$$\frac{dV_{\mathrm{L}}}{dt} = -\frac{dV_{\mathrm{V}}}{dt} \tag{4.5}$$

combining equations (4.3), (4.4) and (4.5):

$$-\frac{dB}{dt} = V_{\mathrm{L}}\frac{d\rho_{\mathrm{L}}}{dt} + \rho_{L}\frac{dV_{\mathrm{L}}}{dt} + (V - V_{\mathrm{L}})\frac{d\rho_{\mathrm{V}}}{dt} - \rho_{\mathrm{V}}\frac{dV_{\mathrm{L}}}{dt} \tag{4.6}$$

after some rearrangement, eq. (4.6) can be expressed as:

$$\frac{1}{\rho_{\mathrm{V}}}\frac{dB}{dt} = \frac{dV_{\mathrm{V}}}{dt}\left(\frac{\rho_{L}}{\rho_{\mathrm{V}}} - 1\right) - \frac{V_{\mathrm{V}}}{\rho_{\mathrm{V}}}\frac{d\rho_{\mathrm{V}}}{dt} - \frac{V_{\mathrm{L}}}{\rho_{\mathrm{L}}}\frac{d\rho_{\mathrm{L}}}{dt} \tag{4.7}$$

where dV_{V}/dt is the rate of evaporation of LNG.

Substituting eq. (4.7) into eq. (4.1) the outcome is the equation that governs how the ingress of heat changes the thermodynamic state of the stored LNG:

$$\dot{Q}_{in} = \frac{dH_{\mathrm{V}}}{dt} + \frac{dH_{\mathrm{L}}}{dt} + \left(\frac{dV_{\mathrm{V}}}{dt}(\rho_{\mathrm{L}} - \rho_{\mathrm{V}}) - V_{\mathrm{V}}\frac{d\rho_{\mathrm{V}}}{dt} - V_{\mathrm{L}}\frac{\rho_{\mathrm{V}}}{\rho_{\mathrm{L}}}\frac{d\rho_{\mathrm{L}}}{dt}\right)h_{\mathrm{V}} \tag{4.8}$$

As the right-hand side of the resulting equation contains only thermodynamic quantities and their evolution with time, it can be obtained from an appropriate thermodynamic model.

4.3 LNG WEATHERING MODELLING

Based on first principles the modelling of LNG weathering requires solving the heat balance and the VLE equations which are valid within the LNG storage tank. The mathematical solution to describe the weathering phenomena is achieved by integrating a

rigorous LNG vapour-liquid equilibrium (VLE) model and a realistic heat transfer model, and combining both into an overall model to predict the compositional evolution of the stored LNG over time.

The conventional approach to stored LNG weathering analysis assumes the system (LNG storage tank) is in vapour-liquid equilibrium. In this research project, two modelling approaches are considered when assessing the effect of the heat ingress from the surrounding into the LNG tank, the isothermal approach, where the vapour-liquid system is in thermodynamic equilibrium during the weathering process; and the superheated vapour approach, where the system does not follow the thermodynamic equilibrium.

Within the isothermal approach the whole system (LNG storage tank) is in VLE over the course of the weathering process; hence, the temperature of the vapour and liquid phases are the same, then all the heat entering into the LNG tank is used to vaporize the LNG. The outcome of this approach is the tank achieving full thermodynamic equilibrium state at the end of the weathering process.

In the second approach, the superheated vapour, the influence of the heat influx from the surrounding into the vapour and liquid spaces in the tank are separated. Within that approach, the vapour phase does not follow the VLE as it gets superheated during the weathering process. As vapour has a much lower specific heat, C_p, it will heat up much faster and, in the process, will transfer some of that heat to the liquid giving rise to further vaporization/weathering. The vapour and liquid phases will have a different temperature at the end of the weathering period; therefore, the tank will not be in thermodynamic equilibrium.

Sections 4.5 and 4.6 respectively describe the equations that govern both weathering models, for the isothermal model and superheated vapour model developed.

4.4 HEAT INGRESS FROM TANK ROOF AND BOTTOM SLAB

The heat ingress into the storage tank comprises heat transfer through the roof, bottom slab and lateral wall. Based on industry standards, that boil-off rate (BOR) should not exceed 0.05% per day, a total heat input into the tank is estimated assuming pure methane boil-off.

Roughly 30% to 40% of the total heat entering into the tank enters through the lateral tank wall; the remaining 60% to 70% comes from the roof, Q_{roof}, and the bottom thermal slab, Q_{slab}. This is in good agreement with estimates based on operation of real storage tanks, as studied by Adom *et al.* [1], who estimated the heat leakage of each part of the LNG tank: roof, side wall and bottom. Table 4.1 below, shows the heat leakage results of four kinds of LNG tanks used in industry [1].

Table 4.1 Heat leakage in LNG storage tanks of different nominal capacity [1]

Tank section (heat ingress)	Tank volume capacity, m^3			
	140,000	160,000	180,000	200,000
Roof, kW	40.3	37.3 (without deck)	46.6	45.4
Lateral walls, kW	51.7	53.9	49.3	49.9
Bottom, kW	77.9	72.0	70.6	68.0

For the modelling of stored LNG weathering within this research project, a standard 165,000 m^3 full containment LNG storage tank is considered.

In industrial storage tanks the bottom is maintained at constant temperature using an electrical heating element and temperature sensors to prevent ground freezing. In respect to the roof heat transfer, the external concrete section is separated from the tank by the insulated suspended deck. The space between the roof and the suspended deck is filled with BOG (refer to Figure 2.14 in Chapter 2). Thus, the inner face of the concrete roof is not directly exposed to the cryogen atmosphere [2].

Based on the previous observations for bottom and roof, the heat ingress through bottom slab, Q_{slab}, and tank roof, Q_{roof}, are assumed to be constant and independent of the temperature of the surroundings in this research. The heat rate input from the bottom thermal slab and roof were respectively estimated as 60 kW and 40 kW, based on the operation of an actual standard 165,000 m^3 full containment LNG storage tank [2]. With

regard to the bottom thermal slab heat input, the estimated value of 60 kW is around 15% lower to that observed in Adom *et al.* study [1], and presented before in Table 4.1.

4.5 ISOTHERMAL MODEL

The isothermal model approach considers the LNG storage tank as a system in thermodynamic equilibrium. There are two implications from this consideration to model LNG weathering. The first comes from the energy balance, representing the storage tank as a system in which all the heat that have entered goes into the liquid (LNG), though the heat in-leak is fully used as total latent heat to vaporize the LNG.

The second implication comes from the vapour-liquid equilibrium, in which the system (the storage tank) is in thermodynamic equilibrium throughout the weathering process.

In respect to the heat input within the isothermal model approach, the system accounts for the heat ingress through the roof, bottom slab and lateral wall.

Figure 4.2 illustrates the isothermal approach to model stored LNG weathering, showing the heat entering through the lateral wall into the vapour, Q_{Vin}, and liquid, Q_{Lin}, sides of the tank, as well as the heats input from roof, Q_{roof}, and bottom thermal slab, Q_{slab}.

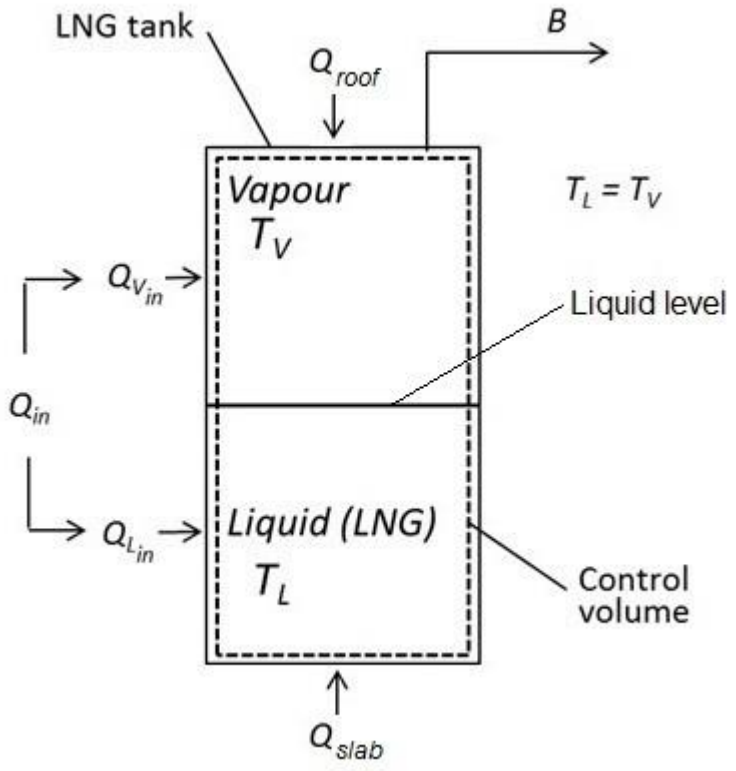

Figure 4.2 Isothermal approach scheme to model LNG weathering

T_L and T_V in Figure 4.2 are the liquid and vapour temperatures respectively, which in the isothermal model case are equal ($T_L = T_V$), as the system is considered to be in thermodynamic equilibrium, and B is the BOG leaving the storage tank.

Equation (4.1) is the differential equation that governs the process represented in Figure 4.2, as it links the heat entering into the tank, to the rate of vapour removal. The numerical solution to equation (4.1) is achieved by finite difference.

The heat balance over the LNG storage tank (refer to Figure 4.2), within a time period from $t = t_0$ to $t = t_1$, is then defined as follows:

$$Q_{in} + Q_{slab} + Q_{roof} = H_{V,t_1} - H_{V,t_0} + H_{L,t_1} - H_{L,t_0} + B_{t_1} h_{V,t_1} \qquad (4.9)$$

When Q_{in} is the sum of the heat input through the lateral wall to vapour $Q_{V_{in}}$ and liquid $Q_{L_{in}}$ sides.

The heat rate input through the lateral wall to the vapour and liquid sides are calculated as follows:

$$\dot{Q}_{\mathrm{V}_{in}} = \left(U_{dry}A_{dry}\right)(T_{air} - T_{\mathrm{V}}) \tag{4.10}$$

$$\dot{Q}_{\mathrm{L}_{in}} = (U_{wet}A_{wet})(T_{air} - T_{\mathrm{L}}) \tag{4.11}$$

$$\dot{Q}_{in} = (U_{wet}A_{wet})(T_{air} - T_{L}) + \left(U_{dry}A_{dry}\right)(T_{air} - T_{\mathrm{V}}) \tag{4.12}$$

where U_{wet} is the overall wet LNG heat transfer coefficient, U_{dry} is the overall dry vapour heat transfer coefficient, A_{wet} is the wet (LNG) heat transfer area, A_{dry} is the dry (vapour) heat transfer area, T_{air} is the air outside temperature, T_{L} is the LNG temperature and T_{V} is the vapour temperature.

The prediction of stored LNG weathering over the defined time period, using the isothermal model approach, requires solving the VLE by the Rachford-Rice equation (3.29), and the heat balance equation (4.9), simultaneously, to get the system temperature ($T = T_{\mathrm{L}} = T_{\mathrm{V}}$), by means of finite difference solution.

The calculation procedure to solve simultaneously the VLE and the heat balance (VLE-HB) is presented in Section 4.7 of this chapter.

4.6 SUPERHEATED VAPOUR MODEL

The superheated vapour model provides a more advanced approach to model stored LNG weathering, as compared to the isothermal model, incorporating additional features.

Industrial evidence shows that the vapour temperature in the LNG tank being higher than liquid (LNG) temperature [2]. In this respect, the superheated vapour model approach separates the influence of the heat influx from the surrounding into the vapour and liquid spaces of the storage tank, considering each phase ensues a different thermodynamic pattern during the weathering process. That is in line with the non equilibrium approach used in blowdown simulation, where the heat transfer into the vapour and liquid phases of the containing vessel are separated to calculate the individual temperature evolution of the vapour and liquid phases during the depressurization process (refer to section 2.7.2).

Furthermore, the model does not account for the heat ingress from the tank roof into the system. This is a suitable approach to incorporate, as the suspended deck and the deck insulation act as a thermal barrier. As previously discussed, the inner face of the tank roof is not directly exposed to the cryogen atmosphere, since the space between the roof and the suspended deck is filled with BOG. Hence, within the superheated vapour model approach, the heat input into the system accounts for the heat ingress through the bottom slab and lateral wall only.

Figure 4.3 illustrates the superheated vapour model approach, showing the heat contributions to vapour, Q_{Vin}, and liquid, Q_{Lin}, sides through the lateral wall, plus the heat input from the bottom thermal slab, Q_{slab}. Also illustrated the heat contribution from the vapour phase to the liquid phase, Q_{vap}, as vapour is at higher temperature with respect to the LNG ($T_V > T_L$).

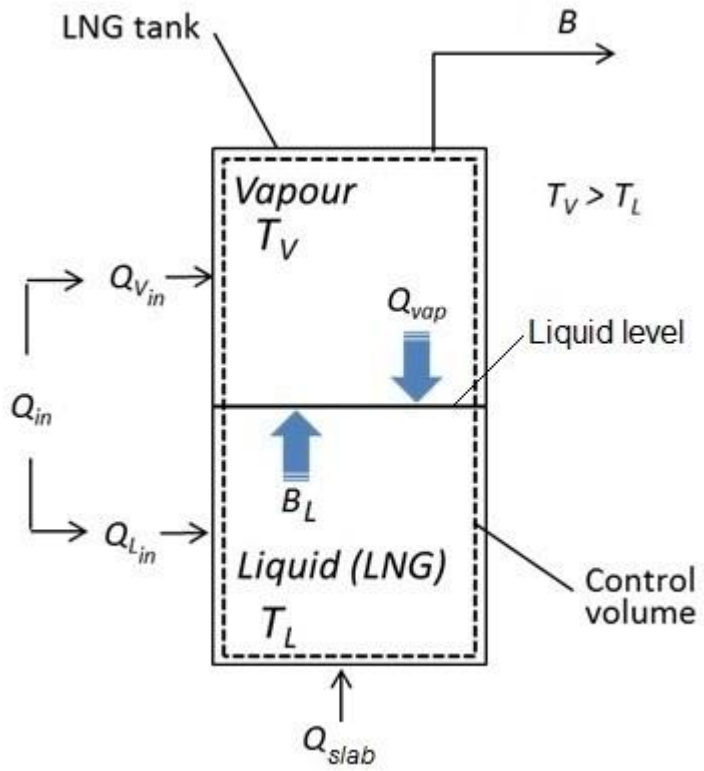

Figure 4.3 Superheated vapour approach scheme to model LNG weathering.

B_L in Figure 4.3 is the BOG leaving the liquid (LNG) phase.

As in the isothermal model, equation (4.1) is the differential equation that governs the process represented in Figure 4.3, as it links the heat entering into the tank, to the rate of vapour removal. The numerical solution to equation (4.1) is achieved by discrete time analysis.

The heat balance over the LNG storage tank (refer to Figure 4.3), within a time period from $t = t_0$ to $t = t_1$, is then defined as follows:

$$Q_{in} + Q_{slab} = H_{V,t_1} - H_{V,t_0} + H_{L,t_1} - H_{L,t_0} + B_{t_1} h_{V,t_1} \quad (4.13)$$

The heat entering into the system, Q_{in}, which is the sum of the heat input through the lateral wall to liquid, $Q_{L_{in}}$, and vapour sides, $Q_{V_{in}}$, plus the constant heat entering through the bottom thermal slab Q_{slab}. Within the superheated vapour model approach, it is assumed that all the heat entering through the bottom thermal slab Q_{slab} goes to the liquid (LNG) and is used to vaporize the LNG.

The heat rate input into the vapour and liquid through the lateral wall are then calculated as follows:

$$\dot{Q}_{V_{in}} = \left(U_{dry} A_{dry}\right)(T_{air} - T_V) \quad (4.14)$$

$$\dot{Q}_{L_{in}} = (U_{wet} A_{wet})(T_{air} - T_L) \quad (4.15)$$

The prediction of stored LNG weathering over the defined time period in the superheated vapour model, taking into account the heat contribution from vapour to liquid, is carried out by solving the energy balance in the liquid and vapour sides of the tank separately, given the heat input in each phase over the time period considered. Within that approach, the calculation sequence is set up by solving first the liquid and thereafter the vapour. In this respect, the liquid (LNG) phase is solved first following the isothermal model approach as in Section 4.5, considering the liquid phase as the control volume, and at its bubble point. The VLE and heat balance are solved simultaneously, taking into account the heat entering into the liquid only. The heat input into the liquid is used to vaporize the

LNG. The outcome of this calculation is the new liquid temperature T_L and the amount of BOG leaving the liquid (LNG vaporized).

The heat balance for the liquid side, within a time period from $t = t_0$ to $t = t_1$, is defined as follows:

$$Q_{\mathrm{L}_{in}} + Q_{slab} + Q_{vap,t_0} = H_{\mathrm{Vo},t_1} - H_{\mathrm{Vo},t_0} + H_{\mathrm{L},t_1} - H_{\mathrm{L},t_0} + B_{\mathrm{L},t_1} h_{\mathrm{Vo},t_1} \quad (4.16)$$

where H_{Vo} is the enthalpy of the vapour in equilibrium with the LNG, H_{L} is the liquid (LNG) enthalpy, h_{Vo} is the specific enthalpy of the vapour in equilibrium with the LNG, B_{L} is the BOG generated and Q_{vap} is the heat contribution from vapour to liquid. To highlight that the equilibrium vapour when solving the liquid side, corresponds to the vapour generated (LNG vaporized) from the liquid heat input, that is different from the initial vapour inside the storage tank.

Once the liquid phase is calculated, the heat balance in the vapour side is next solved to determine the vapour phase temperature T_{V}. The heat balance in the vapour side (control volume) takes into account the energy contributions by the BOG stream coming from the liquid B_{L}, the BOG stream leaving the tank B, and the heat input into the vapour side $Q_{\mathrm{V}in}$.

As mentioned earlier, within the superheated vapour model approach the heat input from the roof Q_{roof} is not taken into account, considering that the suspended deck and the deck insulation act as a thermal barrier.

The heat balance for the vapour side then, within a time period from $t = t_0$ to $t = t_1$, is defined as follows:

$$Q_{\mathrm{V}_{in}} = H_{\mathrm{V},t_1} - H_{\mathrm{V},t_0} + B_{\mathrm{L},t_1} h_{\mathrm{Vo},t_1} - B_{\mathrm{L},t_1} h_{\mathrm{V},t_1} \quad (4.17)$$

The total heat entering into the tank:

$$Q_{in} + Q_{slab} = Q_{\mathrm{L}_{in}} + Q_{\mathrm{V}_{in}} + Q_{slab} \quad (4.18)$$

Figures 4.4 and 4.5 illustrate the energy change in the liquid and vapour sides respectively, over the weathering period (from $t = t_0$ to $t = t_1$), considering the superheated vapour modelling approach.

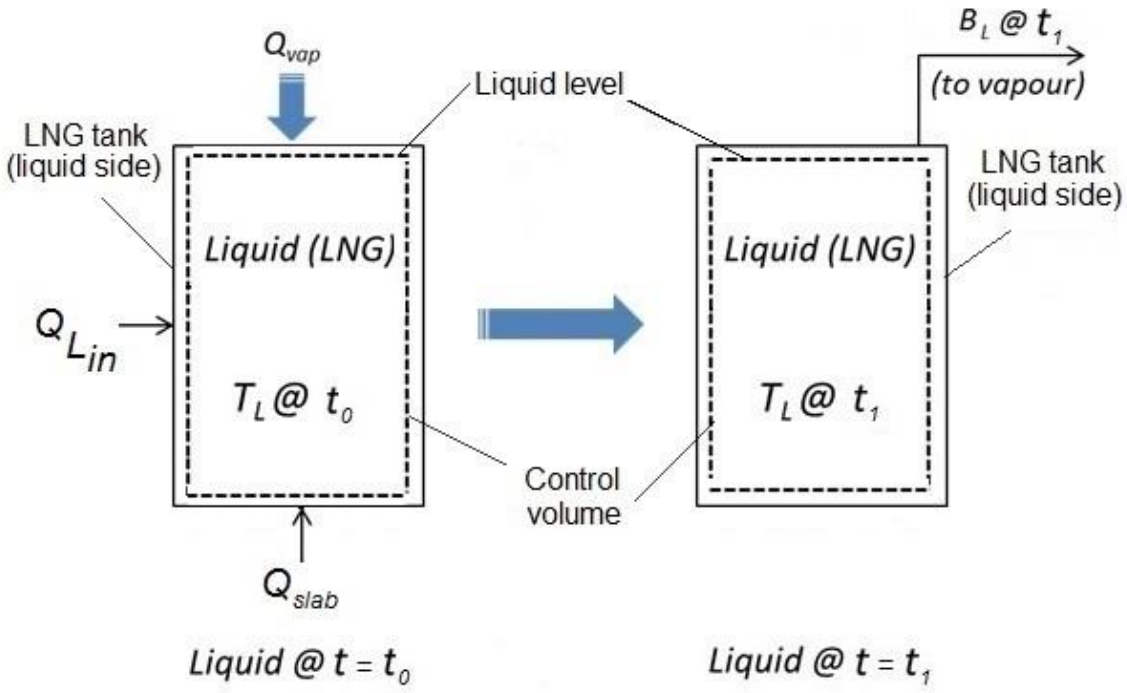

Figure 4.4 Energy change in the liquid side from $t = t_0$ to $t = t_1$. superheated vapour model

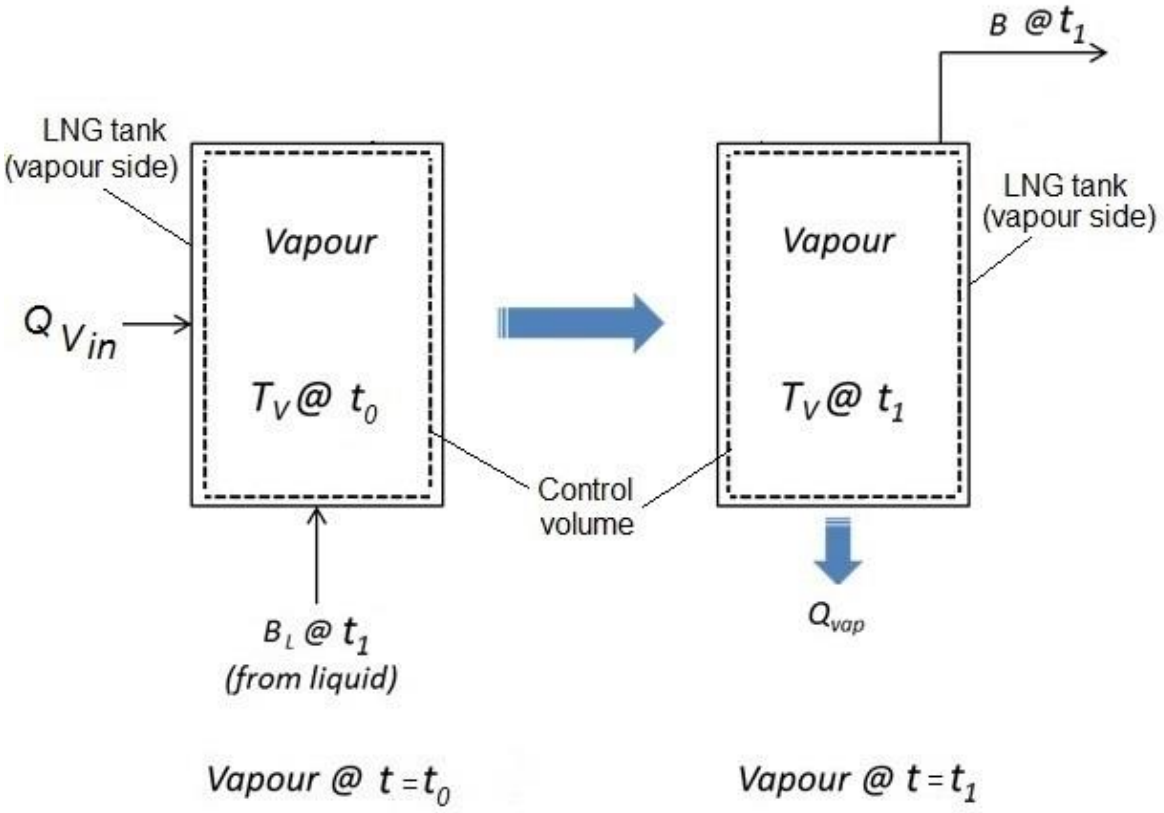

Figure 4.5 Energy change in the vapour side from $t = t_0$ to $t = t_1$. superheated vapour model

The solution of eq. (4.17) gives the initial vapour temperature T_{Vo}. Due to the presence of the liquid, the vapour is normally cooled within the time step to the average vapour temperature $T_{V,avg}$ from T_{V_o}. Once the $T_{V,avg}$ is calculated, then it is possible to calculate the heat contribution from the vapour phase to the liquid Q_{vap}. The following section explains the procedure to calculate $T_{V,avg}$, and describes the equations that govern the heat contribution from the vapour phase to the liquid phase, within the superheated vapour modelling approach.

4.6.1 HEAT EXCHANGE BETWEEN VAPOUR AND LIQUID PHASES

Heat transfer through the vapour is by convection and conduction. In this case, convection heat transfer is not considered; it would require implementing a full numerical computational fluid dynamics (CFD) solution. The problem is approached by assuming

that the heat transfer through the vapour is by conduction only. Thus the equation that governs the heat contribution from the vapour to the liquid can be derived from Fourier's law and the conservation of energy equation.

By Fourier's law, the magnitude of the heat flux q through a surface is directly proportional to the negative temperature gradient across the surface. This is summarized by eq. (3.101) when applied to one dimension [3]:

$$q = -k\frac{\partial T}{\partial x} \tag{3.101}$$

In the absence of work, the negative gradient of the vapour enthalpy is proportional to the change in temperature, and is defined by [4]:

$$-\nabla q = \rho C_p \frac{\partial T}{\partial t} \tag{4.19}$$

Combining equations (3.101) and (4.19), one gets:

$$\rho C_p \frac{\partial T}{\partial t} = k\frac{\partial^2 T}{\partial x^2} \tag{4.20}$$

The thermal diffusivity α is defined as [4]:

$$\alpha = \frac{k}{\rho C_p} \tag{4.21}$$

Combining equations (4.20) and (4.21), the heat contribution from the vapour to the liquid is then governed by the following equation:

$$\frac{\partial T_V}{\partial t} = \alpha\frac{\partial^2 T_V}{\partial x^2} \tag{4.22}$$

The vapour phase differential equation (4.22) is solved considering the initial condition:

$$(i) \qquad t=0 \qquad T_V=T_{Vo}$$

and the following boundary conditions:

$$(ii) \quad x=0 \quad T_V=T_L$$

$$(iii) \quad x=z \quad T_V=T_{Vo}$$

where T_V is the vapour temperature, T_{Vo} is the initial temperature of the vapour, T_L is the temperature of the liquid, x is the vertical length of the vapour space (where x=0 is at liquid level), z is the height of the tank space filled with vapour and α is the thermal diffusivity.

The solution is in the form of the error function producing the vapour temperature T_V as a function of x [5]:

$$T_V = \left(T_{V_o} - T_L\right) erf\left(\frac{x}{2\sqrt{\propto t}}\right) + T_L \tag{4.23}$$

Equation (4.23) is the solution of combining the Fourier's law and the conservation of energy equation, considering the approach of conduction heat transfer through the vapour. Equation (4.23) gives the variation of T_V vs. x for the time that is equal to the selected time step.

As discussed earlier, due to the presence of the liquid, the vapour is normally cooled within the time step to average vapour temperature T_{Vavg} from T_{V_o}. The $T_{V,avg}$ at the end of the time step is calculated by integrating equation (4.23) for T_{V,t_s} as a function of x, along the height z of the vapour space, as follows:

$$T_{Vavg} = \int_0^z T_V . dx \tag{4.24}$$

The amount of heat contribution from the vapour to the liquid Q_{vap}, within the time step, is then calculated by:

$$Q_{vap} = M_V C_p^V \left(T_{V_o} - T_{Vavg}\right) \tag{4.25}$$

where M_{V} are the moles in the vapour phase, C_p^{v} is the specific heat of the vapour, $T_{\mathrm{V}o}$ is the initial temperature of the vapour and $T_{\mathrm{V}avg}$ is the temperature of the vapour at the end of the time step.

4.7 LNG WEATHERING MODEL CALCULATION PROCEDURE

4.7.1 ASSUMPTIONS AND INPUT DATA

The LNG weathering model is based on the following assumptions:

- Homogeneous liquid composition and temperature (no stratification)
- Homogeneous vapour composition and temperature
- Constant tank operating pressure
- LNG storage tank is fully cooled down to cryogenic temperature, so heat transfer through the lateral wall is in steady state, no heat loss due to heat retention in the lateral wall
- Heat flux through tank lateral wall as a function of two overall heat transfer coefficients, one for the liquid side, U_{wet}; and another for the vapour side, U_{dry}
- Constant heat flux from the bottom slab and roof

The input data component of the model is the module where all data on the independent parameters needed to carry out the LNG weathering calculation are provided. The module is structured in four blocks as follows:

1. Stored LNG input data
2. Tank system input data
3. Heat transfer input parameters
4. Calculation input preferences

Following the specific content of each block:

Stored LNG input data

- LNG composition, x_i
- LNG inventory, V_L

Tank system input data

- Internal tank diameter, D_i
- External tank diameter, D_o
- Tank volume, V
- Tank operating pressure, P

Heat transfer input parameters

- Ambient temperature, T_{air}
- Heat rate input from thermal slab, $\dot{Q}_{slab}$
- Heat rate input from tank roof, $\dot{Q}_{roof}$

Calculation input preferences

- Final weathering time, t
- Time step size, t_s
- Temperature step size, ΔT
- Maximum number of iterations, *iter*
- Convergence tolerance, *tol*

4.7.2 INITIAL VLE AND PHASE ENTHALPIES CALCULATION

Figure 4.6 shows the flow diagram summarizing the calculation procedure for the initial VLE of the LNG storage system.

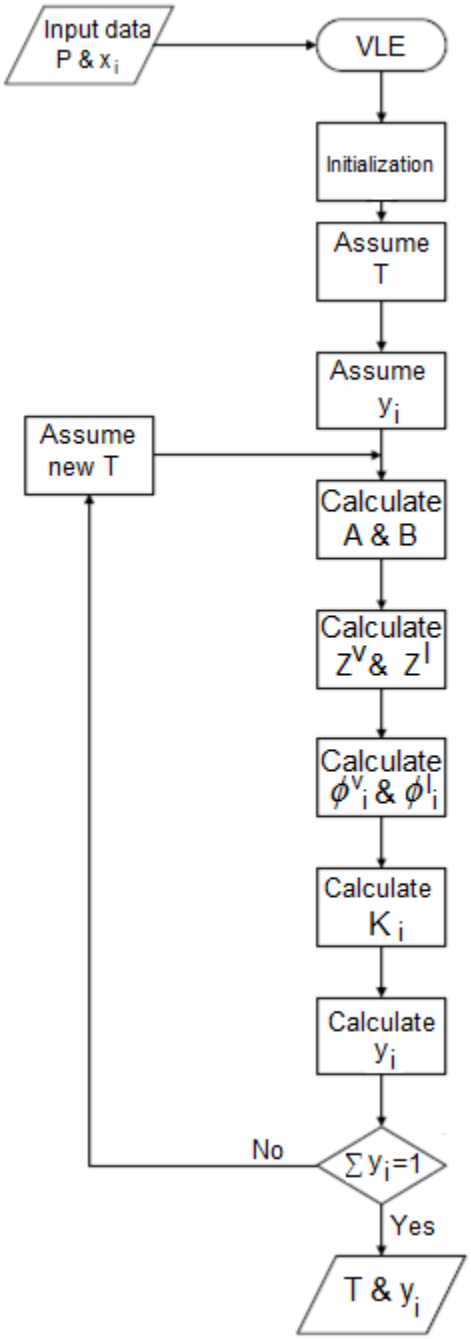

Figure 4.6 Calculation procedure for the initial VLE.

The initial VLE and phase enthalpies calculation module defines the initial thermodynamic conditions (at t=0) of the system.

Below, the description of the calculation procedure implemented within this module, following the flow diagram presented in Figure 4.6:

1. Reading the input data parameters, as defined in section 4.7.1, assumptions and input data.
2. Initialization of LNG components thermodynamic and physicochemical data.
3. Definition of the initial conditions of the system. The initial VLE of the system is calculated considering the operating pressure and the liquid composition, following the iterative procedure presented below:

    i. Assume equilibrium temperature to start the calculation. As a first estimate, the corresponding pure methane equilibrium temperature, at the tank operating pressure, is assumed:

    $$T = T(methane)\ @\ P \qquad (4.26)$$

    The equilibrium temperature for methane can be calculated using the Antoine equation (3.37).

    ii. Assume the vapour composition is the same as the liquid (LNG), for the first iteration:

    $$y_i = x_i \qquad (4.27)$$

    iii. Calculate *A* and *B* parameters in the PR-EOS using equations (3.57) and (3.58), respectively.

    iv. Solve the PR-EOS cubic equation, eq. (3.56), to get compressibility factors Z^V and Z^L. Equation (3.56) is solved twice to get Z^V and Z^L as follows:

        a) once considering the vapour phase composition y_i, to calculate *A* and *B* parameters for Z^V

b) once considering the liquid phase composition x_i, to calculate *A* and *B* parameters for Z^{L}

To solve the PR-EOS cubic equation, Cardano's method [6] is used. Refer to Appendix I for the details of the Cardano's method to solve cubic equations.

v. Calculate fugacity coefficients ϕ_i^{V} and ϕ_i^{L} by equations (3.72) and (3.73) respectively

vi. Calculate distribution constants K_i based on the fugacity coefficients, ϕ_i^{V} and ϕ_i^{L}, by eq. (3.33)

vii. Calculate the vapour phase composition based on the equilibrium constants K_i, by:

$$y_i = K_i x_i \tag{4.28}$$

viii. Check whether $\sum y_i$=1 at the assumed equilibrium temperature. If that is not the case, then a new equilibrium temperature is assumed, and a new iteration calculation is performed from step (*iii*) onwards, until convergence is reached.

The Newton-Raphson [7] numerical method is used to estimate each new iteration temperature, based on the temperature step size ΔT defined in the calculation input preferences. Refer to Appendix II for the details of the Newton-Raphson numerical method.

4. Once the VLE is defined (phase compositions and temperature), initial phase densities are calculated.

Liquid density ρ_L is calculated as per the Klosek-McKinley method, as explained in section 3.2.1, and using eq. (3.78); whilst vapour density ρ_V is calculated as per ideal gases equation corrected by Z^{V}, as follows:

$$\rho_V = \frac{P}{Z^V RT} \tag{4.29}$$

5. Initial material balance, and liquid and vapour phase mol quantities, M_{L} and M_{V} respectively, are then calculated using the VLE information, phase densities, and input data, as follows:

$$M_{\mathrm{L}} = V_{LNG}\,\rho_{\mathrm{L}} \tag{4.30}$$

$$M_{\mathrm{V}} = (V - V_{LNG})\rho_{\mathrm{V}} \tag{4.31}$$

Total moles M_{F}, liquid fraction L_f, and overall component mol fraction z_i inside the storage tank are calculated as follows:

$$M_{\mathrm{F}} = M_{\mathrm{L}} + M_{\mathrm{V}} \tag{4.32}$$

$$L_f = \frac{M_{\mathrm{L}}}{M_{\mathrm{F}}} \tag{4.33}$$

$$z_i = \frac{x_i M_{\mathrm{L}} + y_i M_{\mathrm{V}}}{M_{\mathrm{F}}} \tag{4.34}$$

6. Calculate of initial phase specific enthalpies h_{L} and h_{V} using Z^{L} and Z^{V} respectively, by the enthalpy eq. (3.71):

$$\frac{h-h^{id}}{RT} = Z - 1 - \frac{1}{2\sqrt{2}bRT}\left(a - T\frac{da}{dT}\right)\ln\left(\frac{v+(1+\sqrt{2})b}{v+(1-\sqrt{2})b}\right) \tag{3.71}$$

where h^{id} is the ideal gas enthalpy given by:

$$h^{id} = \sum_i x_i\, h_i^{id} \tag{4.35}$$

The ideal gas enthalpies of each species in eq. (4.35) can be calculated from a thermodynamic database such as REFPROP [8].

4.7.3 INTEGRATED VLE-HB CALCULATION

As mentioned earlier the prediction of stored LNG weathering over the defined time period requires solving simultaneously the VLE by the Rachford-Rice equation (3.29), and the heat balance (HB) eq. (4.9) for the isothermal model, and eq. (4.13) for the liquid side of

the superheated vapour model, to get system temperature by means of discrete time unit steps.

Figure 4.7 shows the flow diagram summarizing the integrated VLE-HB calculation procedure.

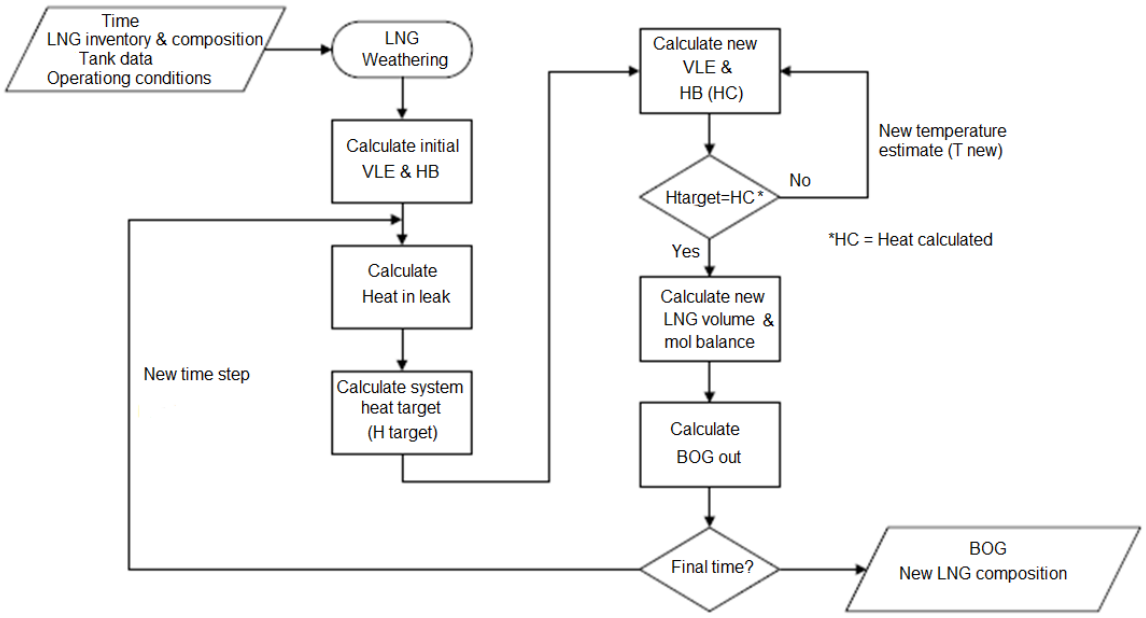

Figure 4.7 Integrated VLE-HB calculation procedure

The calculation procedure to solve the (VLE-HB) simultaneously within the time step t_s is presented below, following the flow diagram showing in Figure 4.7, as heat enters into the LNG storage tank. The calculation procedure follows a finite difference solution approach in which t_{s-1} designates the previous time step and when linked to a physical or thermodynamic variable it refers to the state of the system in the preceding time step.

The calculation procedure to solve the VLE and HB simultaneously is as follows

1. Start of iterative calculation, $t = t_s$
2. Calculation of heat ingress during the time step based on heat input through the LNG storage tank lateral wall, bottom slab and roof (isothermal model approach

only), following the model approach used, whether it is the isothermal or superheated vapour model.

As explained in Section 4.4, in this research, the heat ingress through the tank roof $\dot{Q}_{roof}$ and bottom slab $\dot{Q}_{slab}$ are considered to be constant, and are respectively estimated as 40 kW and 60 kW for a standard 165,000 m^3 full containment LNG storage, which is in good agreement with estimates based on operation of real storage tanks [2].

The heat ingress through the lateral wall is calculated considering the following heat transfer equation:

$$Q_{wall,t_s} = Q_{\mathrm{L}_{in},t_s} + Q_{\mathrm{V}_{in},t_s} \tag{4.36}$$

where $Q_{L_{in}}$ and $Q_{V_{in}}$ correspond to the heat input into the liquid (LNG) and vapour sides respectively of the LNG storage tank, which are delimited by the liquid level inside the tank; t_s is the finite time step interval.

$Q_{L_{in}}$ and $Q_{V_{in}}$ are calculated as follows:

$$Q_{\mathrm{L}_{in},t_s} = U_{wet}A_{wet,t_s}\left(T_{air} - T_{\mathrm{L},t_s}\right)t_s \tag{4.37}$$

$$Q_{\mathrm{V}_{in},t_s} = U_{dry}A_{dry,t_s}\left(T_{air} - T_{\mathrm{V},t_s}\right)t_s \tag{4.38}$$

Substituting eq. (4.37) and (4.38) in eq. (4.36), one gets:

$$Q_{wall,t_s} = \left[U_{wet}A_{wet,t_s}\left(T_{air} - T_{\mathrm{L},t_s}\right) + U_{dry}A_{dry,t_s}\left(T_{air} - T_{\mathrm{V},t_s}\right)\right]t_s \tag{4.39}$$

The tank heat transfer area *A* is defined as:

$$A = \pi D_o L_j \tag{4.40}$$

where the subscript *j* refers to the wet and dry sections inside the tank. The lengths of wet L_{wet} and dry L_{dry} sections in the LNG tank lateral walls, are calculated as follows:

$$L_{wet} = \frac{V_{\mathrm{L},t_S}}{A_T} \tag{4.41}$$

$$L_{dry} = \frac{V - V_{\mathrm{L},t_S}}{A_T} = \frac{V}{A_T} - \frac{V_{\mathrm{L},t_S}}{A_T} = \frac{V}{A_T} - L_{wet} \tag{4.42}$$

where A_T is the LNG storage tank cross sectional area, and is calculated as follows:

$$A_T = \frac{\pi {D_i}^2}{4} \tag{4.43}$$

Figure 4.8 shows a diagram of an LNG storage tank indicating the wet and dry lengths, delimited by the liquid level.

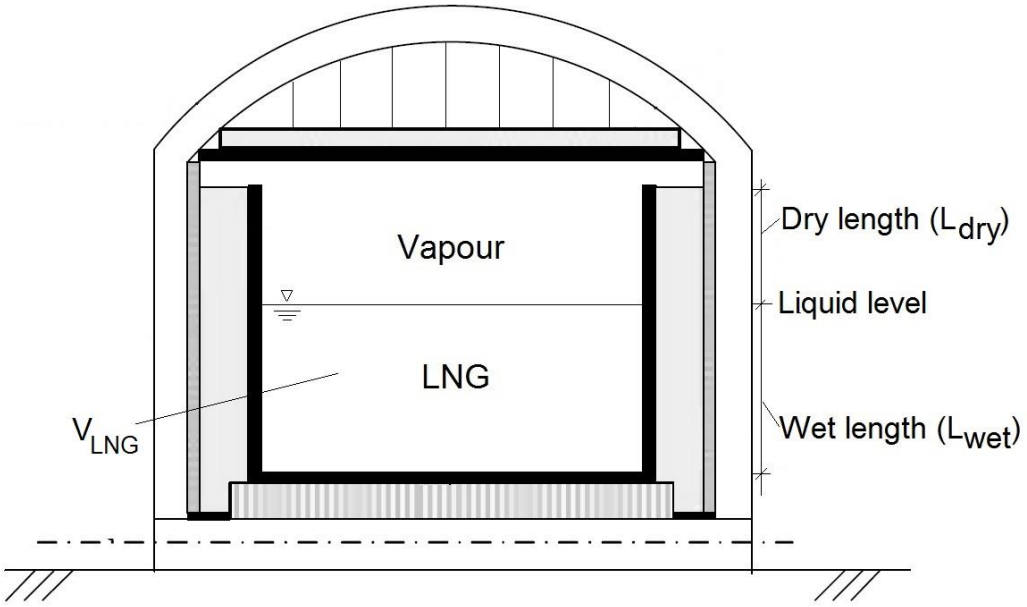

Figure 4.8 LNG storage tank showing the wet and dry lengths

Substituting equations (4.40), (4.41) and (4.42) in eq. (4.39):

$$Q_{wall,t_s} = \pi D_o \left[U_{wet} \frac{V_{\mathrm{L},t_S}}{V} \left(T_{air} - T_{\mathrm{L},t_s} \right) + U_{dry} \frac{(V - V_{\mathrm{L},t_S})}{V} \left(T_{air} - T_{\mathrm{V},t_s} \right) \right] t_s \tag{4.44}$$

In the isothermal model, and in the liquid side of the superheated vapour model (as the liquid side is considered to be at its bubble point), the temperature of the LNG (wet) and vapour (dry) is the same (T=T_L=T_V), since the mixture is at

thermodynamic equilibrium. The equilibrium temperature of the system calculated for the initial VLE (following the calculation procedure presented in Section 4.7.2), is used as first estimate for (T=T_L=T_V).

Equation (4.44) then can be simplified as:

$$Q_{wall,t_s} = \pi D_o \left(U_{wet} \frac{V_{L,t_S}}{V} + U_{dry} \frac{\left(V - V_{L,t_S}\right)}{V} \right) \left(T_{air} - T_{L,t_s} \right) t_s \qquad (4.45)$$

Calculate (D_{eq}) from equation (3.109):

$$D_{eq} = \frac{D_o - D_i}{\ln(D_o / D_i)} \qquad (3.109)$$

Calculate the overall heat transfer coefficients U_{wet} and U_{dry} from equation (3.110):

$$\frac{1}{U_j} = \frac{1}{h_o} + \frac{D_o}{D_i h_{ij}} + \sum_{i=1}^{3} \frac{D_o}{D_{eq\,i}} \frac{e_i}{k_i} \qquad (3.110)$$

where subscript j refers to the wet and dry sections inside the tank, and the summation index i denotes the different layer sections of the tank wall.

Table 4.2 shows the LNG storage tank data used under this research project. The table also includes the dimensions to calculate U_{wet} and U_{dry} by equation (3.110).

Table 4.2 LNG storage tank data.

Tank volume capacity, V	165,000 m^3
LNG volume, V_L	160,000 m^3
Tank height, z	37.3 m
Internal diameter, D_i	76.4 m
External diameter, D_o	80.0 m
Wall section thermal conductivities, k:	
• Resilient blanket [9]	0.015 W/m K
• Expanded perlite [10]	0.035 W/m K
• Concrete [11]	1.6 W/m K
Convection heat transfer coefficients	
• External heat transfer coefficient, h_o	5.7 W/m^2 K
• Internal heat transfer coefficient wet, $h_{i,wet}$	112.0 W/ m^2 K
• Internal heat transfer coefficient dry, $h_{i,dry}$	18.0 W/ m^2 K
Heat rate input bottom thermal slab, $\dot{Q}_{slab}$ [2]	60 kW
Heat rate input roof, $\dot{Q}_{roof}$ [2]	40 kW

The external and internal convection heat transfer coefficients, h_o and h_i (wet and dry respectively), were calculated using the free convection heat transfer expressions presented in Section 3.3.2.

Figure 4.9 shows the LNG storage tank wall section with the equivalent insulation thickness e, to calculate U_{wet} and U_{dry} using equation (3.110).

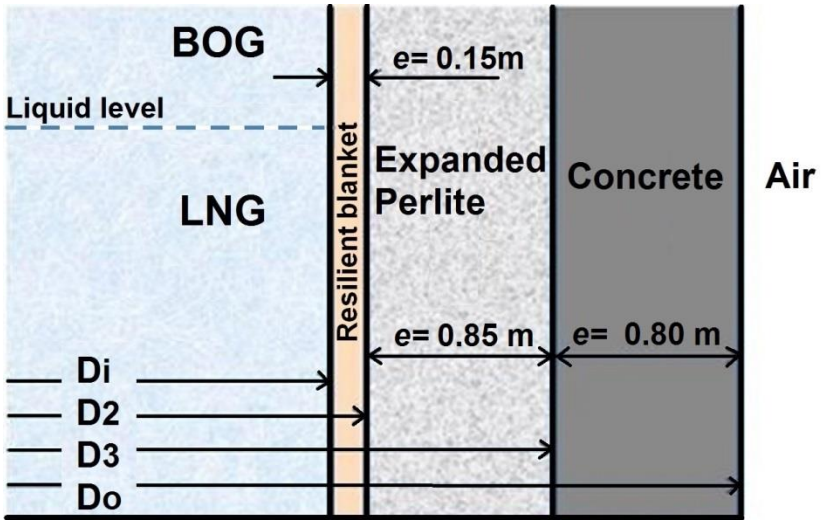

Figure 4.9 LNG storage tank wall section characteristics.

From equation (3.110), and using the external area dimensions, Table 4.3 shows the calculated overall heat transfer coefficients, U_{wet} and U_{dry}.

Table 4.3 Overall heat transfer coefficients U_{wet} and U_{dry}.

Overall wet heat transfer coefficient, U_{wet}	0.02836 W/m^2 K
Overall dry heat transfer coefficient, U_{dry}	0.02832 W/m^2 K

3. Calculate the total heat content of the system within the time step (new energy content), based on the system heat content at previous time step t_{s-1} and the heat ingress calculated in Step 2.

   The total heat content within the time step defines the new enthalpy stage of the system, due to the heat ingress within the time step. This new system enthalpy stage sets the target enthalpy H_{target} numerical solution to be achieved, in terms of the discrete time step calculation. The target enthalpy is defined as follows:

$$H_{target,t_s} = \left(Q_{wall,t_s} + Q_{roof} + Q_{slab}\right)t_s + \left(M_{\mathrm{L},t_{s-1}} h_{\mathrm{L},t_{s-1}} + M_{\mathrm{V},t_{s-1}} h_{\mathrm{V},t_{s-1}}\right) \quad (4.46)$$

4. The heat ingress will cause an increase in temperature and the change of VLE in the system. Hence, a new equilibrium temperature is assumed to recalculate the VLE within the new time step.

5. The new VLE is calculated following the procedure shown in Figure 4.6, with x_i calculated as a function of liquid fraction L_f. Following the calculation steps:

    a. Calculate the equilibrium constants K_i based on the new equilibrium temperature

    b. Calculation of x_i as for Rachford-Rice equation (3.29):

$$x_i = \frac{z_i}{K_i + L_f(1-K_i)} \tag{4.47}$$

    c. Calculation of y_i as:

$$y_i = K_i x_i \tag{4.48}$$

    d. Check whether $\sum(x_i - y_i) = 0$. If that is not the case, the liquid fraction L_f is adjusted and x_i and y_i are recalculated from Step 5a onwards. The new L_f is calculated using the King equation [12] as follows:

$$L_{f_{new}} = L_{f_{old}} - \frac{\sum \frac{z_i(K_i-1)}{K_i+(1-K_i)L_f}}{\sum \frac{z_i(K_i-1)^2}{\left[K_i+(1-K_i)L_f\right]^2}} \tag{4.49}$$

6. Once $\sum(x_i - y_i) = 0$ is achieved, the phase specific enthalpies h_{L,t_s} and h_{V,t_s} are calculated by eq. (3.71), based on the calculated equilibrium temperature and phase compositions.

7. Calculate the new total heat content of the system, taking into account liquid and vapour phases remaining in the tank, and the BOG leaving the system to maintain tank operating pressure. Hence, the system heat content is calculated as follows:

$$H_{t_s} = M_{\mathrm{L},t_s} h_{\mathrm{L},t_s} + M_{\mathrm{V},t_s} h_{\mathrm{V},t_s} + B_{t_s} h_{\mathrm{V},t_s} = M_{\mathrm{L},t_s} h_{\mathrm{L},t_s} + \left(M_{\mathrm{F},t_{s-1}} - M_{\mathrm{L},t_s}\right) h_{\mathrm{V},t_s} \tag{4.50}$$

where M_{F} is the total number of moles.

8. Check whether $H_{target,t_s} - H_{t_s} = 0$. If that is not the case, then a new equilibrium temperature T_{t_s} is assumed and the calculation procedure is repeated from Step 5 onwards.

9. Calculate phase densities and phase volumes. Liquid density $\rho_{\mathrm{L}}(T)_{t_s}$ is calculated as per the Revised Klosek-McKinley method, as explained in Section 3.2.1, and using eq. (3.78); whilst vapour density $\rho_{\mathrm{V}}(T)_{t_s}$ is calculated as per ideal gases equation corrected by Z^{V}, using eq. (4.29).

10. Calculate the new liquid phase volume as follows:

$$V_{\mathrm{L},t_s} = \frac{M_{\mathrm{L},t_s}}{\rho_{\mathrm{L}}(T)_{t_s}} \tag{4.51}$$

11. The vapour stream *B* leaving the system is calculated based on the tank volume balance. The new (total) moles in the tank vapour side M_{V,t_s} are calculated first, taking into account the new volume available in the tank for the vapour phase V_{V,t_s}, considering the liquid volume reduction due to the vaporization of the LNG; thereafter, the moles of vapour leaving the system are determined by material balance.

    The new vapour phase volume is calculated by volume balance with the tank volume capacity *V*, as follows:

$$V_{\mathrm{V},t_s} = V - V_{\mathrm{L},t_s} \tag{4.52}$$

    The moles in the tank vapour side are calculated by the following equation:

$$M_{\mathrm{V},t_s} = V_{\mathrm{V},t_s}\, \rho_{\mathrm{V}}(T)_{t_s} \tag{4.53}$$

    The moles of vapour leaving tank are calculated by material balance, based on the system total moles of the preceding time step, $M_{\mathrm{F},t_{s-1}}$:

$$B_{t_s} = \left(M_{\mathrm{F},t_{s-1}} - M_{\mathrm{L},t_s}\right) - M_{\mathrm{V},t_s} \quad (4.54)$$

12. Calculate the new global composition z_i considering a material balance in the tank, taking into account the moles of vapour stream *B* that has left the LNG tank.

    The material balance to calculate the new total moles in the system, M_{F,t_s}, is written as follows:

$$M_{\mathrm{F},t_s} = M_{t_{s-1}} - B_{t_s} \quad (4.55)$$

    The new global composition is calculated by:

$$z_{i,t_s} = \frac{z_{i,t_{S-1}} M_{\mathrm{F},t_{S-1}} - B_{t_S} y_{i,t_S}}{M_{t_S}} \quad (4.56)$$

13. Iterate from Step 2 for a new time step t_{s+1}, until the final weathering time *t* is reached.

4.7.4 VLE-HB CALCULATION WITH VAPOUR HEAT CONTRIBUTION

As discussed previously, within the superheated vapour model approach, the heat contribution from vapour phase to the liquid phase is taken into account. In this regard, the vapour temperature is estimated first, and thereafter the heat contribution from vapour to liquid is calculated by solving the energy balance in the vapour side of the storage tank.

The calculation procedure to estimate the vapour phase temperature and the heat contribution from vapour to liquid, within each time step, is presented below:

1. Start by solving the VLE-HB in the liquid side following the calculation procedure as presented in Section 4.7.3, considering that the liquid phase is at its bubble point

2. Calculate the heat ingress through the lateral wall into the liquid Q_{L,t_s}, for the new time step $t=t_s$, using the wet tank area A_{wet}, liquid temperature T_{L}, and overall wet heat transfer coefficient U_{wet}:

$$Q_{\mathrm{L}_{in},t_s} = U_{wet} A_{wet,t_s} \left(T_{air} - T_{\mathrm{L},t_s}\right) t_s \quad (4.57)$$

The equilibrium temperature of the system calculated for the initial VLE (following the calculation procedure in Section 4.7.2), is used as a first estimate of T_{L,t_s}.

The overall wet heat transfer coefficient U_{wet} is estimated by equation (3.110):

$$\frac{1}{U_{wet}} = \frac{1}{h_{\mathrm{o}}} + \frac{D_{\mathrm{o}}}{D_{\mathrm{i}} h_{\mathrm{i},wet}} + \sum_{i=1}^{3} \frac{D_{\mathrm{o}}}{D_{\mathrm{eq}\,i}} \frac{e_i}{k_i} \qquad (3.110)$$

where summation index *i* denotes the different layer sections of the tank wall.

Calculate the new total heat content of the system (liquid side) within the time step, based on the system heat content at previous time step ts-1 and the liquid heat ingress calculated in Step 2, plus the heat input from the bottom thermal slab Qslab. Following the assumption of the superheated vapour model approach, the energy balance in the liquid phase to consider that all the heat entering through the bottom thermal slab Qslab goes to the liquid (LNG) and is used to vaporize it.

The new system energy stage becomes the target enthalpy Htarget numerical solution to be achieved, in terms of the discrete time step calculation. The target enthalpy for the liquid side is then defined as follows:

$$H_{target,t_s} = \left(\dot{Q}_{\mathrm{L}_{in},t_s} + \dot{Q}_{slab}\right) t_s + M_{\mathrm{L},t_{s-1}} h_{\mathrm{L},t_{s-1}} \qquad (4.58)$$

3. Following the calculation procedure for VLE-HB presented in section 4.7.3, calculate the new liquid temperature T_{L,t_s}, and the new liquid volume V_{L,t_s}. The new liquid temperature T_{L,t_s} is the liquid temperature that solves equation (4.58).

4. Calculate the amount of vapour leaving the liquid B_{L,t_s} within the time step, by solving the material balance in the liquid, based on the liquid total moles of the preceding time step, $M_{\mathrm{L},t_{s-1}}$, as follows:

$$B_{\mathrm{L},t_s} = M_{\mathrm{L}_{t_{s-1}}} - M_{\mathrm{L}_{t_s}} \qquad (4.59)$$

5. Once the new liquid temperature T_{L,t_s}, and the amount of vapour generated B_{L,t_s} is estimated, the calculation sequence proceeds to solving the vapour phase.

6. Calculate the heat entering into the vapour Q_{V,t_s} (using the dry tank area), vapour temperature T_{V,t_s} and the corresponding overall heat transfer coefficient U_{dry}, by:

$$Q_{\mathrm{V},t_s} = U_{dry} A_{dry,t_s} \left(T_{air} - T_{V,t_s}\right) t_s \tag{4.60}$$

U_{dry} estimated by equation (3.110):

$$\frac{1}{U_{dry}} = \frac{1}{h_{\mathrm{o}}} + \frac{D_{\mathrm{o}}}{D_{\mathrm{i}} h_{\mathrm{i},dry}} + \sum_{i=1}^{3} \frac{D_{\mathrm{o}}}{D_{\mathrm{eq}\,i}} \frac{e_i}{k_i} \tag{3.110}$$

where summation index *i* denotes the different layer sections of the tank wall.

As a first estimate T_{V,t_s} is assumed to be equal as the liquid temperature (T_{V}=T_{L}).

7. Calculate moles in the vapour phase M_{V,t_s} by tank volume balance as follows:

$$V_{\mathrm{V},t_s} = V - V_{\mathrm{L},t_s} \tag{4.61}$$

$$M_{\mathrm{V},t_s} = V_{V,t_s} \cdot \rho_{\mathrm{V}}(T)_{t_s} \tag{4.62}$$

8. Calculate the BOG leaving the tank B_{t_s} for the new time step by solving the material balance for the vapour side:

$$B_{t_s} = \left(M_{t_{s-1}} - M_{\mathrm{L}t_s}\right) - M_{\mathrm{V},t_s} \tag{4.63}$$

9. Calculate the new heat content of the vapour side within the time step, based on the vapour heat content at previous time step, $t_{s\text{-}1}$, and the heat ingress calculated in Step 6.

The calculated total heat content defines the new enthalpy stage of the vapour, due to the heat ingress within the time step. This new system enthalpy stage becomes the target enthalpy H_{target} numerical solution to be achieved, in terms of the discrete time step calculation. The target enthalpy for the vapour side is then defined as follows:

$$H_{target,t_s} = Q_{\mathrm{V}in,t_s}\, t_s + M_{\mathrm{V},t_{s-1}} h_{\mathrm{V},t_{s-1}} + B_{\mathrm{L},t_s} h_{\mathrm{Vo},t_s} - B_{t_s} h_{\mathrm{V},t_s} \tag{4.64}$$

Where $B_{\mathrm{L}} h_{\mathrm{Vo}}$ is the energy contributions of the vaporized LNG stream coming from the liquid, and $B_t h_V$ is the energy leaving the system with the BOG.

10. Following the calculation procedure for VLE-HB presented in Section 4.7.3, calculate the initial vapour temperature T_{V_0,t_s}, that is the vapour temperature that solves equation (4.64)

11. Calculate the average vapour temperature $T_{\mathrm{V}avg,t_s}$ by integrating $T_{\mathrm{V},t_s}(x)$, equations (4.23) and (4.24):

$$T_{\mathrm{V},t_s} = \left(T_{\mathrm{V_o},t_s} - T_{\mathrm{L},t_s}\right) erf\left(\frac{x_{t_s}}{2\sqrt{\alpha t}}\right) + T_{\mathrm{L},t_s} \tag{4.23}$$

$$T_{Vavg,t_s} = \int_0^h T_{V,t_s}(x).\, dx \tag{4.24}$$

Equation (4.24) is solved by numerical integration using the trapezoidal rule [6] to get T_{Vavg,t_s}. Refer to Appendix III for the details of the trapezoidal rule numerical method.

12. Once the average vapour temperature T_{Vavg,t_s} is determined, the heat contribution from vapour to liquid Q_{vap,t_s} can be calculated by eq. (4.25):

$$Q_{vap,t_s} = M_{\mathrm{V},t_s}\, C_p^{\mathrm{v}}\left(T_{\mathrm{V_o},t_s} - T_{\mathrm{V}avg,t_s}\right) \tag{4.25}$$

13. Repeat the calculation from Step 2 for a new time step t_{s+1}, until the final weathering time t is reached.

The energy balance in the liquid side for the new time step is calculated taken into account the heat contribution from vapour to liquid $Q_{vap,t_{s-1}}$. In this respect, equation (4.58) is rewritten as follows:

$$H_{target,t_s} = \left(\dot{Q}_{\mathrm{L}_{in},t_s} + \dot{Q}_{slab}\right)t_s + M_{\mathrm{L},t_{s-1}} h_{\mathrm{L},t_{s-1}} + Q_{vap,t_{s-1}} \tag{4.65}$$

Equation (4.65) becomes the new liquid energy content (H_{target,t_s}) equation for the new time step.

4.8 CHAPTER SUMMARY

This chapter describes the mathematical analysis and the calculation procedure to predict stored LNG weathering as a function of time, based on mass and energy balance and thermodynamic equilibrium. Two modelling approaches are considered in this PhD research project, the isothermal model and the superheated vapour model.

Within the isothermal model, the whole system (LNG storage tank) is considered to be in thermodynamic equilibrium over the course of the weathering process; hence, the temperature of the vapour and liquid phases are the same. Therefore all the heat entering into the LNG tank is used to vaporize the LNG. The outcome of this approach is the tank achieving full thermodynamic equilibrium state at the end of the weathering process.

The superheated vapour model provides a more advanced approach to model stored LNG weathering, as compared to the isothermal model, incorporating additional features. In the superheated vapour model the influence of the heat influx from the surrounding into the vapour and liquid spaces of the tank is separated. Within this approach, the system is considered under non-equilibrium thermodynamic condition, thus the heat contribution from the vapour, which will heat up much quicker due to its lower specific heat, to the liquid can be taken into account, giving rise to further vaporization/weathering. At the end of the weathering process vapour and liquid phases will have a different temperature.

The following chapter describes the tests and simulation runs performed using both weathering models developed, to check for their robustness and to ensure both models are able to provide realistic results.

4.9 REFERENCES

[1] Adom E., Islam S. Z., Ji X. (2010) Modelling of boil-off gas in LNG tanks: A case study. *International Journal of Engineering and Technology*, 2 (4), 292-296.

[2] Operations supervisor, LNG regasification facility. (Personal communication, 28th March 2014).

[3] Lienhard IV, J. H., Lienhard V, J. H. (2008) *A heat transfer textbook, 3rd edition*. Cambridge, Phlogiston Press.

[4] Vidal, J. (2003) *Thermodynamics – Applications in chemical engineering and the petroleum industry*. Paris, Institut Française du Pétrole Publications, Editions Technip.

[5] Bird, R., Warren, S., Lightfoot, E. (2007) *Transport phenomena, 2nd edition*. USA, John Wiley & Sons, Inc.

[6] Ramana, B. V. (2007) *Higher engineering mathematics*. New Delhi, Tata McGraw-Hill Publishing Company Limited.

[7] Nocedal, J., Wright, S. (1999) *Numerical optimization*. USA, Springer series in operations research.

[8] Lemmon, E. W., Huber, M. L., McLinden, M. O., 2013. NIST standard reference database 23: reference fluid thermodynamic and transport properties-REFPROP, Version 9.1, Standard reference data program. National Institute of Standards and Technology, Gaithersburg, MD.

[9] Anco Products (2006) *Resilient blanket product information – System 9000*. USA, Anco Products Inc.

[10] Arkema Group (2006) *Expanded perlite product information – CECA*. France, Arkema, S. A.

[11] Perry, H., Green, D. (1985) *Perry's chemical engineers' handbook 50th anniversary edition*. USA, McGraw-Hill.

[12] Poling, B., Prausnitz, J., O'Connell, J. (2007); *The properties of gases and liquids, 5th edition*. McGraw-Hill.

5 MODEL TESTING AND VERIFICATION

Three assessments were designed for testing and verification of both weathering models developed under this PhD research project. The first assessment compared the predictions of the thermodynamic vapour-liquid equilibrium (VLE) module, against the results obtained with the accredited process simulator Aspen Hysys [1]. The second assessment was performed by validating the estimated latent heat of the weathered LNG mixture, against a full thermodynamic calculation. Finally, as a third assessment, a comparison of weathered LNG estimates, using the models developed with previous studies and measured data was carried out [2].

This chapter also discusses on the discrepancies of the LNG density estimate by the empirical correlation the Revised Klosek-McKinley method eq. (3.78), to that estimated when considering ideal mixture and the COSTALD correlation method, as it is widely used in the oil and gas industry to predict hydrocarbon liquid density.

5.1 VLE MODULE TEST

The vapour-liquid equilibrium (VLE) module is the same for both the isothermal and the superheated vapour weathering models developed in this work. The VLE module was initially validated by comparing the predictions against the results obtained with the process simulator Aspen-Hysys [1] for vapour composition y_i and equilibrium temperature, knowing the liquid composition x_i and pressure. The lack of reliable experimental data on LNG mixtures has led us to selecting Aspen-Hysys [1] to validate the VLE module. The Aspen-Hysys package has been tested extensively on hydrocarbon systems including binary and multicomponent mixtures. The binary interaction parameters have been fitted to the phase envelopes, which is sometimes not the case for some of the scientific thermodynamic packages that are more development/research oriented. Moreover, not all the thermodynamic packages are reliable at low temperatures. Additionally, Aspen-Hysys [1] has demonstrated to be thermodynamically consistent, so that there are no concerns about incompatibilities that might arise when using experimental data from different sources.

The VLE module verification was performed considering two typical LNG commercial compositions, including LNG with nitrogen content (0.57% mol N_2) and heavy LNG (87% mol C_1 and 13% mol C_{2+}), and two hypothetical mixtures, heavy (75% mol C_3 and 25% mol nC_5) and light mix (95% mol C_1 and 5% N_2). The aim was to assess the robustness of the VLE module within a wide compositional range.

The deviation *Dev* was calculated as the difference between the reference value obtained with Aspen-Hysys and the value predicted by the VLE module, as follows:

$$Dev = x_{ref} - x_{mod} \tag{5.1}$$

where x_{ref} and x_{mod} are respectively the reference value and the model predicted value, either for vapour mol fraction or equilibrium temperature.

The deviation percentage *% Dev* is calculated from the following equation:

$$\%\ Dev = \frac{x_{ref} - x_{mod}}{x_{ref}} . 100 \tag{5.2}$$

It is important to highlight that, although eq. (5.2) is a good approach to evaluate deviation between two values, it does not work well when assessing the deviation of small and near zero mol fractions. Within that range, the deviation reported as percentage basis can be misleading. Therefore, we use absolute deviation calculated from eq. (5.1).

Tables 5.1 and 5.2 respectively show the results obtained for the LNG with nitrogen and Heavy LNG; and Tables 5.3 and 5.4 show the results for the Heavy and Light hypothetical mixtures, respectively.

Table 5.1 Predicted vapour mol fraction and equilibrium T for LNG with N_2 at 116.3 kPa (150 mbarg).

Composition	x_i	VLE Module y_i	Aspen Hysys y_i	VLE comparison	
				Dev	% Dev
Methane	0.9055	0.8516	0.8520	0.0004	0.05
Ethane	0.0585	0.0001	0.0001	0.0000	0.00
Propane	0.0207	3.45E-07	3.49E-07	3.50E-09	1.00
Isobutane	0.0096	6.45E-09	6.54E-09	9.00E-11	1.38
Butane	-	-	-	-	-
Isopentane	-	-	-	-	-
Pentane	-	-	-	-	-
Nitrogen	0.0057	0.1483	0.1479	-0.0004	-0.27
Temperature (K)		112.44	112.39	0.05	-0.04

Table 5.2 Predicted vapour mol fraction and equilibrium T for Heavy LNG at 116.3 kPa (150 mbarg).

Composition	x_i	VLE Module y_i	Aspen Hysys y_i	VLE comparison	
				Dev	% Dev
Methane	0.8757	0.9998	0.9998	0.0	0.00
Ethane	0.0760	0.0002	0.0002	0.0	0.00
Propane	0.0312	7.79E-07	7.86E-07	7.00E-09	0.89
Isobutane	0.0080	8.63E-09	8.73E-09	1.00E-10	1.15
Butane	0.0085	2.53E-09	2.56E-09	3.00E-11	1.17
Isopentane	0.0005	7.40E-12	7.50E-12	1.00E-13	1.33
Pentane	0.0001	3.98E-13	4.07E-13	9.00E-15	2.21
Nitrogen	-	-	-	-	-
Temperature (K)		114.86	114.80	-0.06	-0.05

Table 5.3 Predicted vapour mol fraction and equilibrium T for Heavy mix at 116.3 kPa (150 mbarg).

Composition	x_i	VLE Module y_i	Aspen Hysys y_i	VLE comparison	
				Dev	% Dev
Methane	-	-	-	-	-
Ethane	-	-	-	-	-
Propane	0.7500	0.9891	0.9890	-0.001	-0.01
Isobutane	-	-	-	-	-
Butane	-	-	-	-	-
Isopentane	-	-	-	-	-
Pentane	0.2500	0.0109	0.0110	0.0001	0.55
Nitrogen	-	-	-	-	-
Temperature (K)		241.19	241.09	-0.1	-0.04

Table 5.4 Predicted vapour mol fraction and equilibrium T for Light mix at 116.3 kPa (150 mbarg).

Composition	x_i	VLE Module y_i	Aspen Hysys y_i	VLE comparison	
				Dev	% Dev
Methane	0.9500	0.3490	0.3500	0.001	0.29
Ethane	-	-	-	-	-
Propane	-	-	-	-	-
Isobutane	-	-	-	-	-
Butane	-	-	-	-	-
Isopentane	-	-	-	-	-
Pentane	-	-	-	-	-
Nitrogen	0.0500	0.6510	0.6500	-0.001	-0.15
Temperature (K)		101.78	101.75	-0.03	-0.03

In all the cases the mol fractions of major components ($x > 0.01$) in the vapour phase were in agreement to better than 1%. Within the major components, the difference for methane is negligible (below 0.05%), except for the light mix case which is 0.29%.

For minor components (heavier hydrocarbons) deviations up to 2% were observed. Nevertheless, the amount in the vapour phase of such components is so small that the absolute deviation is negligible.

The temperature in all cases is in full agreement; the calculated deviations are below 0.05% in all cases.

5.2 LATENT HEAT VERIFICATION

The second assessment was performed by comparing the overall latent heat predicted by both weathering models against the calculations based on the reference thermodynamic relationships. The overall latent heat predicted by both models was estimated simply by dividing, at each time step, the heat ingress by the vaporization rate. The verification was carried out for three binary mixtures, in order to take advantage of relatively simple thermodynamic relationships for the latent heat of binary mixtures. Table 5.5 shows the mixtures used for the model verification.

Table 5.5 Binary mixtures composition used for the weathering models verification.

Mixture / mol %	Mol Weight g/mol	C_1	C_2	N_2
1 - LNG-like	16.60	96	4	-
2 - C_2 rich	17.59	89	11	-
3 - N_2 rich	16.52	96	-	4

As discussed in Section 3.2.3, for mixtures that are undergoing isobaric phase change one needs to distinguish between the overall and differential latent heat. The former is simply the difference between the molar or specific enthalpy of the vapour and liquid phase at equilibrium and corresponds to the amount of heat necessary to evaporate the whole mixture. The latter corresponds to the amount of heat necessary to evaporate an infinitesimal amount of liquid mixture under isobaric conditions.

As the liquid phase gets progressively richer in the heavier component its boiling temperature increases and it is customary to separate the differential latent heat into direct and indirect latent heats [3-5]. The direct component can be ascribed to the change in entropy during isobaric evaporation between a mol of liquid (x_1, x_2) and a mol of vapour

(y_1, y_2), whilst indirect component arises due to change in temperature which accompanies isobaric evaporation.

The direct and indirect differential latent heats for a binary mixture, can be expressed in terms of thermodynamic quantities by the following relationships [3-5].

$$L_{direct} = \frac{M^{l}(\frac{\partial x_1}{\partial T})_{P,b} T[y_1(s_1^{v} - s_1^{l}) + y_2(s_2^{v} - s_2^{l})] + M^{v}(\frac{\partial y_1}{\partial T})_{P,d} T[x_1(s_1^{v} - s_1^{l}) + x_2(s_2^{v} - s_2^{l})]}{M^{l}(\frac{\partial x_1}{\partial T})_{P,b} + M^{v}(\frac{\partial y_1}{\partial T})_{P,d}} \quad (5.3)$$

$$L_{indirect} = \frac{(x_1 - y_1)(M^{l}C_p^{l} - M^{v}C_p^{v})}{M^{l}(\frac{\partial x_1}{\partial T})_{P,b} + M^{v}(\frac{\partial y_1}{\partial T})_{P,d}} \quad (5.4)$$

where C_p, s and M are molar specific heat, molar entropy and number of moles, respectively, of each phase.

To determine L_{direct} from eq. (5.3) knowledge is required of the partial entropies, s^{v} and s^{l}. To get them accurate advanced equations of state are necessary, which are not straight forward to implement. To avoid doing that we have opted in this research project to obtain the thermodynamic quantities entering equations from Aspen-Hysys [1] process simulator for each assessed mixture. Evaluating $L_{indirect}$ instead, is more direct to implement from eq. (5.4). The derivatives for liquid and vapour composition in eq. (5.4) were calculated by the finite difference method for each modelling approach.

The simulations were run for a storage tank of 165,000 m^3 capacity, initially filled with 160,000 m^3 liquid volume, 52 weeks weathering time and tank pressure of 116.3 kPa (150 mbarg).

Values of L_{direct} for different mixture composition were obtained from Aspen-Hysys [1]. In order to estimate L_{direct} at each time step, taking into account the compositional change of the mixture over time, a polynomial function was fitted to Aspen results as a function of the methane content in the binary mixture. The resulting polynomial fit was integrated into both weathering models (isothermal and superheated vapour).

Table 5.6 and Figure 5.1 respectively show the L_{direct} data series for the methane-ethane mixture, and the plot of the L_{direct} for the methane-ethane mixture as function of methane mol fraction.

Table 5.6 L_{direct} data series for the methane-ethane mixture [1] at 116.3 kPa (150 mbarg).

CH_4	C_2H_6	L_{direct}, J/mol
0.9993	0.0007	8,290
0.9980	0.0020	8,434
0.9970	0.0030	8,513
0.9950	0.0050	8,630
0.9898	0.0102	8,838
0.9793	0.0207	9,112
0.9691	0.0309	9,313
0.9577	0.0423	9,504
0.9055	0.0945	10,200
0.8043	0.1957	11,300
0.7022	0.2978	12,300
0.6103	0.3897	13,140
0.5057	0.4943	14,050
0.4167	0.5833	14,780
0.3066	0.6934	15,580
0.2075	0.7925	16,140
0.1037	0.8963	16,290
0.0575	0.9425	15,940
0.0001	0.9999	14,570

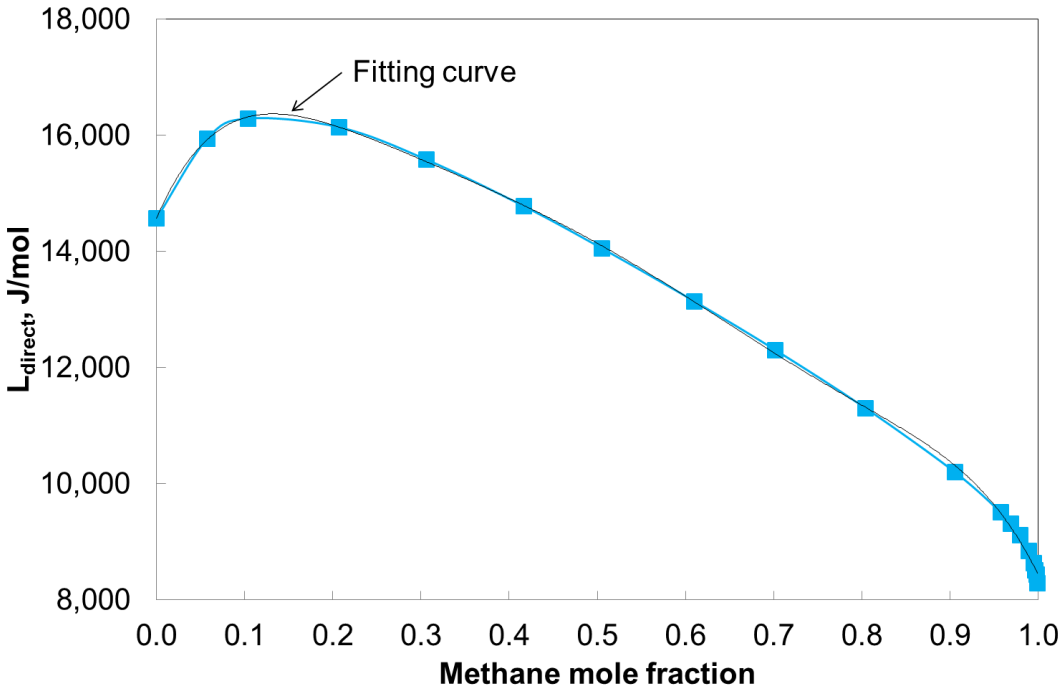

Figure 5.1 L_{direct} **for the methane-ethane mixture vs. methane mol fraction. (-■- L_{direct})**

The polynomial function obtained by regression of L_{direct} as a function of the methane mol fraction x_{C_1}, for the methane-ethane mixture, is written as follows:

$$L_{direct} = -314088.71x_{C_1}^6 + 972500.04x_{C_1}^5 - 1186501.82x_{C_1}^4 + 728610.84x_{C_1}^3 - 241997.18x_{C_1}^2 + 35343.99x_{C_1} + 14566.69 \quad (5.5)$$

Equation (5.5) gives a coefficient of determination R^2 = 0.99952, confirming a very good fit of the L_{direct} regression.

Table 5.7 and Figure 5.2, respectively show the L_{direct} data series for the methane-nitrogen mixture, and the plot of the L_{direct} for the methane-nitrogen mixture as function of methane mol fraction.

Table 5.7 L_{direct} **data series for the methane-nitrogen mixture [1] at 116.3 kPa (150 mbarg).**

CH_4	N_2	L_{direct}, J/mol
0.0509	0.9491	5,877
0.0987	0.9013	6,120
0.1954	0.8046	6,527
0.2932	0.7068	6,902
0.3920	0.6080	7,271
0.4889	0.5111	7,628
0.5957	0.4043	8,010
0.6919	0.3081	8,331
0.7915	0.2085	8,607
0.8998	0.1002	8,719
0.9497	0.0503	8,584
0.9999	0.0001	8,172

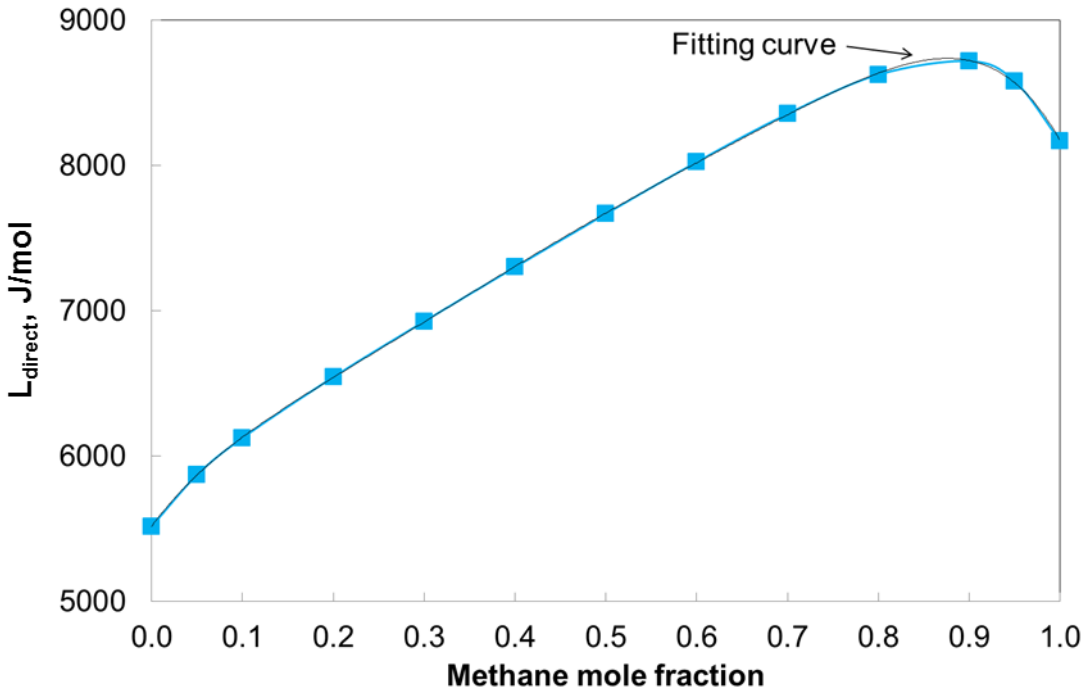

Figure 5.2 L_{direct} **for the methane-nitrogen mixture vs. of methane mol fraction.** (-■- L_{direct})

The polynomial function for L_{direct} as a function of the methane mol fraction for the methane-nitrogen mixture is written as follows:

$$L_{direct} = -69259.87x_{C_1}^6 + 189853.86x_{C_1}^5 - 206162.90x_{C_1}^4 + 111724.75x_{C_1}^3 - 31896.40x_{C_1}^2 + 8397.75x_{C_1} + 5517.52 \quad (5.6)$$

In the methane-nitrogen case, eq. (5.6) gives a coefficient of determination R^2 = 0.99997, also confirming a very good fit of the L_{direct} regression in this case.

The reference latent heat L_{ref} calculated for each modelling approach taking into account the corresponding $L_{indirect}$, is compared to the overall latent heat predicted by both models L_{iso} and L_{shv} that is obtained by dividing, at each time step, the vaporization rate by the heat ingress. Subscripts *iso* and *shv* refer to the isothermal and superheated vapour models respectively.

L_{ref} for each model is defined as follows:

$$L_{ref} = L_{direct} + L_{indirect} \quad (5.7)$$

where L_{direct} is calculated from eq. (5.5), whilst $L_{indirect}$ is calculated from eq. (5.4) for each modelling approach.

L_{iso} and L_{shv} at each time step are calculated as follows:

$$L_{iso} = \frac{Q_{L_{in}} + Q_{V_{in}} + Q_{roof} + Q_{slab}}{B} \quad (5.8)$$

$$L_{shv} = \frac{Q_{L_{in}} + Q_{slab}}{B} \quad (5.9)$$

Figures 5.3 and 5.4 respectively show the results of the latent heat verification test for the isothermal and superheated vapour weathering models for the LNG-like and C_2 rich mixtures cases. As the reference latent heats L_{ref} for the LNG-like and C_2 rich mixtures for both models are nearly the same, they are shown as one line in the figures.

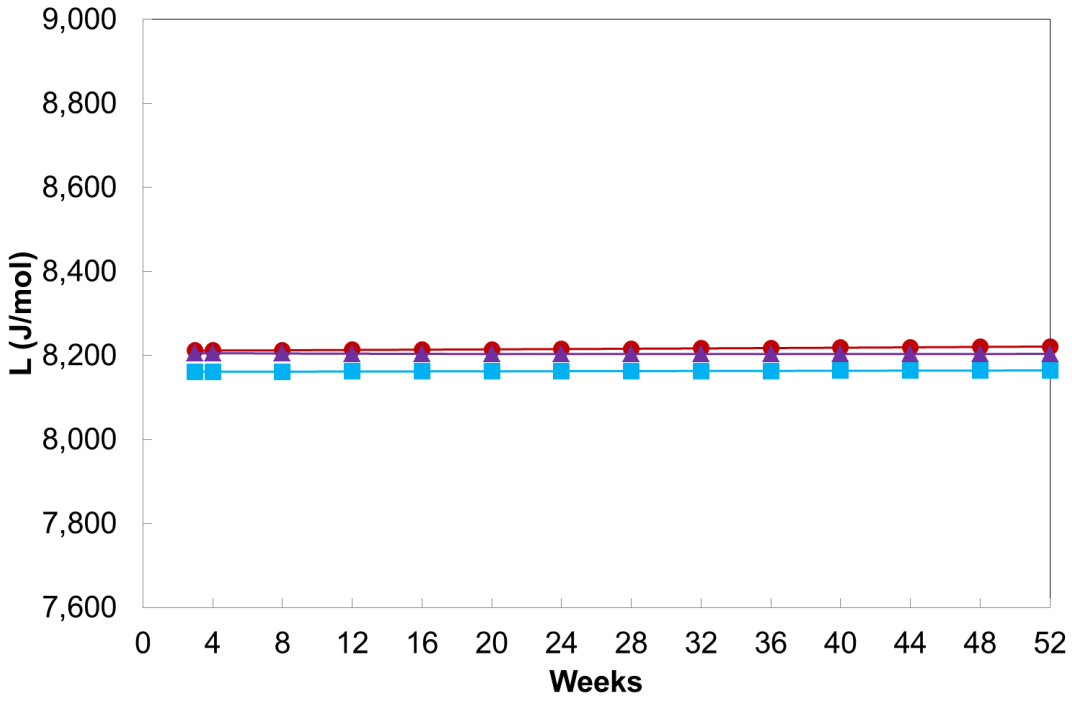

Figure 5.3 **Latent heat verification isothermal & superheated vapour – LNG-like.**
(C_1: 96% mol, C_2: 4% mol; -●- L_{ref}; -■- L_{iso}; -▲- L_{shv})

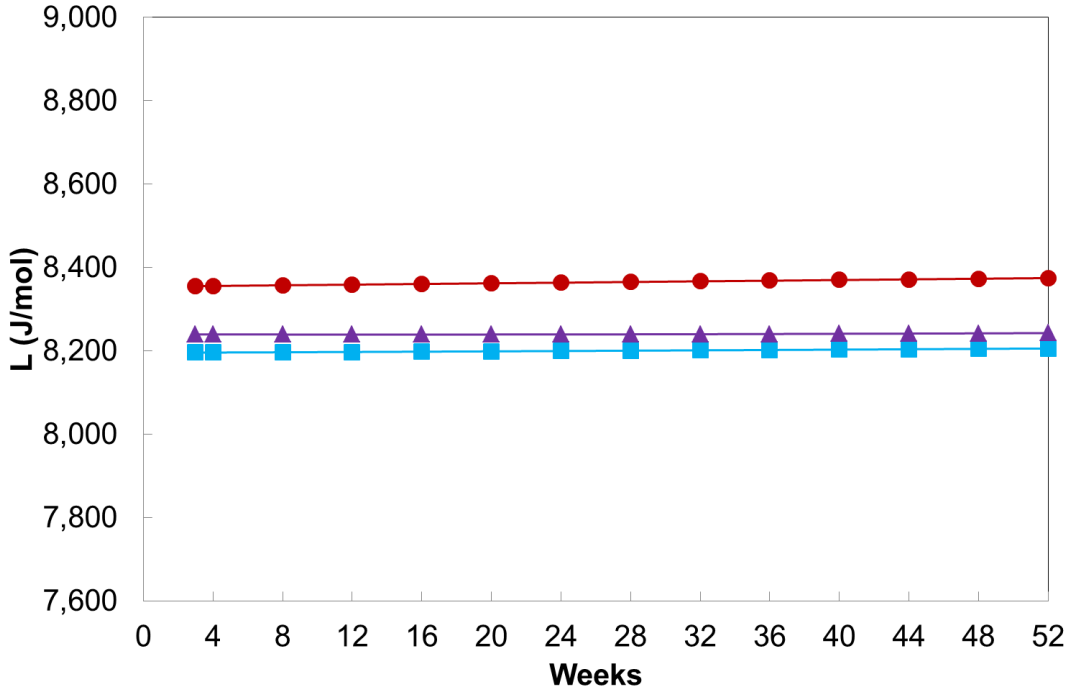

Figure 5.4 **Latent heat verification isothermal & superheated vapour – C_2 rich.**
(C_1: 89% mol, C_2: 11% mol; -●- L_{ref}; -■- L_{iso}; -▲- L_{shv})

For the LNG-like mixture case (Figure 5.3), the deviation of predicted latent heat over the weathering period by both models is lower than 0.7%, when compared to the reference latent heat; whilst in the C_2 rich mixture case (Figure 5.4) the deviation is within 1%-2%.

Latent heat for both mixtures is nearly constant, and very close to pure methane latent heat, over the weathering period. In the LNG-like mixture case, average latent heat is 8,216 J/mol vs. 8,170 J/mol for pure methane. For the C_2 rich case, the average latent heat is 8,364 J/mol (vs. 8,170 J/mol for pure methane). Those estimates of latent heats, and its behaviour over the weathering period, are an indication that boiling temperature hardly changes and so indirect latent heat for both mixtures, as a result of vapour being mainly methane. Moreover, it can be also deduced from Figures 5.3 and 5.4 that indirect latent heat is very low, and is a very small portion of the overall latent heat for both mixtures. That is confirmed by Figure 5.5, showing the indirect latent heat evolution (calculated from eq. (5.4)). For the LNG-like case, the $L_{indirect}$ contribution represents 0.3% of the overall latent heat at the beginning of the weathering period, and 0.4% by the end, for both, the isothermal and superheated vapour models; whilst for the C_2 rich case, that contribution represents around 1.6% at the beginning of the weathering process, and 1.8% by the end, for both modelling approaches.

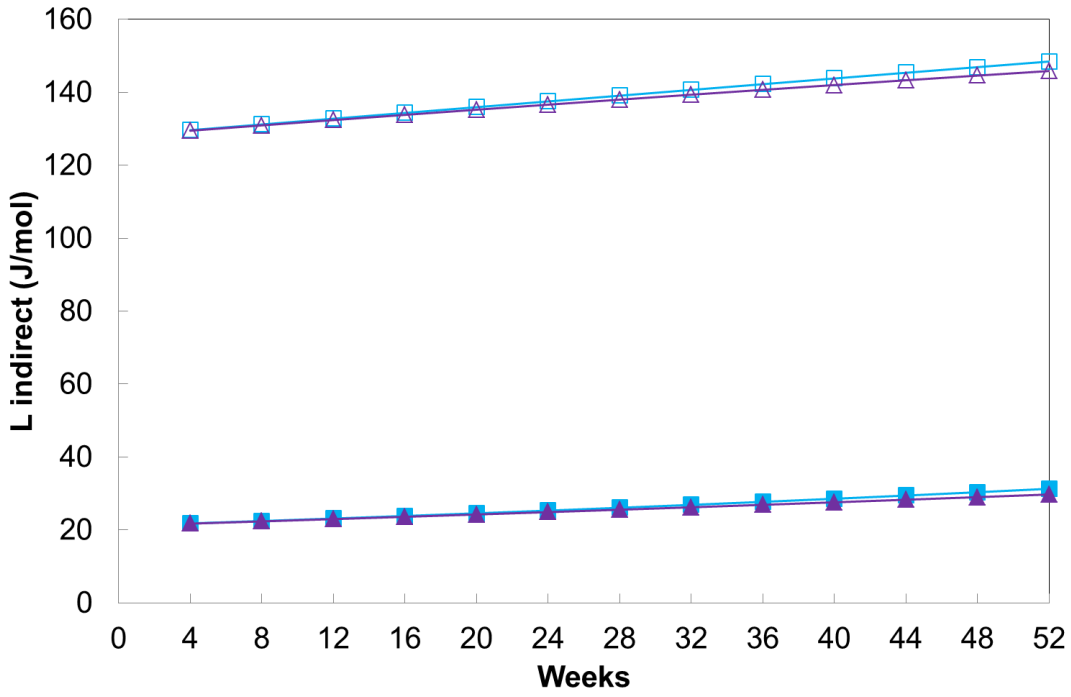

Figure 5.5 Indirect latent heat evolution.
(-■- Iso. LNG-like, -▲- Sup. LNG-like - C_1: 96% mol, C_2: 4% mol;
-□- Iso. C_2 rich , -△- Sup. C_2 rich - C_1: 89% mol, C_2: 11% mol)

Figures 5.6 and 5.7 respectively show the boiling temperature evolution and methane mol vapour fraction for both mixtures (LNG-like and C_2 rich mixtures), using both weathering models, isothermal and superheated vapour.

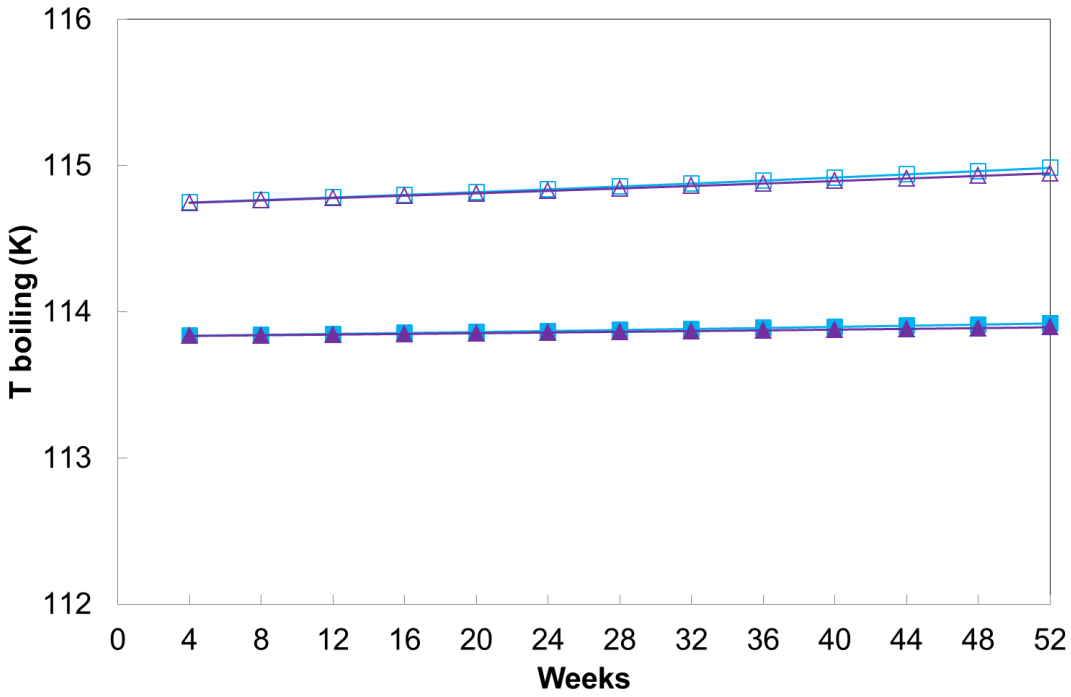

Figure 5.6 Boiling temperature evolution.
(-■- Iso. LNG-like, -▲- Sup. LNG-like - C_1: 96% mol, C_2: 4% mol;
-□- Iso. C_2 rich , -△- Sup. C_2 rich - C_1: 89% mol, C_2: 11% mol)

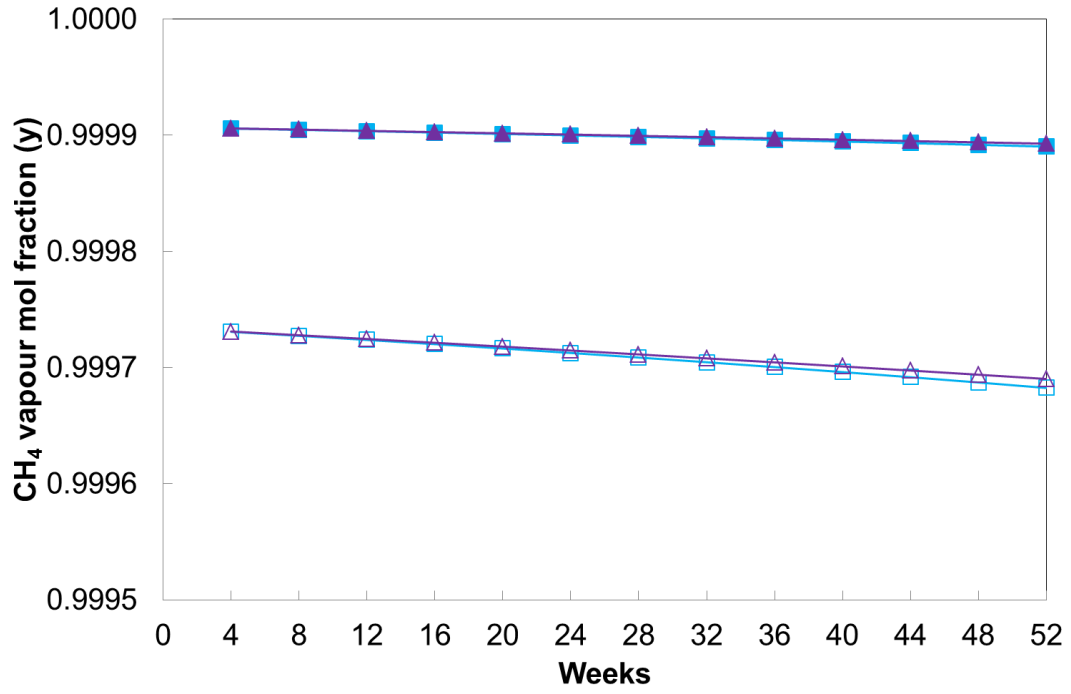

Figure 5.7 Methane vapour mol fraction evolution.
(-■- Iso. LNG-like, -▲- Sup. LNG-like - C_1: 96% mol, C_2: 4% mol;
-□- Iso. C_2 rich, -△- Sup. C_2 rich - C_1: 89% mol, C_2: 11% mol)

In the C_2 rich case, it is shown that by the end of the assessment period (near week 52) the boiling temperature of the weathered mixture reaches 115 K (refer to Figure 5.6), which is the maximum temperature validity limit for the Revised Klosek-McKinley method, used by both LNG weathering models to calculate the liquid density. Using that method at the temperature specification limit, may lead to estimation errors when calculating the liquid density of the weathered mixture. In the LNG-like mixture case, methane content and boiling temperature are within the specification limits of the density calculation method at all times along the assessed weathering period.

Figures 5.8 and 5.9 show the heat input into the LNG and the LNG volume evolution respectively, over the assessed weathering period.

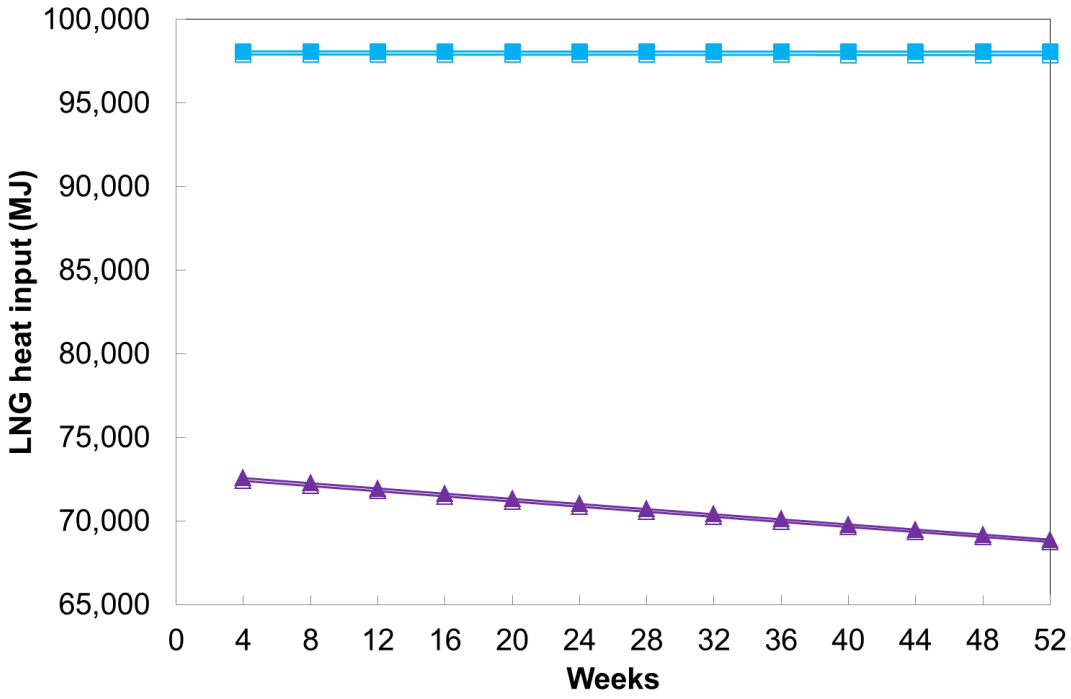

Figure 5.8 LNG heat input vs. time.
(-■- Iso. LNG-like, -▲- Sup. LNG-like - C_1: 96% mol, C_2: 4% mol;
-□- Iso. C_2 rich, -△- Sup. C_2 rich - C_1: 89% mol, C_2: 11% mol)

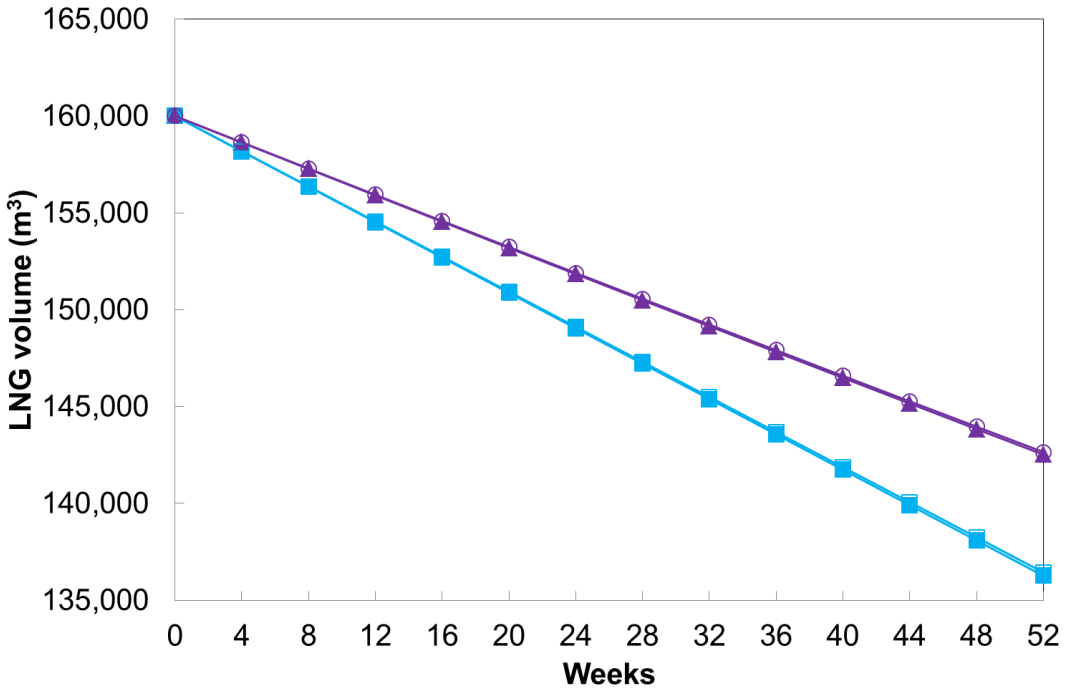

Figure 5.9 Liquid volume evolution.
(-■- Iso. LNG-like, -▲- Sup. LNG-like - C_1: 96% mol, C_2: 4% mol;
-□- Iso. C_2 rich, -△- Sup. C_2 rich - C_1: 89% mol, C_2: 11% mol)

From Figure 5.8 it is observed that the heat input into the LNG in the isothermal model case is greater than the superheated vapour case at all times over the weathering period, thus following the expected behaviour. As discussed in Chapter 4, for the isothermal model case all the heat entering into the tank is used to vaporize the liquid; whilst in the superheated vapour model the heat used for vaporization is a portion of the total, since the influence of the heat influx is separated into the liquid and vapour sides of the tank. Furthermore, the heat input evolution in the superheated vapour case progressively decreases in time, concurrently with the liquid drop in the storage tank (refer to Figure 5.9), owing the reduction of the wet heat transfer area as the mixture is vaporized from the tank. In this regard, at the beginning of the weathering process the LNG heat input in the superheated vapour represents 74.0% of the heat used in the isothermal model case; after 52 weeks that contributions drops to 70.2%.

From Figure 5.9 one can observe that the liquid volume drops quicker for the isothermal model case than in the superheated vapour. That is not surprising as more liquid is

vaporized in the isothermal case due to the greater heat input. Whilst for the superheated vapour the liquid volume drops by around 11% over the weathering period, for the isothermal model the decrease is around 15%.

Figure 5.10 and 5.11 show the results of the latent heat verification test for the N_2 rich case, for the isothermal and superheated vapour models respectively.

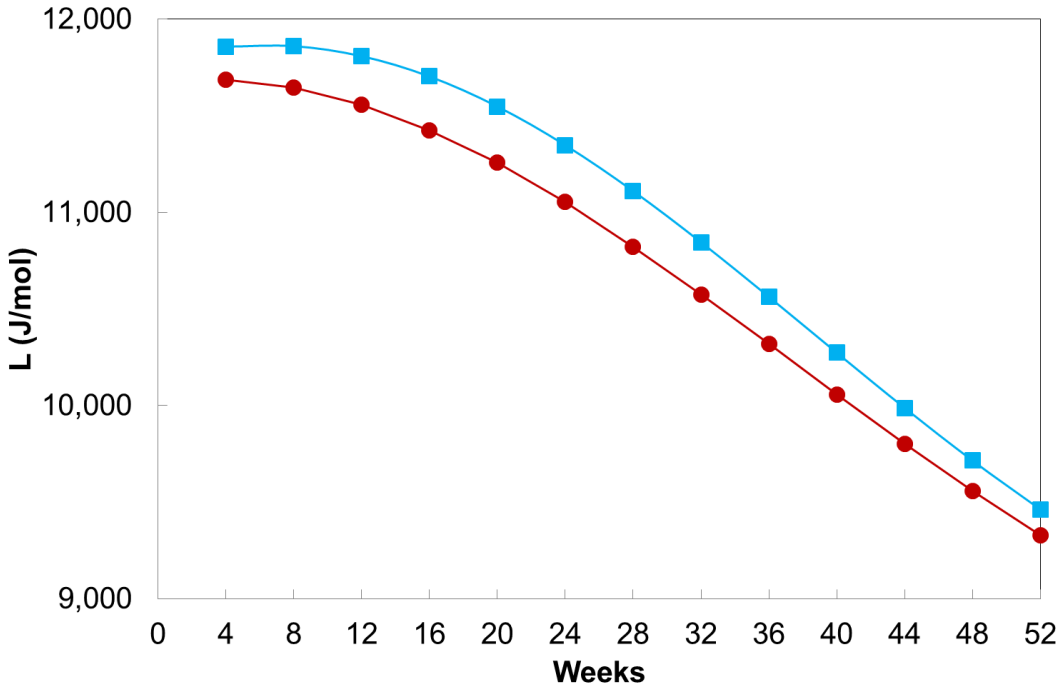

Figure 5.10 Latent heat verification Isothermal model - N_2 rich.
(C_1: 96% mol, N_2: 4% mol; -●- L_{ref}; -■- L_{iso})

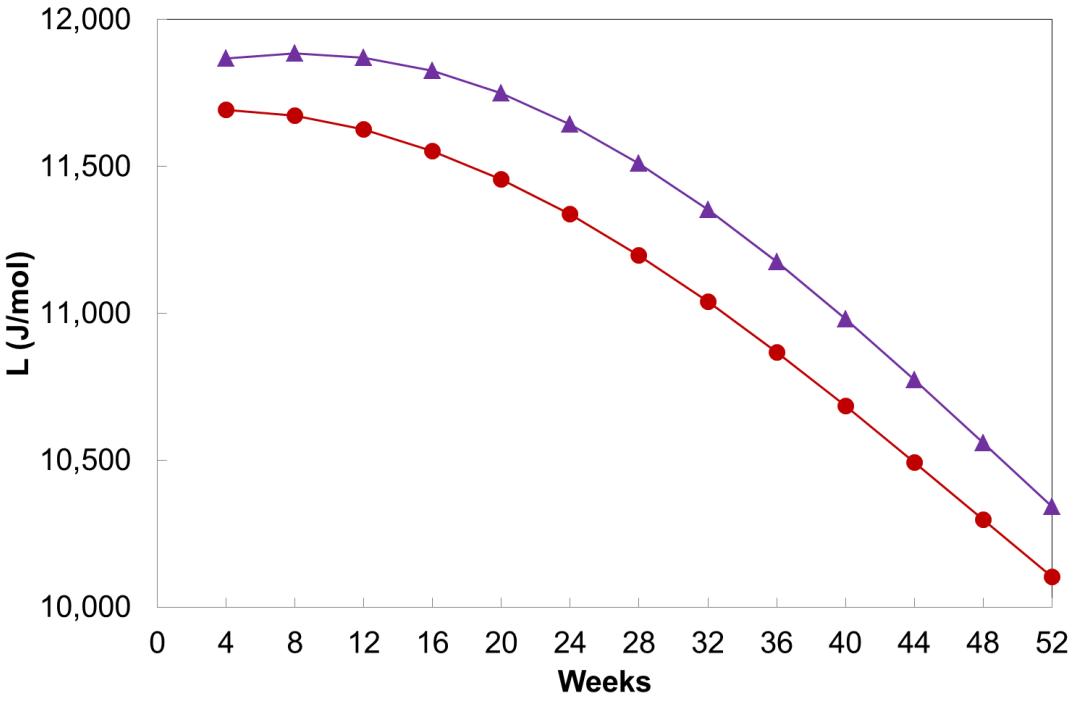

Figure 5.11 Latent heat verification superheated vapour model - N_2 rich.
(C_1: 96% mol, N_2: 4% mol; -●- L_{ref}, -▲- L_{shv})

In the N_2 rich case (Figures 5.10 and 5.11), the observed deviation between the corresponding reference latent heat and the value predicted by both models is of the order of 2.0%.

Although there is a good agreement between predicted L and L_{ref}, it is important to mention that at the early stage of weathering the initial N_2 content of the mixture is 4% mol, which is the maximum specification validity limit of the Revised Klosek-McKinley method for the liquid density.

It is worth noting for this verification that at the early stage of weathering, as the tank is nearly full, the latent heat approximation could be a good one. As the tank begins to empty, the contact area will play an important part in the heat ingress, which is particularly important within the superheated vapour model approach.

Figure 5.12 shows the $L_{indirect}$ evolution for the N_2 rich mixture case, using both models.

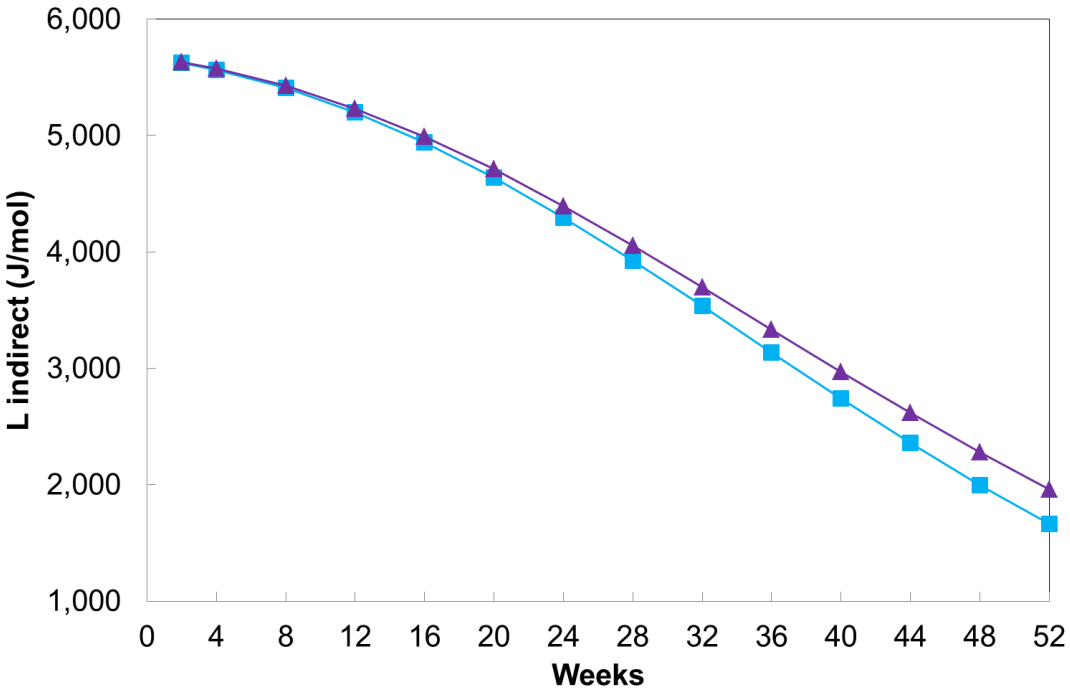

Figure 5.12 Indirect latent heat evolution - N_2 rich.
(-■- Iso. Model, -▲- Sup. vapour model; C_1: 96% mol, N_2: 4% mol)

In the N_2 rich mixture case the contribution of the $L_{indirect}$ to the overall latent heat is significantly higher compared to the full alkane mixture cases (LNG-like and C_2 rich case), with the evolution pattern having a reverse effect. Whilst for the C_1-C_2 mixtures the contribution of the $L_{indirect}$ slightly increases by the end of the weathering process, in the N_2 rich mix the contribution decreases as N_2 is exhausted from the mixture. At the beginning of the weathering process the contribution of $L_{indirect}$ to the overall latent heat represents 42.8% and 42.9% for the isothermal and superheated vapour models respectively; and by the end that contribution is reduced down to 16.0% and 18.4% for the isothermal and superheated vapour models respectively.

Figures 5.13, 5.14 and 5.15 show the boiling temperature evolution, vapour methane mol fraction and heat input respectively, for the N_2 rich mixture using both weathering models.

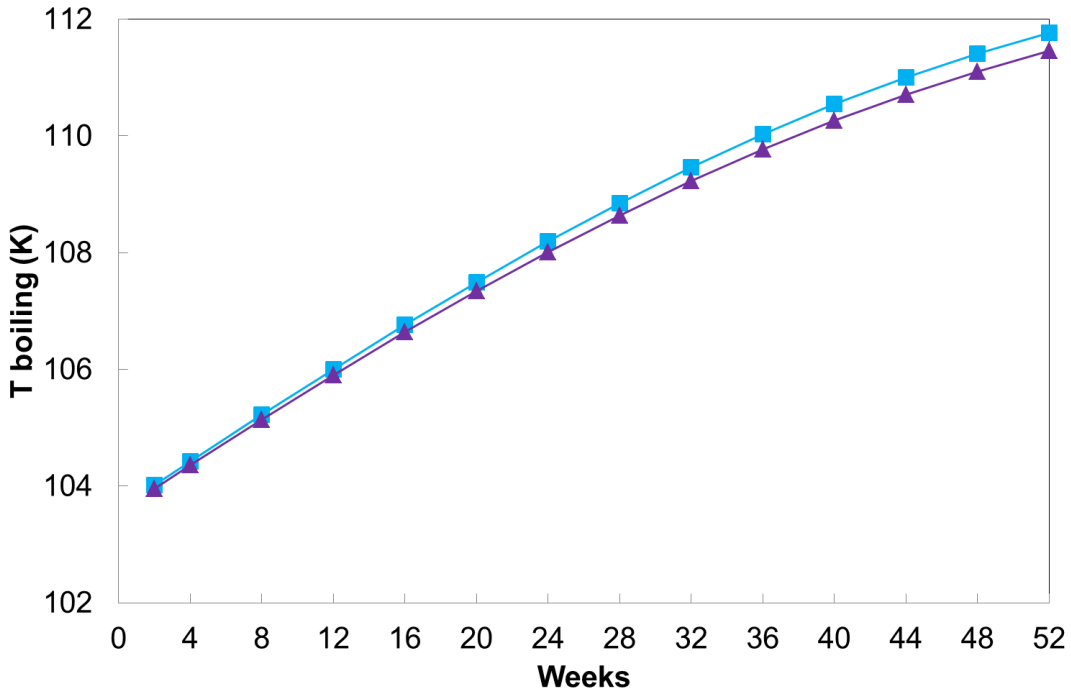

Figure 5.13 Boiling temperature evolution – N_2 rich.
(-■- Iso. Model, -▲- Sup. vapour model; C_1: 96% mol, N_2: 4% mol)

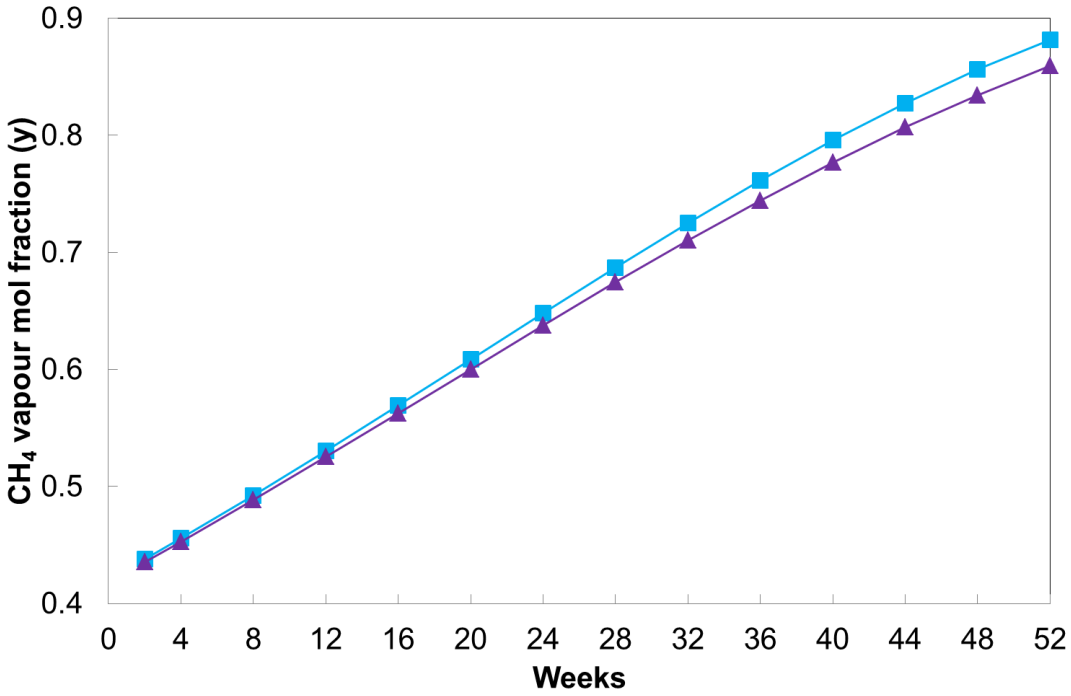

Figure 5.14 Methane vapour mol fraction evolution – N_2 rich.
(-■- Iso. Model, -▲- Sup. vapour model; C_1: 96% mol, N_2: 4% mol)

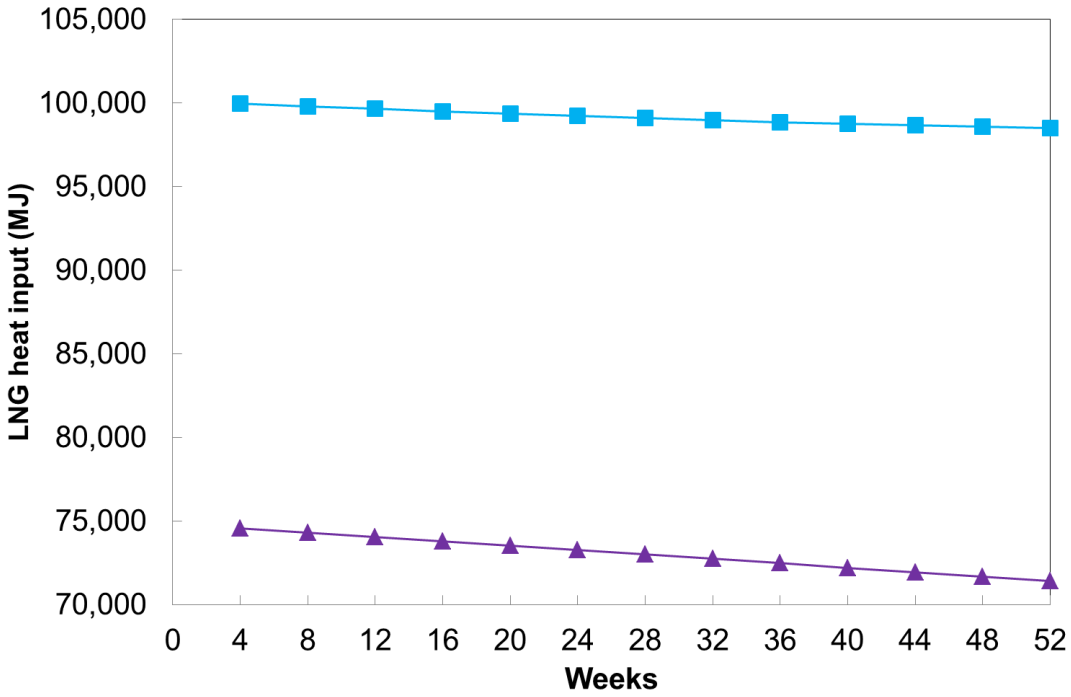

Figure 5.15 LNG heat input vs. time – N_2 rich.
(-■- Iso. Model, -▲- Sup. vapour model; C_1: 96% mol, N_2: 4% mol)

Heat input into the LNG in the isothermal model case is greater than the superheated vapour case at all times over the weathering period, and follows the expected behaviour. As discussed earlier, that is due to the larger heat input into the LNG estimated by the isothermal model over the superheated vapour model approach.

The heat input evolution for both models progressively decreases in time, although the reasons behind the drop are different for each modelling approach. The drop in the isothermal model case is due to the increase of the boiling temperature of the weathered liquid remaining in the tank, as N_2 is exhausted from the mixture.

In the superheated vapour case however, as the liquid is vaporized from the tank the heat transfer area is reduced, thus less heat enters into the LNG. The heat input into the LNG decrease concurrently with the liquid drop in the storage tank (refer to Figure 5.16). At the beginning of the weathering process the heat input in the superheated vapour represents 74.6% of the isothermal model case, and after 52 weeks that contributions drops to 72.5%.

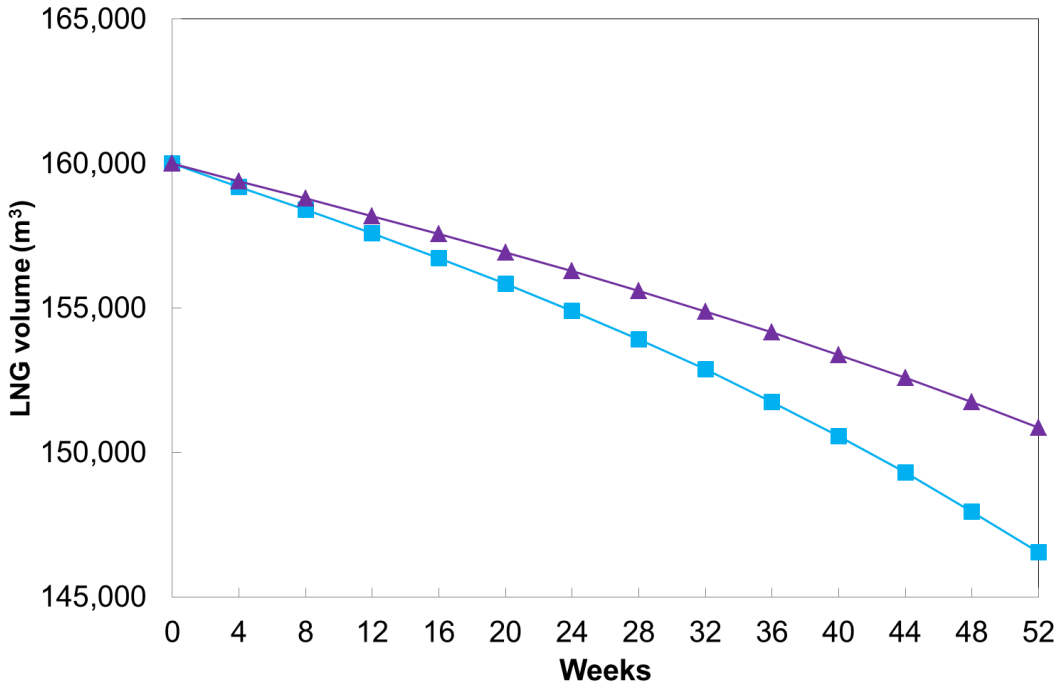

Figure 5.16 Liquid volume evolution.
(-■- Iso. Model, -▲- Sup. vapour model; C_1: 96% mol, N_2: 4% mol)

Concerning the liquid volume, it drops quicker for the isothermal model case than the superheated vapour. Same as in the C_1-C_2 mixtures cases before, that is the expected performance as more liquid is vaporized in the isothermal case due to the greater heat input into the LNG. Whilst for the superheated vapour the liquid volume drops 5.7% over the weathering period, for the isothermal model the estimated decrease is around 8.4%.

As a general conclusion it is shown that the differential latent heat calculated by the two modelling methods for the three mixtures is in good agreement. For the C_2 rich case the agreement is within 1% to 2%; less than 0.7% for the LNG-like case and within 2% for the N_2 rich case.

5.3 COMPARISON AGAINST PREVIOUS STUDIES AND MEASURED DATA

As an additional verification test the weathering predictions of both models were compared with selected LNG weathering data obtained from historical cargo measurements [2]. The

same data were used by Miana *et al.* [2] to assess their models (physical model and i-model), specifically developed for LNG weathering during ship transportation.

Same as in LNG storage tanks, LNG is continuously vaporized as BOG during ship transport. The amount of BOG generated depends on a number of factors, such as ship and cargo tank design, storage insulation and operating conditions, and sea condition during voyage. A BOR around 0.10-0.15% v/v of the full transported cargo content per day is typical over a 20 days journey [6]. Within this context, the amount of BOG produced is of order of 2-3% v/v of the total volume transported. Considering the total LNG trade movement in 2014 was 333.3 Gm^3 [7], then the BOG generated can reach up to 10 Gm^3 in one year, in ship transport only. That amount is equivalent to the annual gas consumption of countries like Singapore and Vietnam, with 9.7 Gm^3 and 9.2 Gm^3 [7], respectively; and is close to the total LNG imported by the United Kingdom in 2014, 11.3 Gm^3 [7]. The BOG generated in an LNG carrier during the voyage is used in its propulsion system, in most of the cases. Most of the LNG fleet currently in operation is equipped with a steam plant that uses BOG and liquid fuel to fire the boilers to produce steam. The steam is used to drive the turbines that propels the ship.

As measured data were obtained for LNG weathering during the marine transport, a minor change was incorporated in the heat transfer module of the isothermal and superheated vapour weathering models. By making use of a constant BOR of 0.15% v/v of the total cargo per day quoted Miana *et al.* [2] and routinely used in the LNG shipping industry, the overall heat transfer coefficient for the LNG (wet) side has been adjusted to U_{wet} = 0.3756 W/m^2 K in equations (4.11) and (4.15). Hence this verification tests only the thermodynamic module and mass balance equations that have been implemented in both models. An additional assessment is presented later in this section using the adjusted (U_{wet}) for LNG shipping (U_{wet} = 0.3756 W/m^2 K), to compare the BOG generation predicted by both models to that predicted by Hasan *et al.* [6] during LNG ship transport.

In both comparison assessments, to Miana *et al.* [2] and to Hasan *et al.* [6], the overall heat transfer coefficient for the vapour (dry) side and for both weathering models has been kept to U_{dry} = 0.02832 W/m^2 K, as presented in Table 4.3 in Chapter 4.

The following sections explain the assumptions and the calculation procedure to adjust U_{wet} (U_{wet} = 0.3756 W/m^2 K), and presents the performance comparison of both weathering models to the published work by Miana *et al.* [2] and Hasan *et al.* [6].

5.3.1 OVERALL HEAT TRANSFER COEFFICIENT ADJUST

Assuming the LNG storage tank is fully loaded with pure methane, the adjusted wet overall heat transfer coefficient is calculated based on an allowable heat input into the storage tank that fulfils the target BOR of 0.15% v/v that has evaporated in one day relative to the initial gross tank volume. Assuming that all heat enters through the tank lateral wall, the wet overall heat transfer coefficient is calculated from the heat transfer equation (3.104) as follows:

$$U_{wet} = \frac{\dot{Q}}{A_m(T_{air} - T_{LNG})} \tag{5.10}$$

Where $\dot{Q}$ is the heat rate input through the tank lateral wall into the LNG, A_m is the mean heat transfer area, T_{air} is the air outside temperature and T_{LNG} is the LNG temperature. It is assumed that all heat entering into the LNG comes from the LNG tank lateral wall, and then the heat contributions from roof and bottom thermal slab are omitted from the adjusted U_{wet} calculation.

Table 5.8 summarizes the LNG storage tank characteristics, data and assumptions used to calculate the adjusted overall wet heat transfer coefficient.

Table 5.8 LNG storage tank data and assumptions to calculate U_{wet}.

LNG volume, V_L	160,000 m^3
Tank operating pressure, P	116.3 kPa (150 mbarg)
Air temperature, T_{air}	298.2 K
LNG (methane) temperature, T_{LNG}	113.2 K
LNG density (pure methane), d	421.0 kg/m^3
Methane molecular weight, MW	16.04 kg/kmol
Methane heat of vaporization, L [1]	8,170 kJ/kmol
Tank internal diameter, D_i	76.4 m
Tank external diameter, D_o	80.0 m

To determine the adjusted overall wet heat transfer coefficient, one calculates first the heat input into the LNG from the target BOR that is the amount of LNG vaporized in one day.

The amount of LNG vaporized in one day $\dot{m}_{LNG}$ is calculated as follows:

$$\dot{m}_{LNG} = \frac{0.15 V_{LNG} d}{100} = 101{,}040 \ \frac{kg}{d} \qquad (5.11)$$

The heat rate input into the LNG is calculated by:

$$\dot{Q} = \frac{\dot{m}_{LNG} L}{M} = 51.465 \,.\, 10^6 \ \frac{kJ}{d} = 595.66 \ kW \qquad (5.12)$$

The mean heat transfer area (wet side) is calculated from the lateral wall of the LNG storage tank. That is considering the storage tank as a cylinder and using the equivalent diameter D_{eq}, as shown in Figure 5.17.

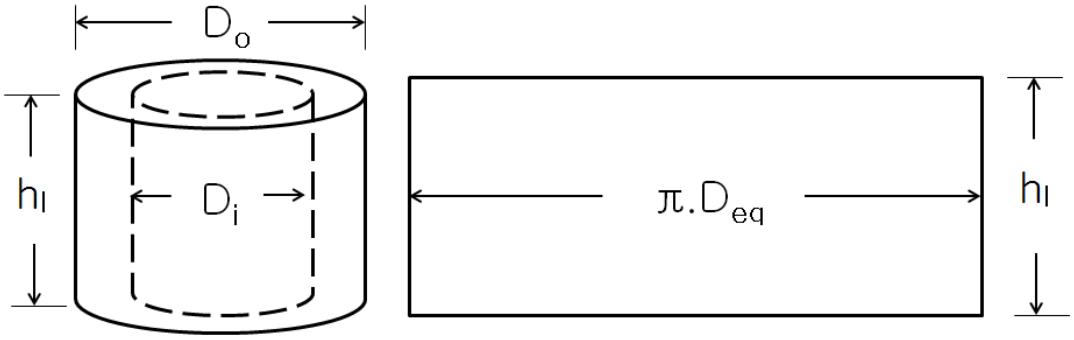

Figure 5.17 Wet heat transfer area (lateral wall) LNG storage tank.

The mean heat transfer area is calculated as follows:

$$A_m = \pi D_{eq} h_l \tag{5.13}$$

where h_l is the tank liquid height.

The tank liquid height is calculated from the stored LNG volume V_L in the tank, using the internal diameter:

$$V_L = \frac{\pi {D_i}^2}{4} h_l \tag{5.14}$$

$$h_l = \frac{4.}{\pi {D_i}^2} V_L = 34.90\ m \tag{5.15}$$

The equivalent diameter D_{eq} is calculated as follows:

$$D_{eq} = \frac{D_o - D_i}{\ln(D_o/D_i)} = 78.19\ m \tag{5.16}$$

Substituting h_l and D_{eq} in eq. (5.13), the mean heat transfer area is:

$$A_m = \pi D_{eq} h_l = 8{,}572.90\ m^2 \tag{5.17}$$

The adjusted wet overall heat transfer coefficient U_{wet} is then calculated with $\dot{Q}$, A_m, T_{LNG} and T_{air}:

$$U_{wet} = \frac{\dot{Q}}{A_m(T_{air} - T_{LNG})} = 0.3756 \ \frac{w}{m^2 K} \quad (5.18)$$

5.3.2 COMPARISON TO SELECTED LNG WEATHERING DATA

Miana *et al.* [2], in their study, compared the predictions of their weathering models (physical and i-model) with selected data obtained from historical cargo measurements received at different LNG regasification facilities located in Spain. The isothermal and superheated vapour weathering models were tested against the Miana *et al*. [2] models predictions, as well as the actual measured data (aimed for custody transfer purposes) from the regasification terminals published in Miana *et al*. [2].

Concerning the comparison to actual measured data, it is important to take into account the uncertainty associated to those measurements. The GIIGNL Handbook [8] refers to a US National Bureau of Standards (NBS) study [9] for estimation of uncertainty in measured composition and calculated gross or higher heating value for LNG custody transfer. The uncertainty in the measured LNG composition can be considered to be composed of two main elements. The first is from the sampling system and its operating conditions, and the second is from the gas analysis by chromatography. The GIIGNL Handbook [8] indicates by reference to the NBS study [9] that the combined uncertainty in measured LNG composition due to sampling and analysis is ±0.3%. With regards to the calculated higher heating value, the only source that contributes to the uncertainty is the higher calorific value of the components contained in the mixture, which is estimated to be ±0.04% according to the NBS [9].

The following tables (Tables 5.9 to 5.13) show the results obtained for five selected journeys. The tables are presented following the same setups and terminology used by Miana *et al*. [2] in their study, adding additional columns for the LNG weathering prediction of each model, as well as the absolute difference (deviation *Dev*) to the actual measured composition value at the receiving terminal (weathered LNG). The absolute deviation *Dev* is calculated using equation (5.1), where x_{ref} is the measured value and x_{mod} is the value predicted by the corresponding model. For the rest of the variables the percentage of deviation % *Dev*, calculated using equation (5.2), is presented.

Reported HHV and WI values of the LNG cargo were measured at the destination port with temperature and pressure of 0 ºC and 0.1 MPa, respectively, as the reference conditions.

Table 5.9 LNG weathering prediction for a cargo example Journey 1.

Trip duration (h) =	126.5
Tank capacity (m^3) =	138,500
Volume (m^3) =	136,102
Pressure origin (mbar) =	1128
P destination (mbar) =	1138

Component, mol %	Port origin measured	Port destination measured	Port destination physical model	Physical model Dev	Port destination i-model	i-model Dev	Port destination isothermal model	Isothermal model Dev	Port destination Superheated vapour model	Superheated vapour model Dev
N2	0.00030	0.00028	0.00030	-0.00002	0.00039	-0.00011	0.00025	0.00003	0.00025	0.00003
C1	0.97180	0.97294	0.97156	0.00138	0.97581	-0.00287	0.97162	0.00132	0.97160	0.00134
C2	0.02480	0.02410	0.02504	-0.00094	0.02102	0.00308	0.02500	-0.00090	0.02502	-0.00092
C3	0.00170	0.00156	0.00170	-0.00014	0.00170	-0.00014	0.00171	-0.00015	0.00172	-0.00016
iC4	0.00060	0.00057	0.00060	-0.00003	0.00052	0.00005	0.00060	-0.00003	0.00061	-0.00004
nC4	0.00030	0.00029	0.00030	-0.00001	0.00030	-0.00001	0.00030	-0.00001	0.00030	-0.00001
iC5	0.00000	0.00019	0.00000	0.00019	0.00020	-0.00001	0.00000	0.00019	0.00000	0.00019
nC5	0.00050	0.00007	0.00050	-0.00043	0.00008	-0.00001	0.00050	-0.00043	0.00050	-0.00043
BOR (%)	-	0.16	0.15	0.01	0.23	-0.07	0.15	0.01	0.17	-0.01
				% Dev		% Dev		% Dev		% Dev
Temperature (K)	113.4	113.4	113.2	0.18	113.6	-0.18	113.4	0.00	113.4	0.00
Volume (m^3)	136,102	134,984	135,034	-0.04	134,486	0.37	135,014	-0.02	134,908	0.06
WI (kWh/m^3) 0°C/0°C	15.039	15.031	15.042	-0.07	15.014	0.11	15.041	-0.07	15.041	-0.07
HHV (kWh/m^3)	11.367	11.347	11.367	-0.18	11.322	0.22	11.368	-0.19	11.366	-0.17
Density (kg/m^3)	429.596	429.052	429.964	-0.21	427.982	0.25	429.694	-0.15	429.698	-0.15

Table 5.10 LNG weathering prediction for a cargo example Journey 2.

Trip duration (h) =	390.0
Tank capacity (m^3) =	137,661
Volume (m^3) =	136,089
P origin (mbar) =	1084
P destination (mbar) =	1140

Component, mol %	Port origin measured	Port destination measured	Port destination physical model	Physical model Dev	Port destination i-model	i-model Dev	Port destination isothermal model	Isothermal model Dev	Port destination Superheated vapour model	Superheated vapour model Dev
N2	0.00360	0.00186	0.00193	-0.00007	0.00146	0.00040	0.00222	-0.00036	0.00213	-0.00027
C1	0.90300	0.90142	0.90273	-0.00131	0.90100	0.00042	0.90219	-0.00077	0.90204	-0.00062
C2	0.06160	0.06399	0.06315	0.00084	0.06495	-0.00096	0.06304	0.00095	0.06320	0.00079
C3	0.02250	0.02300	0.02289	0.00011	0.02291	0.00009	0.02303	-0.00003	0.02309	-0.00009
iC4	0.00370	0.00389	0.00370	0.00019	0.00403	-0.00014	0.00379	0.00010	0.00380	0.00009
nC4	0.00550	0.00578	0.00550	0.00028	0.00550	0.00028	0.00563	0.00015	0.00564	0.00014
iC5	0.00010	0.00005	0.00010	-0.00005	0.00012	-0.00007	0.00010	-0.00005	0.00010	-0.00005
nC5	0.00000	0.00001	0.00000	0.00001	0.00003	-0.00002	0.00000	0.00001	0.00000	0.00001
BOR (%)	-	0.13	0.15	-0.02	0.16	-0.03	0.13	0.00	0.14	-0.01
				% Dev		% Dev		% Dev		% Dev
Temperature (K)	113.3	113.3	113.5	-0.18	114.4	-0.97	113.5	-0.18	113.5	-0.18
Volume (m^3)	136,089	133,147	132,816	0.25	132,553	0.45	133,305	-0.12	132,993	0.12
WI (kWh/m^3) 0°C/0°C	15.439	15.494	15.483	0.07	15.506	-0.08	15.480	0.09	15.483	0.07
HHV (kWh/m^3) 0°C/0°C	12.178	12.236	12.217	0.16	12.247	-0.09	12.220	0.13	12.221	0.12
Density (kg/m^3)	457.035	457.710	456.891	0.18	456.236	0.32	457.495	0.05	457.498	0.05

Table 5.11 LNG weathering prediction for a cargo example Journey 3.

Trip duration (h) =	98.0
Tank capacity (m^3) =	30,000
Volume (m^3) =	28,818
P origin (mbar) =	1100
P destination (mbar) =	1125

Component, mol %	Port origin measured	Port destination measured	Port destination physical model	Physical model Dev	Port destination i-model	i-model Dev	Port destination isothermal model	Isothermal model Dev	Port destination Superheated vapour model	Superheated vapour model Dev
N2	0.00715	0.00383	0.00615	-0.00232	0.00463	-0.00080	0.00632	-0.00249	0.00595	-0.00212
C1	0.87417	0.87722	0.87450	0.00272	0.87539	0.00183	0.87441	0.00281	0.87447	0.00275
C2	0.08950	0.09018	0.09007	0.00011	0.09079	-0.00061	0.08995	0.00023	0.09018	0.00000
C3	0.02226	0.02210	0.02236	-0.00026	0.02238	-0.00028	0.02237	-0.00027	0.02243	-0.00033
iC4	0.00286	0.00276	0.00286	-0.00010	0.00275	0.00001	0.00287	-0.00011	0.00288	-0.00012
nC4	0.00370	0.00355	0.00370	-0.00015	0.00370	-0.00015	0.00372	-0.00017	0.00373	-0.00018
iC5	0.00019	0.00020	0.00019	0.00001	0.00019	0.00001	0.00019	0.00001	0.00019	0.00001
nC5	0.00017	0.00016	0.00017	-0.00001	0.00016	0.00000	0.00017	-0.00001	0.00017	-0.00001
BOR (%)	-	0.06	0.15	-0.09	0.12	-0.06	0.09	-0.03	0.14	-0.08
				% Dev		% Dev		% Dev		% Dev
Temperature (K)	111.8	113.1	112.3	0.71	113.4	-0.27	112.0	0.92	112.1	0.80
Volume (m^3)	28,818	28,748	28,643	0.37	28,672	0.26	28,709	0.14	28,652	0.33
WI (kWh/m^3) 0°C/0°C	15.467	15.528	15.489	0.25	15.519	0.06	15.486	0.27	15.495	0.21
HHV (kWh/m^3) 0°C/0°C	12.311	12.347	12.312	0.28	12.336	0.09	12.328	0.15	12.332	0.12
Density (kg/m^3)	465.735	462.959	464.973	-0.44	463.188	-0.05	466.111	-0.68	458.569	0.95

Table 5.12 LNG weathering prediction for a cargo example Journey 4.

Trip duration (h) =	258.0
Tank capacity (m^3) =	134,487
Volume (m^3) =	129,969
P origin (mbar) =	1090
P destination (mbar) =	1185

Component, mol %	Port origin measured	Port destination measured	Port destination physical model	Physical model Dev	Port destination i-model	i-model Dev	Port destination isothermal model	Isothermal model Dev	Port destination Superheated vapour model	Superheated vapour model Dev
N2	0.00065	0.00035	0.00043	-0.00008	0.00047	-0.00012	0.00045	-0.00010	0.00044	-0.00009
C1	0.92753	0.92605	0.92658	-0.00053	0.92612	-0.00007	0.92650	-0.00045	0.92641	-0.00036
C2	0.04843	0.04789	0.04922	-0.00133	0.04945	-0.00156	0.04926	-0.00137	0.04933	-0.00144
C3	0.01976	0.02037	0.02008	0.00029	0.02002	0.00035	0.02010	0.00027	0.02013	0.00024
iC4	0.00191	0.00260	0.00194	0.00066	0.00220	0.00040	0.00194	0.00066	0.00195	0.00065
nC4	0.00161	0.00265	0.00164	0.00101	0.00161	0.00104	0.00164	0.00101	0.00164	0.00101
iC5	0.00011	0.00008	0.00011	-0.00003	0.00009	-0.00001	0.00011	-0.00003	0.00011	-0.00003
nC5	0.00000	0.00001	0.00000	0.00001	0.00004	-0.00003	0.00000	0.00001	0.00000	0.00001
BOR (%)	-	0.20	0.15	0.05	0.18	0.02	0.15	0.05	0.16	0.04
				% Dev		% Dev		% Dev		% Dev
Temperature (K)	113.7	114.5	114.4	0.09	114.4	0.09	114.4	0.09	114.4	0.09
Volume (m^3)	129,969	127,168	127,894	-0.57	127,513	-0.27	127,867	-0.55	127,685	-0.41
WI (kWh/m^3) 0°C/0°C	15.336	15.367	15.347	0.13	15.350	0.11	15.347	0.13	15.348	0.12
HHV (kWh/m^3) 0°C/0°C	11.914	11.914	11.928	-0.12	11.936	-0.18	11.930	-0.13	11.928	-0.12
Density (kg/m^3)	446.697	446.832	446.042	0.18	446.224	0.14	446.260	0.13	446.287	0.12

Table 5.13 LNG weathering prediction for a cargo example Journey 5.

Trip duration (h) =	283.5
Tank capacity (m^3) =	140,500
Volume (m^3) =	137,936
Pressure origin (mbar) =	1117
P destination (mbar) =	1126

Component, mol %	Port origin measured	Port destination measured	Port destination physical model	Physical model Dev	Port destination i-model	i-model Dev	Port destination isothermal model	Isothermal model Dev	Port destination Superheated vapour model	Superheated vapour model Dev
N2	0.00011	0.00020	0.00011	0.00009	0.00029	-0.00009	0.00008	0.00012	0.00007	0.00013
C1	0.96691	0.96519	0.96635	-0.00116	0.96427	0.00092	0.96633	-0.00114	0.96627	-0.00108
C2	0.02758	0.02931	0.02814	0.00117	0.02973	-0.00042	0.02809	0.00122	0.02814	0.00117
C3	0.00447	0.00448	0.00447	0.00001	0.00447	0.00001	0.00455	-0.00007	0.00456	-0.00008
iC4	0.00042	0.00032	0.00042	-0.00010	0.00038	-0.00006	0.00043	-0.00011	0.00043	-0.00011
nC4	0.00033	0.00036	0.00033	0.00003	0.00033	0.00003	0.00034	0.00002	0.00034	0.00002
iC5	0.00018	0.00008	0.00018	-0.00010	0.00008	0.00000	0.00018	-0.00010	0.00018	-0.00010
nC5	0.00000	0.00006	0.00000	0.00006	0.00005	0.00001	0.00000	0.00006	0.00000	0.00006
BOR (%)	-	0.17	0.17	0.00	0.23	-0.06	0.15	0.02	0.17	0.00
				% Dev		% Dev		% Dev		% Dev
Temperature (K)	113.6	113.4	113.3	0.09	113.6	-0.18	113.3	0.03	113.3	0.03
Volume (m^3)	137,936	135,144	135,199	-0.04	134,121	0.76	135,439	-0.22	135,201	-0.04
WI (kWh/m^3) 0°C/0°C	15.075	15.078	15.075	0.02	15.078	0.00	15.078	0.00	15.078	0.00
HHV (kWh/m^3) 0°C/0°C	11.422	11.433	11.428	0.04	11.436	-0.03	11.429	0.03	11.428	0.04
Density (kg/m^3)	431.079	431.089	431.685	-0.14	431.726	-0.15	431.604	-0.12	431.621	-0.12

From tables 5.9 to 5.13 it can be observed that the agreement of predicted values from both models with measured data is very good for all journeys.

Journey 1 is of short duration (126.5 h) and LNG is of high methane content. Both models reproduce the measured compositional data to better than 0.001 of mol fraction. Predicted volume at the port of destination is better than 0.02% for the isothermal model, and 0.06% for the superheated vapour model. The predicted density is within 0.15% of the measured value for both models, whilst the temperature is estimated with no deviation respect to measured value.

When examining Journey 2, which lasted 3 times longer (390 h) and where the initial content of methane was much lower, it can be observed that the agreement is still very good. Both models reproduce the measured compositional data to better than 0.001 of mol fraction, the final volume and temperature to better than 0.12% and 0.18% respectively; whilst the predicted density is within 0.05% of the measured value.

All the measured data on other journeys reported by Miana *et al*. [2] are reproduced with similar accuracy. The only exception is Journey 3, where both models reproduce the measured compositional data to within 0.002 of mol fraction, the final volume to better than 0.33%, and the predicted temperature within 0.92% and 0.80% of the measured value for the isothermal and superheated vapour models respectively. The results are surprising as this is the shortest journey (98 h), although the methane content is lower and nitrogen content higher than in other reported journeys. However, the cursory analysis of actual data indicates that some of the measurements might have a larger uncertainty than previously assumed. For instance, based on the quoted volumes and nitrogen content measured at the port of origin and destination, one can estimate that nitrogen evaporation alone led to 96 m^3 decrease in the amount of LNG. However, based on quoted total volumes only 70 m^3 of LNG has evaporated as BOG. It is also worth noting that the experimental error in measuring the composition of trace components (nC_5 & iC_5) at the two ports is large, which is not surprising as they both constitute less than 0.05% of the overall mixture. During the weathering process it is expected the composition of heavy components in LNG

to increase. As can be seen from the measured values (see Table 5.11) that is not always the case.

Figures 5.18 to 5.22 illustrate the deviation percentage *% Dev*, calculated using equation (5.2), of the isothermal and superheated vapour models to those of Miana *et al.* [2] from the measured data x_{ref} for the five selected journeys.

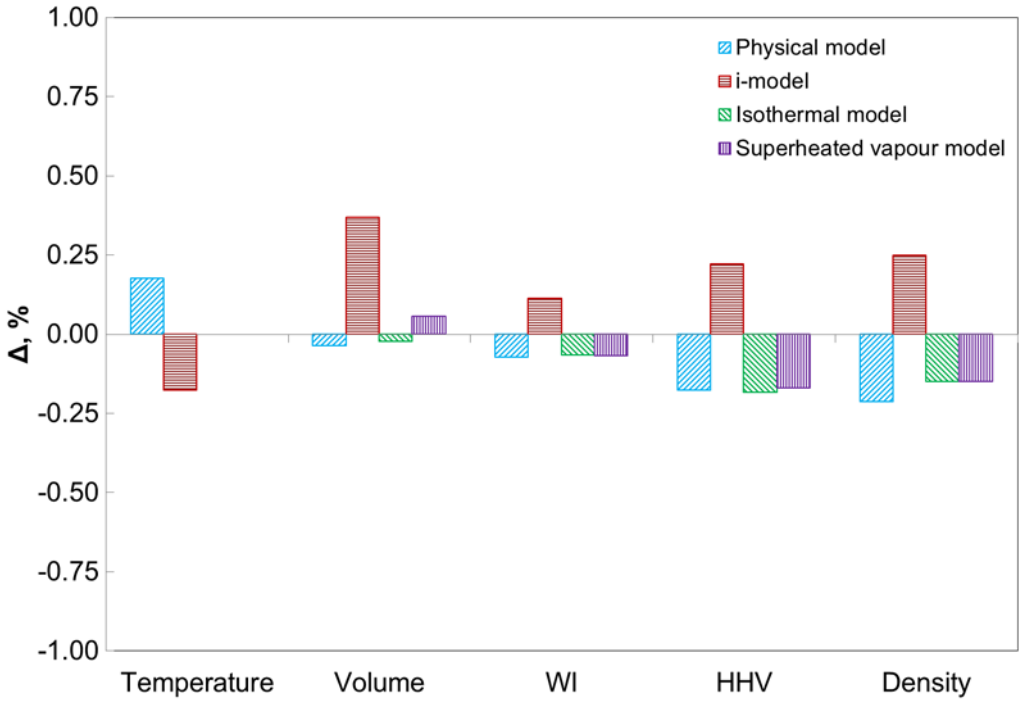

Figure 5.18 Relative percentage deviation for Journey 1.
(of both models and Miana *et al.* models from the measured data)
[$\Delta=100\ (x_{ref} - x_{mod}) / x_{ref}$]

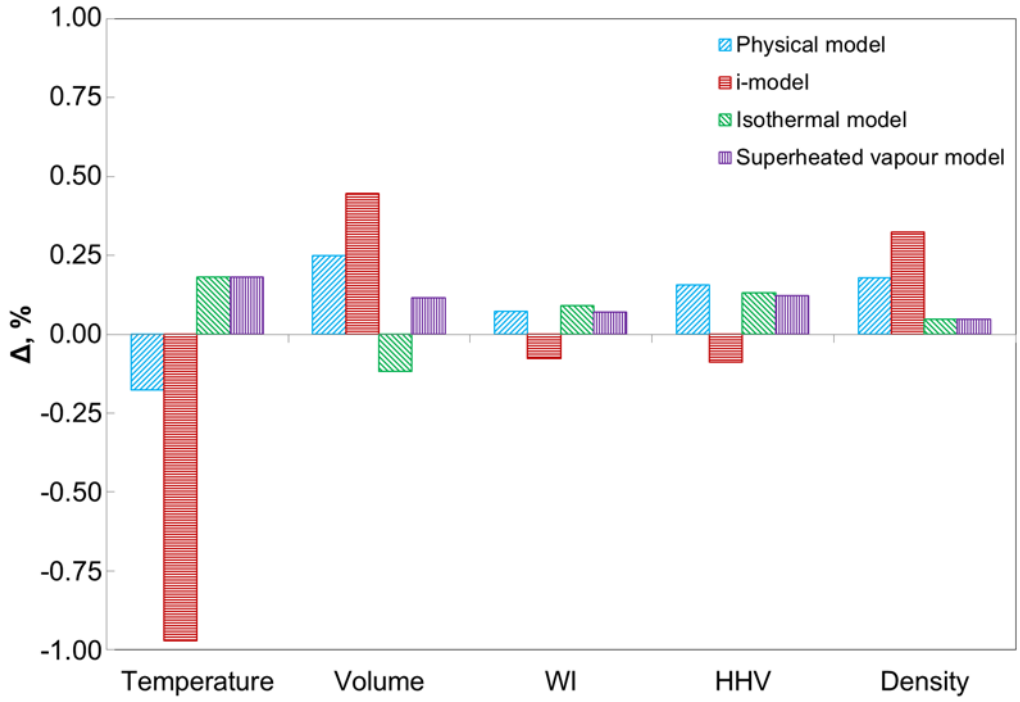

Figure 5.19 Relative percentage deviation for Journey 2.
(of both models and Miana *et al.* models from the measured data)
[$\Delta=100\ (x_{ref} - x_{mod}) / x_{ref}$]

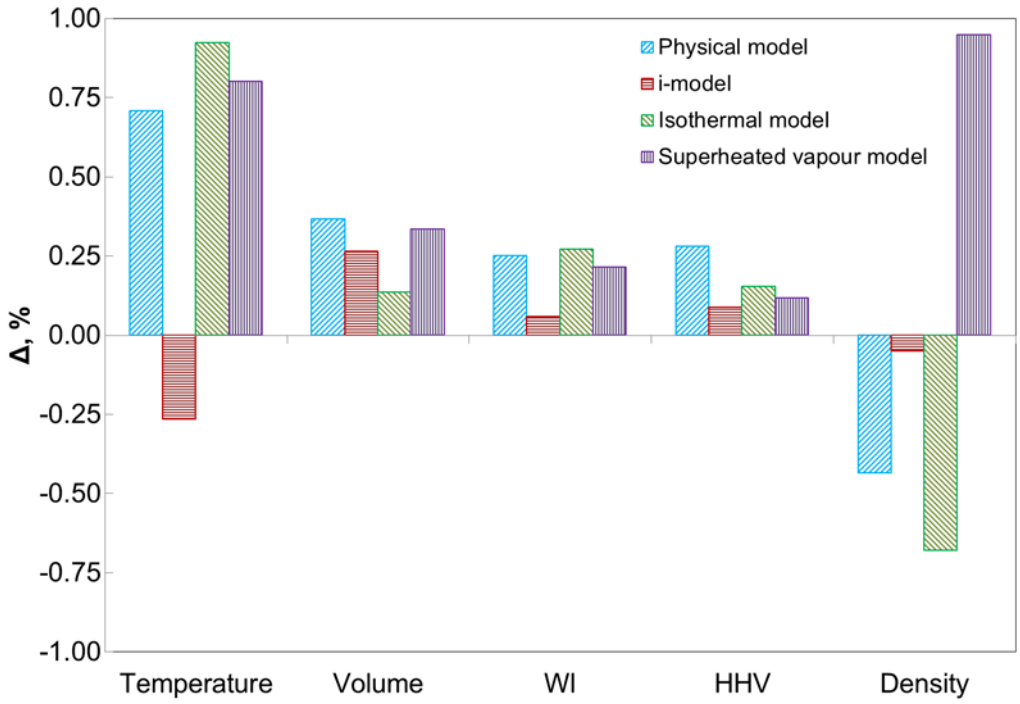

Figure 5.20 Relative percentage deviation for Journey 3.
(of both models and Miana *et al.* models from the measured data)
[$\Delta=100\ (x_{ref} - x_{mod}) / x_{ref}$]

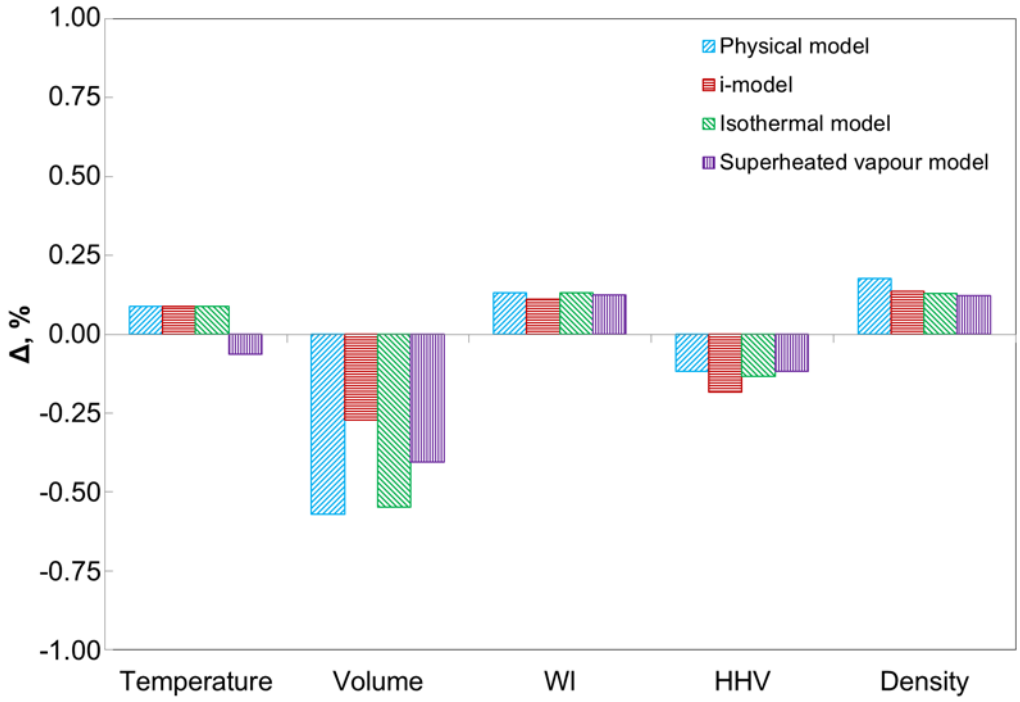

Figure 5.21 Relative percentage deviation for Journey 4.
(of both models and Miana *et al.* models from the measured data)
[$\Delta=100\ (x_{ref} - x_{mod}) / x_{ref}$]

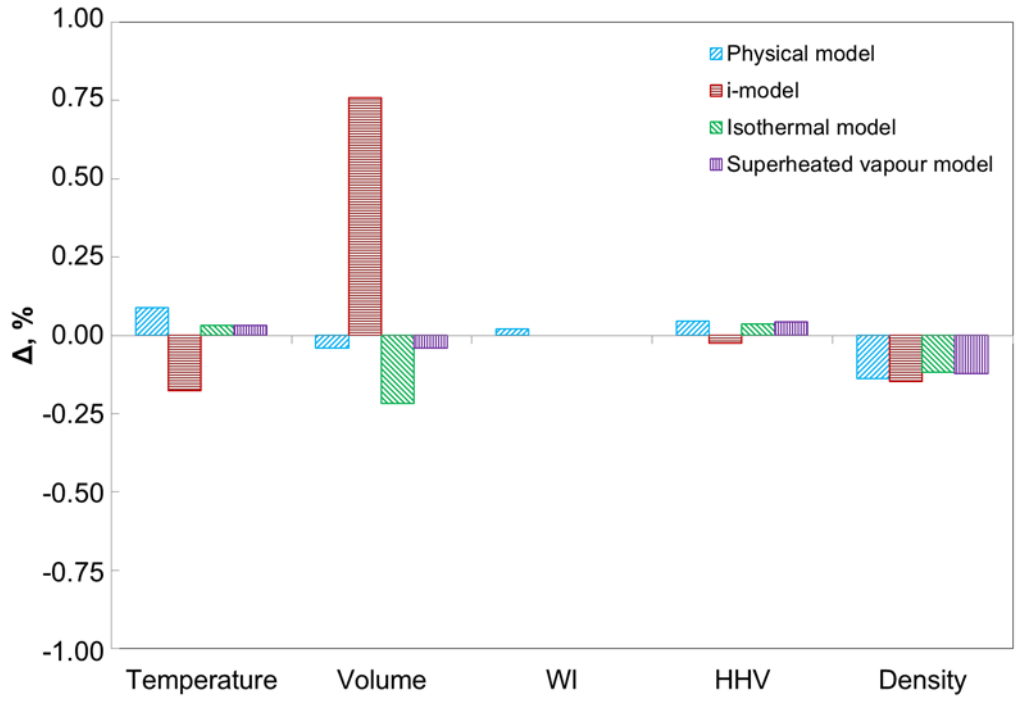

Figure 5.22 Relative percentage deviation for Journey 5.
(of both models and Miana *et al.* models from the measured data)
[$\Delta=100\ (x_{ref} - x_{mod}) / x_{ref}$]

Figures 5.18 to 5.22 illustrate that the predicted values of HHV and WI from both the isothermal and the superheated vapour are better than 0.3%. The HHV is obtained as mol average of heat of combustions at standard conditions by means of eq. (3.88) and WI is calculated using eq. (3.89). The values of heat of combustion for each relevant species where obtained from reference [10].

It is also shown that the isothermal and superheated vapour models give very similar deviations to Miana *et al.* [2] physical model, with differences not exceeding 0.9 % which is well within the uncertainty of both models. None of the models exhibit a bias, as there is neither systematic overestimation nor underestimation of measured variables. The improvement that the current models bring is that: (*i*) BOR is not fixed and can be predicted as part of the simulation; (*ii*) it can account for variable heat input during the weathering process and (*iii*) the LNG density is accurately calculated by means of experimentally based correlation.

Another useful study, for the purposes of comparison, which has been published recently, is that of Hasan *et al.* [6]. They analysed the effect of ambient temperature and overall heat transfer on the BOG generated during LNG ship transport, considering a voyage length of 20 days. Hasan *et al.* [6] estimated the BOG generated, reported as CBOG, which is the weight percentage of BOG generated to initial cargo load, over the full length of the journey for different ambient temperatures ranging from -10 ºC to 25 ºC, and overall heat transfer coefficients of 0.11, 0.14 and 0.17 W/m^2 K. These overall heat transfer coefficients values are in agreement with typical cargo shells used in industry where U is about 0.1142 W/m^2 K, assuming that it only depends on the thermal conductivities and thickness of insulation and tank support, and the ratio of support junction area to total surface area [11].

Those overall heat transfer coefficients considered by Hasan *et al.* [6] are lower when compared to the adjusted U_{wet} = 0.3756 W/m^2 K used in the developed weathering models for the verification. The difference has to do with the assumptions taken to calculate the adjusted U_{wet}, where the heat inputs from roof and bottom slab are omitted. If the heat ingress from roof and bottom slab is taking into account, then the amount of heat coming

through the lateral wall would be roughly 50-60% smaller, which makes the adjusted U_{wet} roughly in the region of that used by Hasan *et al.* [6] in their study.

In Hasan *et al.* [6] work CBOG is an equivalent indicator for BOR over the weathering time, but in mass basis.

Table 5.14 shows the input data used by Hasan *et al.* [6] in their study.

Table 5.14 Input data for the CBOG vs. ambient temperature analysis.

LNG composition	Mol %
Methane	81.5
Ethane	8.5
Propane	5.0
Butane	4.0
Nitrogen	1.0
Pressure, kPa	101.3
Tanker capacity, m^3	145,000
LNG volume, m^3	142,100

Figure 5.23 shows the result found by Hasan *et al.* [6], the effect of the ambient temperature and overall heat transfer coefficient on CBOG for the LNG mixture as presented in Table 5.14.

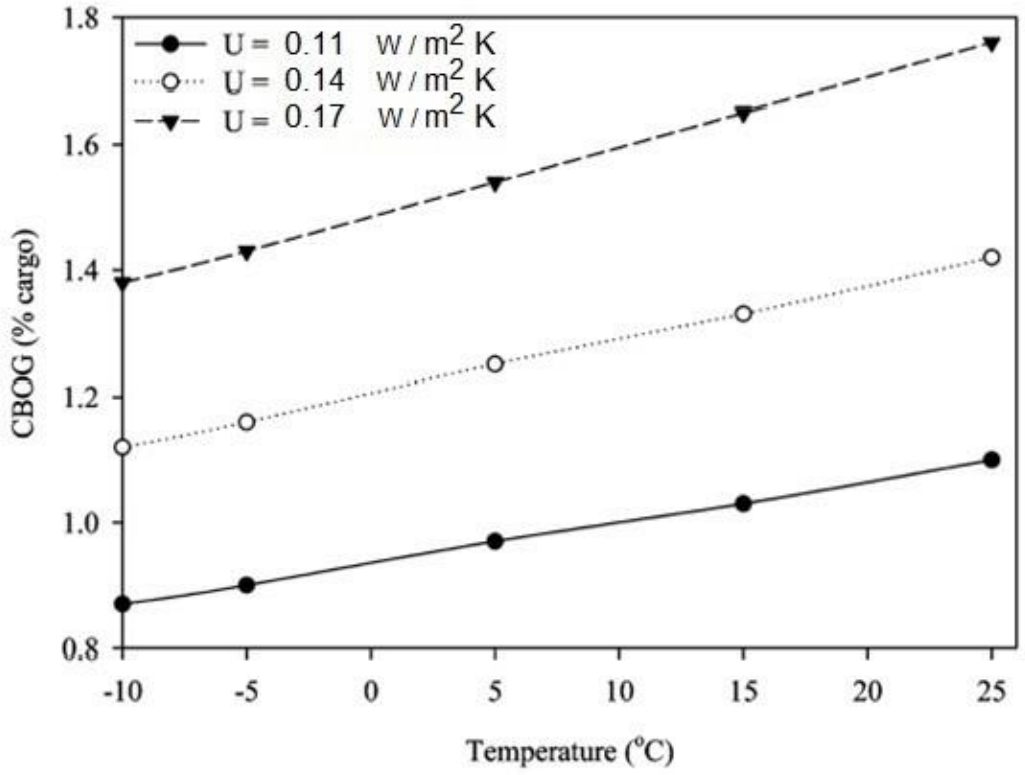

Figure 5.23 CBOG vs. T_{air} for different overall heat transfer coefficient [6].

By means of using the same data as Hasan *et al*. [6] study the isothermal and superheated vapour models were run, but applying the overall heat transfer coefficient as adjusted to validate Miana *et al*. [2] work (U_{wet} = 0.3756 W/m^2 K), to compare the predicted BOG generation by both models to that calculated by Hasan *et al.* [6] during LNG shipping.

Figure 5.24 shows the effect of surrounding temperature on CBOG, considering the adjusted overall heat transfer coefficient of U_{wet} = 0.3756 W/m^2 K, for the LNG mixture included in Table 5.14.

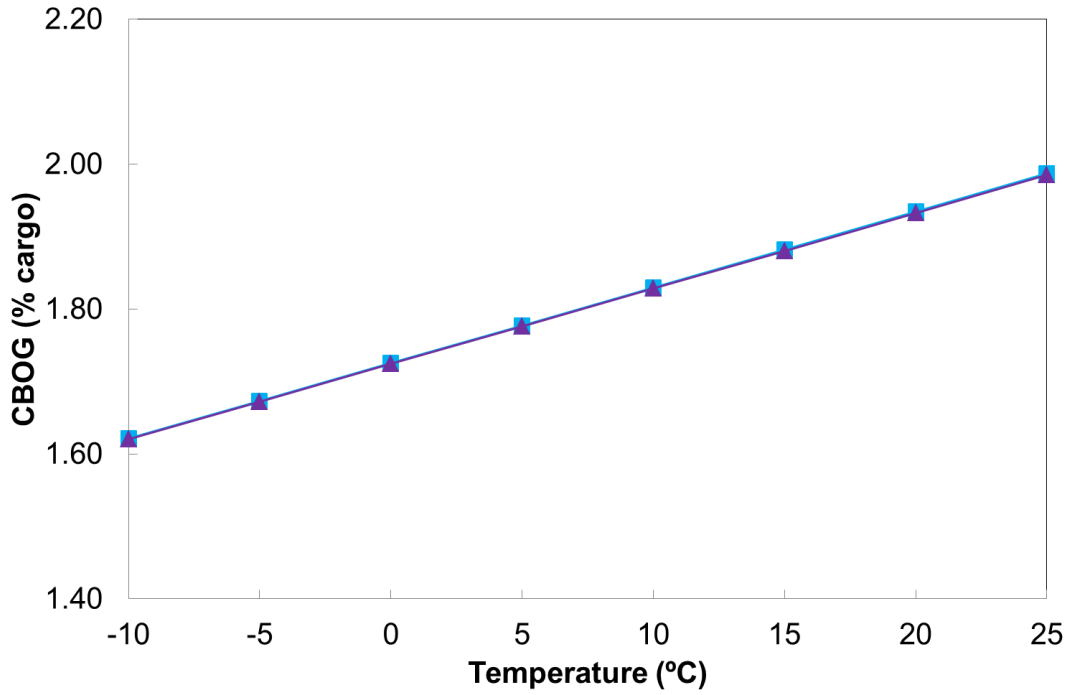

Figure 5.24 CBOG vs. T_{air} considering U_{wet} = 0.3756 W/m^2 K.
(-■- Isothermal model; -▲- Superheated vapour model)

From Figure 5.24 one can observe that the BOG estimated by the isothermal and superheated vapour models are essentially the same, following the same linear pattern as the one predicted by Hasan *et al.* [6], BOG increases as surrounding temperature increases.

The BOG estimates from Hasan *et al.* [6] study are lower when compared to the predicted value by both models, and that is due to the lower overall heat transfer coefficients used by Hasan *et al.* [6] in their simulations. However, as discussed earlier, a BOR between 0.1-0.15% v/v of the full transported cargo content per day is typical in the LNG industry, thus after 20 days journey the expected vaporized volume should be around 2-3% v/v of the original cargo. To calibrate that, the CBOG shown in Figure 5.24 (1.99% for both models at 25 ºC surrounding temperature) has been corrected to volume basis obtaining a BOR of 2.38% v/v, which is in agreement with current industry standards.

From Figure 5.24 one can assume a rule-of-thumb that in LNG shipping 1 ºC change in the surrounding temperature will change the BOG generation by approximately 0.01 %.

5.4 LIQUID DENSITY CORRELATION TEST

As discussed in Chapter 3, although the use of cubic EOS with the corrected volume is standard practice when estimating liquid density in the oil and gas industry, in this research project the Revised Klosek-McKinley method [8] was rather used. As it is an empirical correlation that has been developed specifically for estimating the density of LNG, it is a reliable and accurate method that is frequently used for LNG custody transfer purposes, and is the recommended option by the GIIGNL [8] and the ISO 6578 [12]. It is valid over the compositions and boiling temperatures of interest to LNG industry, and has a claimed uncertainty of ±0.1%, providing either the nitrogen or butane content does not exceed 4%.

The LNG density prediction by the Revised Klosek-McKinley method [8], were compared to that estimated when considering ideal mixture and to that estimated by the COSTALD correlation method [13]. The COSTALD correlation method [13] has been selected to test the Revised Klosek-McKinley method [8], as it has a claimed average absolute percent error (between calculated and experimental) for cryogenic liquids of 0.5% [13]. Moreover, the COSTALD correlation method [13] is the standard liquid density prediction method adopted by the American Petroleum Institute (API) [14], and is the default method used by the process simulator Aspen Hysys [1].

To calculate LNG density ρ_L, the ideal mixture and Revised Klosek-McKinley methods make use of the molar volume υ of the LNG mixture. The LNG density is calculated as the inverse of the molar volume, as follows:

$$\rho_L = \frac{1}{\upsilon} \tag{5.19}$$

The molar volume within the ideal mixture approach is calculated as follows:

$$\upsilon = \sum \upsilon_i x_i \tag{5.20}$$

where subscript i denotes the component within the mixture, and x_i refers to component molar fraction.

The Revised Klosek-McKinley method [8], equation (3.79), is based on an empirical correlation of the molar volume of the mixture in the thermodynamic state of the LNG considered, and is written as follows:

$$\upsilon = \sum v_i x_i - \left[k_1 + (k_2 - k_1)\left(\frac{x_{N_2}}{0.0425}\right)\right] x_{CH_4} \qquad (3.79)$$

where k_1 and k_2 are temperature dependent correction factors (refer to Tables 3.3 and 3.4 in Chapter 3), and x_{N_2} and x_{CH_4} are respectively the nitrogen and methane molar fractions present in the LNG mixture.

The difference between both methods resides in the correction factor used by the Revised Klosek-McKinley method, and the approach taken to adjust υ of the LNG mixture, as the ideal mixture approach makes no use of correction factor for υ.

Concerning the COrresponding STAte Liquid Density (COSTALD) correlation, it was developed by Hankinson and Thompson [13] and liquid density is calculated from the saturated liquid volume (V_s) as follows:

$$\rho_L = \frac{1}{V_s} \qquad (5.21)$$

The COSTALD [13] correlation determines the saturated liquid volume of a pure component from two parameters, the optimized value of the acentric factor based on the SRK EOS ω, and the characteristic volume, V^*.

The COSTALD [13] correlation method to estimate V_s for a pure component is described below:

$$\frac{V_s}{V^*} = V_r^{(0)}\left[1 - \omega\, V_r^{(\delta)}\right] \qquad (5.22)$$

where $V_r^{(0)}$ and $V_r^{(\delta)}$ are determined from the reduced temperature T_r as follows:

$$V_r^{(0)} = 1 + a(1 - T_r)^{1/3} + b(1 - T_r)^{2/3} + c(1 - T_r) + d(1 - T_r)^{4/3} \qquad (5.23)$$

for:

$$0.25 < T_r < 0.95; \qquad T_r = T/T_c$$

where T_c is the critical temperature for each component.

$$V_r^{(\delta)} = \frac{[e + f\,T_r + g\,{T_r}^2 + h\,{T_r}^3]}{(T_r - 1.00001)} \tag{5.24}$$

for:

$$0.25 < T_r < 1.00$$

Table 5.15 shows the parameters for equations 5.23 and 5.24 [13].

Table 5.15 Parameters for COSTALD correlation.

a	-1.5281600
b	1.4390700
c	-0.814460
d	0.1904540
e	-0.2961230
f	0.3869140
g	-0.0427258
h	-0.0480645

Table 5.16 shows the characteristic volume *V** of components usually present in LNG.

Table 5.16 *V (l/mol) of components usually present in LNG.**

Methane	0.09939
Ethane	0.14580
Propane	0.20010
Isobutane	0.25680
Butane	0.25440
Isopentane	0.30960
Pentane	0.31130
Nitrogen	0.09012

For the mixtures case, to calculate the saturated liquid volume V_s with the COSTALD [13] correlation method the following mixing rule is used:

$$T_{cm} = \left[\sum_i \sum_j x_i\, x_j\, V_{ij}^*\, T_{c_{ij}}\right] / V_m^* \tag{5.25}$$

$$V_m^* = 0.25\left[\sum_i x_i V_i^* + 3\left(\sum_i x_i\, V_i^{*0.67}\right)\left(\sum_i x_i\, V_i^{*0.33}\right)\right] \tag{5.26}$$

$$V_{ij}^* T_{c_{ij}} = \left(V_i^* T_{c_i} V_j^* T_{c_j}\right)^{0.5} \tag{5.27}$$

$$\omega_m = \sum_i x_i\, \omega_i \tag{5.28}$$

where *i* and *j* refer to any component.

The comparison of the liquid density predictions, using the three methods described before, has been done for the mixtures shown in Tables 5.1, 5.2 and 5.4. Those are the LNG with N_2, Heavy LNG and Light mix, as they allow assessing the influence of nitrogen and heavy hydrocarbons. Heavy mix (Table 5.3) has been excluded from this comparison as it falls well outside the validity limits of the Revised Klosek-McKinley method range (CH_4 > 60 % mol; iC_5+nC_5 < 2 % mol; $T_{boiling}$ < 115 K) [8].

Table 5.17 shows the liquid density predictions with the three methods, Ideal Mixture (IM), COSTALD (CD) and Revised Klosek-McKinley (KM), for each binary mixture. Table 5.17 also includes the deviation percentage % *Dev*, calculated using equation (5.2), between the estimated values by IM and CD to the KM. The x_{ref} in this calculation is either the density value estimated by IM or CD; whilst x_{mod} refers to the density value calculated by the Revised Klosek McKinley method [8].

Table 5.17 Liquid density predictions in (kmol/m^3) for each assessed mixture.

Mixture mol %	$T_{boiling}$ K	Ideal Mixture IM	COSTALD CD	Rev. Klosek McKinley KM	% *Dev* IM-KM	% *Dev* AH-KM
LNG with N_2	112.4	25.254	25.597	25.552	-1.18	0.18
Heavy LNG	114.9	24.623	25.049	24.960	-1.37	0.36
Light mix	101.8	27.035	27.263	27.227	-0.71	0.13

Comparing the density estimates of the Revised Klosek-McKinley method [8] to that of COSTALD [13], one can observe that the agreement between the two is within 0.4 % in all cases. It is interesting to note that for the LNG with N_2 case, the deviation percentage between the predicted values of the Revised Klosek-McKinley method [8] and COSTALD [13] is less than 0.2 %. Furthermore, in the Light mix case, although the N_2 content is above the maximum limit of the method (5 % mol vs. 4 % mol maximum) [8], the deviation percentage to COSTALD [13] is also less than 0.2 %.

When comparing to the ideal mixture behaviour method, the prediction based on the Revised Klosek-McKinley [8] for the LNG like mixtures, LNG with N_2 and Heavy LNG, would overpredict density by 1.2 % and 1.4% respectively. For the Light mix case the difference between the two methods is around 0.7%.

With regards to LNG density calculation, the work of Ajetunmobi [15] is of special interest. Ajetunmobi [15] compared the performance of different equations of state in the calculation of saturated liquid density of LNG like mixtures. He concluded that

cubic equations of state tend to have major shortcomings in the prediction of LNG properties within the range of temperatures and pressures encountered during the liquefaction of natural gas. Concerning the influence of N_2 composition, Ajetunmobi [15] found that the presence of N_2 has a mild effect of increasing the saturated liquid density of LNG mixtures; however, regarding the accurate calculation of saturated liquid density, the higher the N_2 content in the LNG the greater the deviation of the predicted estimate to actual value.

5.5 CHAPTER SUMMARY

The tests and simulation runs used to evaluate the performance of both weathering models developed in this PhD research project have been described in this chapter.

The performance was evaluated by three assessments. The first one compared the predictions of the thermodynamic vapour-liquid equilibrium (VLE) module, against the results obtained with the accredited process simulator Aspen Hysys [1]. The second assessment was performed by validating the estimated latent heat of the weathered LNG mixture, against a full thermodynamic calculation. In the third assessment a comparison of weathered LNG estimates using the models developed with previous studies and measured data was carried out [2]. None of the models exhibit a bias, as there was neither systematic overestimation nor underestimation of referenced and measured variables.

The chapter also reviews the discrepancies of the LNG density estimate by the empirical correlation the Revised Klosek-McKinley method, to that estimated when considering ideal mixture and the COSTALD correlation method [13], as it is commonly used in the oil and gas industry to predict hydrocarbon liquid density. The agreement when comparing the density estimates of the Revised Klosek-McKinley method [8] to that of COSTALD [13] is within 0.4 % in all cases, which is well below industry requirements.

Next chapter presents the sensitivity assessments carried out to model the weathering process in a standard 165,000 m^3 full containment above ground LNG storage tank as used in industry, using both models, the isothermal and superheated vapour.

5.6 REFERENCES

[1] Aspen Technology (2007) *Aspen Hysys process simulator* (version 2006.5) [Software] USA. Aspen Technology, Inc.

[2] Miana M., Del Hoyo R., Rodrigálvarez V., Valdés J. R., Llorens R. (2010) Calculation models for prediction of liquefied natural gas (LNG) ageing during ship transportation. *Applied Energy*, 87 (5), 1687–1700.

[3] Bett, K. E., Rowlinson J. S., Saville, G. (1975) *Thermodynamics for chemical engineers*. USA, the MIT press.

[4] Strickland-Constable R. F. (1951) Two-Phase equilibrium in binary and ternary systems. VII. Calculation of latent heats and some other similar properties. *Proceedings of The Royal Society A*, 8 October 1951. London.

[5] Conrado, C., Vesovic, V. (2000) The influence of chemical composition on vaporisation of LNG and LPG on unconfined water surfaces. *Chemical Engineering Science*, 55, 4549−4562

[6] Hasan M. M. F., Zheng A. M., Karimi I. A. (2009) Minimizing Boil-Off Losses in Liquefied Natural Gas Transportation. *Industrial Engineering and Chemistry Research*, 48, 9571–9580

[7] BP Statistical Review of World Energy (2015). BP p.l.c., London, UK.

[8] Groupe International des Importateurs de Gaz Naturel Liquéfié – GIIGNL (2010) *LNG Custody Transfer Handbook, 3rd edition*, Paris

[9] National Bureau of Standards Publications (NBS). (1985) NBSIR 85-3028. *LNG Measurement, A User's Manual for Custody Transfer*. USA, NBS.

[10] Lemmon, E. W., Huber, M. L., McLinden, M. O. (2013) NIST Standard Reference Database 23. *Reference Fluid Thermodynamic and Transport Properties REFPROP*, Version 9.1. Gaithersburg, National Institute of Standards and Technology (NIST).

[11] Chen, Q. S., Wegrzyn, J., Prasad, V. (2004) Analysis of Temperature and Pressure Changes in Liquefied Natural Gas (LNG) Cryogenic Tanks. *Cryogenics*, 44 (10), 701–709

[12] International Organization for Standardization (ISO). (2009) ISO 6578: 1991. *Refrigerated hydrocarbon liquids - Static measurement - Calculation procedure*. Switzerland, ISO.

[13] Hankinson, R. W., Thompson, G. H. (1979) A New Correlation for Saturated Densities of Liquids and Their Mixtures. *AIChE Journal*, 25 (4), 653-663.

[14] American Petroleum Institute. (2007). *Manual of petroleum measurement standards chapter 17 - Marine measurement*. Section 10 - Measurement of refrigerated and/or pressurized cargoes on board marine gas carriers. Part 2 - Liquefied petroleum and chemical gases. API publishing services. Washington, D.C. USA.

[15] Ajetunmobi, T. (2010) *LNG Phase Behaviour*. MSc thesis. Imperial College of London.

6 WEATHERING SIMULATIONS RESULTS

A sensitivity assessment was carried out using the described LNG weathering models, isothermal and superheated vapour, wherein four cases were analysed on a long term basis for better understanding of the LNG weathering phenomenon.

The weathering simulations were performed for a standard 165,000 m^3 full containment above ground LNG storage tank used in industry. The storage tank characteristics are summarized in Table 6.1.

The simulations were run considering the tank being isolated (no LNG loading or unloading), and assuming an outside temperature of 25 ºC[10].

Table 6.1 LNG storage tank characteristics and sensitivity assumptions.

Tank volume, V	165,000 m^3
LNG volume[11], V_L	160,000 m^3
Tank height, z	37.3 m
Tank internal diameter, D_i	76.4 m
Tank external diameter, D_o	80.0 m
Tank operating pressure	116.3 kPa (150 mbarg)
Wall section thermal conductivities, k:	
• Resilient blanket [1]	0.015 W/m K
• Expanded perlite [2]	0.035 W/m K
• Concrete [3]	1.6 W/m K
Heat rate input bottom thermal slab, $\dot{Q}_{slab}$ [4]	60 kW
Heat rate input roof [12], $\dot{Q}_{roof}$ [4]	40 kW
Ambient temperature, T_{air}	25 ºC
Atmospheric pressure, P_{atm}	101.33 kPa

[10] Except for sensitivity to outside temperature variations
[11] Except for sensitivity to initial inventory
[12] $\dot{Q}_{roof}$ is only taken into account in the Isothermal model approach, as dicussed in Chapter 4

The sensitivity assessment was performed over a period of 52 weeks, which slightly exceeds the normal time that LNG is stored in LNG peak-shaving facilities. Compared to regular regasification terminals, LNG peak-shaving facilities store LNG for longer periods of time, thus they are more subject to LNG weathering.

For LNG subject to weathering, particularly in long term LNG storage such as 52 weeks duration, the risk of rollover is present as a result of the density stratification between the upper and lower layers in the tank. As discussed in Chapter 1, due to lighter components being preferentially evaporated from the liquid (LNG) surface, the heavier fractions that remain form a dense layer at the top of the storage tank trapping the layer below, which gets less dense. As the LNG stock continues to warm the situation becomes unstable, generating a rapid mixing event where the dense layer at the top rolls over to the bottom of the tank, causing a sudden increase in the generation of vapour, with a subsequent heavy release of it. In this work rollover phenomenon was not investigated. The primary reason for this is that the industrial focus of the project was on examining the routine operation of the storage tank and BOG generation. Although for an isolated tank left to weather the rollover is possible, in industrial operations the LNG is continuously monitored. In the event that LNG density stratification is identified, warm LNG from the lower layer is circulated back to the top of the tank, promoting the stored LNG to mix up therefore, preventing the density stratification and rollover occurrence.

The following sections present the sensitivity cases studied for both modelling approaches: (*i*) initial LNG composition, (*ii*) initial LNG inventory, (*iii*) initial N_2 content, (*iv*) outside temperature variations and (*v*) time step size.

6.1 ISOTHERMAL LNG WEATHERING MODEL RESULTS

6.1.1 SENSITIVITY TO INITIAL LNG COMPOSITION

In order to capture the variety of LNG mixtures available in the market, the initial analysis has been performed using three commercial LNG mixtures that adequately describe a range of actual LNG compositions. They include: (*i*) a ‘Light LNG’ that primarily consists

of methane with small amount of ethane present; (*ii*) a 'Heavy LNG' where the amount of methane is around 91% mol and (*iii*) 'LNG with N_2', containing 0.26% mol of nitrogen.

Table 6.2 shows the LNG compositions used for the analysis, including boiling temperature and overall latent heat. Boiling temperature and overall latent heat values are at the operating pressure of the tank, which in this simulation is 116.3 kPa (150 mbarg).

Table 6.2 LNG mixtures composition (mol fraction) used for the sensitivity case.

Component	Light LNG	Heavy LNG	LNG with N_2
C_1	0.9613	0.9164	0.9307
C_2	0.0340	0.0576	0.0661
C_3	0.0039	0.0204	0.0006
iC_4	0.0004	0.0029	0.0000
nC_4	0.0003	0.0022	0.0000
iC_5	0.0000	0.0002	0.0000
N_2	0.0001	0.0003	0.0026
$T_{boiling}$, °C	-159.4	-158.9	-159.9
Overall Latent Heat, J/mol [5]	10,290	11,548	9,980

Figures 6.1, 6.2 and 6.3 respectively show the BOR, BOG generation rate and boiling temperature evolutions over the weathering period, using the isothermal weathering model, for the three LNG mixtures compositionally described in Table 6.2.

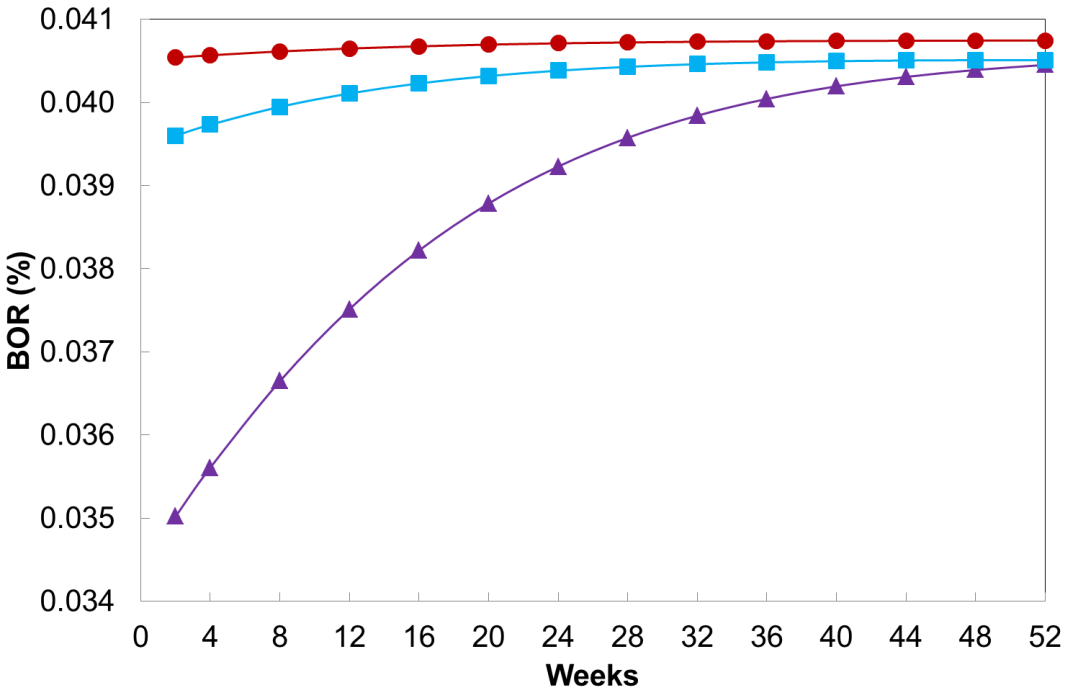

Figure 6.1 BOR vs. time - isothermal model.
(-●- Light LNG; -■- Heavy LNG; -▲- LNG with N_2)

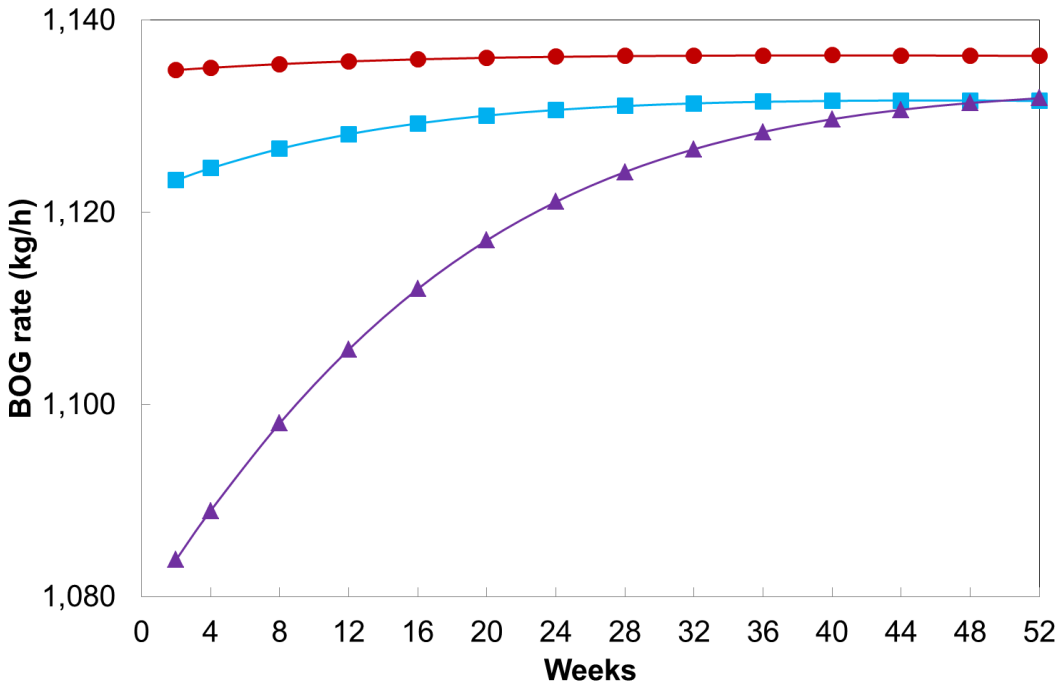

Figure 6.2 BOG generation rate vs. time - isothermal model.
(-●- Light LNG; -■- Heavy LNG; -▲- LNG with N_2)

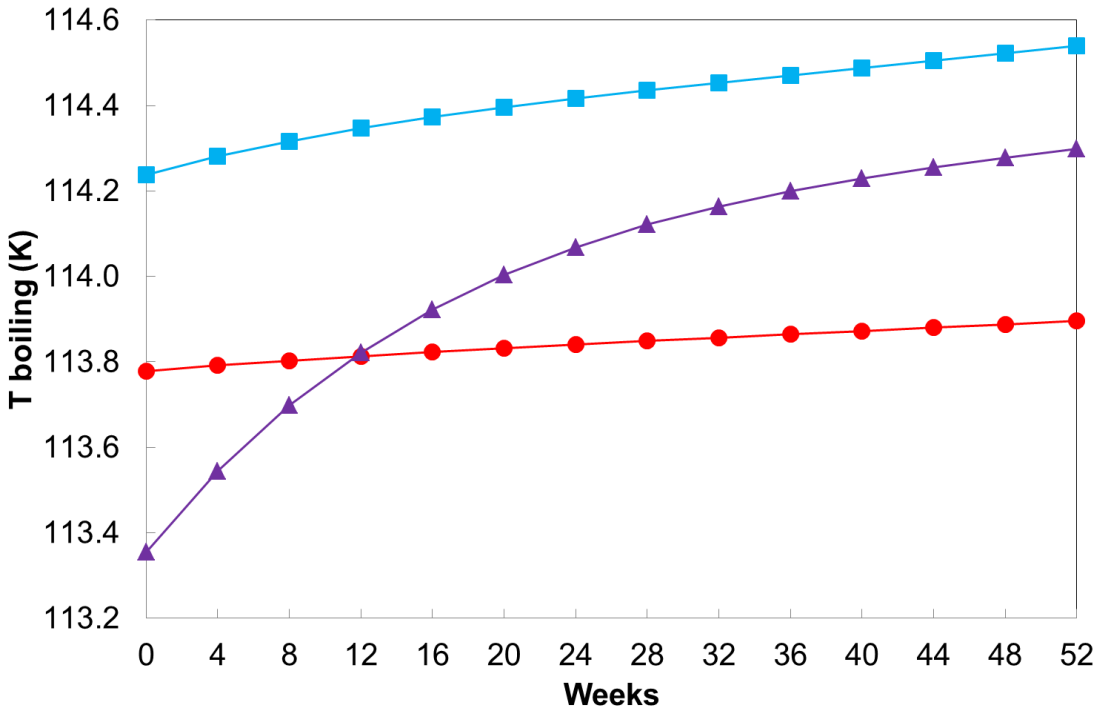

Figure 6.3 Boiling temperature vs. time – isothermal model.
(-●- Light LNG; -■- Heavy LNG; -▲- LNG with N_2)

It is shown that Light LNG evaporates at constant BOG of the order of 1,135 kg/h, which is only 0.5% smaller than the BOG of pure methane. This is not surprising as the simulations conducted in this research and previously published work [6] indicate that for boiling LNG that contains no nitrogen, the vapour consists primarily of methane, $y_{CH4} > 0.99$ (refer to Figure 6.4). The Heavy LNG also boils at approximately constant BOG, but at the rate 1 % lower than that for Light LNG. In this case the vapour is also primarily methane, but the boiling temperature and latent heat are slightly higher (see Table 6.2). As less heat enters the system and it takes more energy to evaporate the unit mass of LNG resulting in marginally lower evaporation rate. The most interesting case is that of LNG with N_2. The BOG increases rapidly in the initial stages of weathering from the value of 1,089 kg/h to 1,132 kg/h. This behaviour is entirely due to the presence of nitrogen that vaporizes preferentially to methane. The simulations indicate that the initial vapour composition consists of only 94% methane and only when all of the nitrogen has evaporated does vapour revert to being essentially pure methane. As addition of nitrogen increases the overall latent heat of nitrogen-methane mixture (as discussed in Chapter 5),

the amount of LNG vaporized will decrease. What is interesting is that even a very small amount of nitrogen present in LNG, in this case 0.26%, can have a substantial influence on the initial BOG, leading to nearly 5% decrease. The decrease of BOG in the initial stages of weathering will result in BOR starting at a lower value, and gradually increasing to 0.04 % that corresponds to nearly pure methane case. This strong sensitivity of BOG on nitrogen content is further explored in Section 6.1.3.

The differences in BOG evolution and the methane content have important consequences on the quality of LNG. Figure 6.4 shows the methane content in the vapour for the three mixtures over the weathering period.

Quality assessment of LNG during the weathering process is carried out using recourse to standard industry measures, namely High Heating Value (HHV) and Wobbe Index (WI). For illustrations purposes the interim guidelines set for the US regulatory specifications in the White Paper on Natural Gas Interchangeability and Non-Combustion End Use [7] are used, for the HHV and WI (15.5 ºC/15.5 ºC and 0.1 MPa) for natural gas to be traded in US markets. The regulation sets targets values for maximum HHV and WI, but not for the minimum, which are defined by limiting the amount of butanes and inerts in the gas. In this respect, the minimum (HHV and WI) based on the regulation has been chosen [7], which is limiting the amount of non-methane species to less than 4% on molar basis. The minimum and maximum for HHV are set to 36.23 MJ/m^3 and 41.36 MJ/m^3 respectively, whilst for the WI are set to 47.93 MJ/m^3 and 52.16 MJ/m^3, minimum and maximum respectively.

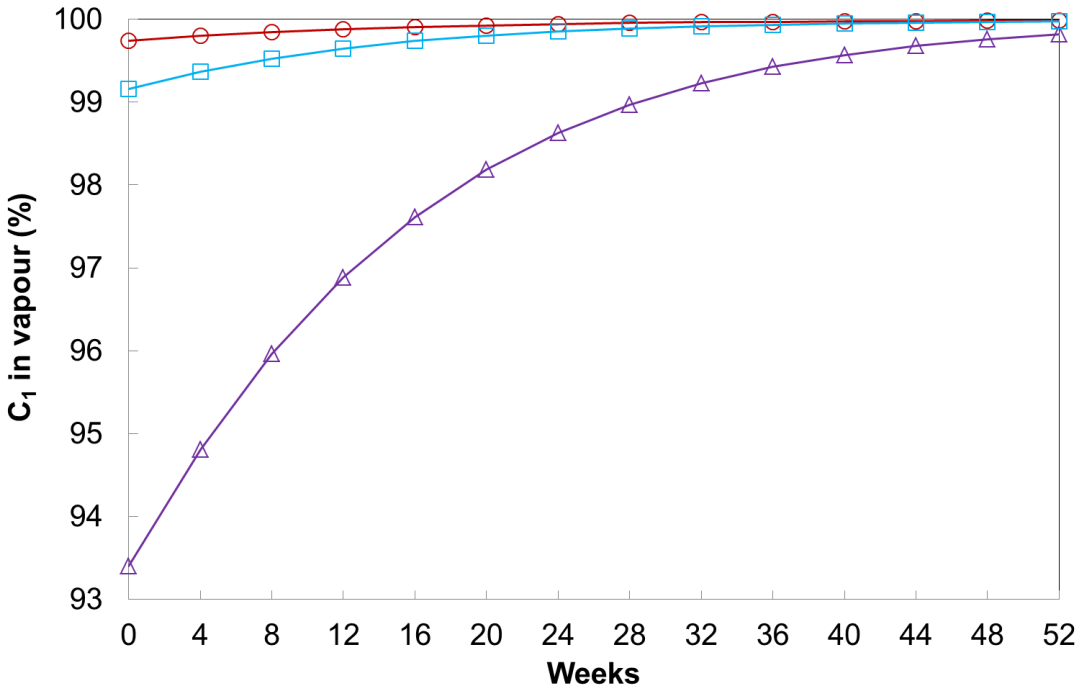

Figure 6.4 Methane content in the vapour vs. time – isothermal model.
(-○- Vapour from Light LNG; -□- Vapour from Heavy LNG;
-△- Vapour from LNG with N_2)

Figures 6.5 and 6.6 illustrate the weathering effect on HHV and WI, of both LNG remaining in the tank and BOG generated.

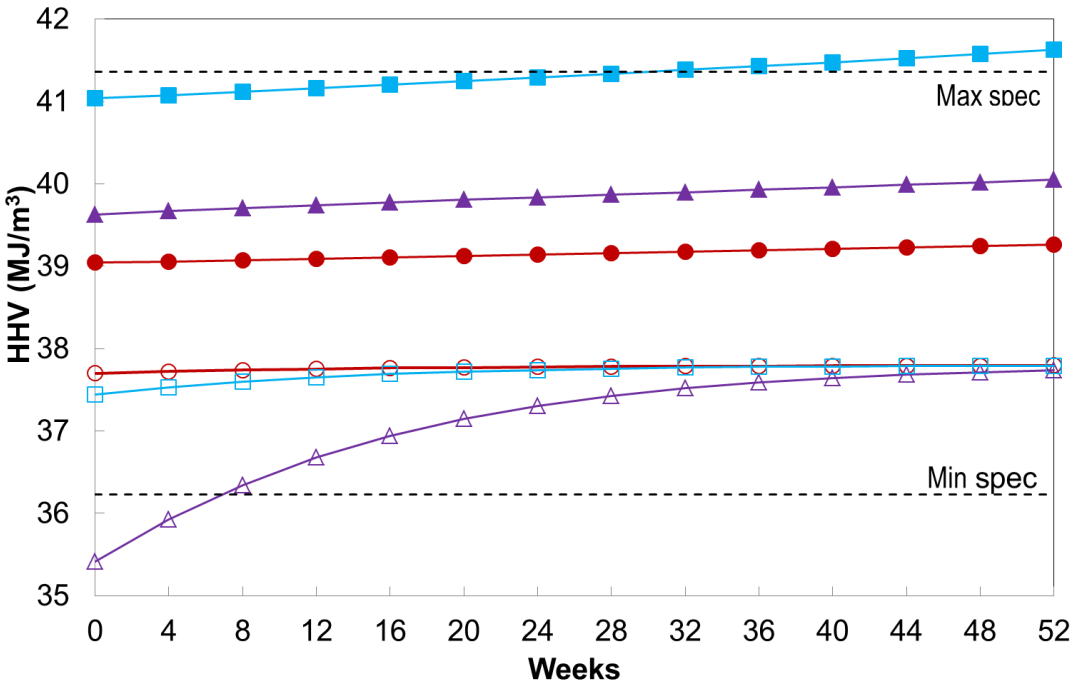

Figure 6.5 HHV vs. time for LNG and BOG - isothermal model.
(-●- Light LNG; -■- Heavy LNG; -▲- LNG with N_2; -○- BOG from Light LNG; -□- BOG from Heavy LNG; -△- BOG from LNG with N_2)

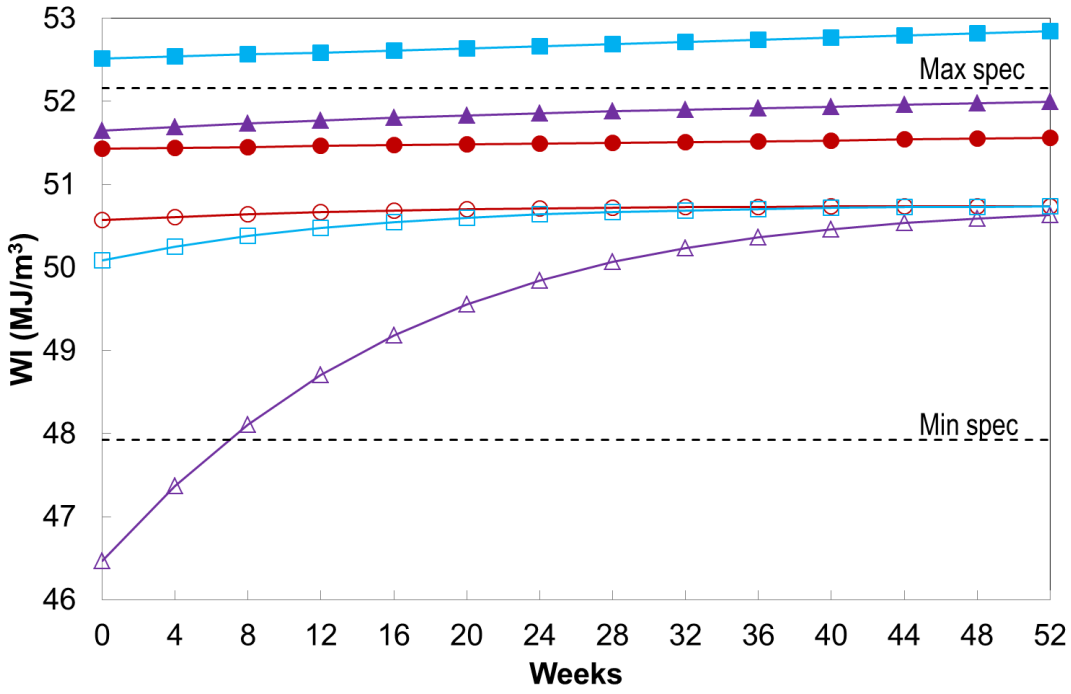

Figure 6.6 WI vs. time for LNG and BOG - isothermal model.
(-●- Light LNG; -■- Heavy LNG; -▲- LNG with N_2; -○- BOG from Light LNG; -□- BOG from Heavy LNG; -△- BOG from LNG with N_2)

Although for all three LNG mixtures the HHV and WI increase with time, the Light LNG and LNG with N_2 remain within the US market quality specifications during the whole period of weathering. The Heavy LNG behaviour is interesting as the two measures (HHV and WI) give slightly different results. If using the WI measure the Heavy LNG is outside the US spec and could not be traded in the US markets, whilst the HHV measure indicates that initially it starts just within the spec but after 33 weeks gets sufficiently weathered to become out of spec.

In the quality assessment of the BOG generated, the key parameter is the initial content of nitrogen. If it is sufficiently high the BOG will contain a large amount of nitrogen making the natural gas out of spec in the initial stages of weathering. As the nitrogen content of the BOG decreases with time, the natural gas will become marketable based on US HHV and WI specifications. In this case the BOG from Light and Heavy LNG are within the US market quality specifications at all times over the weathering period, however the BOG from the LNG with N_2 is outside the US spec at the beginning of the weathering period, with a N_2 content of 6.3% (refer to Figure 6.7). It is not until after week 7, when N_2 content goes down to around 4% mol, that HHV and WI reach the minimum quality spec, 36.23 MJ/m^3 and 47.93 MJ/m^3 respectively. Furthermore, it is shown that both HHV and WI of BOG, for the three mixtures, tend to the value for pure methane ($HHV_{methane}$=37.69 MJ/m^3 and $WI_{methane}$=50.87 MJ/m^3) as the amount of nitrogen in BOG progressively decreases.

Figure 6.7 shows the nitrogen content in the BOG over the weathering period.

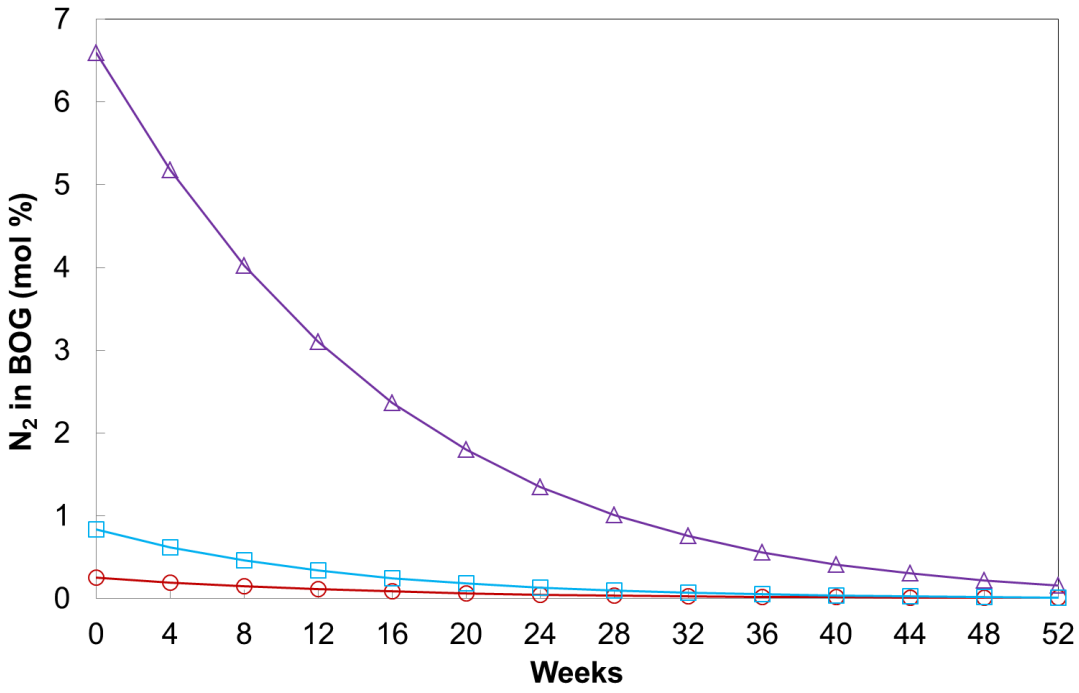

Figure 6.7 N_2 content in the BOG vs. time – isothermal model.
(-○- BOG from Light LNG; -□- BOG from Heavy LNG;
-△- BOG from LNG with N_2)

6.1.2 SENSITIVITY TO INITIAL LNG INVENTORY

A sensitivity analysis has been carried out to investigate the effect of variation in the initial LNG inventory on the generated BOG. The LNG inventory was varied between 15,000 and 160,000 m^3, in a storage tank of capacity of 165,000 m^3 and the simulations were performed for both the Light LNG and Heavy LNG mixtures, compositionally described in Table 6.2.

Figures 6.8 and 6.9 illustrate the vaporization rate expressed as BOR and BOG rate respectively, as a function of the amount of LNG evaporated. BOR defined as the ratio of volume, in liquid terms of LNG that has evaporated in one day relative to the initial LNG volume in the tank. The amount of LNG evaporated was measured in terms of number of moles evaporated divided by the initial number of moles of LNG, expressed as a percentage. Expressing the results in terms of percentage of LNG evaporated using volumetric or mass basis has only the effect of resizing the x-axis, but no impact on any of

the features observed. For clarity only results for the smallest inventory (15,000 m^3) and highest inventory (160,000 m^3) are presented, for both LNG mixtures.

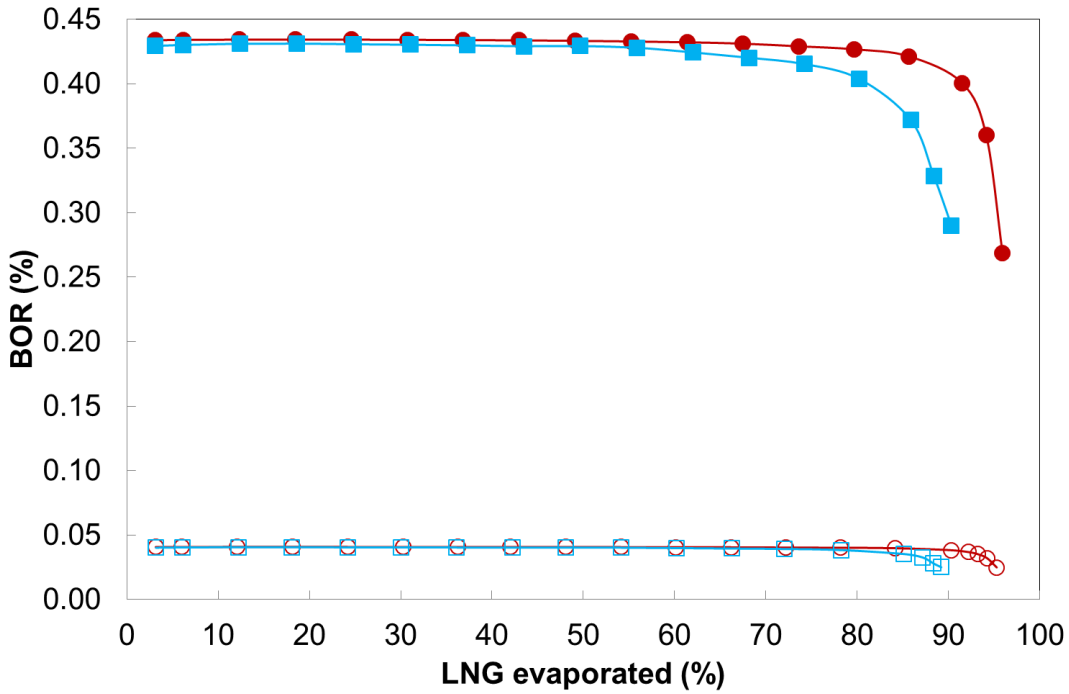

Figure 6.8 BOR vs. LNG evaporated - isothermal model.
(-●- Light LNG, 15,000m^3 inventory; -○- Light LNG, 160,000m^3 inventory;
-■- Heavy LNG 15,000m^3 inventory; -□- Heavy LNG 160,000m^3 inventory)

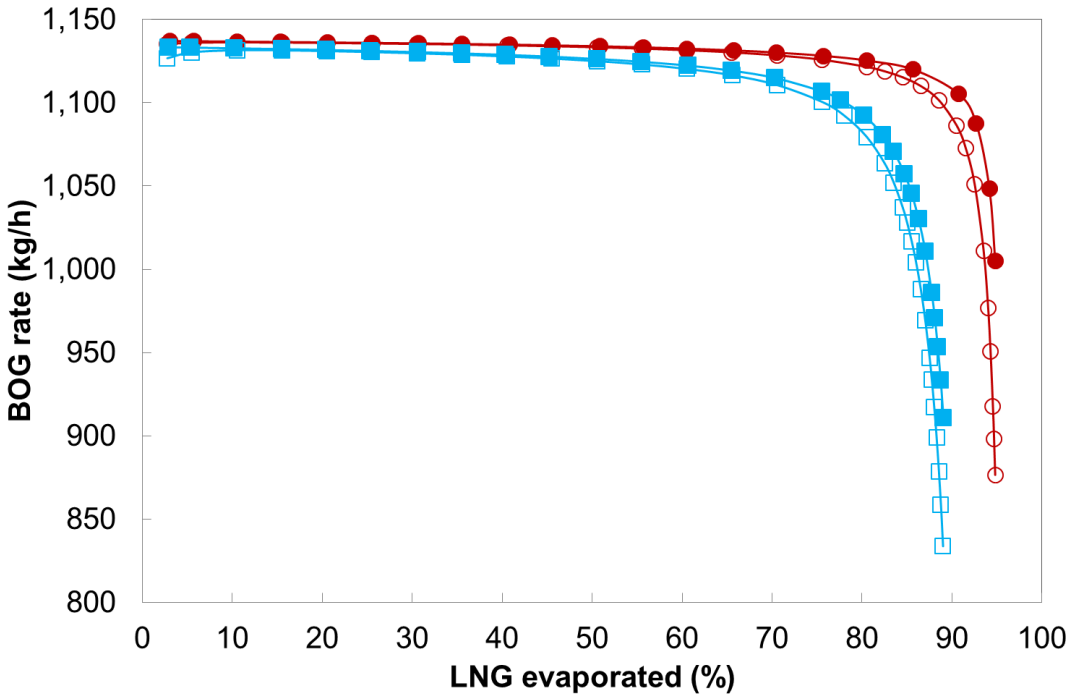

Figure 6.9 BOG generation rate vs. LNG evaporated - isothermal model.
(-●- Light LNG, 15,000m^3 inventory; -○- Light LNG, 160,000m^3 inventory;
-■- Heavy LNG 15,000m^3 inventory; -□- Heavy LNG 160,000m^3 inventory)

Figure 6.8 shows that the BOR increase as the stored volume of LNG decreases in the tank. From Figure 6.9, one can observe that in the initial stages of weathering the BOG rate is constant of the order of 1,140 kg/h, and is independent of the amount of LNG present. This is not surprising as in the beginning the vapour consist exclusively of methane, hence neither the boiling temperature (refer to Figure 6.10) nor the differential latent heat (refer to Figure 6.11) change appreciable. As a result the BOR is also essentially constant, around 0.04 % for tank initially filled with 160,000 m^3 LNG, and 0.43 % for the tank initially filled with 15,000 m^3.

As the LNG evaporates the remaining liquid gets richer in heavier hydrocarbons. This has two thermodynamic consequences [6]. The boiling temperature (refer to Figure 6.10) and the differential latent heat (refer to Figure 6.11) increase. The resulting reduction in the heat ingress and the need to provide more energy to vaporize the same amount of LNG, now richer in heavy components, results in drastic decrease of BOG, as observed in Figure 6.9. As expected the Heavy LNG gets richer in heavy components quicker than the

Light LNG and BOG starts decreasing earlier, at approximately 60% compared with 85% for Light LNG. It can be also observed in Figure 6.9, that the tank filled up to 160,000 m^3 capacity exhibits a slightly earlier decrease in BOG than the tank with the smaller initial amount of LNG. This is a direct consequence of the indirect differential latent heat. As the LNG gets richer in heavier hydrocarbons its boiling temperature increases, and hence some of the heat ingress will go towards heating up the remaining LNG. For a given amount of LNG evaporated the storage tank with initially more LNG will have more liquid remaining. Hence more heat will be required to increase its temperature to a new boiling point, thus reducing the amount of heat available for evaporating the LNG. The overall result will be an earlier decrease in BOG for an initially more filled storage tank.

Figure 6.10 and 6.11 show the boiling temperature and the differential latent heat as a function of the amount of LNG evaporated.

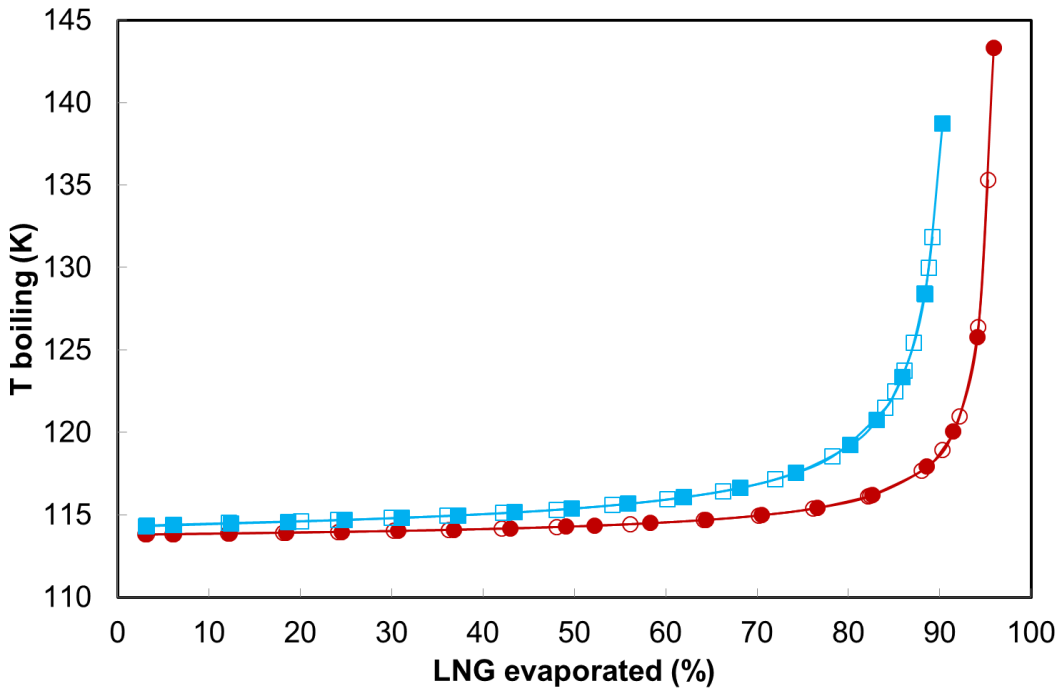

Figure 6.10 Boiling temperature vs. LNG evaporated - isothermal model.
(-●- Light LNG, 15,000m^3 inventory; -○- Light LNG, 160,000m^3 inventory;
-■- Heavy LNG 15,000m^3 inventory; -□- Heavy LNG 160,000m^3 inventory)

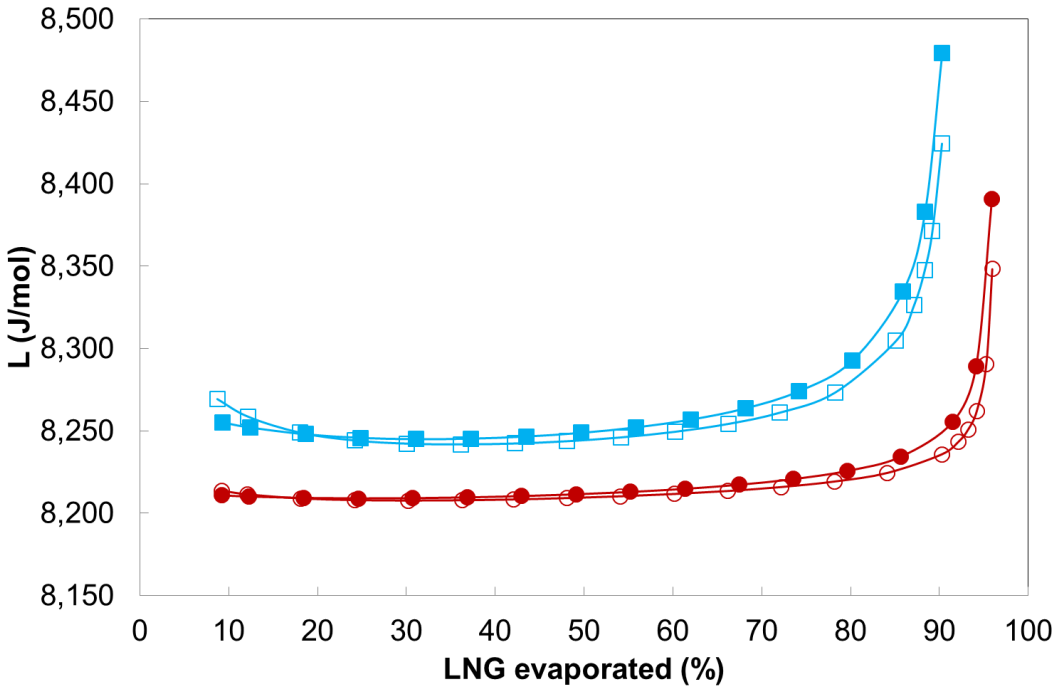

Figure 6.11 Latent heat vs. LNG evaporated - isothermal model.
(-●- Light LNG, 15,000m^3 inventory; -○- Light LNG, 160,000m^3 inventory;
-■- Heavy LNG 15,000m^3 inventory; -□- Heavy LNG 160,000m^3 inventory)

Due to range of validity of Klosek-McKinley equation to calculate liquid density the simulations have been stopped before the complete evaporation of the LNG in the tank. This late stage is usually of marginal interest to the weathering process and the thermodynamic behaviour has been already extensively analysed [6].

6.1.3 SENSITIVITY TO INITIAL N_2 CONTENT

It's been already observed (refer to Figure 6.2) that the presence of nitrogen in LNG decreases the BOG markedly during the initial stages of weathering. Here this effect is examined further by analysing the sensitivity of BOG to the amount of N_2 present in stored LNG. The analysis is performed by comparing an actual Light LNG composition to three hypothetical N_2 enriched LNG mixtures of up to 1.5% N_2 content. Table 6.3 summarizes the composition of the four mixtures. In order to make the comparison on the equal footing the ratios of the hydrocarbon species were maintained constant for all four mixtures.

Boiling temperature and overall latent heat are also included in the table, and are reported at the operating pressure of the tanks, which in this simulation is 116.3 kPa (150 mbarg).

Table 6.3 Nitrogen enriched LNG mixtures.

Component (mol fraction)	Light LNG	0.5% N_2	1.0% N_2	1.5% N_2
C_1	0.9613	0.9566	0.9517	0.9470
C_2	0.0340	0.0338	0.0337	0.0335
C_3	0.0039	0.0039	0.0039	0.0038
iC_4	0.0004	0.0004	0.0004	0.0004
nC_4	0.0003	0.0003	0.0003	0.0003
N_2	0.0001	0.0050	0.0100	0.0150
$T_{boiling}$, ºC	-159.4	-160.9	-162.4	-163.8
Overall Latent Heat, J/mol [5]	10,290	10,351	10,410	10,461

Figures 6.12, 6.13 and 6.14 respectively show the evolution of the BOG generation rate expressed in terms of BOR, mass and molar basis using the isothermal model, for four different N_2 enriched LNG mixtures as described in Table 6.3.

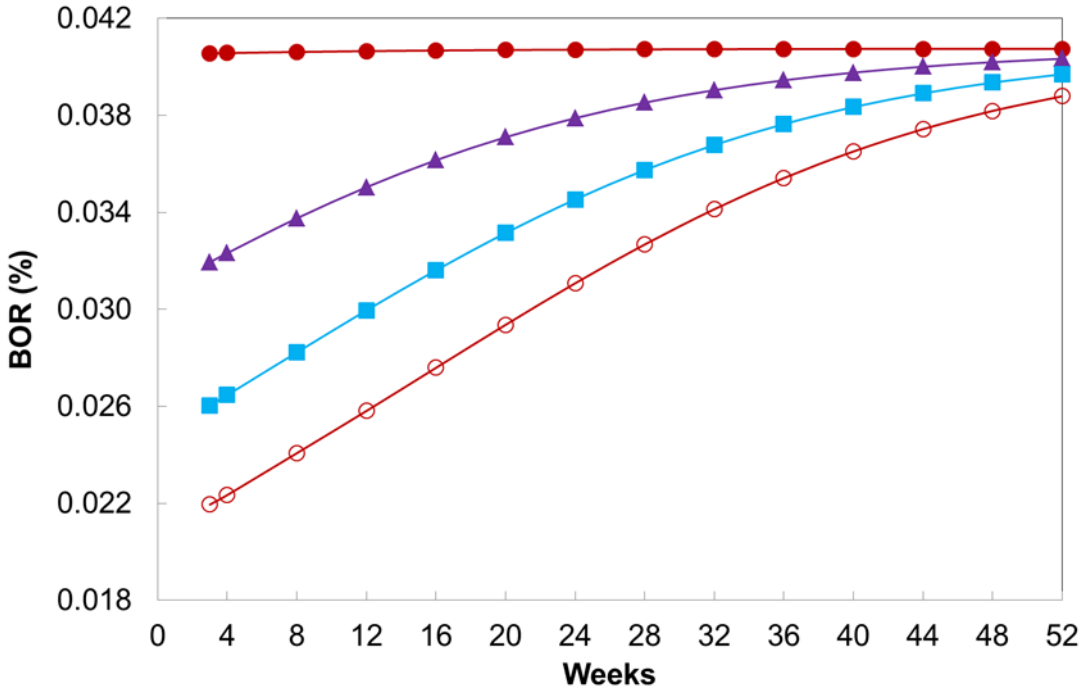

Figure 6.12 BOR vs. time - isothermal model.
(-●- Light LNG; -▲- LNG 0.5% N_2; -■- LNG 1.0% N_2; -○- LNG 1.5% N_2)

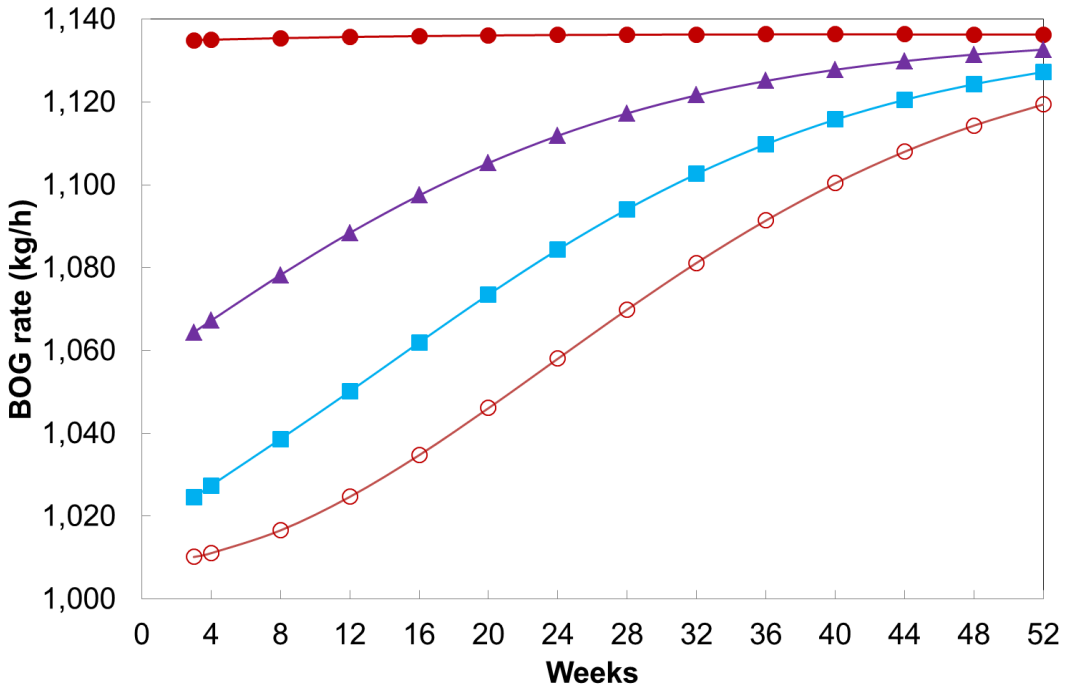

Figure 6.13 BOG rate (kg/h) vs. time - isothermal model.
(-●- Light LNG; -▲- LNG 0.5% N_2; -■- LNG 1.0% N_2; -○- LNG 1.5% N_2)

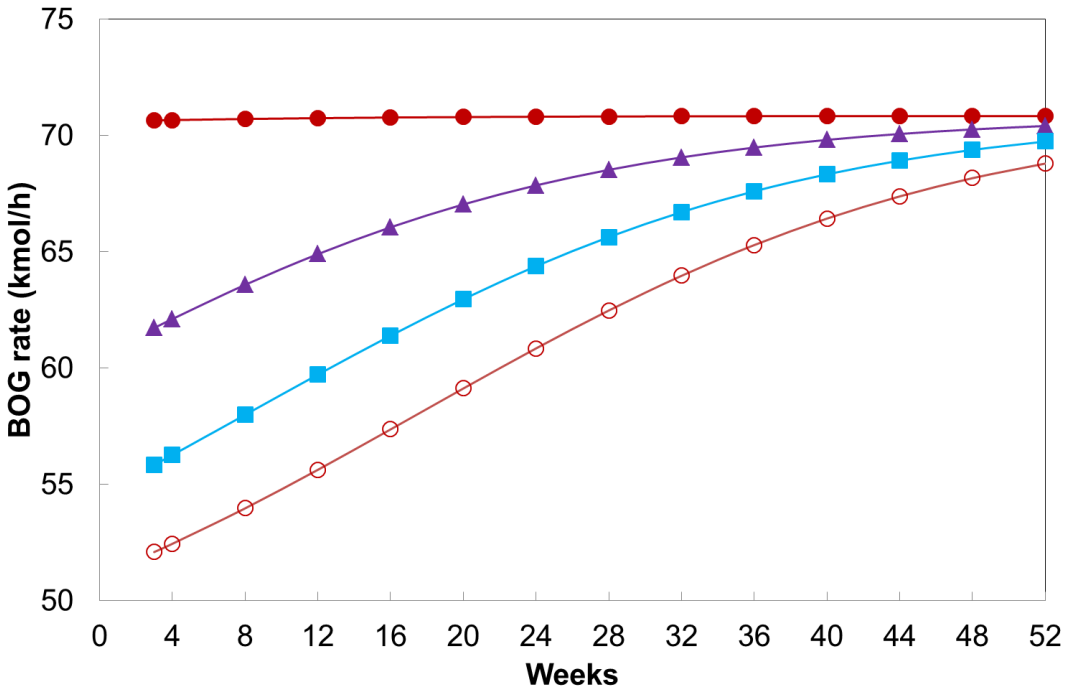

Figure 6.14 BOG rate (kmol/h) vs. time - isothermal model.
(-●- Light LNG; -▲- LNG 0.5% N_2; -■- LNG 1.0% N_2; -○- LNG 1.5% N_2)

One can observe a marked decrease in the BOG in the initial stages of weathering of up to 12% mass basis, between the low N_2 mixture and the 1.5% N_2 mixture, with the rest of N_2 enriched mixtures in between. The difference in BOG generation between the four mixtures nearly disappears towards the end of the weathering period as N_2 is depleted from the enriched N_2 mixtures. These curves indicate that the presence of nitrogen in the liquid has a predominant effect on weathering.

In order to understand the mechanism behind the decrease, the thermodynamics of the mixture are examined. The increase of the amount of N_2 in the LNG mixtures leads to two thermodynamic effects, namely lowering the boiling point of the mixture and increasing the latent heat needed to vaporize an LNG drop as summarized in Table 6.3. As LNG starts to weather, N_2, being the most volatile component in the mixture, will vaporize preferentially.

Figure 6.13 shows that the BOG generation rate (mass basis) gradually increases for the N_2 rich mixtures, which is due to the decrease of the molecular weight of the vapour and the latent heat, over the assessed weathering period.

Figures 6.15 and 6.16 illustrate the change in N_2 composition of the liquid and vapour phases as a function of time.

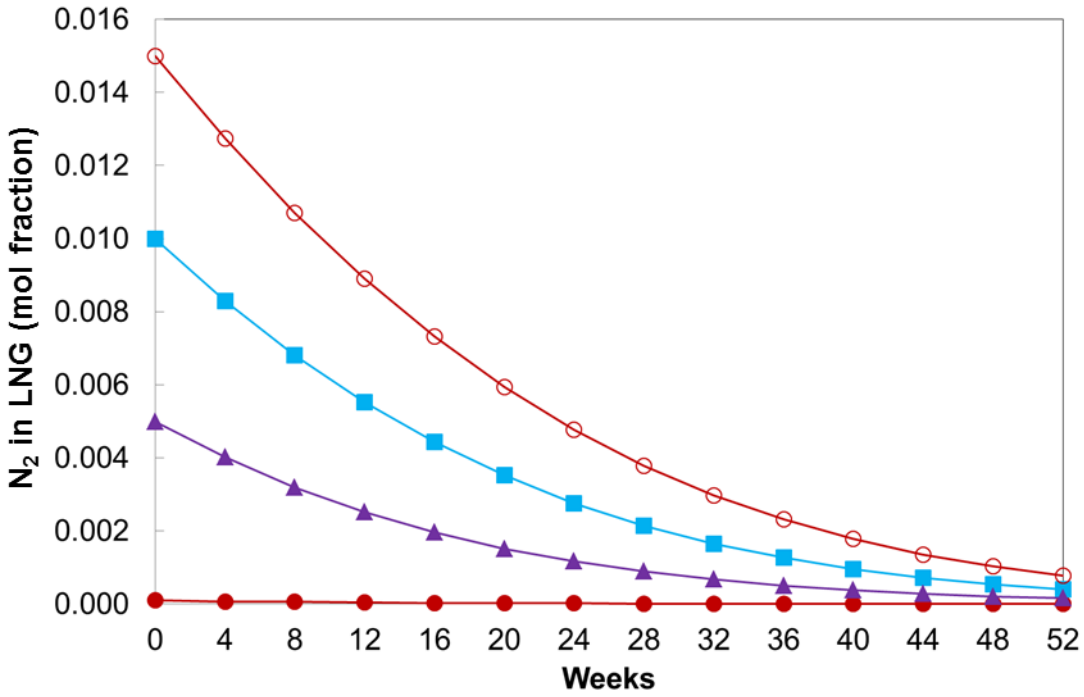

Figure 6.15 N_2 content (mol fraction) in LNG vs. time - isothermal model.
(-●- Light LNG; -▲- LNG 0.5% N_2; -■- LNG 1.0% N_2; -○- LNG 1.5% N_2)

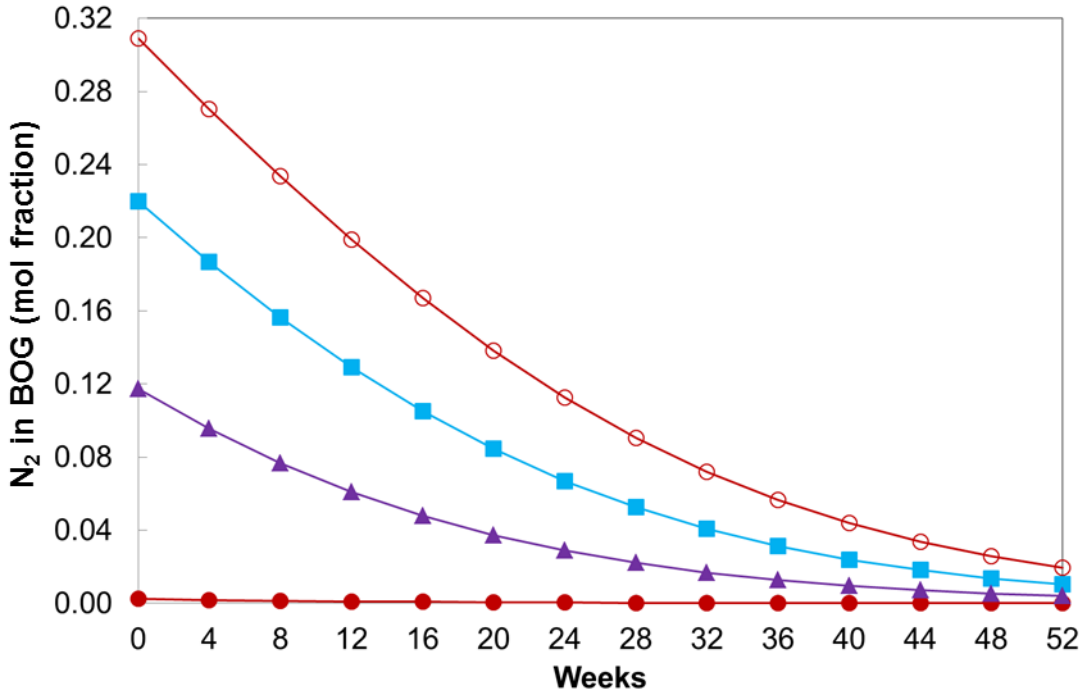

Figure 6.16 N_2 content (mol fraction) in BOG vs. time - isothermal model.
(-●- Light LNG; -▲- LNG 0.5% N_2; -■- LNG 1.0% N_2; -○- LNG 1.5% N_2)

One can observe a rapid decrease in the nitrogen concentration. As a consequence of it, the boiling temperature of the remaining LNG will increase. The simulations indicate that within the 52 weeks period examined the boiling temperature of all mixtures will reach around 114 K (refer to Figure 6.17 below). Such a small change in the boiling temperature during the weathering process will result in a rather small indirect differential latent heat component. The simulations indicate that the indirect differential latent heat is less than 0.1% of the total differential latent heat.

Figure 6.17 shows the boiling temperature evolution over the assessed weathering period for the four mixtures.

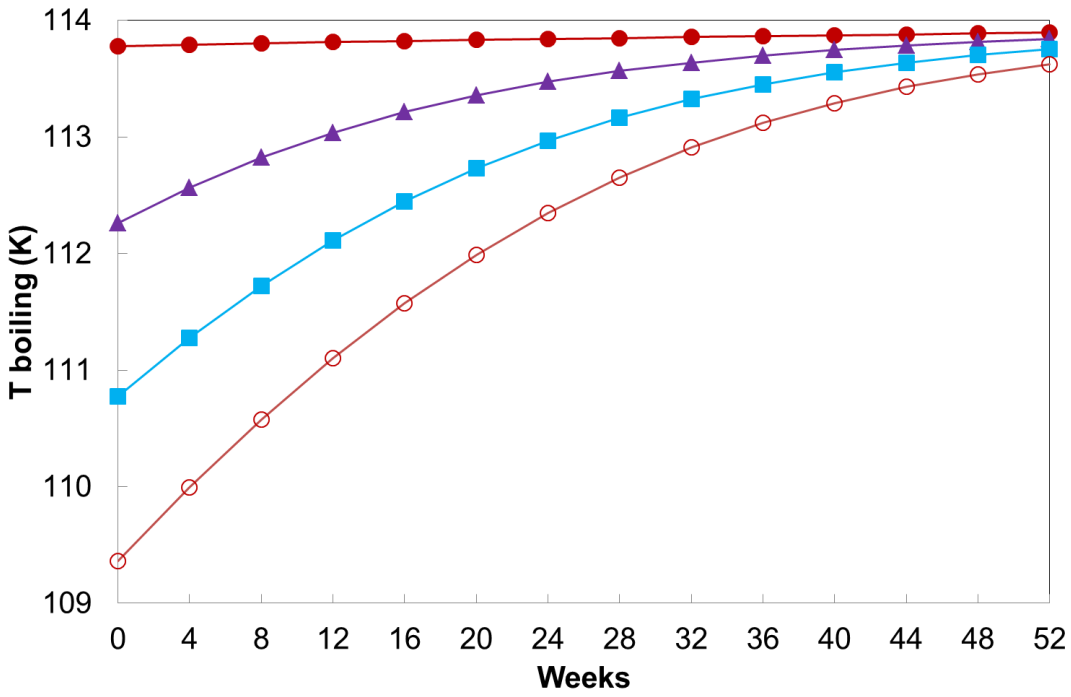

Figure 6.17 Boiling temperature vs. time - isothermal model.
(-●- Light LNG; -▲- LNG 0.5% N_2; -■- LNG 1.0% N_2; -○- LNG 1.5% N_2)

One can observe that the initial steep rise in the liquid temperature is due to the preferential vaporization of nitrogen which was originally present in the mixture.

Although the decrease in the boiling temperature (as the N_2 content in the mixture increases) has minimal effect on the differential latent heat, it will lead to a larger temperature differential between the LNG and the surroundings, at least in the initial stages

of the process. As a consequence the heat flux into the tank will increase. However, the effect is again only minor and the heat flux will increase by at most 1.0 %. Therefore, the determining factor in the reduction of BOG for N_2 rich mixtures is due to the increase in the direct latent heat required to vaporize a drop of LNG. Judging by results in Table 6.3 the difference in the latent heat between four mixtures is relatively small. However, that is the overall latent heat required to completely evaporate the mixture. As the mixture experiences preferential evaporation of lighter components the initial LNG vaporized will consist of a large amount of nitrogen as illustrated in Figure 6.15. Hence, the differential molar latent heat required to vaporize a drop of LNG at each stage of the process needs to be considered. At the initial stage of vaporization of LNG containing 1.5 % N_2, the vapour phase will consists of 31 % nitrogen, see Figure 6.16. The differential latent heat needed to evaporate a mixture consisting of 31 % nitrogen and 69 % methane will be approximately 40 % higher than the latent heat of pure methane. This roughly translates into a decrease of molar based BOG (measured in kmol/h) by a similar amount. However, if it is examined, as traditionally done, the mass based BOG, expressed in kg/h, then the decrease is smaller and no longer proportional to the direct latent heat. This is the consequence of the increase in the molecular weight of the generated vapour which is initially higher than in the base case, due to a large amount of N_2 present in the vapour.

As shown in Figure 6.16, the nitrogen content of the vapour can reach up to 30 %. The increase in molecular weight of vapour compared to the base case (Light LNG) explains the different initial slope of BOG for 1.5% N_2 rich LNG in Figure 6.13. As the preferential evaporation of nitrogen continues the amount of nitrogen decreases in time, that is illustrated in Figure 6.15. The direct differential molar latent heat will consequently decrease, resulting in increase in BOG in later stages of weathering, as illustrated in Figure 6.13.

Table 6.4 shows the LNG weathered compositions after 52 weeks predicted by the isothermal model, for the LNG mixtures compositionally described in Table 6.3.

Table 6.4 Predicted LNG weathered composition after 52 weeks.

Component (mol fraction)	Light LNG	Weathered Light LNG	0.5% N_2	Weathered 0.5% N_2	1.0% N_2	Weathered 1.0% N_2	1.5% N_2	Weathered 1.5% N_2
C_1	0.9613	0.9545	0.9566	0.9551	0.9517	0.9554	0.9470	0.9556
C_2	0.0340	0.0400	0.0338	0.0394	0.0337	0.0389	0.0335	0.0384
C_3	0.0039	0.0046	0.0039	0.0045	0.0039	0.0045	0.0038	0.0044
iC_4	0.0004	0.0005	0.0004	0.0005	0.0004	0.0005	0.0004	0.0005
nC_4	0.0003	0.0004	0.0003	0.0003	0.0003	0.0003	0.0003	0.0003
N_2	0.0001	0.0000	0.0050	0.0002	0.0100	0.0004	0.0150	0.0008
$T_{boiling}$, °C	-159.4	-159.2	-160.9	-159.3	-162.4	-159.4	-163.8	-159.5

Figures 6.18 and 6.19 show respectively the graphs of molecular weight versus nitrogen content, and molecular weight vs. time, of the LNG mixture remaining in the tank over 52 weeks of weathering period.

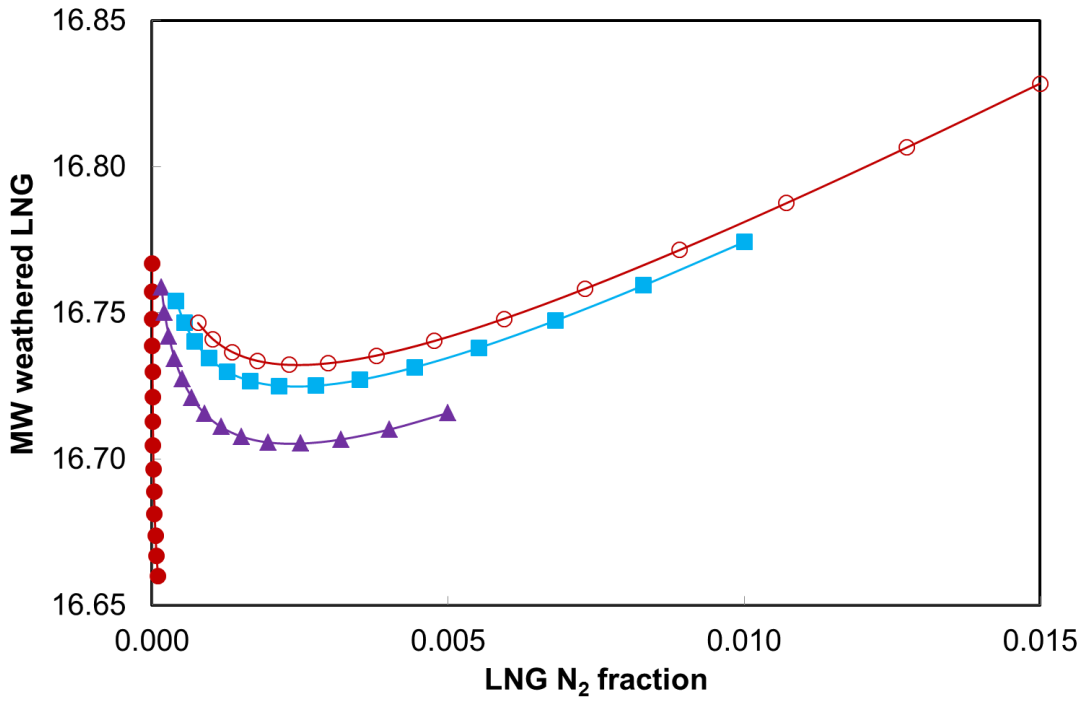

Figure 6.18 LNG molecular weight vs. N_2 content - isothermal model.
(-●- Light LNG; -▲- LNG 0.5% N_2; -■- LNG 1.0% N_2; -○- LNG 1.5% N_2)

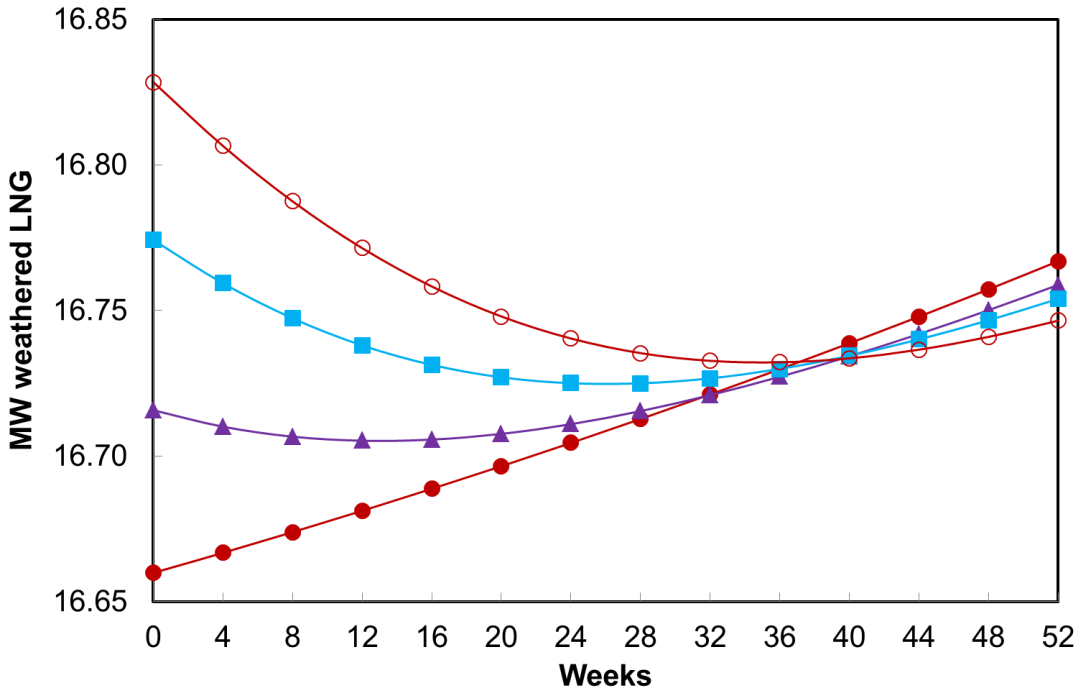

Figure 6.19 LNG molecular weight vs. time - isothermal model.
(-●- Light LNG; -▲- LNG 0.5% N_2; -■- LNG 1.0% N_2; -○- LNG 1.5% N_2)

What is interesting to observe is that further increase in the initial nitrogen content does not lead to further decrease of BOG. Figure 6.20 shows the variation of the initial BOG rate after 24 hours of weathering, with the initial amount of N_2 in the LNG up to 4% mol (refer to Table 6.5 for detail composition). It is observed that a minimum exists at around 1.5% of N_2. The minimum is a direct consequence of the increase in the molecular weight of the generated vapour, which is rich in nitrogen.

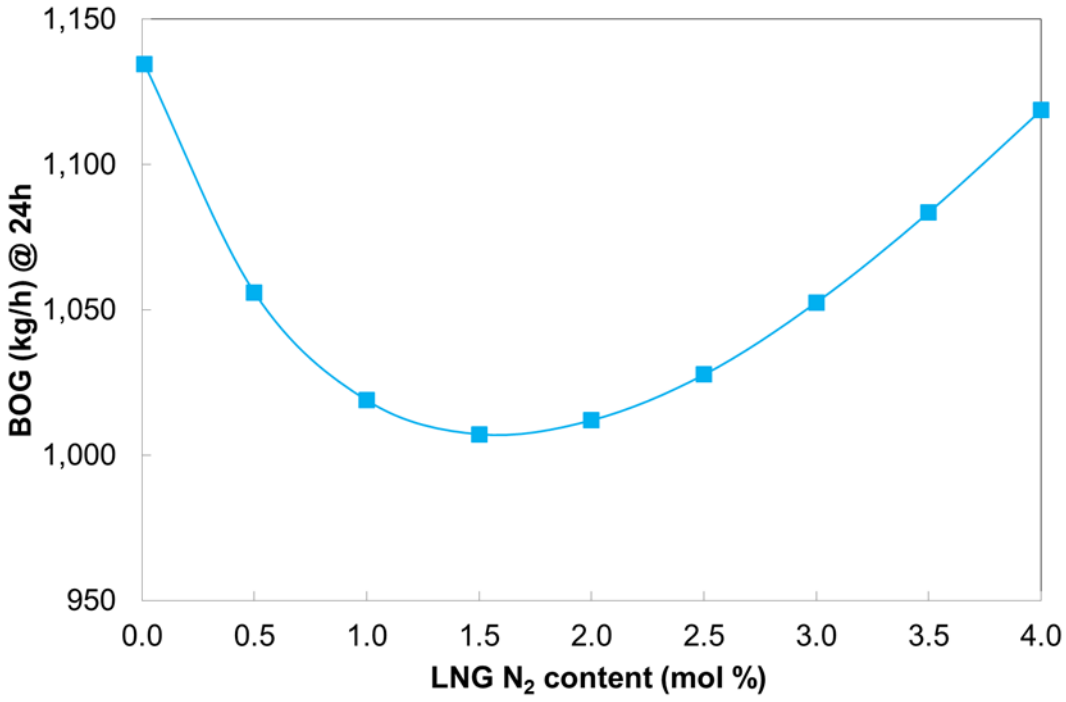

Figure 6.20 BOG rate after 24h vs. initial N_2 content - isothermal model.

Table 6.5 below shows the nitrogen enriched compositions used for the further increase in the initial nitrogen content analysis

Table 6.5 Extended nitrogen enriched LNG mixtures.

Component	Light	N_2 content in the mixture							
mol fraction	LNG	0.5%	1.0%	1.5%	2.0%	2.5%	3.0%	3.5%	4.0%
C_1	0.9613	0.9566	0.9517	0.9470	0.9422	0.9373	0.9325	0.9277	0.9229
C_2	0.0340	0.0338	0.0337	0.0335	0.0333	0.0332	0.0330	0.0328	0.0326
C_3	0.0039	0.0039	0.0039	0.0038	0.0038	0.0038	0.0038	0.0038	0.0038
iC_4	0.0004	0.0004	0.0004	0.0004	0.0004	0.0004	0.0004	0.0004	0.0004
nC_4	0.0003	0.0003	0.0003	0.0003	0.0003	0.0003	0.0003	0.0003	0.0003
N_2	0.0001	0.0050	0.0100	0.0150	0.0200	0.0250	0.0300	0.0350	0.0400
$T_{boiling}$, ºC	-159.4	-160.9	-162.4	-163.8	-165.2	-166.5	-167.7	-168.8	-169.9

Two additional graphs are plotted to further investigate what is the effect on the BOG generation behaviour after some time, since part or all N_2 has evaporated from the mixture.

Figures 6.21 and 6.22 respectively show the variation of the initial BOG rate after 14 days and 52 weeks of weathering, with the initial amount of N_2 in the LNG.

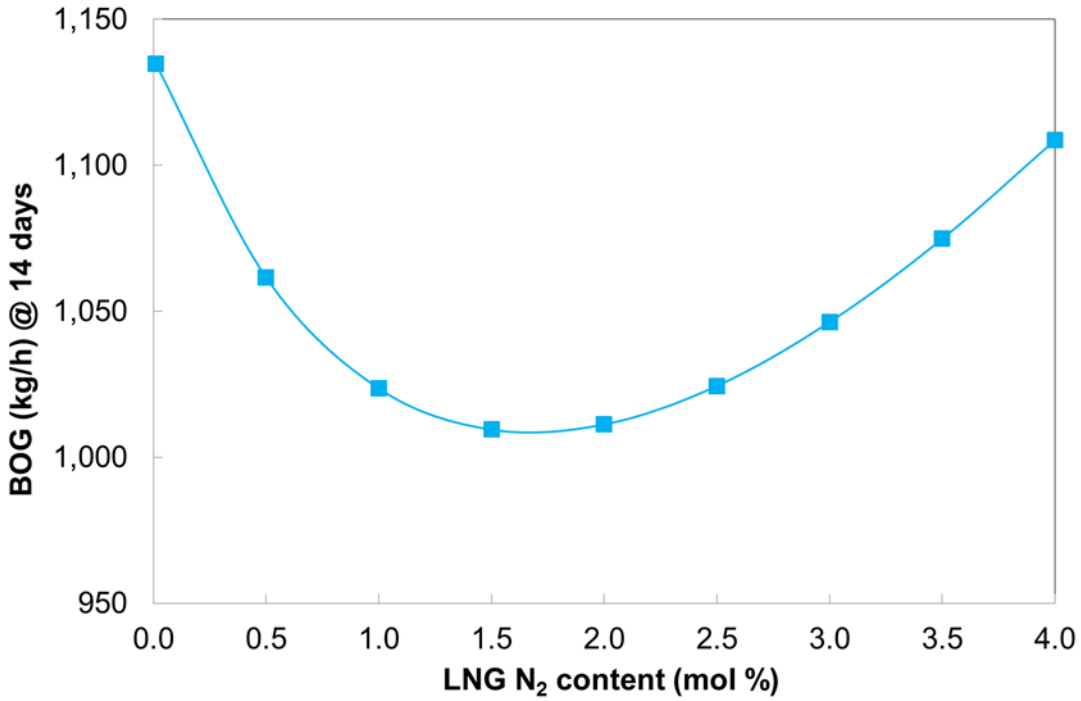

Figure 6.21 BOG rate after 14 days vs. initial N_2 content - isothermal model.

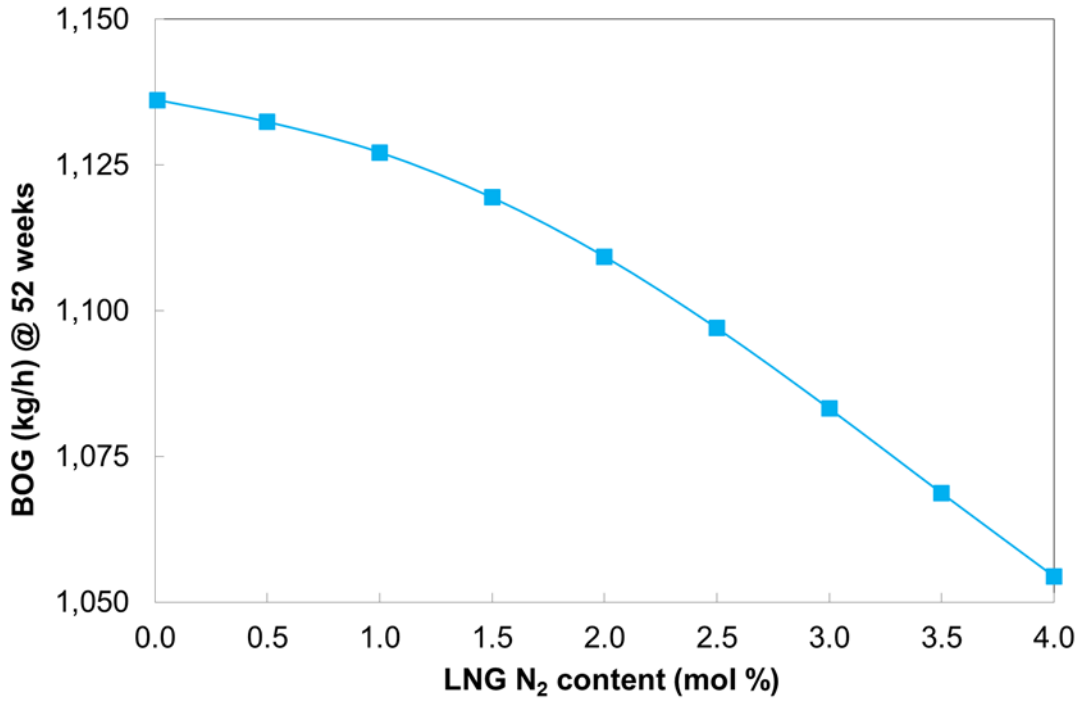

Figure 6.22 BOG rate after 52 weeks vs. initial N_2 content – isothermal model.

As the amount of nitrogen in the initial LNG increases, the boiling temperature will decrease (refer to Table 6.5) and the direct differential molar latent heat will increase (refer to Figure 6.23 below). For instance, for an LNG mixture that contains 4% by mol of nitrogen, the boiling temperature will drop by approximately 6 ^{o}C and direct differential molar latent heat will increase by approximately 8%, compared to an LNG mixture that contains 1.5% by mol of nitrogen. The effect of temperature is small resulting in 1% increase in BOG, whilst the effect of the latent heat will dominate and will lead to the overall decrease of BOG by approximately 7%. However, in the initial stages of boiling the BOG being released by 4% N_2 LNG mixture will consist of approximately 60% nitrogen, compared to 30% for 1.5% N_2 LNG mixture. The increase in the *MW* of the resulting vapour will result in lower total differential latent heat per unit mass. Hence, the standard BOG expressed in mass terms, rather than in terms of number of moles, will be higher for the LNG mixture that contains 4% by mol of nitrogen. This offers an intriguing possibility of using nitrogen to minimize the BOG, during the storage stage, as long as the generated BOG vapour is not transferred to the outside gas network.

Figure 6.22 shows that after 52 weeks of weathering there is a change in the BOG generation rate behaviour, which progressively decreases as the initial N_2 content increases. The BOG generation drop is due to the progressive increase of the molar latent heat, as shown by Figure 6.23. The increase in the molecular weight of the BOG generated after 52 weeks from Light LNG to 4% mol N_2 content is very small (compared to 24 hours), and hence the effect of the vapour molecular weight on BOG generation (after 52 weeks) is negligible, compared to the effect of the molar latent heat.

Figures 6.23 and 6.24 respectively show the molar latent heat and the vapour molecular weight for the three durations (24 hours, 14 days and 52 weeks), with the initial amount of N_2 in the LNG.

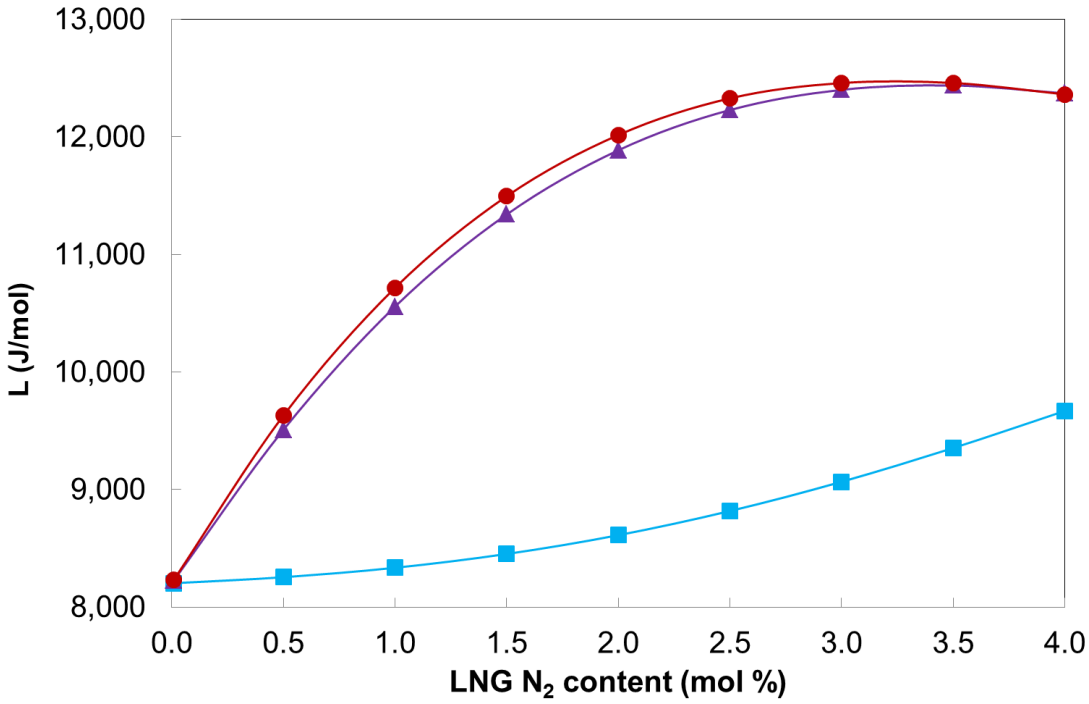

Figure 6.23 Latent heat (J/mol) vs. initial N_2 content - isothermal model.
(-●- 24 hours; -▲- 14 days; -■- 52 weeks)

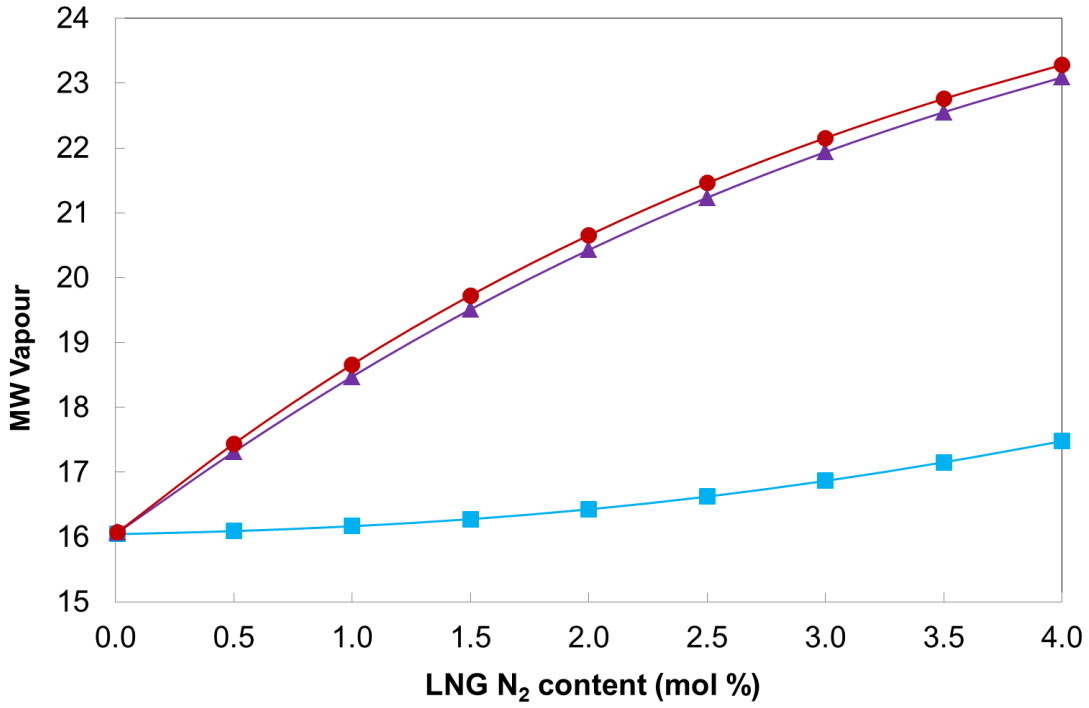

Figure 6.24 Vapour MW vs. initial N_2 content – isothermal model.
(-●- 24 hours; -▲- 14 days; -■- 52 weeks)

Figure 6.25 shows the mass latent heat for the three durations, with the initial nitrogen content. The graph illustrates the interplay between the molar latent heat and the molecular weight of the vapour at the early stage of weathering (after 24 hours and 14 days), and the progressive increase of the mass latent heat for the late stage of weathering (after 52 weeks), as the nitrogen content increases in the LNG.

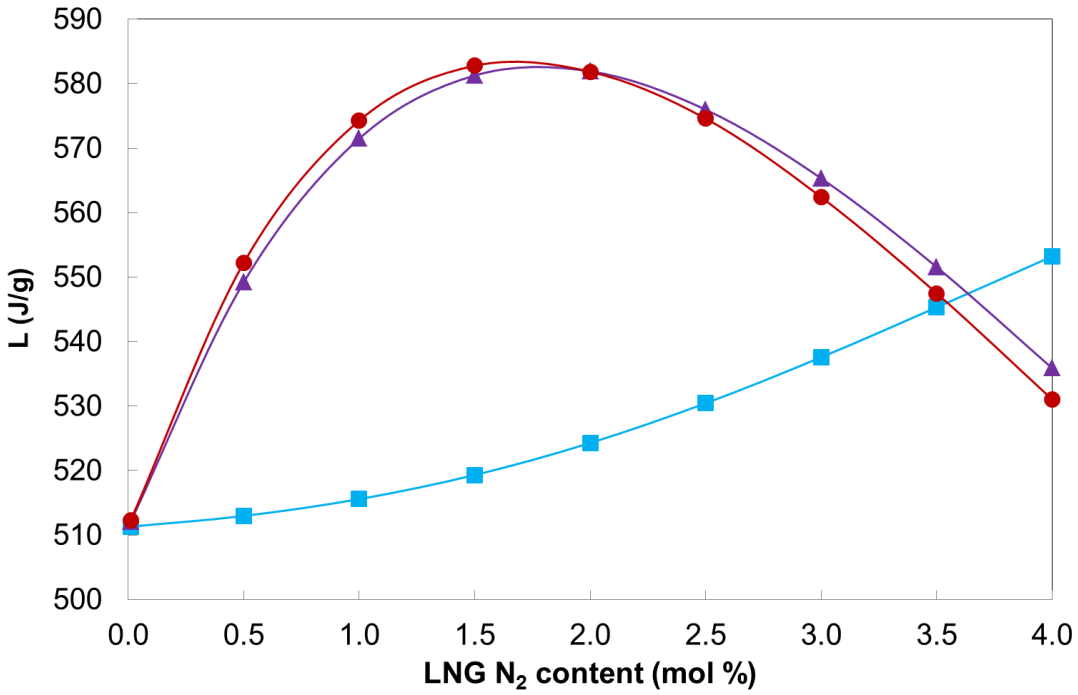

Figure 6.25 Latent heat (J/g) vs. initial N_2 content - isothermal model.
(-●- 24 hours; -▲- 14 days; -■- 52 weeks)

6.1.4 SENSITIVITY TO OUTSIDE TEMPERATURE VARIATION

A sensitivity case is presented to analyse the effect of outside temperature variations on BOG generation from stored LNG. The analysis is based on the initial filling of 160,000 m^3 of LNG and the outside temperature has varied in 10 ºC stages from 5 ºC to 35 ºC. The LNG mixture containing 1.5% of N_2 on molar basis compositionally defined in Table 6.3 is used in the illustrations, as it showed greatest variation of BOG (see Figure 6.13) over the period of interest.

Figure 6.26 and 6.27 respectively illustrate the sensitivity of BOG vaporization rate and BOR, to the outside temperature variation; the BOR defined as the ratio of volume in liquid terms of LNG that has evaporated in one day, relative to the initial LNG volume.

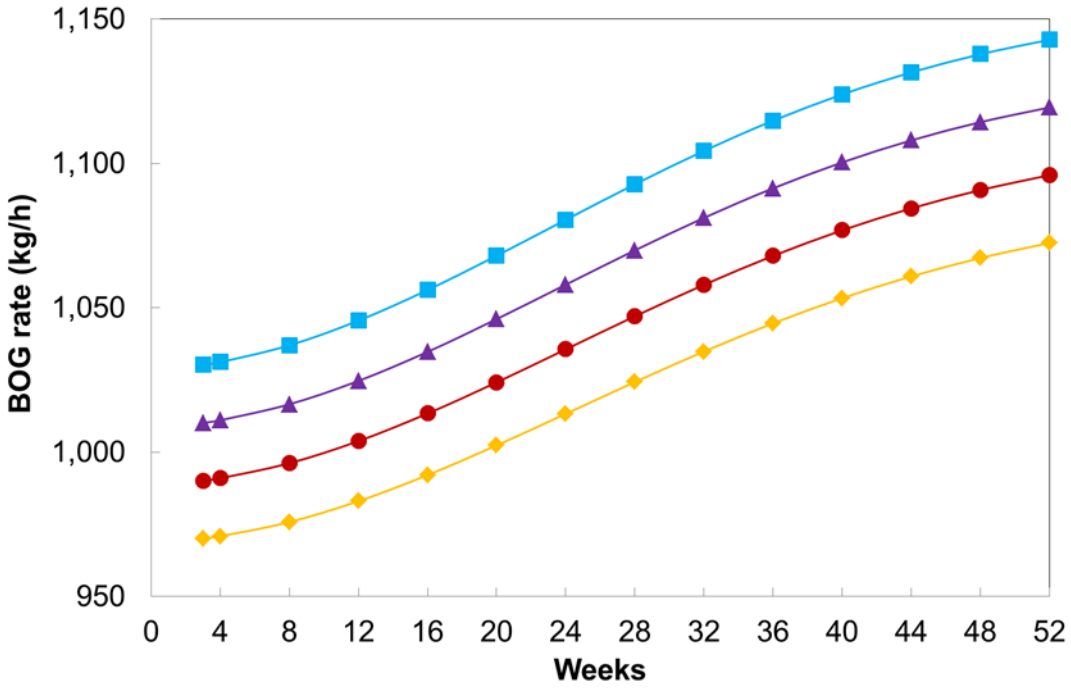

Figure 6.26 BOG rate due to variation of T air - isothermal model.
(-◆- T_{air}=5 °C; -●- T_{air}=15 °C ; -▲- T_{air}=25 °C; -■- T_{air}=35 °C)

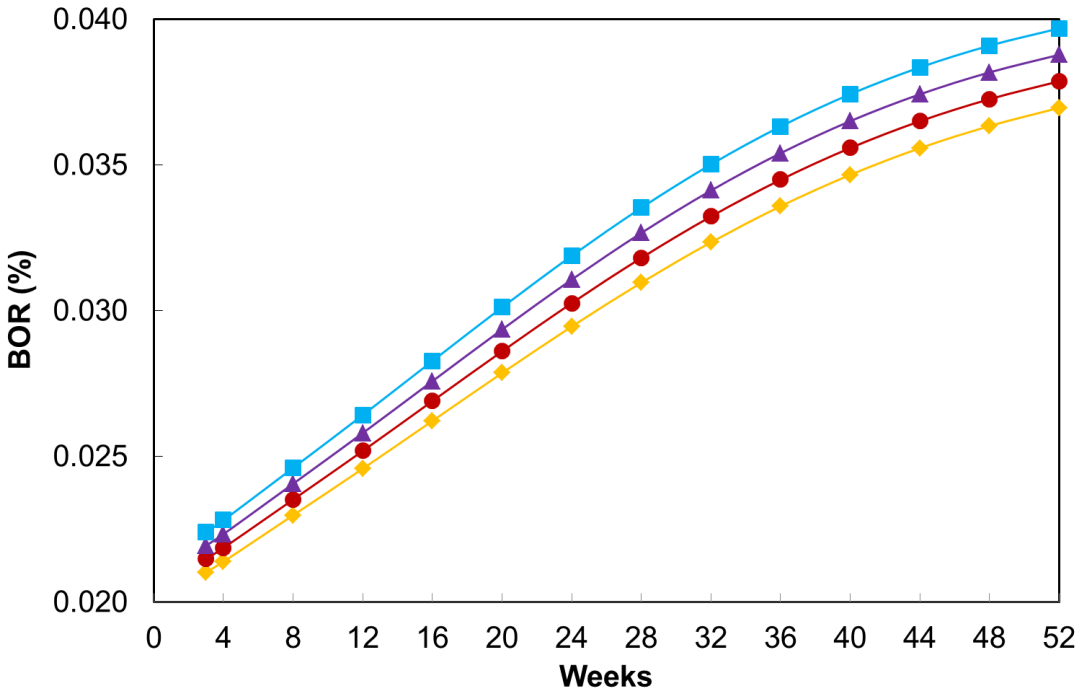

Figure 6.27 BOR due to variation of T air - isothermal model.
(-◆- T_{air}=5 °C; -●- T_{air}=15 °C ; -▲- T_{air}=25 °C; -■- T_{air}=35 °C)

On average the BOG rate increases by approximately 2% for every 10 ºC increase in the outside temperature. It is primarily driven by the temperature differential between the tank and the surroundings, taking into account that the heats coming through the slab and roof section of the tank are very weakly dependent on the temperature of surrounding air. Hence, for LNG tanks currently operated by industry one can safely assume a rule-of-thumb that 1 ºC change in the outside temperature will change the BOG by approximately 0.2 %.

6.1.5 EFFECT OF TIME STEP SIZE

As described in Chapter 4, the LNG weathering model is built in a stepwise execution mode using finite differences by specifying a time step. The time step refers to the indexing variable within the model, and characterizes the unit of time in which the system progresses. This section presents the influence of the time step size in the modelling of LNG weathering, as the implication of this is that the solution has converged only when further reduction in time step produces no observable change in the system state.

LNG weathering runs were performed over one year period for the LNG with N_2 mixture (compositionally described in Table 6.2), to compare parameter predictions for different time step sizes. The simulations were conducted for one day, one week and one month time step sizes. Figures 6.28, 6.29 and 6.30 show the results for the predicted BOG generation rate, boiling temperature and LNG methane content respectively.

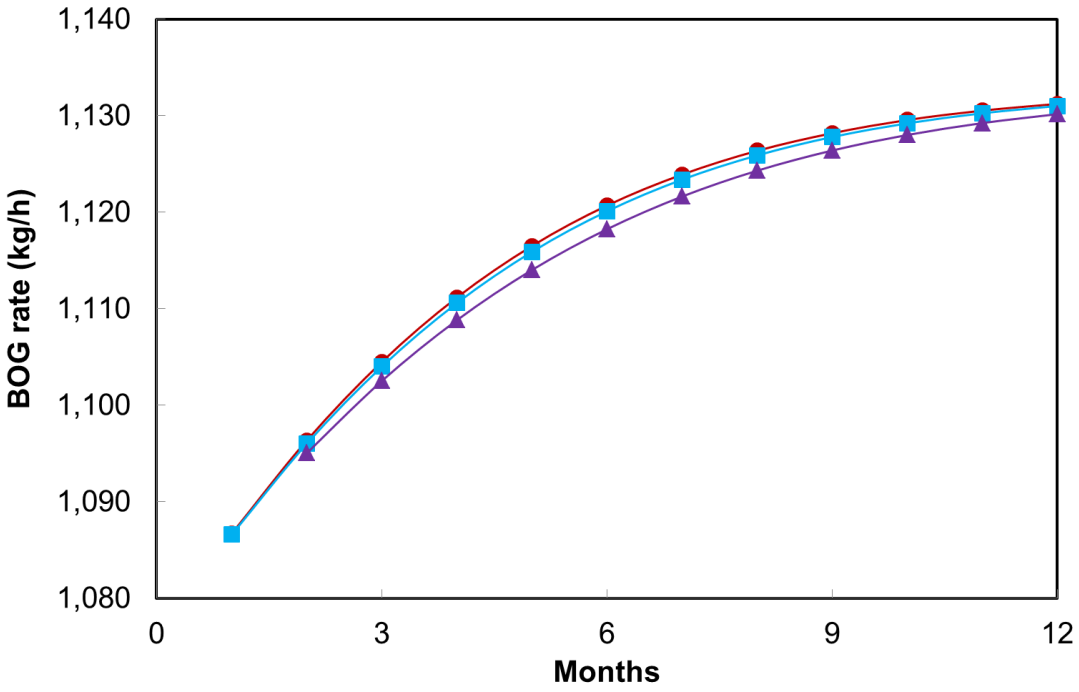

Figure 6.28 BOG rate for different time step sizes – isothermal model.
(-●- t_s: 1 day; -■- t_s: 1 week; -▲- t_s: 1 month)

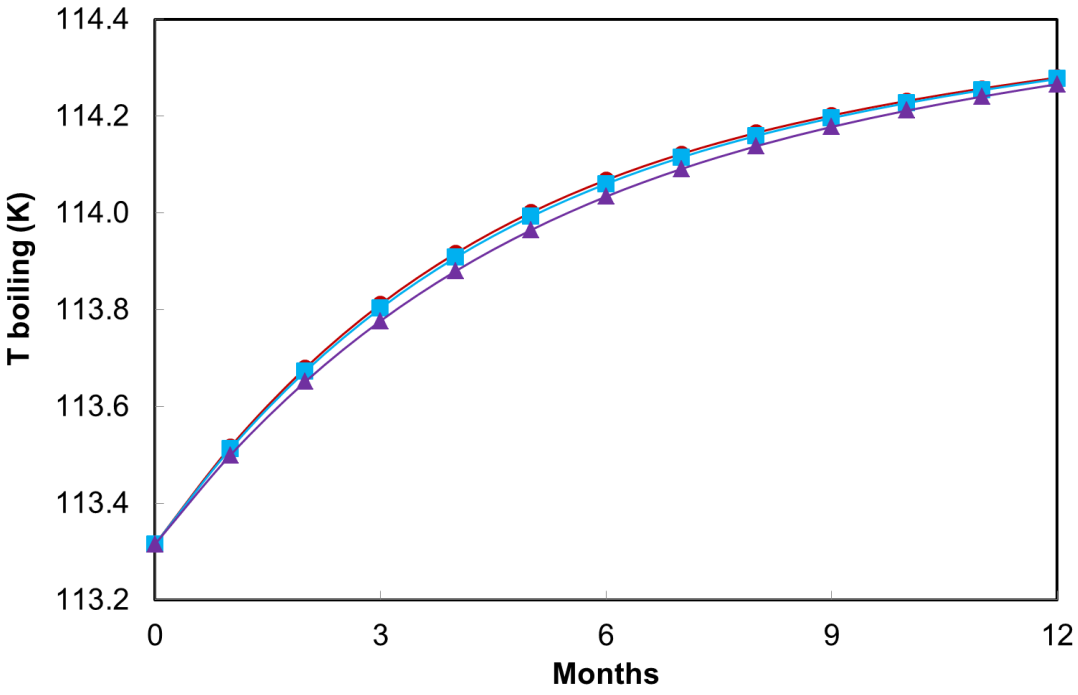

Figure 6.29 T boiling for different time step sizes – isothermal model.
(-●- t_s: 1 day; -■- t_s: 1 week; -▲- t_s: 1 month)

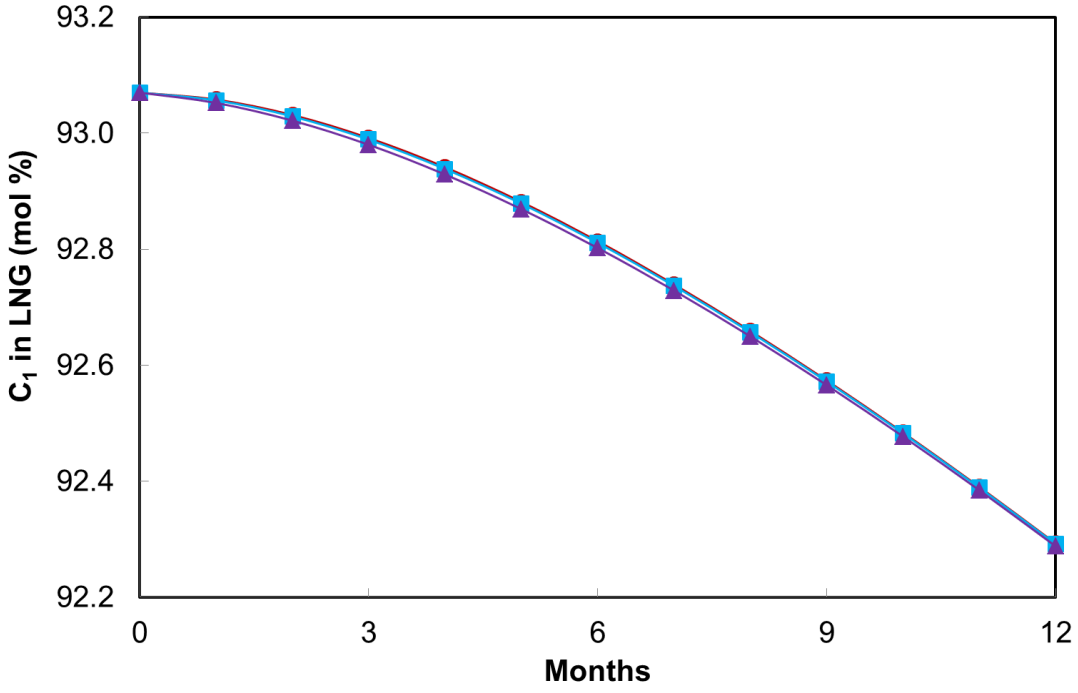

Figure 6.30 CH_4 in LNG for different time step sizes – isothermal model.
(-●- t_s: 1 day; -■- t_s: 1 week; -▲- t_s: 1 month)

The comparative error between the predicted BOG generation rates is lower than 0.25% over the entire weathering period. With regards to boiling temperature and LNG methane content evolution, the errors are within 0.05% and 0.02%, respectively.

Regardless of the time step size the isothermal model produces the same results in key weathering parameters such as BOG generation rate, boiling temperature and methane content in LNG.

The simulations and sensitivity analysis within this research project were run using one week as the time step.

6.2 SUPERHEATED VAPOUR LNG WEATHERING MODEL RESULTS

6.2.1 SENSITIVITY TO INITIAL LNG COMPOSITION

A sensitivity analysis to initial LNG composition was also carried out using the superheated vapour weathering model developed, and for the three commercial LNG mixtures used for the isothermal model sensitivity assessment, as described in Table 6.2.

Figures 6.31 and 6.32 illustrate the BOG rate evolution using the superheated vapour model as a function of the weathering period.

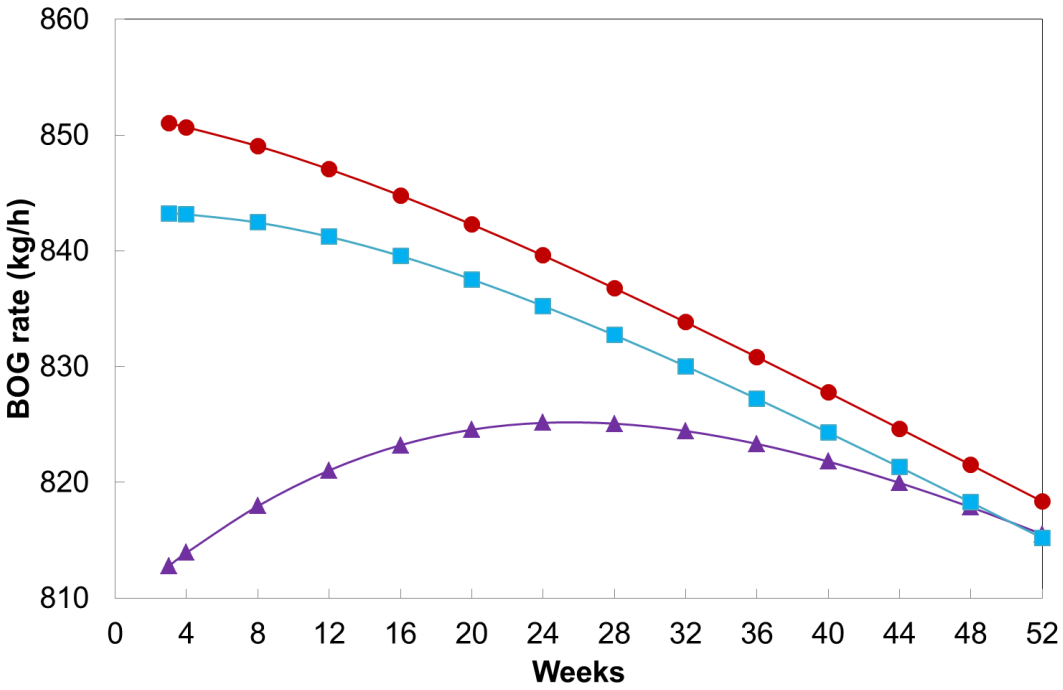

Figure 6.31 BOG rate (mass basis) vs. time - superheated vapour model.
(-●- Light LNG;-■- Heavy LNG; -▲- LNG with N_2)

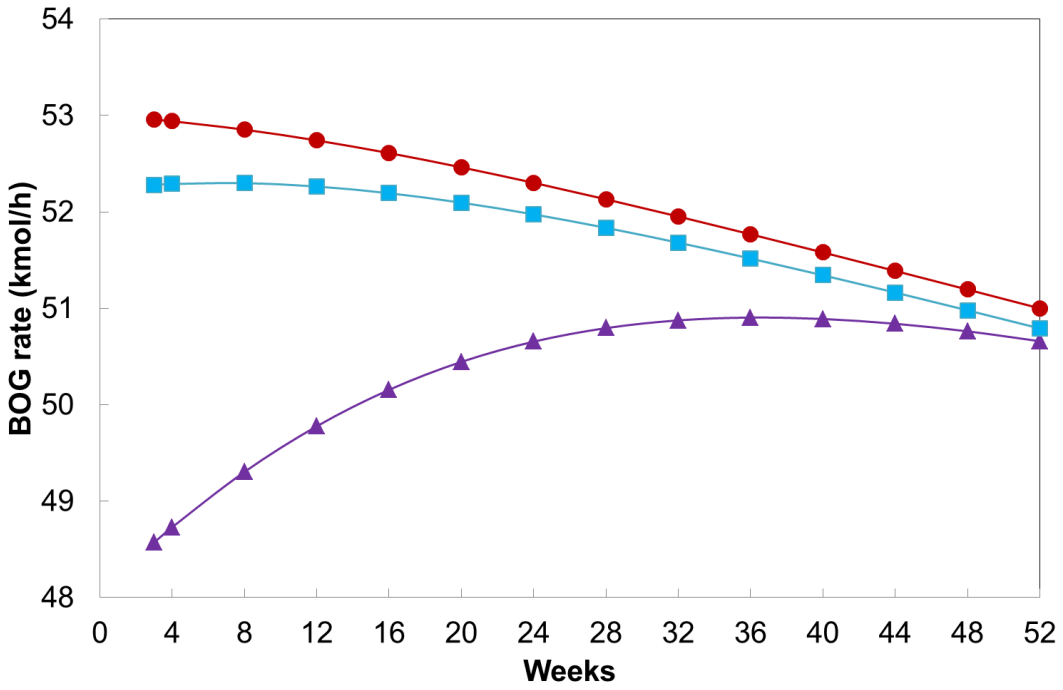

Figure 6.32 BOG rate (mol basis) vs. time - superheated vapour model.
(-●- Light LNG; -■- Heavy LNG; -▲- LNG with N_2)

The BOG generated for the three LNG mixtures progressively drops as the weathering process develops. In the isothermal model the BOG generation is nearly constant over the weathering process, as all the heat entering into the tank is used to vaporize the LNG. Within the superheated vapour approach the vapour is heated up, so less heat is going to vaporize the LNG, thus less BOG is generated. Moreover, as LNG evaporates the wet heat transfer area decreases (the heat transfer contact area reduces); therefore, less heat is available to vaporize the LNG.

The BOG produced at the beginning of the weathering process for the Light LNG mixture is 851 kg/h (53.0 kmol/h), whilst for the Heavy LNG is 843 kg/h (52.3 kmol/h). By the end of weathering period, week 52, the BOG generation rate drops down to 818 kg/h (51.0 kmol/h) and 815 kg/h (50.8 kmol/h), for Light and Heavy LNG respectively, which are very close to the pure methane case, 821 kg/h (51.2 kmol/h). Furthermore, the BOG generation rate for the Light and Heavy LNG mixtures show very similar evaporation behaviour following the same trend as for the pure methane case (refer to Figure 6.33). Later on, within this section, the comparison of the BOG generation rate results between the isothermal and superheated vapour models is presented.

Figure 6.33 show the BOG rate evolution for the pure methane case, using the superheated vapour model.

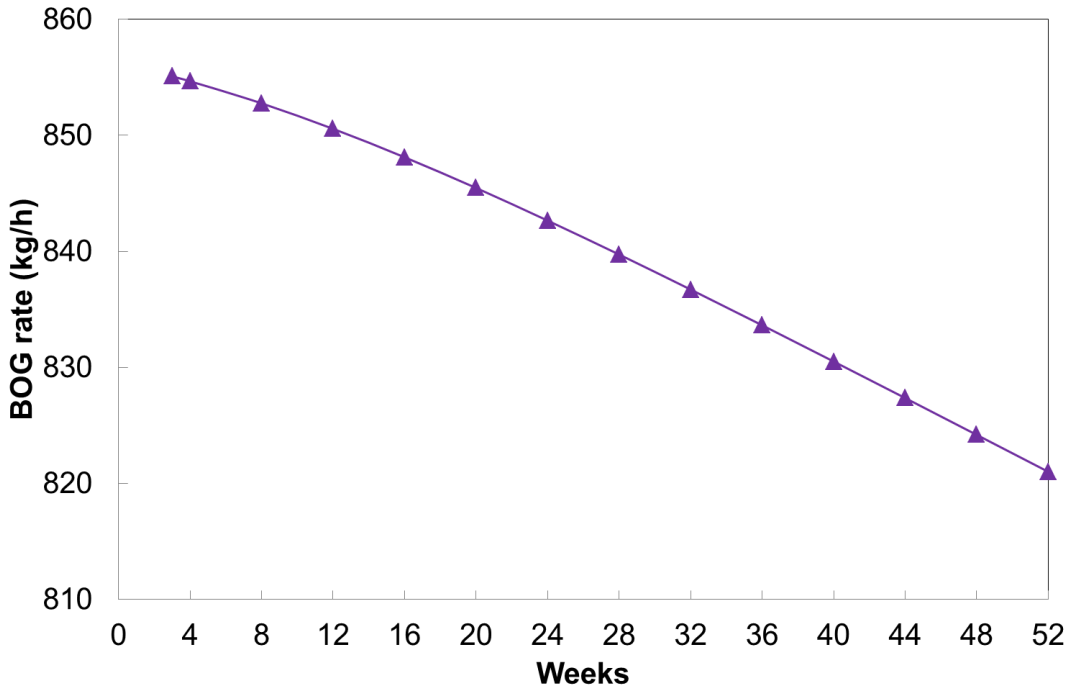

Figure 6.33 BOG rate (mass basis) CH_4 case - superheated vapour model.

Figures 6.31 and 6.32 additionally confirm that a very small amount of nitrogen present in the LNG (0.26% in this case) has a substantial influence on the initial BOG (812 kg/h – 48.6 kmol/h), leading to nearly 5% and 4% decrease compared to Light and Heavy LNG (mixtures with virtually nil nitrogen content), respectively. As addition of nitrogen increases the overall latent heat of the nitrogen-methane mixture, the amount of LNG vaporized will decrease. In this case, LNG with N_2, the initial methane content in the vapour is near 94% (see Figure 6.34). As the amount of nitrogen in BOG progressively decreases the BOG generation rate becomes very similar to that of the pure methane case. The BOG produced by the end of the weathering period is 816 kg/h (50.7 kmol/h). It is also confirmed that the Heavy LNG boils at a lower evaporation rate than the Light LNG mixture, since the boiling temperature and latent heat are slightly higher (see Table 6.3) the system takes more energy to evaporate a unit mass of LNG.

Compared to the isothermal model, the decrease in BOG generation rate estimated by the superheated vapour model (refer to Figures 6.2 and 6.31) is predicted to be beneficial for the industry. In this regard, it is important to highlight that sometimes a conservative model

as the isothermal model may lead to rather conservative results, and relying on them, may lead to conservative practices with an additional cost impact.

Figure 6.34 shows the methane content in the vapour for the three mixtures over the assessed weathering period.

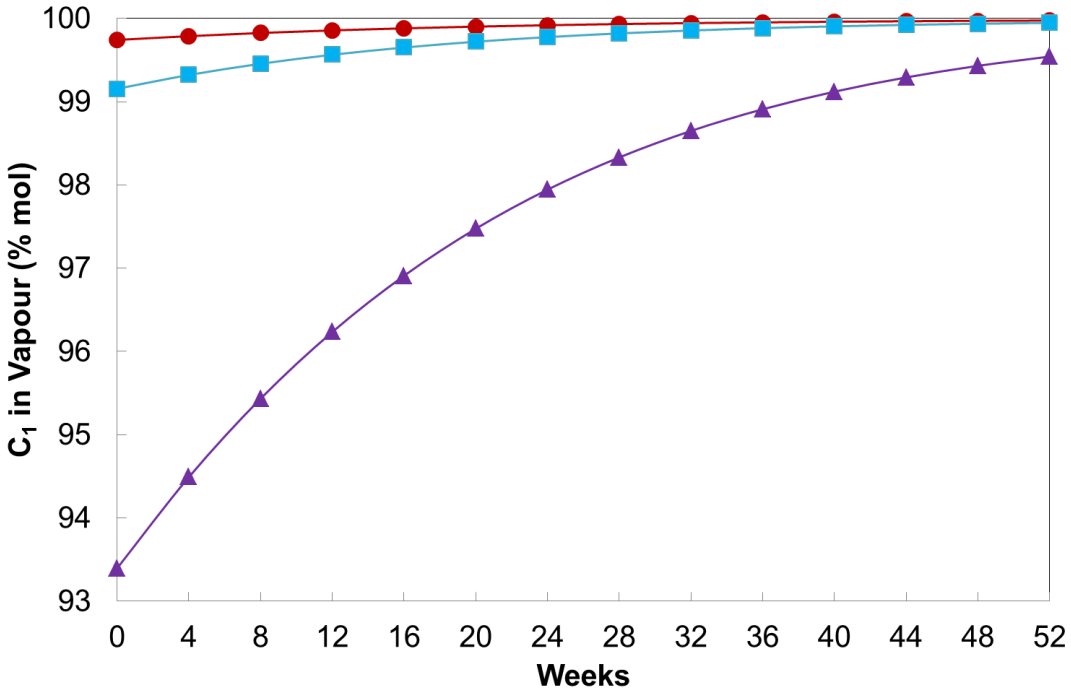

Figure 6.34 CH_4 content in the vapour – superheated vapour model.
(-●- Light LNG; -■- Heavy LNG; -▲- LNG with N_2)

Figures 6.35 and 6.36 respectively show the boiling and vapour temperatures vs. time.

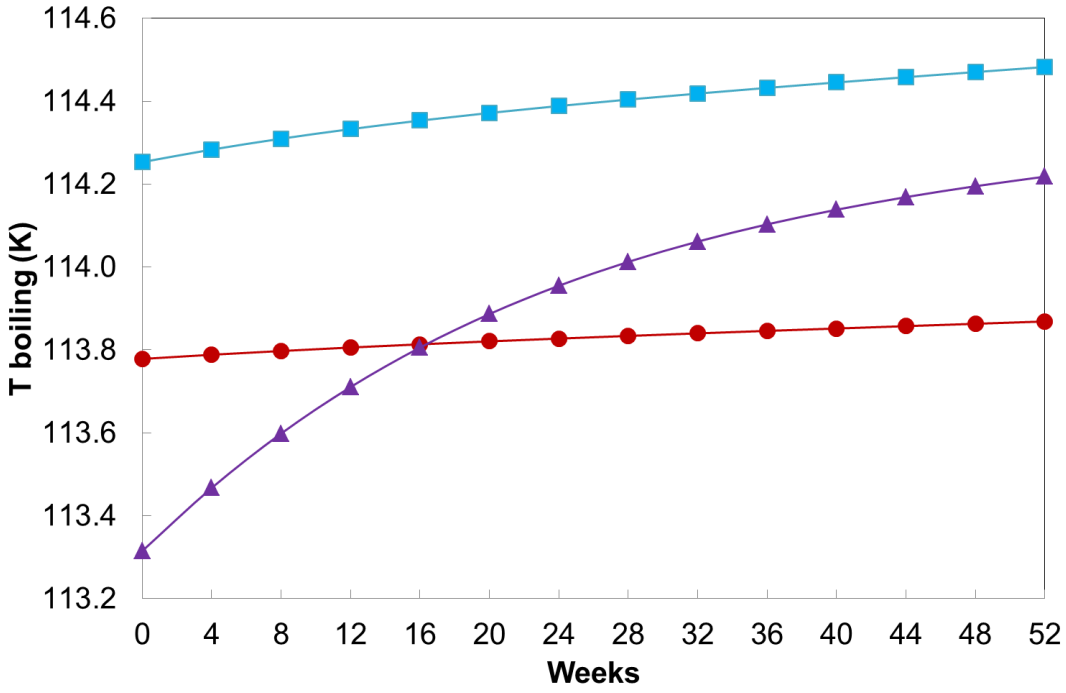

Figure 6.35 Boiling temperature vs. time - superheated vapour model.
(-●- Light LNG; -■- Heavy LNG; -▲- LNG with N_2)

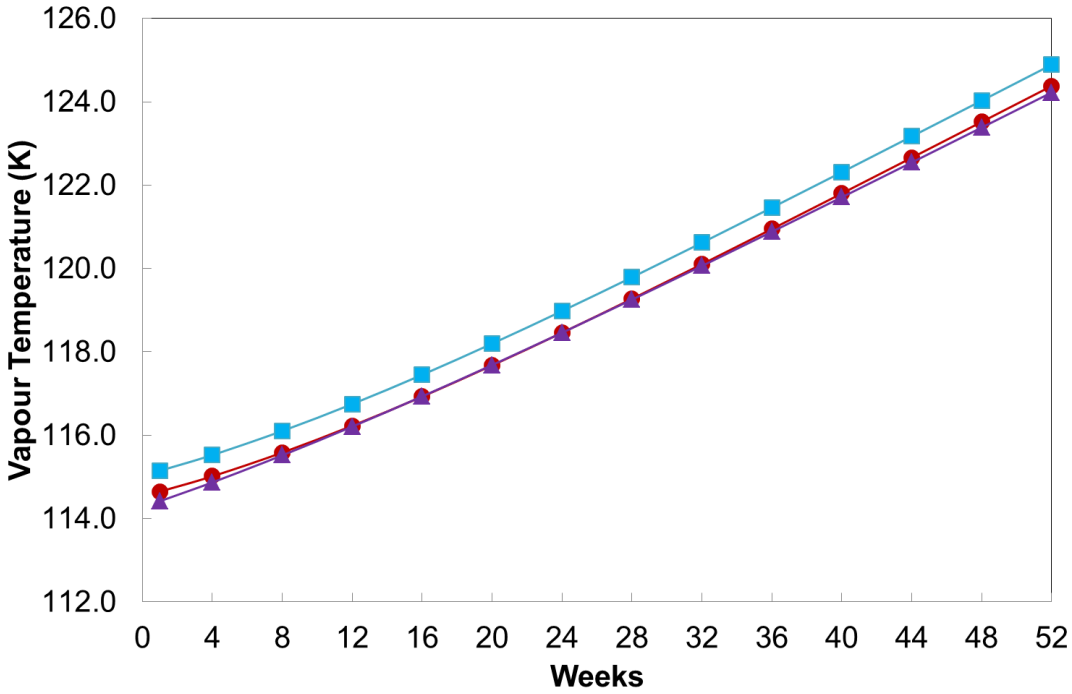

Figure 6.36 Vapour temperature vs. time - superheated vapour model.
(-●- Light LNG; -■- Heavy LNG; -▲- LNG with N_2)

As discussed earlier, in the isothermal model the whole system is considered to be in thermodynamic equilibrium, thus all heat entering into the system is used to vaporize the LNG. In the superheated vapour model instead, the heat ingress from the roof is omitted and the influence of the heat influx into the LNG storage tank is separated between the liquid and the vapour sides. Hence the BOG generated comes from the heat entering into the liquid, which includes the heat contribution from the superheated vapour.

From Figure 6.31 one can observe that compared to the isothermal model (see Figure 6.2), there is a large difference between the BOG generation rate predicted by both models. The mechanistic behind this BOG generation behaviour is due to the less heat used to vaporize the LNG, and the need to heat up the vapour in the superheated vapour model (refer to Figure 6.36). To confirm this explanation a further assessment was carried out to check whether the heat required to vaporize the incremental BOG from the isothermal model is comparable to the total heat input ratio between the isothermal and superheated vapour models. The assessment was carried out by comparing the BOG generation calculated by the isothermal model, scaled by a multiplication factor calculated from the heat input ratio between both models, to the BOG generation estimated by the superheated vapour model. The scaled BOG generation to make the comparison assessment is called *BOG'*, and is written as follows:

$$BOG' = \frac{Q_{shv}}{Q_{iso}} BOG_{iso} \tag{6.1}$$

where (Q_{shv}) and (Q_{iso}) are defined as follows:

$$Q_{shv} = \left(\dot{Q}_{\mathrm{L}_{in}} + \dot{Q}_{slab} + \dot{Q}_{\mathrm{V}_{in}}\right) t_s \tag{6.2}$$

$$Q_{iso} = \left(\dot{Q}_{\mathrm{L}_{in}} + \dot{Q}_{slab} + \dot{Q}_{\mathrm{V}_{in}} + \dot{Q}_{roof}\right) t_s \tag{6.3}$$

where t_s is the time step used for the weathering calculation. $\dot{Q}_{\mathrm{L}_{in}}$ and $\dot{Q}_{\mathrm{V}_{in}}$ are calculated from equations (4.14) and (4.15) respectively:

$$\dot{Q}_{\mathrm{V}_{in}} = \left(U_{dry} A_{dry}\right)(T_{air} - T_{\mathrm{V}}) \tag{4.14}$$

$$\dot{Q}_{\mathrm{L}_{in}} = (U_{wet}A_{wet})(T_{air} - T_{\mathrm{L}}) \qquad (4.15)$$

Figures 6.37, 6.38 and 6.39 show the comparison of the *BOG'* calculated using eq. (6.1) with the BOG generation estimated by the superheated vapour model BOG_{shv}, for the Light LNG, Heavy LNG and LNG with N_2, respectively. Each graph also includes the tank liquid height h_l in the right y-axis.

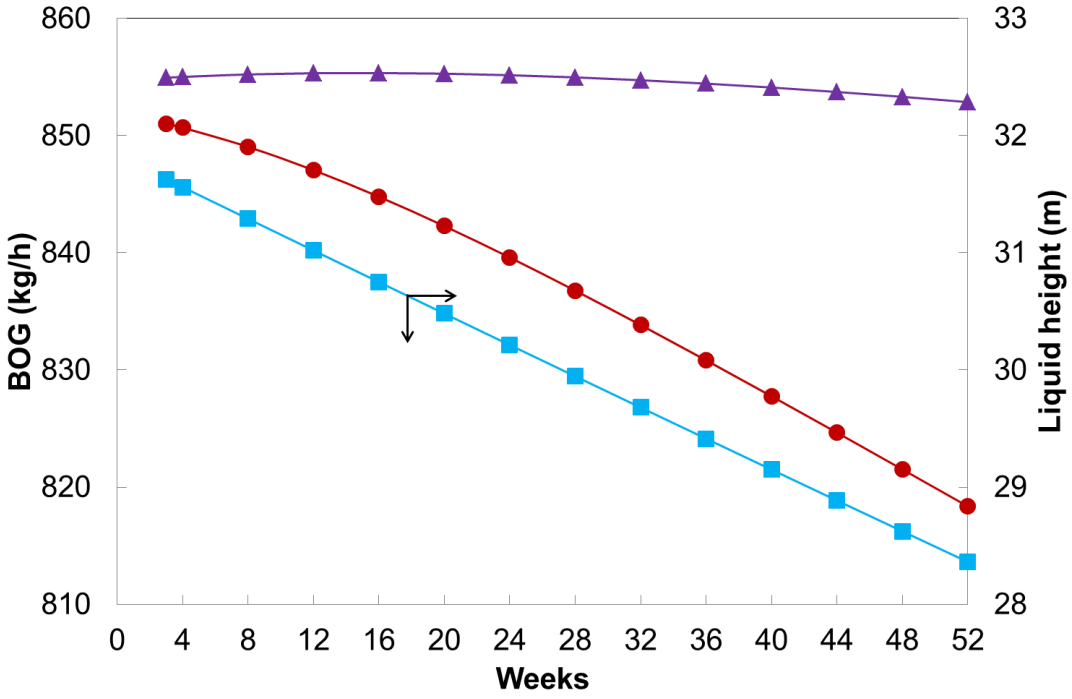

Figure 6.37 *BOG', BOG* and h_l vs. time - Light LNG.
(-▲- BOG'; -●- BOG_{shv}; -■- h_l)

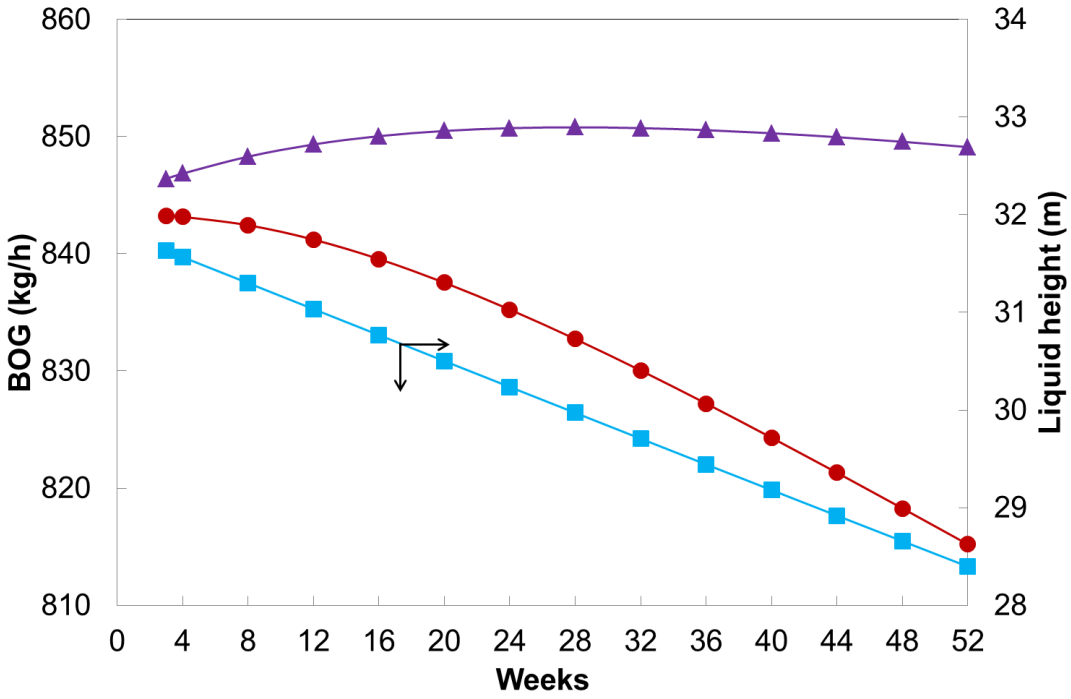

Figure 6.38 ***BOG', BOG*** **and h_l vs. time - Heavy LNG.**
(-▲- BOG'; -●- BOG_{shv}; -■- h_l)

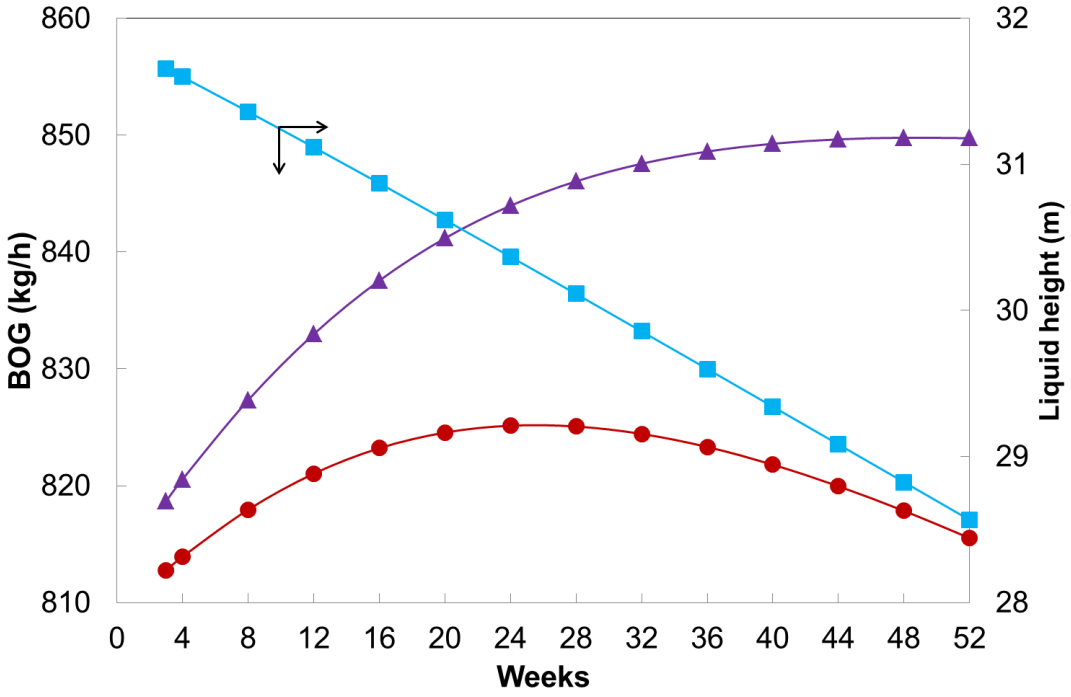

Figure 6.39 ***BOG', BOG*** **and h_l vs. time – LNG with N_2.**
(-▲- BOG'; -●- BOG_{shv}; -■- h_l)

The liquid height h_l is calculated dividing the LNG volume at each time step by the tank transversal area using the internal diameter, as follows:

$$h_l = \frac{V_{LNG}}{\left(\pi.\frac{D_i^2}{4}\right)} \quad (6.4)$$

The deviation percentage between BOG_{shv} and *BOG'* progressively increases, from less than 1% in the early stage of the weathering process to a maximum of 4% by the end. The reason for that deviation increase is ascribed to the progressive decrease of the BOG_{shv} that is linked to the reduction of the wet heat transfer area in the tank. For the superheated vapour model approach, as LNG is vaporized from the tank, less heat enters into the LNG, thus less BOG is produced. This is confirmed by the similar trend observed between the BOG_{shv} and the liquid height in the tank for the Light and Heavy LNG mixtures cases (refer to Figures 6.37 and 6.38). The trend is also similar for the LNG with N_2 case at the late stage of the weathering, once the N_2 is exhausted from the mixture. At the early stage of the weathering the effect is offset owing the presence of N_2; BOG generation increases due to the preferential vaporization of N_2 from the mixture.

Figures 6.37, 6.38 and 6.39 also show the liquid drop for the three mixtures (indicated as liquid height in the graphs). The LNG volume decreases around 10% in the three cases by the end of the assessed period (week 52).

Figures 6.40 and 6.41 show the quality assessment of LNG during the weathering process by HHV and WI measures, using the interim guidelines [7] as in section 6.1.1. The weathering effect on HHV and WI of both, the LNG remaining in the tank and BOG generated, is presented.

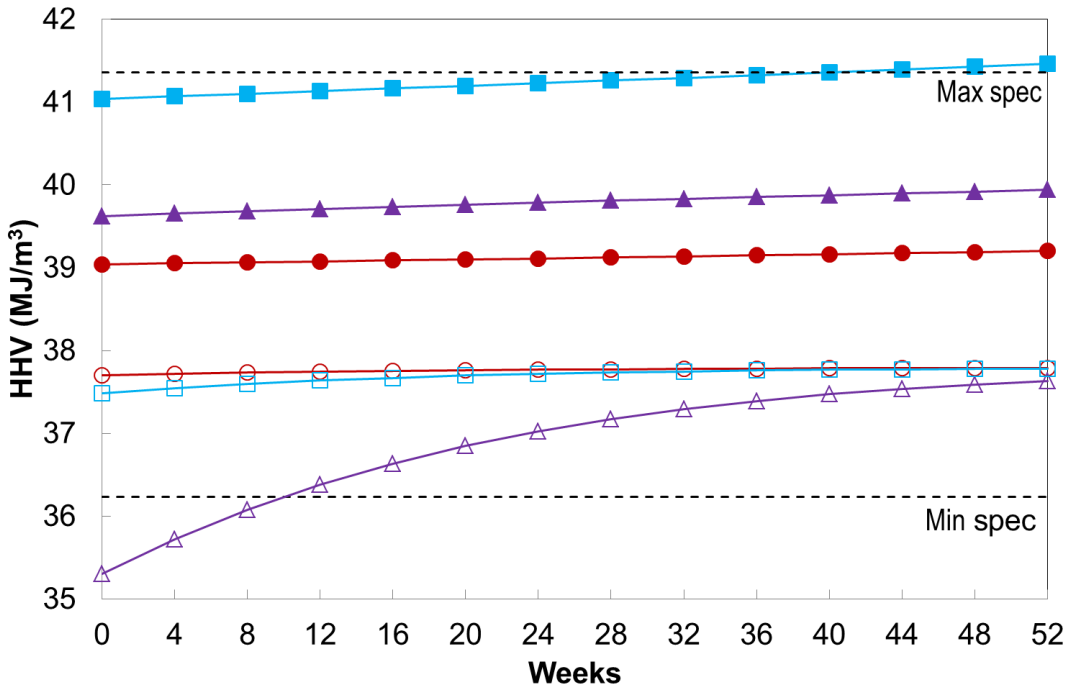

Figure 6.40 HHV vs. time for LNG and BOG - superheated vapour model.
(-●- Light LNG; -■- Heavy LNG; -▲- LNG with N_2; -○- BOG from Light LNG; -□- BOG from Heavy LNG; -△- BOG from LNG with N_2)

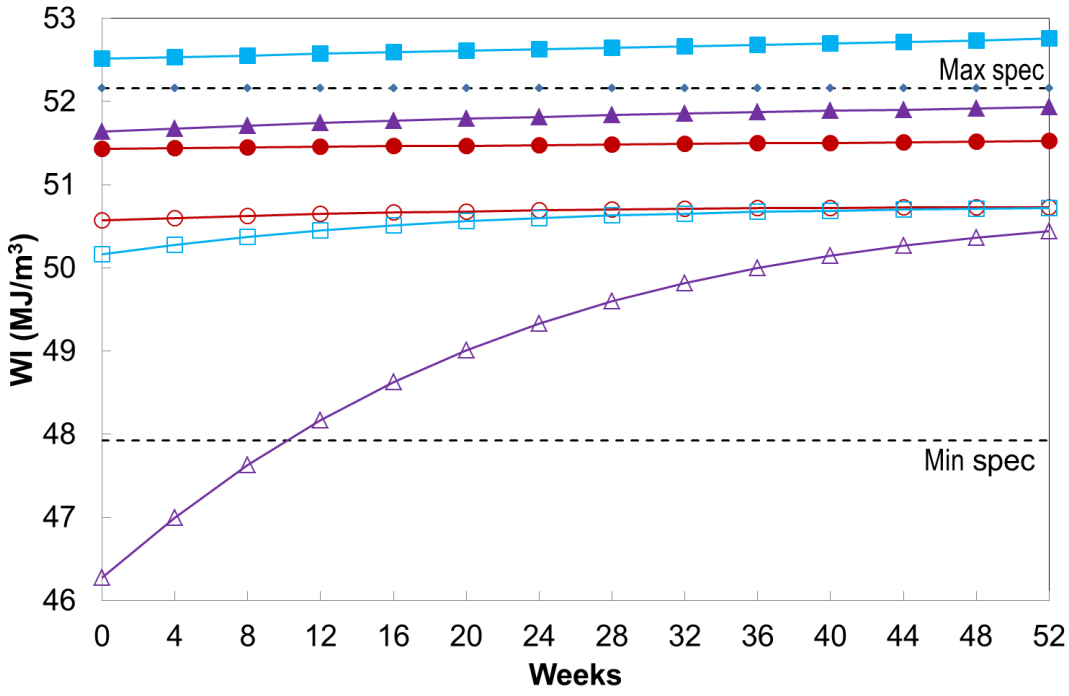

Figure 6.41 WI vs. time for LNG and BOG - superheated vapour model.
(-●- Light LNG; -■- Heavy LNG; -▲- LNG with N_2; -○- BOG from Light LNG; -□- BOG from Heavy LNG; -△- BOG from LNG with N_2)

For all three LNG mixtures the HHV and WI increase with time, the Light LNG and LNG with N_2 remain within the US market quality specifications during the whole weathering period. The Heavy LNG follows the same behaviour as described in the isothermal model approach, as HHV and WI measures give slightly different results. If using the WI measure the Heavy LNG is outside the US spec and could not be traded in the US markets, whilst the HHV measure indicates that initially the LNG starts within the spec but after 40 weeks it gets sufficiently weathered to become out of spec.

When comparing the estimated quality properties HHV and WI for LNG and BOG between the isothermal and superheated vapour models, one can observe that the differences are small. That is due to the estimated weathered compositions (see Table 6.6 below), which are very similar in both cases. The preferential vaporization of C_1 and N_2 over long term weathering, takes the LNG mixture and BOG to a similar composition even with less amount of heat input, as in the case of superheated vapour model. Table 6.6 shows the comparison of the LNG weathered composition predicted by the isothermal and superheated vapour models, at the end of the weathering period (52 weeks).

Table 6.6 Predicted LNG weathered composition after 52 weeks.

Component	Light LNG	Isothermal Model	Superheated Vapour Model	Heavy LNG	Isothermal Model	Superheated Vapour Model	LNG with N_2	Isothermal Model	Superheated Vapour Model
C_1	0.9613	0.9545	0.9567	0.9164	0.9020	0.9063	0.9307	0.9218	0.9251
C_2	0.0340	0.0400	0.0382	0.0576	0.0678	0.0647	0.0661	0.0774	0.0740
C_3	0.0039	0.0046	0.0044	0.0204	0.0240	0.0230	0.0006	0.0007	0.0007
iC_4	0.0004	0.0005	0.0004	0.0029	0.0034	0.0033	-	-	-
nC_4	0.0003	0.0004	0.0003	0.0022	0.0026	0.0025	-	-	-
iC_5	-	-	-	0.0002	0.0002	0.0002	-	-	-
N_2	0.0001	0.0000	0.0000	0.0003	0.0000	0.0000	0.0026	0.0001	0.0002

From Table 6.6 it is shown that in terms of estimated LNG weathered compositions there are no major differences between the models. As mentioned earlier, that is also confirmed when comparing the estimated quality properties such as HHV (see Figures 6.5 and 6.40) and WI (see Figures 6.6 and 6.41) for LNG and BOG. Nevertheless, the weathered composition predicted by the isothermal model is slightly heavier. This is not surprising as in the isothermal model the LNG gets more heat input; therefore, the resulting higher vaporization results to further weathering.

In the quality assessment of the BOG generated the key parameter is the initial nitrogen content, as discussed in the sensitivity with the isothermal model in Section 6.1.1. In this case the BOG from Light and Heavy LNG are within the US specifications at all times over the weathering period. However the BOG from the LNG with N_2 is outside the US spec at the initial stage of the weathering with a N_2 content of 6.6 % mol. This is confirmed by Figure 6.42, where the N_2 content in the BOG over the weathering period for the three mixtures is shown.

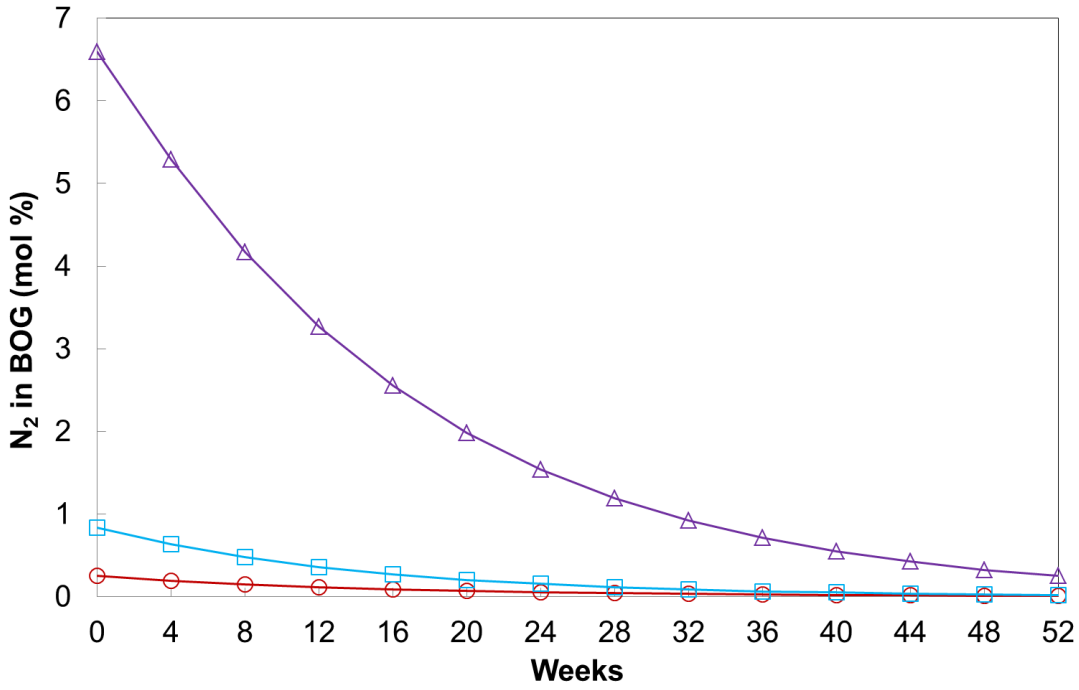

Figure 6.42 N_2 content in the BOG – superheated vapour model.
(-○- BOG from Light LNG; -□- BOG from Heavy LNG;
-△- BOG from LNG with N_2)

It is after week 10 when N_2 content goes down to around 4% mol, the increase in HHV and WI in the BOG reach the minimum quality spec, 36.23 MJ/m^3 and 47.93 MJ/m^3 respectively (refer to Figures 6.40 and 6.41). Moreover, one can observe that both HHV and WI of BOG for all mixtures tend to the value for pure methane ($HHV_{methane}$=37.69 MJ/m^3 and $WI_{methane}$=50.87 MJ/m^3), as the amount of nitrogen in BOG progressively decreases.

Figure 6.43 shows the heat input ratio Q_{ratio} into the LNG between both models over the weathering period for the three LNG mixtures.

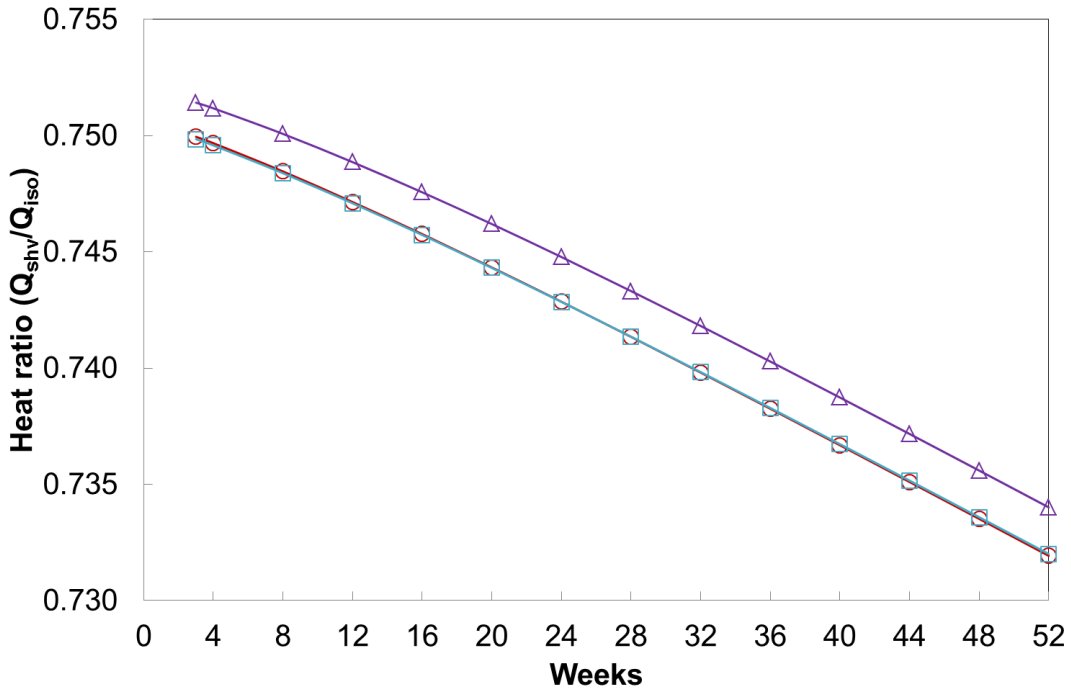

Figure 6.43 Heat input ratio into the LNG vs. time between both models.
(-○- Light LNG; -□- Heavy LNG; -△- LNG with N_2)

The LNG heat input ratio Q_{ratio} is calculated as follows:

$$Q_{ratio} = \frac{Q_{shv}}{Q_{iso}} \tag{6.5}$$

where Q_{shv} is the LNG heat input in the superheated vapour model (it includes the heat contribution from the vapour phase to the liquid phase), and Q_{iso} is the LNG heat input in the isothermal model.

Figure 6.43 shows that the heat input ratio at the beginning of the weathering is approximately 75% for the three mixture cases, and progressively declines down to approximately 73% over the assessed weathering period. This is an indicator of how the contact area in the tank plays a part in the heat transfer calculation of the superheated vapour model. In the beginning of weathering the tank is full and as the tank begins to empty the contact area is reduced, thus less heat is going into the LNG. By the end of the weathering period the estimated LNG heat input for the superheated vapour model drops by 1.8%.

Figure 6.43 also shows that the heat input ratio is nearly the same for the Light and Heavy LNG, whilst is a slightly higher (around 0.25% higher) for the LNG with N_2 case. This is due to the higher heat contribution from vapour to liquid in the superheated vapour model, particularly at the early stage of weathering when the N_2 content is higher. The presence of N_2 lowers the boiling point of the liquid mixture, but also the equilibrium vapour temperature at the beginning of the weathering, thus producing a greater heat input due to the higher temperature difference with the surrounding.

Table 6.7 summarizes the BOG generated and heat input into the LNG for the three mixtures, over the 52 weeks of weathering for both models.

Table 6.7 BOG generated and heat input into the LNG after 52 weeks.

	Isothermal model			Superheated vapour model		
	Light LNG	Heavy LNG	LNG with N_2	Light LNG	Heavy LNG	LNG with N_2
Total LNG, kmol.10^3	4,149.6	4,077.9	4,141.0	4,149.6	4,077.9	4,141.0
Total BOG, kmol.10^3	621.3	617.0	603.6	455.3	452.2	439.3
% Original LNG (mol basis)	14.97	15.13	14.58	10.97	11.09	10.61
Total LNG, kg.10^3	69,138.5	71,998.2	70,474.2	69,138.5	71,998.2	70,474.2
Total BOG, kg.10^3	9,972.4	9,916.9	9,808.3	7,309.8	7,268.9	7,169.9
% Original LNG (mass basis)	14.42	13.77	13.92	10.57	10.10	10.17
Total heat input into LNG, MJ.10^6	5.101	5.095	5.099	3.733	3.729	3.743

The total amount of BOG predicted by the isothermal model is higher in all cases, which is a direct consequence of the less heat input into the LNG used in the superheated vapour model.

6.2.2 SENSITIVITY TO INITIAL LNG INVENTORY

The effect of the variation in the initial LNG inventory on the BOG generated has been investigated using the superheated vapour model. As in the isothermal model case, the LNG inventory was varied between 15,000 and 160,000 m^3, considering a storage tank of 165,000 m^3 capacity, with the simulations performed for both, Light LNG and Heavy LNG mixtures, compositionally described in Table 6.2.

Figure 6.44 and 6.45 show the vaporization rate expressed as BOR and BOG rate respectively, as a function of the amount of LNG evaporated (percentage of moles of LNG vaporized divided by the initial LNG moles). As in Section 6.1.2, for clarity purposes only

results for the smallest inventory (15,000 m^3) and highest inventory (160,000 m^3) are presented, for both LNG mixtures.

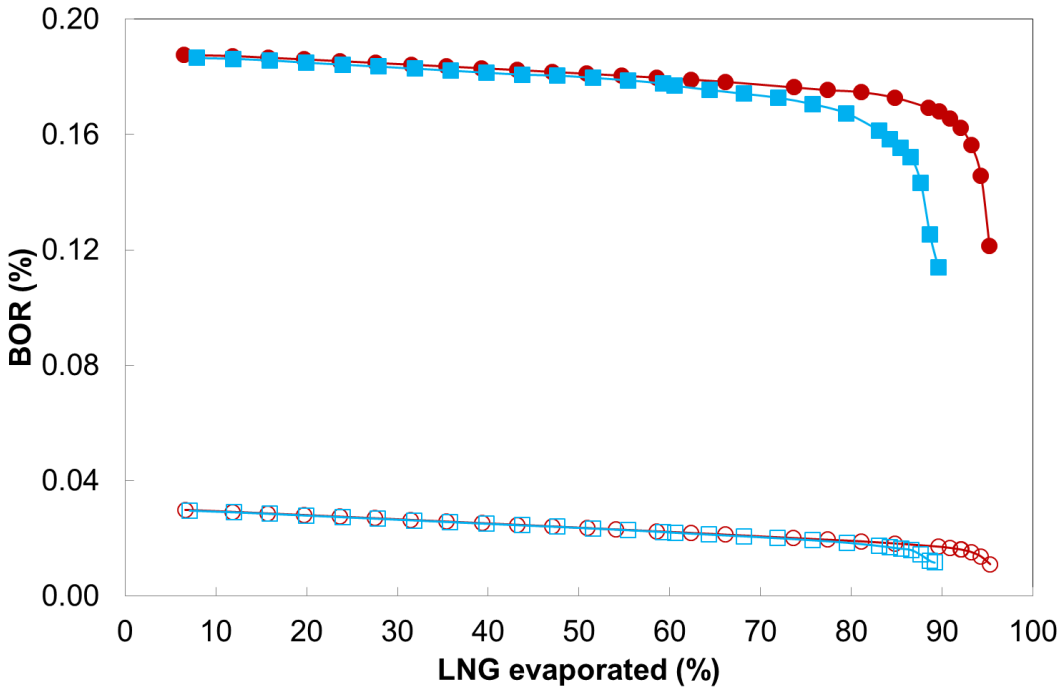

Figure 6.44 BOR vs. LNG evaporated - superheated vapour model.
(-●- Light LNG, 15,000m^3 inventory; -○- Light LNG, 160,000m^3 inventory;
-■- Heavy LNG 15,000m^3 inventory; -□- Heavy LNG 160,000m^3 inventory)

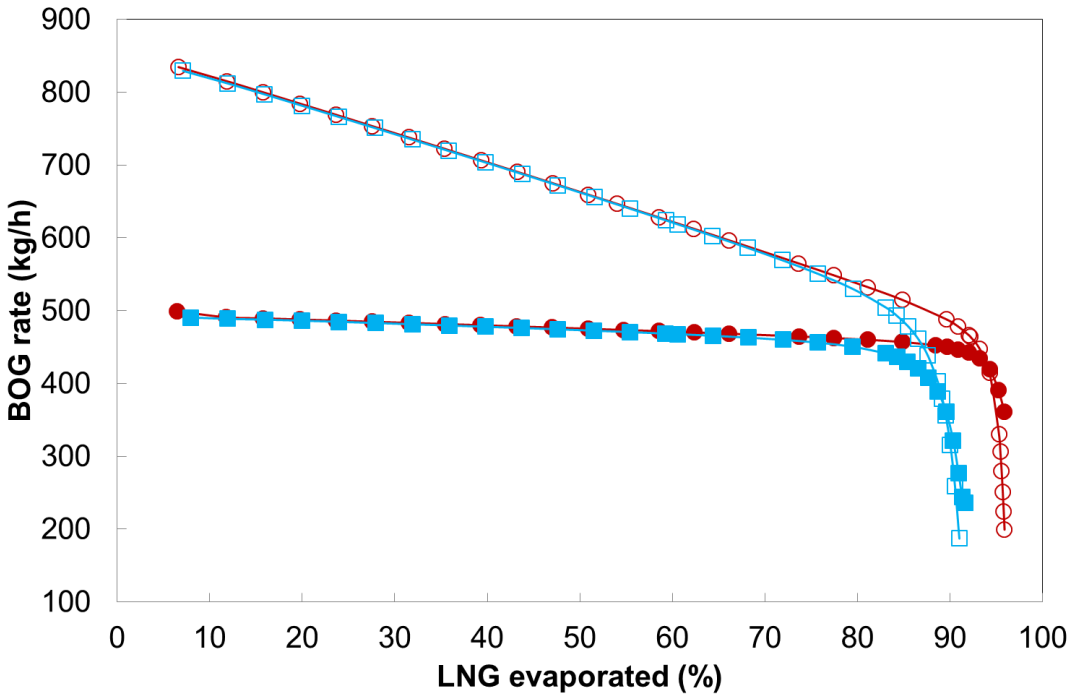

Figure 6.45 BOG generation rate vs. LNG evaporated - superheated vapour model.
(-●- Light LNG, 15,000m^3 inventory; -○- Light LNG, 160,000m^3 inventory;
-■- Heavy LNG 15,000m^3 inventory; -□- Heavy LNG 160,000m^3 inventory)

As in the isothermal model, within the superheated vapour model approach the BOR increase as the stored volume of LNG decreases in the tank (refer to Figure 6.44). In the initial stages of weathering the BOR is essentially constant around 0.19 % for tank initially filled with 15,000 m^3, regardless the LNG composition stored. The BOR remains nearly constant until the mixture is near its complete evaporation (above 80%) when it decreases down to around 0.12%. For the 160,000 m^3 LNG inventory case, the BOR starts around 0.03 %, for both mixtures (Light and Heavy LNG), and progressively decreases as LNG is evaporated from the tank. When the LNG volume is near its full evaporation the BOR is around 0.01%.

As LNG evaporates the remaining liquid gets richer in heavier hydrocarbons. This has, as discussed previously within the isothermal model sensitivity assessment, two thermodynamic consequences, the boiling temperature and the differential latent heat increase (see Figures 6.48 and 6.49 respectively). The resulting reduction in the heat ingress and the need to provide more energy to vaporize the same amount of LNG, then

richer in heavy components, results in drastic decrease of BOG, as observed in Figure 6.45. In this regard, the Heavy LNG gets richer in heavy components quicker than the Light LNG and the BOG rate starts decreasing earlier, at approximately 80% compared with 90% for Light LNG. Figure 6.45 shows two different BOG generation behaviours between the two inventory scenarios. In the 15,000 m^3 case the heat input to vaporize the LNG is dominated by the heat ingress from the bottom slab Q_{slab}, thus explaining the nearly constant BOG generation rate. For the 160,000 m^3 case the heat input from the lateral wall contributes significantly, particularly at the early stage of the weathering; hence, the progressive drop of the BOG generation rate is due to the decrease of the wet heat transfer area. As LNG is evaporated the wet area in the LNG tank progressively reduces, therefore less heat is transferred to the LNG. That is confirmed by Figures 6.46 and 6.47, respectively showing for 15,000 m^3 and 160,000 m^3 volumes the BOG generation rate to the heat input into the liquid considering pure methane.

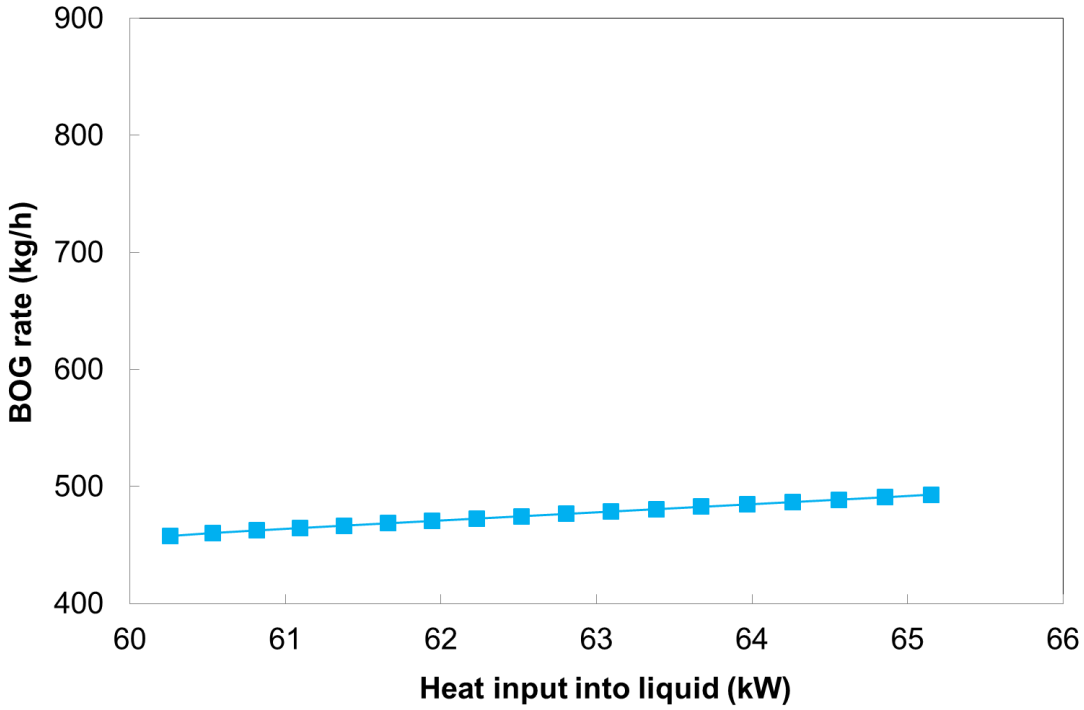

Figure 6.46 BOG rate vs. LNG heat input (CH_4; 15,000 m^3).

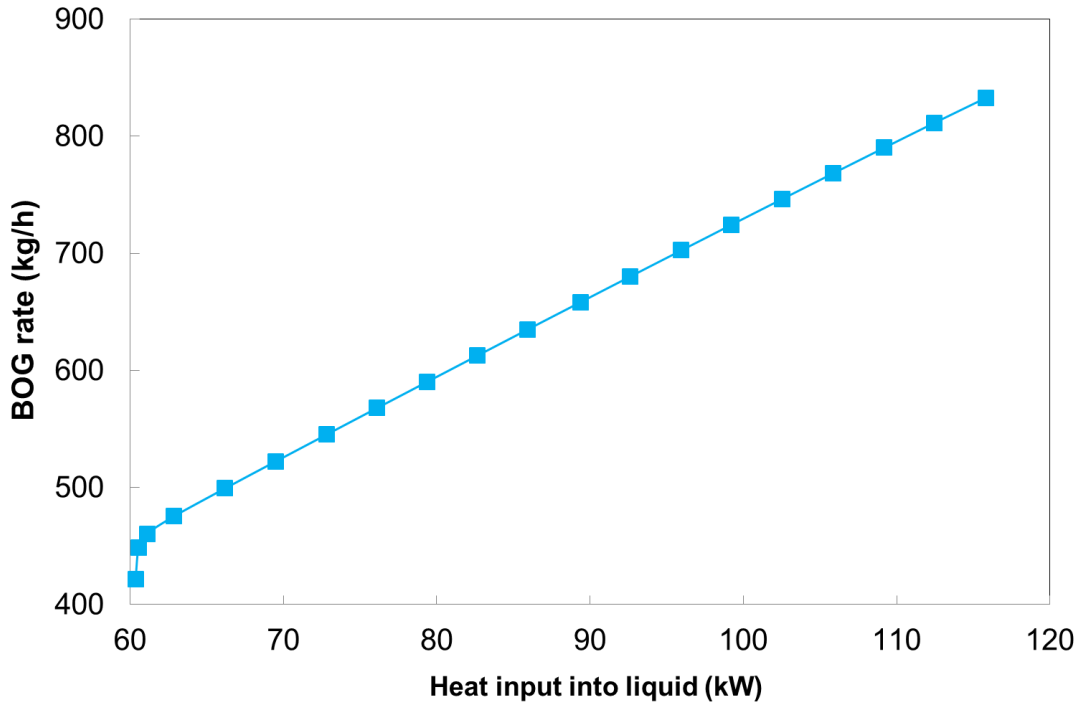

Figure 6.47 BOG rate vs. LNG heat input (CH_4; 160,000 m^3).

One can observe in the 15,000 m^3 case (Figure 6.46) that the heat input into the liquid is approximately the same as the heat entering from the bottom slab, ~60 kW (refer to Table 6.1), thus explaining the nearly constant behaviour of the BOG generation rate in Figure 6.45. In the 160,000 m^3 case (Figure 6.47), the rise of BOG generation rate as the heat input into the liquid increases, describes the progressive decrease BOG generation rate vs. the amount of LNG evaporated. The scale and range of the vertical axis in Figures 6.46 and 6.47 were kept identical to ease the comparison between them.

Figures 6.48 and 6.49 respectively show the boiling temperature and the differential latent heat as a function of the LNG evaporated, within the superheated vapour model approach.

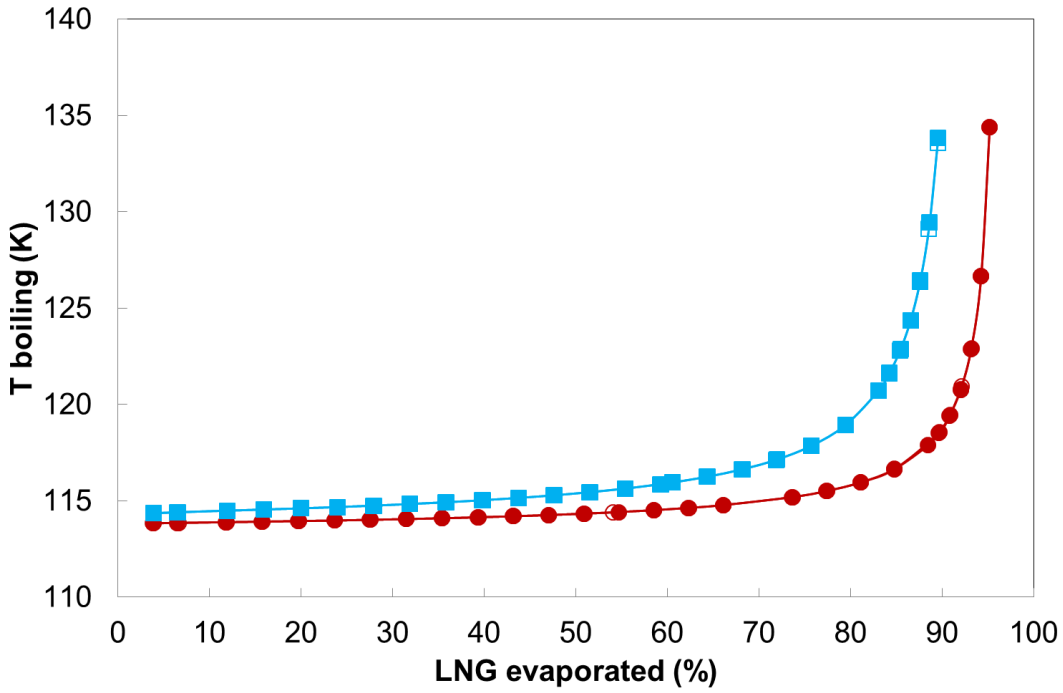

Figure 6.48 T boiling vs. LNG evaporated - superheated vapour model.
(-●- Light LNG, 15,000m^3 inventory; -○- Light LNG, 160,000m^3 inventory;
-■- Heavy LNG, 15,000m^3 inventory; -□- Heavy LNG, 160,000m^3 inventory)

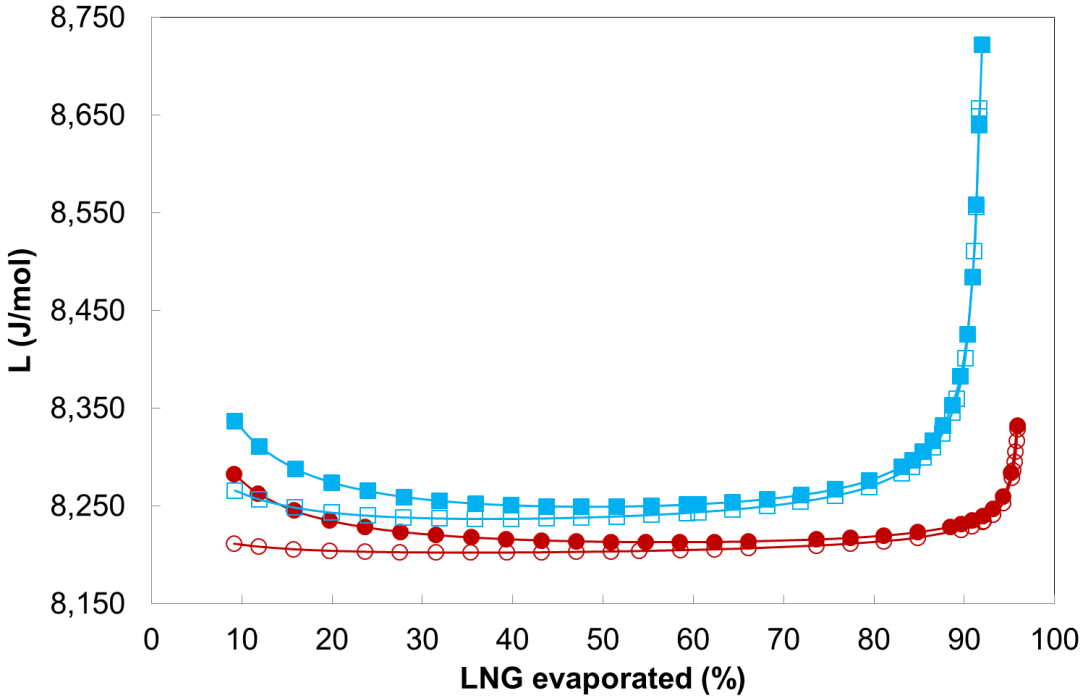

Figure 6.49 Latent heat vs. LNG evaporated - superheated vapour model.
(-●- Light LNG, 15,000m^3 inventory; -○- Light LNG, 160,000m^3 inventory;
-■- Heavy LNG, 15,000m^3 inventory; -□- Heavy LNG, 160,000m^3 inventory)

As in the isothermal model approach, Figure 6.45 also shows that the tank filled up to 160,000 m^3 exhibits a slightly earlier decrease in BOG than the tank with less initial amount of LNG. This is a direct consequence of the indirect differential latent heat. As the LNG gets richer in heavier hydrocarbons its boiling temperature increases, and hence part of the heat ingress will go towards heating up the remaining LNG. For a given amount of LNG evaporated the storage tank with initially higher LNG volume will have more liquid remaining. Hence, more heat will be required to increase its temperature to a new boiling point, thus reducing the amount of heat available for evaporating the LNG. The overall result will be an earlier decrease in BOG for an initially more filled storage tank. That is confirmed by observing Figures 6.45, 6.48 and 6.49, showing that the BOG rate decrease ties up with the boiling temperature and differential latent heat increase in both LNG mixtures. For the Heavy LNG that occurs around 80% evaporation, whilst for the Light LNG is near 90%.

Same as in the isothermal approach, due to range of validity of Klosek-McKinley equation to calculate liquid density the simulations have been stopped before the complete evaporation of the LNG in the tank.

Figure 6.50 shows the heat input ratio Q_{ratio} into the LNG, between the heat contribution from the vapour side to the heat entering through the lateral wall Q_{Lin}, plus the bottom thermal slab Q_{slab}.

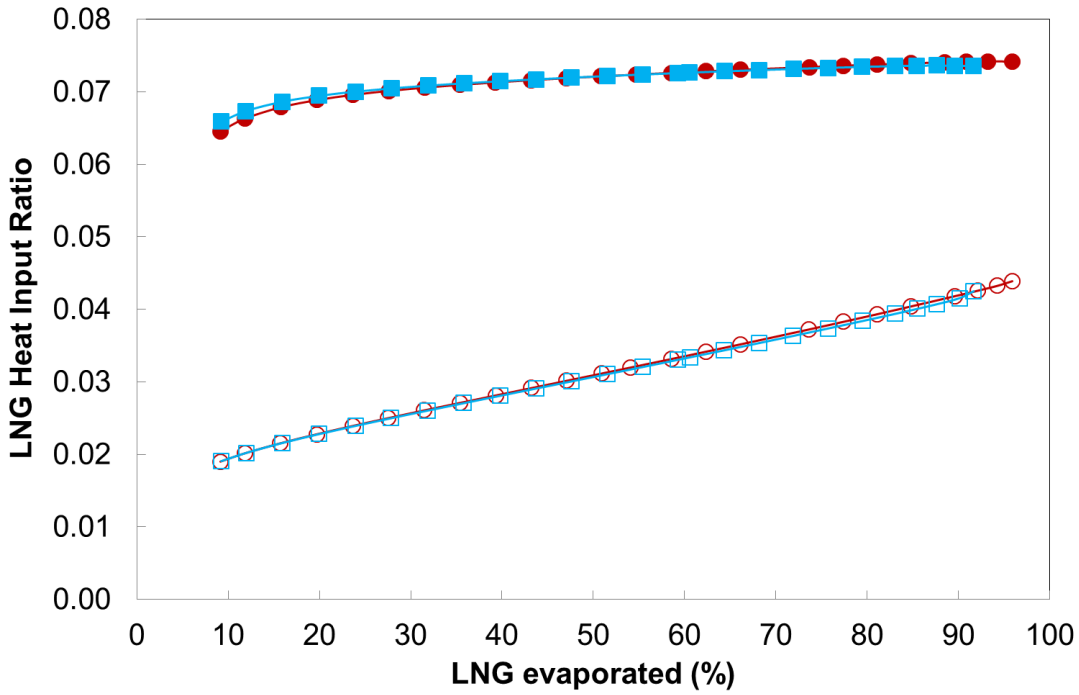

Figure 6.50 LNG heat input ratio vs. LNG evaporated - superheated vapour model.
(-●- Light LNG, 15,000m^3 inventory; -○- Light LNG, 160,000m^3 inventory;
-■- Heavy LNG, 15,000m^3 inventory; -□- Heavy LNG, 160,000m^3 inventory)

The LNG heat input ratio Q_{ratio} is calculated as follows:

$$Q_{ratio} = \frac{Q_{vap}}{Q_{L_{in}} + Q_{slab}} \tag{6.6}$$

Figure 6.50 shows that the heat contribution from vapour to liquid increase as the LNG inventory decreases in the tank, regardless the composition of the LNG stored.

6.2.3 SENSITIVITY TO INITIAL N_2 CONTENT

It's been already observed (refer to section 6.1.3) that the presence of nitrogen in LNG decreases the BOG markedly during the initial stages of weathering. Within this section, the effect is re-examined further using the superheated vapour model approach. As in the isothermal model assessment, the analysis is performed by comparing an actual Light LNG composition to three hypothetical N_2 enriched LNG mixtures of up to 1.5% N_2 content, as described in Table 6.3.

Figure 6.51, 6.52 and 6.53 show the evolution of the vapour generation rate expressed in terms of BOR and BOG, mass and molar basis, using the superheated vapour model.

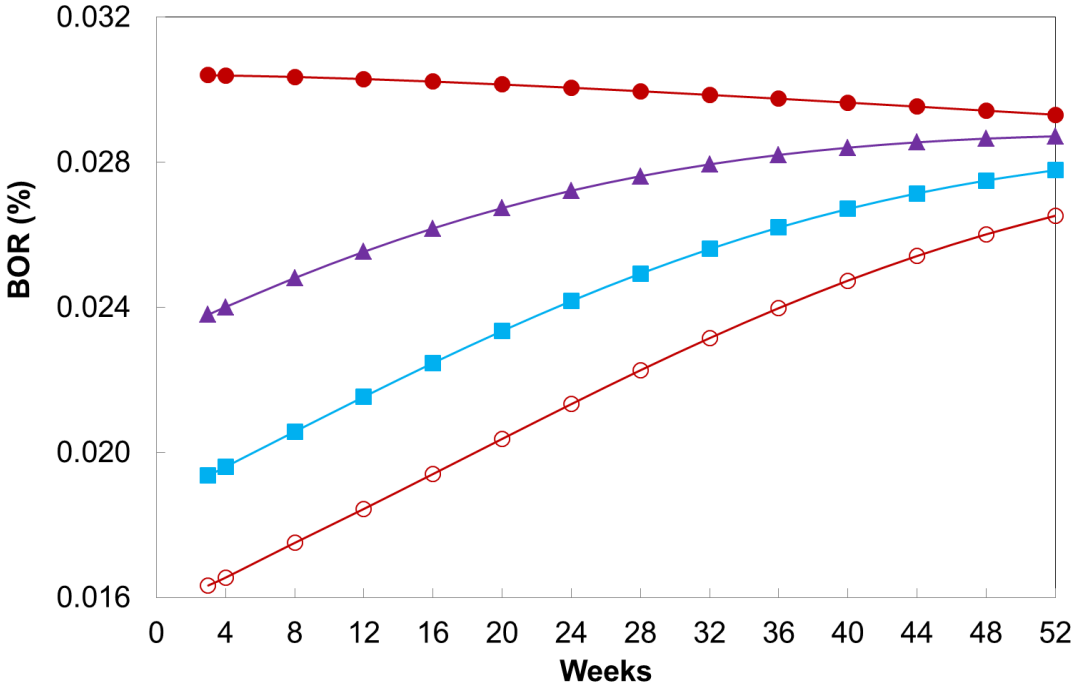

Figure 6.51 BOR vs. time – superheated vapour model.
(-●- Light LNG; -▲- LNG 0.5% N_2; -■- LNG 1.0% N_2; -○- LNG 1.5% N_2)

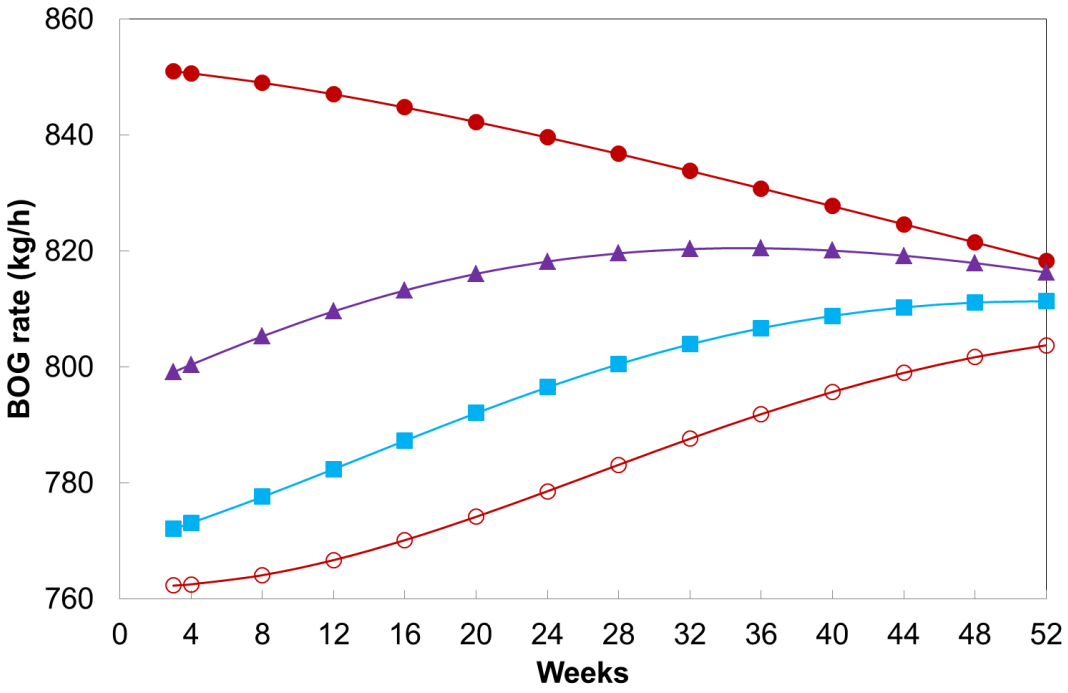

Figure 6.52 BOG rate (mass basis) vs. time - superheated vapour model.
(-●- Light LNG; -▲- LNG 0.5% N_2; -■- LNG 1.0% N_2; -○- LNG 1.5% N_2)

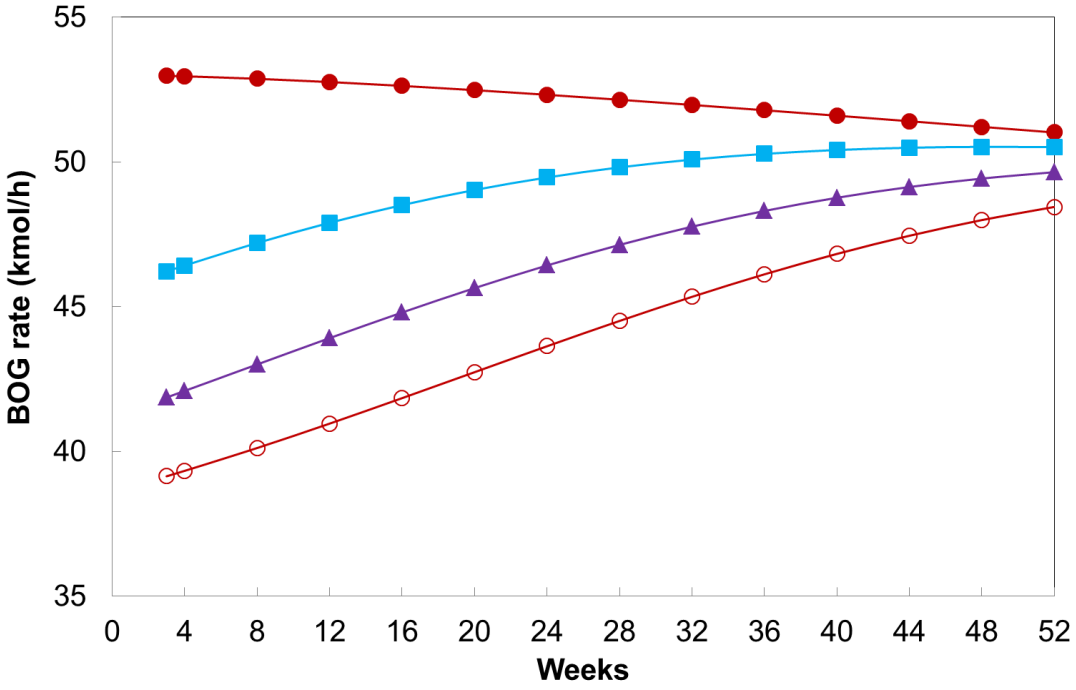

Figure 6.53 BOG rate (mol basis) vs. time - superheated vapour model.
(-●- Light LNG; -▲- LNG 0.5% N_2; -■- LNG 1.0% N_2; -○- LNG 1.5% N_2)

As discussed previously the presence of nitrogen in the liquid has a predominant effect on weathering. From Figure 6.52 one can observe a marked difference, up to 12% higher, in the BOG generation rate at the initial stages of weathering, between the 1.5% N_2 mixture and the Light LNG, with the rest of N_2 enriched mixtures in between. Same as in the isothermal model case, the increase in molecular weight of vapour compared to the Light LNG case, explains the different initial drop of BOG for 1.5% N_2 rich LNG. The determining factor in the reduction of BOG for N_2 rich mixtures is due to the increase in the direct latent heat required to vaporize a drop of LNG. As discussed in section 6.1.3, the increase of the amount of N_2 in the LNG mixtures leads to two thermodynamic effects, namely lowering the boiling point of the mixture and increasing the latent heat needed to vaporize an LNG drop, as summarized in Table 6.3.

Figure 6.52 shows that the BOG generation rate (mass basis) gradually increases for the N_2 rich mixtures, whilst progressively decreases for the Light LNG. As LNG begins to weather, N_2 will vaporize preferentially with the difference in BOG generation rate between the four mixtures nearly disappearing towards the end of the weathering period, after the N_2 is exhausted from the enriched N_2 mixtures.

The increase of the BOG generation rate for the N_2 rich mixtures is due to the decrease of the molecular weight of the vapour (refer to Figure 6.54) and the latent heat (refer to Figure 6.55), over the assessed weathering period. As a result of the preferential evaporation of nitrogen, the direct differential molar latent heat decreases in the later stages of the weathering, thus less heat is needed to vaporize the LNG. Although the heat input into the LNG also decreases (refer to Figure 6.56) that in principle would make the BOG generation rate to go down, there is interplay between the rate of change of vapour molecular weight and latent heat, to the rate of change of the LNG heat input.

The decrease instead of the BOG generation rate for the Light LNG is explained by the drop of the LNG heat input, as the molecular weight of the vapour and latent heat remain nearly constant along the assessed weathering period. The drop of the LNG heat input into the LNG is due to the progressive reduction of the heat transfer area, as LNG is evaporated from the tank. The higher proportional decrease in the heat input into the LNG, since part

of the heat goes to heating up the vapour, results in less BOG generation as weathering progresses.

Figures 6.54, 6.55 and 6.56 respectively show the vapour molecular weight, latent heat and LNG heat input as function of time. Figure 6.56 also shows the tank liquid height as function of time in the right y-axis.

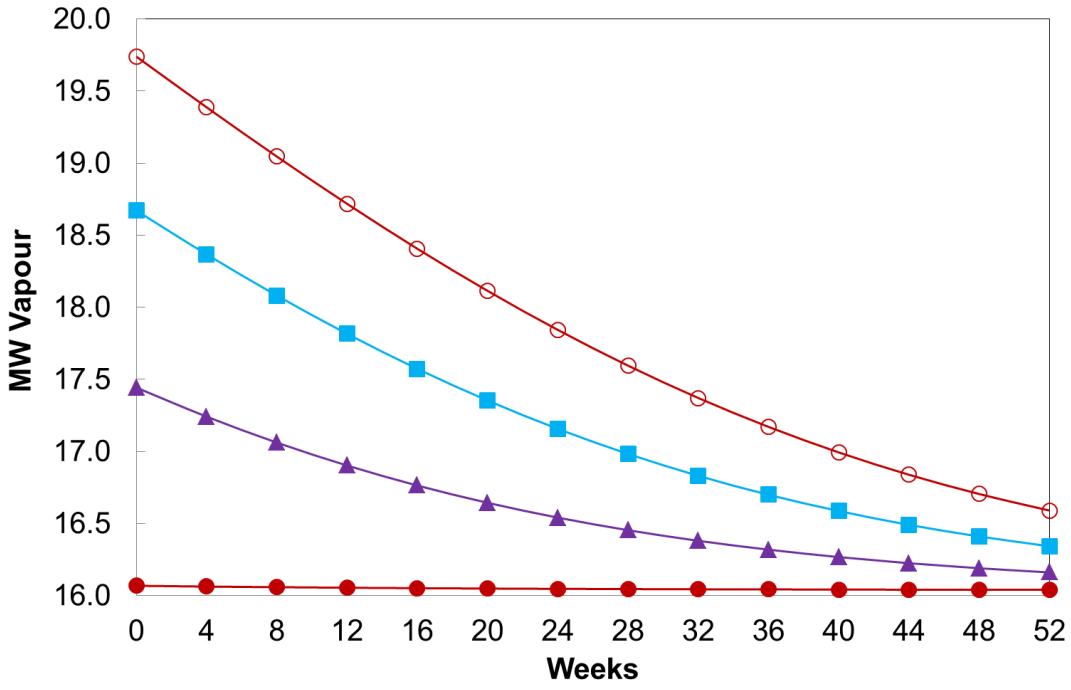

Figure 6.54 MW of vapour vs. time - superheated vapour model.
(-●- Light LNG; -▲- LNG 0.5% N_2; -■- LNG 1.0% N_2; -○- LNG 1.5% N_2)

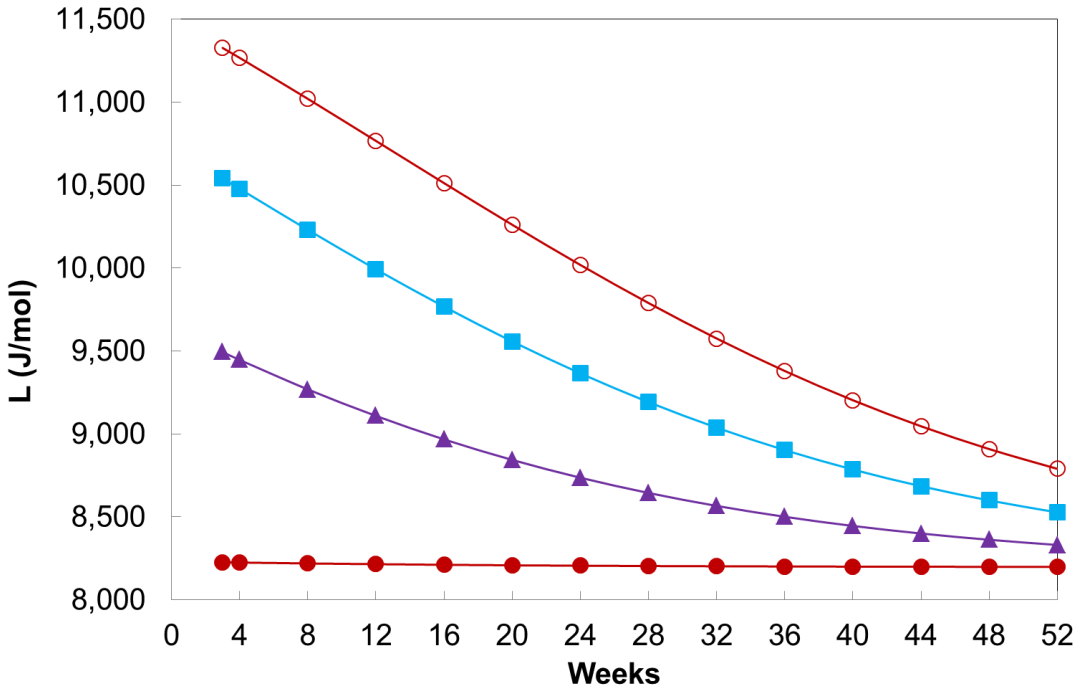

Figure 6.55 Latent heat vs. time - superheated vapour model.
(-●- Light LNG; -▲- LNG 0.5% N_2; -■- LNG 1.0% N_2; -○- LNG 1.5% N_2)

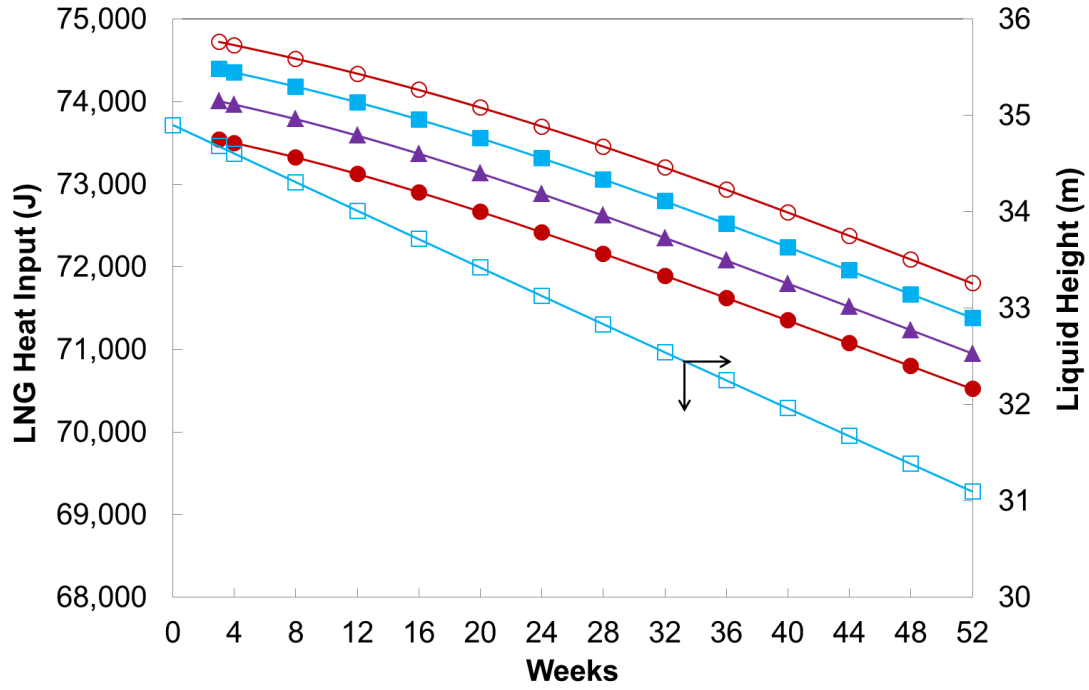

Figure 6.56 LNG heat input and h_l vs. time - superheated vapour model.
(-●- Light LNG; -▲- LNG 0.5% N_2; -■- LNG 1.0% N_2;
-○- LNG 1.5% N_2; -□- h_l)

As the 1.5% N_2 mixture gets weathered the remaining liquid becomes methane richer, hence the molar direct latent heat decrease and the molar BOG rate increase. This is the consequence of the decrease in the molecular weight of the weathered mixture as N_2 is preferentially vaporized. By the end of the weathering period the four mixtures have basically the same BOG generation rate, as the depletion of N_2 essentially takes them to the same weathered composition.

Figures 6.57 and 6.58 respectively illustrate the change in N_2 composition of the liquid and vapour phases as a function of time.

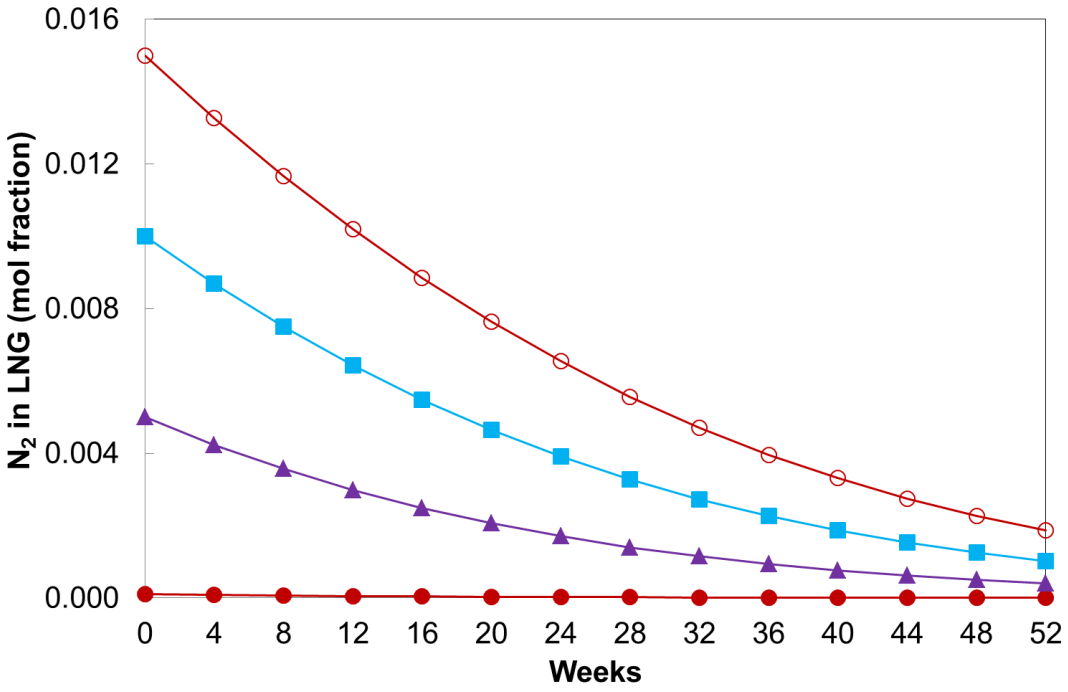

Figure 6.57 N_2 in LNG (mol fraction) – superheated vapour model.
(-●- Light LNG; -▲- LNG 0.5% N_2; -■- LNG 1.0% N_2; -○- LNG 1.5% N_2)

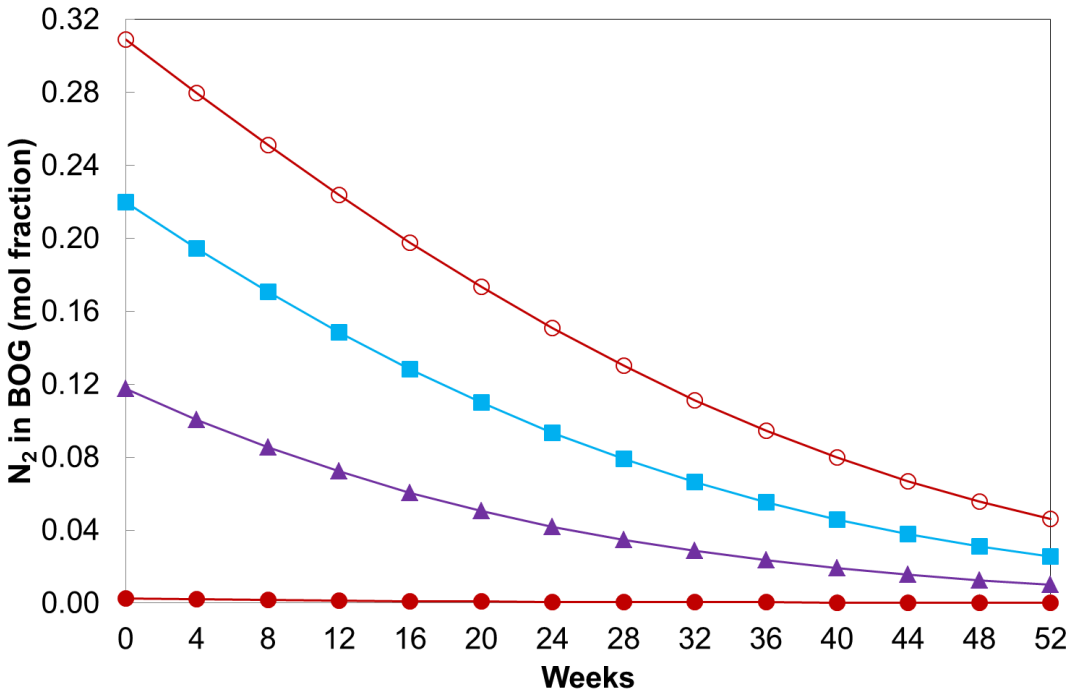

Figure 6.58 N_2 in BOG (mol fraction) – superheated vapour model.
(-●- Light LNG; -▲- LNG 0.5% N_2; -■- LNG 1.0% N_2; -○- LNG 1.5% N_2)

Figure 6.58 shows that nitrogen content of the vapour can reach up to 30 % mol. Same as in the isothermal model case, a rapid decrease in the nitrogen concentration is observed. As a consequence, the boiling temperature of the remaining LNG will increase. Within the 52 weeks period examined, the boiling temperature of the four mixtures will reach around 114 K (refer to Figure 6.59), same as with the isothermal model approach. The minor change in the boiling temperature during the weathering process will result in a rather small indirect differential latent heat component, less than 0.1 % of the total differential latent heat.

Figures 6.59 and 6.60 respectively show the boiling temperature and vapour temperature evolutions over the weathering period, for the four mixtures.

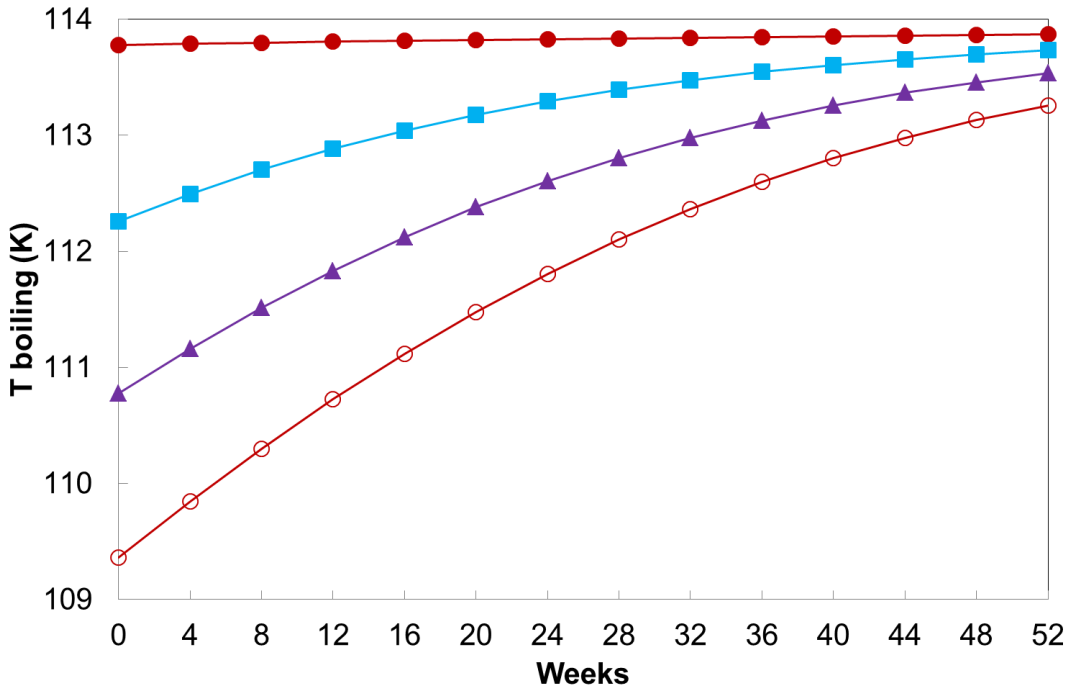

Figure 6.59 T boiling vs. time - superheated vapour model.
(-●- Light LNG; -▲- LNG 0.5% N_2; -■- LNG 1.0% N_2; -○- LNG 1.5% N_2)

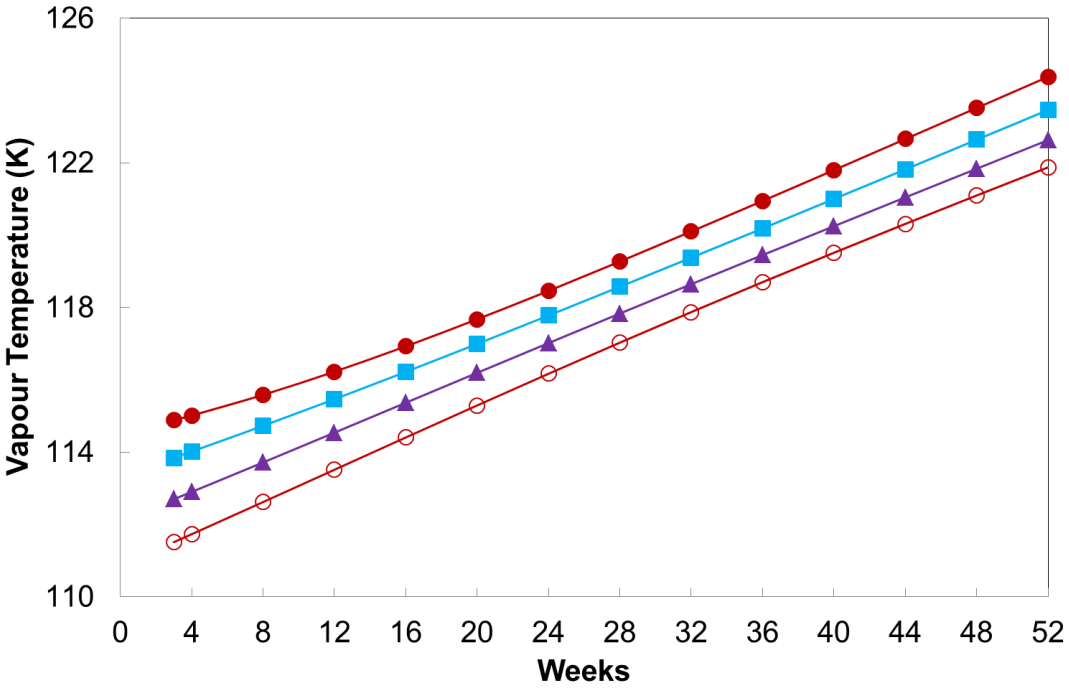

Figure 6.60 Vapour temperature vs. time - Superheated vapour.
(-●- Light LNG; -▲- LNG 0.5% N_2; -■- LNG 1.0% N_2; -○- LNG 1.5% N_2)

Figure 6.59 confirms, as in the isothermal model, that the initial steep rise in the liquid temperature is due to the preferential vaporization of nitrogen, which was originally present in the mixture.

Figure 6.60 shows that the vapour temperature progressively increases for the four LNG mixtures over the weathering period. As weathering develops the temperature of the Light LNG vapour is at higher temperature at all times when compared to the other enriched N_2 mixtures. The reason behind that behaviour is the higher boiling temperature of the Light LNG mixture at the beginning of the weathering process.

Table 6.8 below shows the LNG weathered composition predicted by the superheated vapour model at the end of the weathering period (52 weeks), for the Light LNG and for the assessed N_2 enriched compositions.

Table 6.8 Predicted LNG weathered composition after 52 weeks.

Component (mol fraction)	Light LNG	Weathered Light LNG	0.5% N_2	Weathered 0.5% N_2	1.0% N_2	Weathered 1.0% N_2	1.5% N_2	Weathered 1.5% N_2
C_1	0.9613	0.9567	0.9566	0.9567	0.9517	0.9566	0.9470	0.9563
C_2	0.0340	0.0382	0.0338	0.0379	0.0337	0.0374	0.0335	0.0369
C_3	0.0039	0.0044	0.0039	0.0043	0.0039	0.0043	0.0038	0.0042
iC_4	0.0004	0.0004	0.0004	0.0004	0.0004	0.0004	0.0004	0.0004
nC_4	0.0003	0.0003	0.0003	0.0003	0.0003	0.0003	0.0003	0.0003
N_2	0.0001	0.0000	0.0050	0.0004	0.0100	0.0010	0.0150	0.0019
$T_{boiling}$, ºC	-159.4	-159.3	-160.9	-159.4	-162.4	-159.6	-163.8	-159.9

Figure 6.61 and 6.62 respectively show the graphs of liquid (weathered LNG) molecular weight vs. nitrogen content, and vs. time.

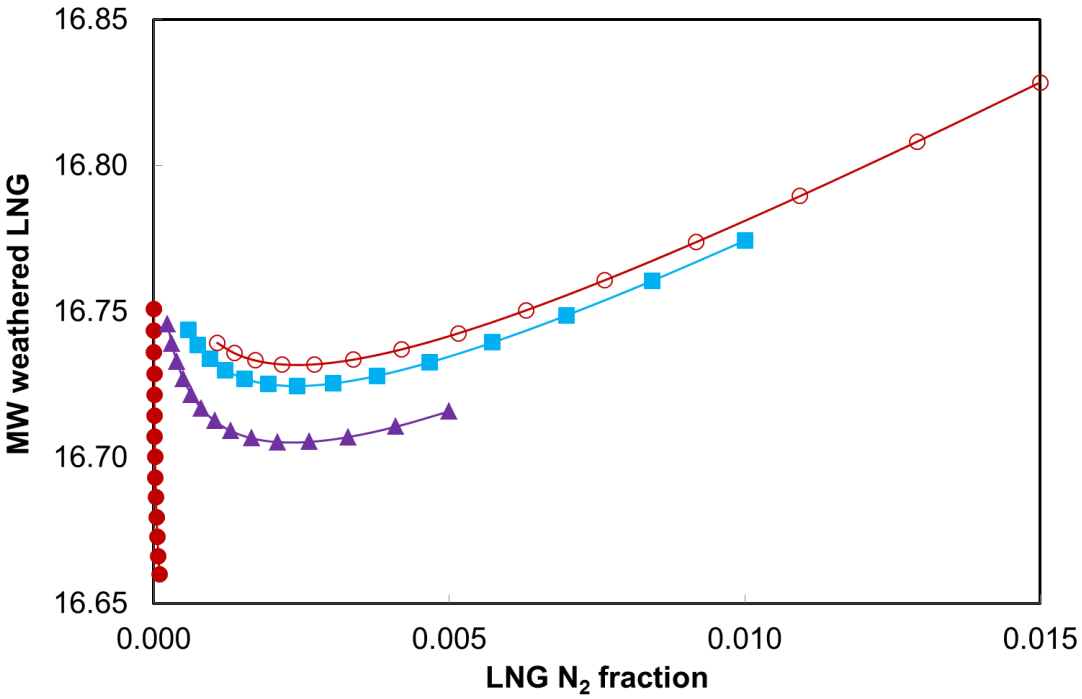

Figure 6.61 MW of LNG vs. N_2 in LNG - superheated vapour model.
(-●-Light LNG; -▲- LNG 0.5% N_2; -■- LNG 1.0% N_2; -○- LNG 1.5% N_2)

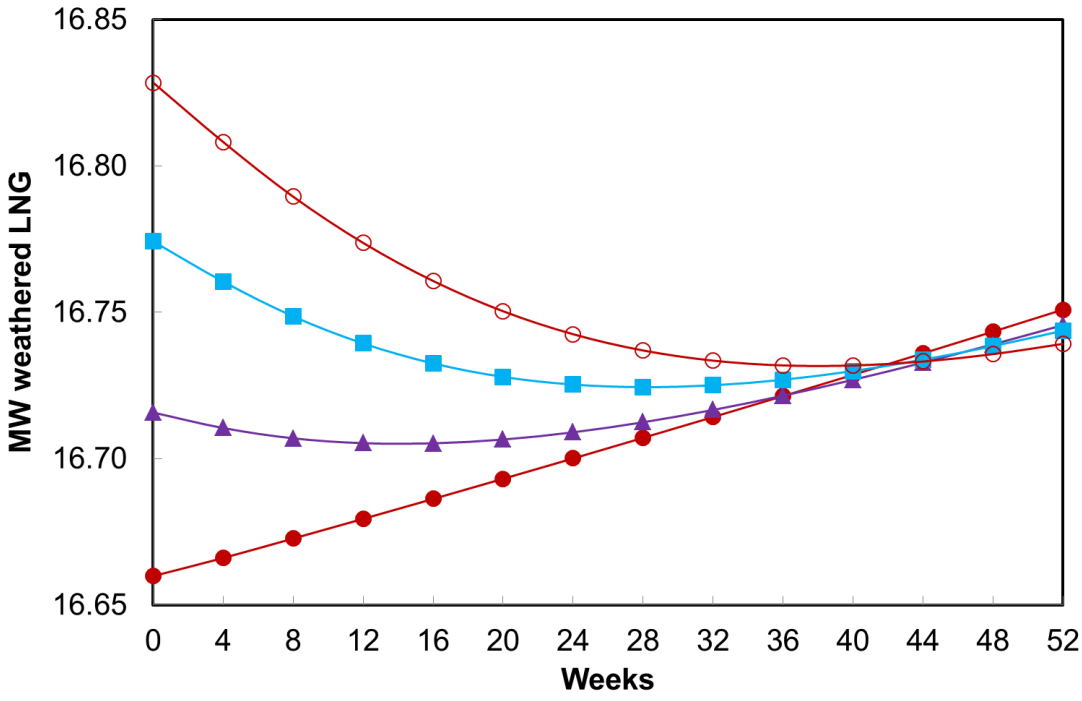

Figure 6.62 MW of LNG vs. time - superheated vapour model.
(-●-Light LNG; -▲- LNG 0.5% N_2; -■- LNG 1.0% N_2; -○- LNG 1.5% N_2)

Figure 6.63 illustrates the variation of the initial BOG rate after 24 hours weathering with the initial amount of N_2 in the LNG, using the extended nitrogen enriched LNG compositions presented in Table 6.5.

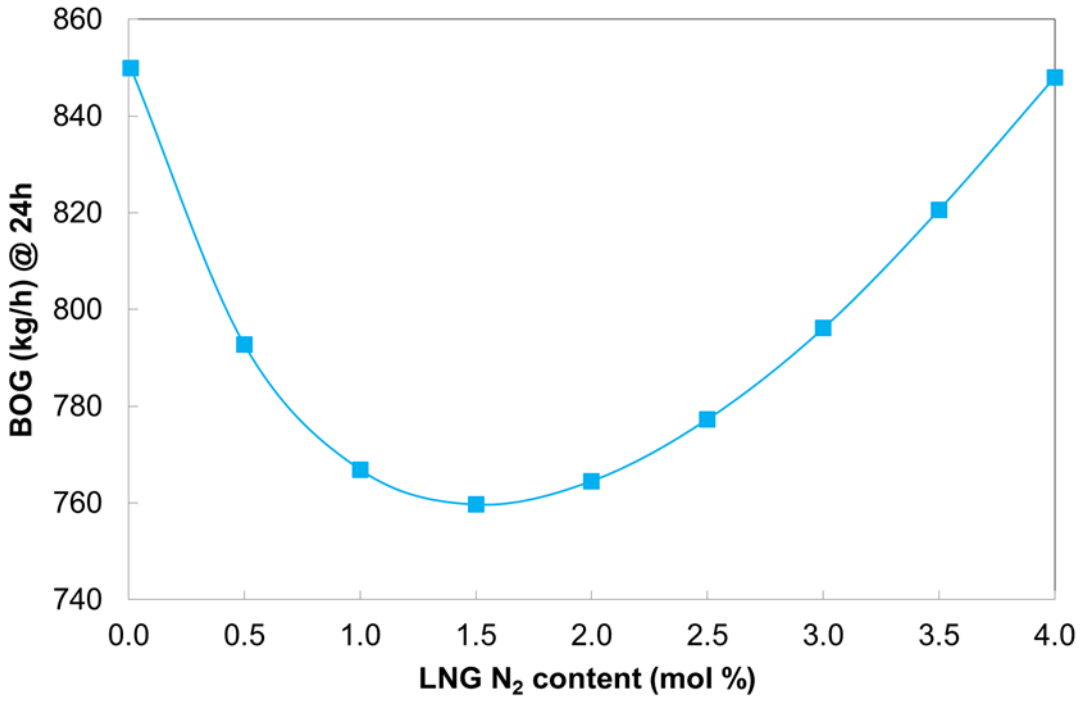

Figure 6.63 BOG rate after 24h vs. LNG N_2 content - superheated vapour model.

Within the superheated model approach, it is observed that further increase in the initial nitrogen content does not lead to further decrease of BOG, which is the same behaviour as observed with the isothermal model approach.

From Figure 6.63 shows that the minimum is achieved at around 1.5% mol of N_2 content, same as in the isothermal model. As explained in section 6.1.3 the minimum is a direct consequence of the increase in the molecular weight of the generated vapour which is rich in nitrogen.

The BOG generation behaviour after some time has also been investigated within this approach. Figures 6.64 and 6.65 respectively show the variation of the initial BOG generation rate after 14 days and 52 weeks of weathering, vs. the initial amount of N_2 in the LNG.

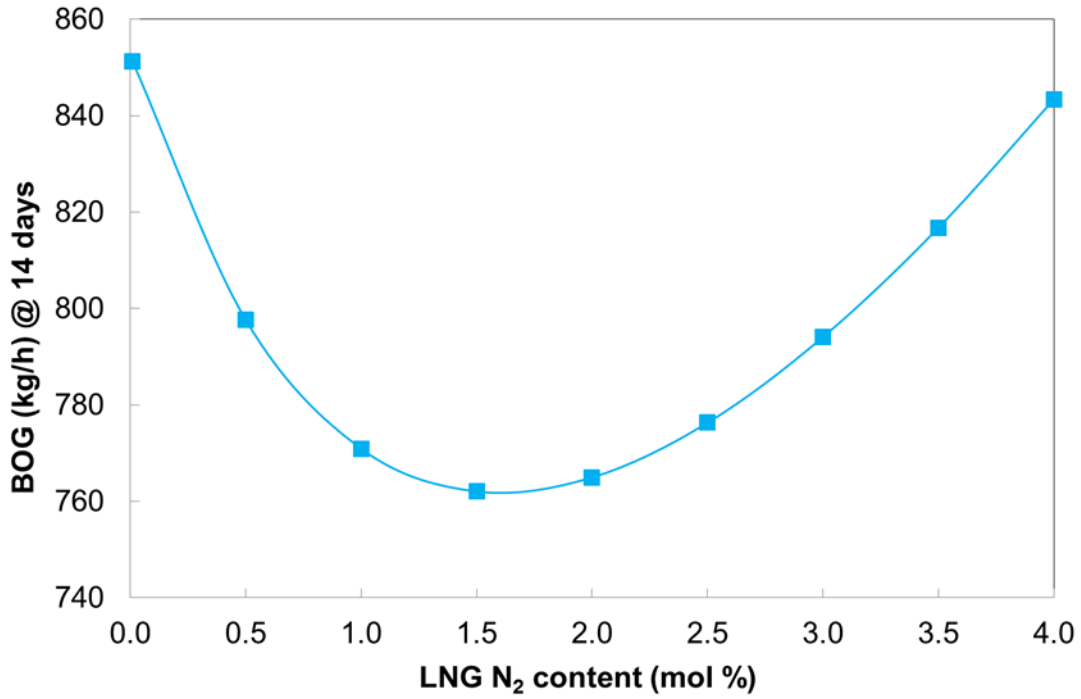

Figure 6.64 BOG rate after 14 days vs. LNG N_2 content - superheated vapour model.

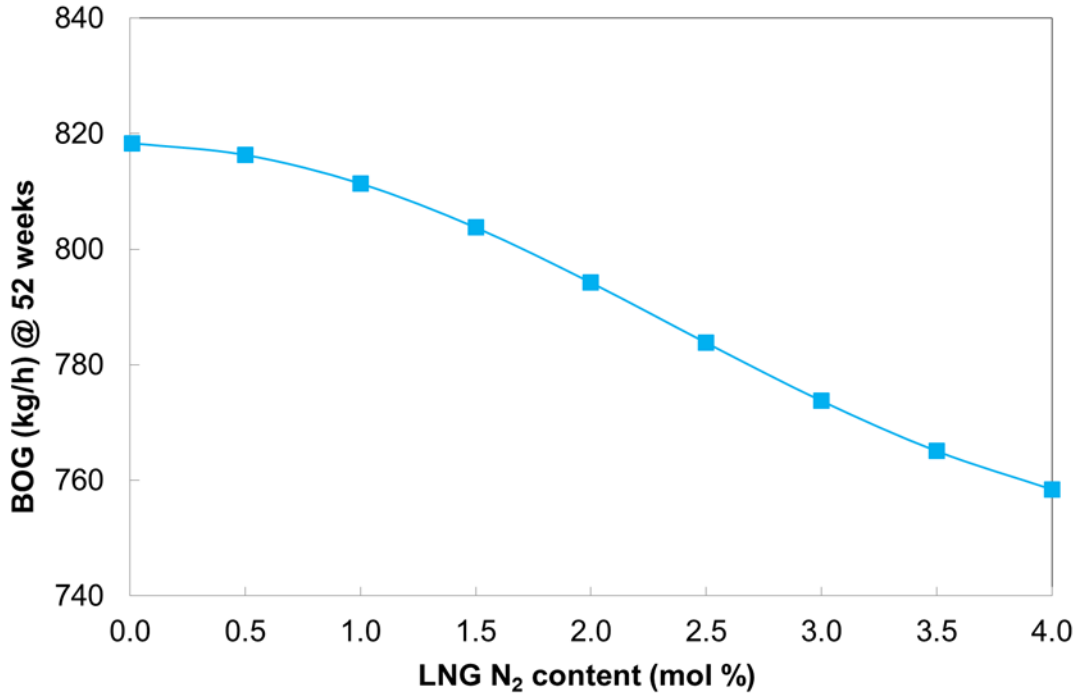

Figure 6.65 BOG rate after 52 weeks vs. LNG N_2 content - superheated vapour model

Figure 6.65 shows the same trend as in the isothermal model case that after 52 weeks of weathering there is a change in the BOG generation rate behaviour, which progressively drops down as the initial N_2 content increases. Same as in the isothermal model case, the BOG generation decrease is explained by the increase in the molar latent heat, as shown by Figure 6.66. Figures 6.67 and 6.68 respectively illustrate the vapour molecular weight and the mass latent heat for the three durations, with the initial N_2 content of the LNG, showing also the similar behaviour as in the isothermal model approach.

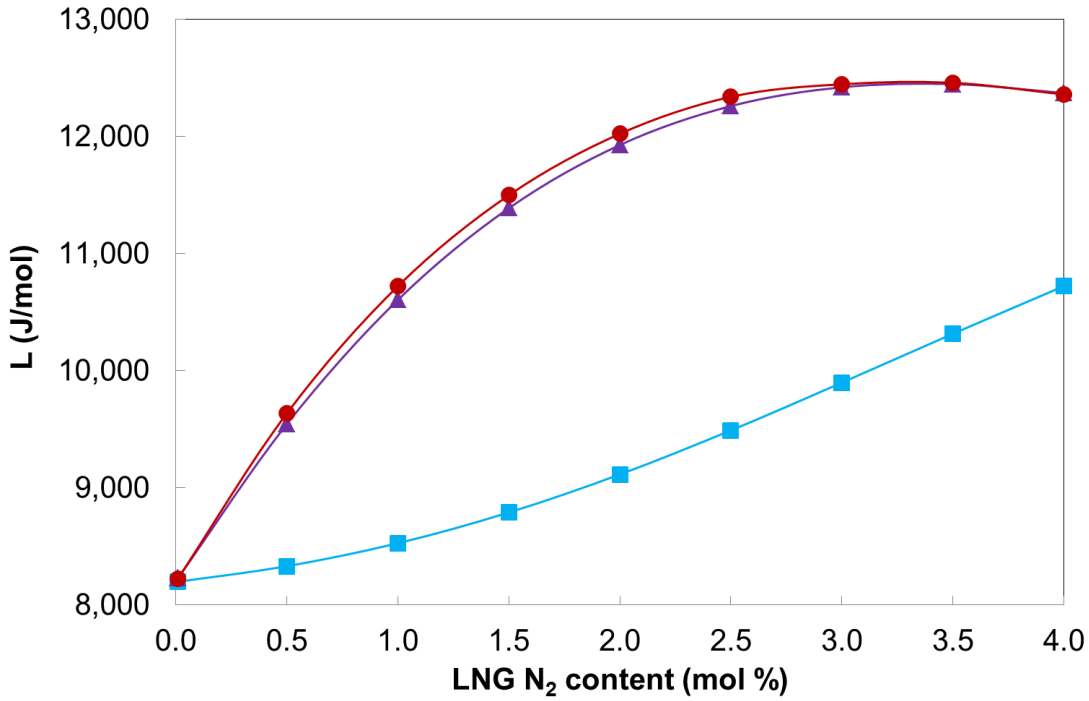

Figure 6.66 Latent heat (J/mol) vs. LNG N_2 content – superheated vapour model.
(-●- 24 hours; -▲- 14 days; -■- 52 weeks)

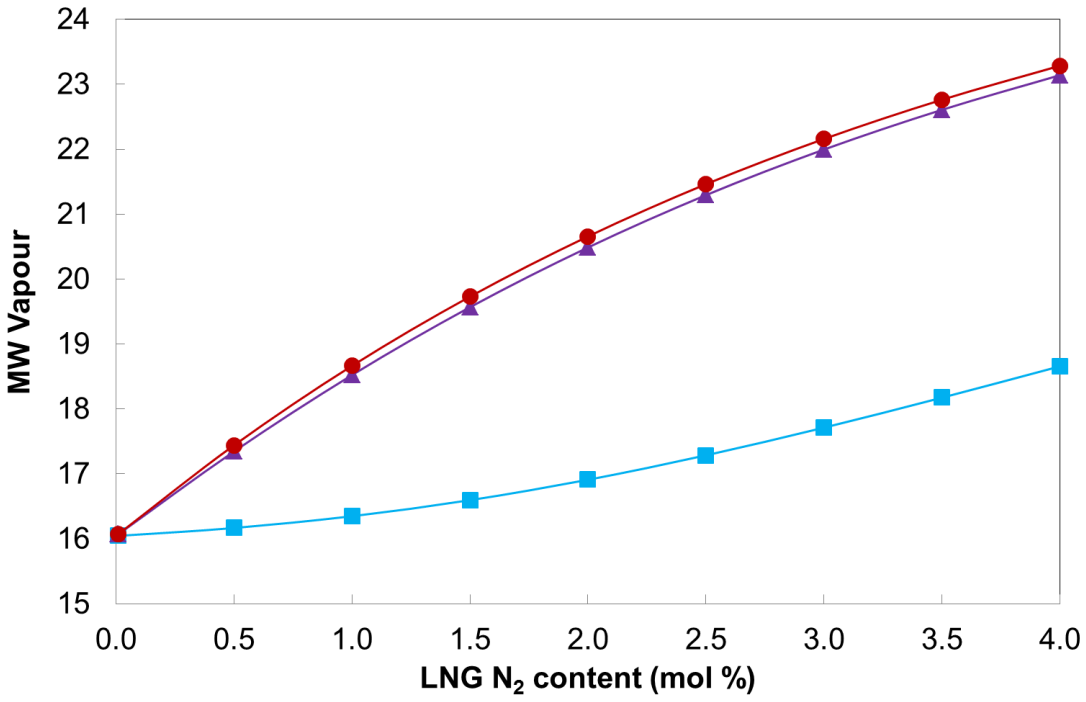

Figure 6.67 Vapour MW vs. LNG N_2 content – superheated vapour model.
(-●- 24 hours; -▲- 14 days; -■- 52 weeks)

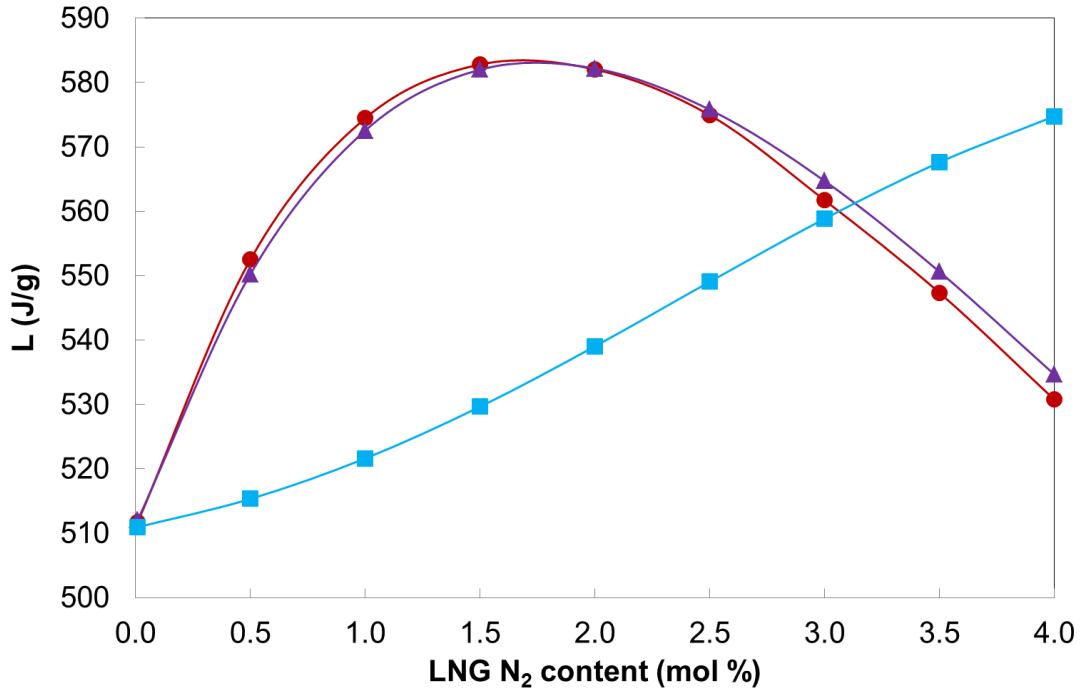

Figure 6.68 Latent heat (J/g) vs. LNG N_2 content – superheated vapour model.
(-●- 24 hours; -▲- 14 days; -■- 52 weeks)

6.2.4 SENSITIVITY TO OUTSIDE TEMPERATURE VARIATION

The effect of outside temperature variations on BOG generation from stored LNG considering the superheated vapour model approach has been analysed. As in the isothermal model approach, the analysis is based on the initial filling of 160,000 m^3 of LNG and the outside temperature being varied by 10 ºC from 5 ºC to 35 ºC, using the LNG mixture containing 1.5% of N_2 on molar basis, compositionally defined in Table 6.3.

Figure 6.69 and 6.70 respectively illustrate the sensitivity of BOR and BOG generation rate to outside temperature variations, using the superheated vapour model approach.

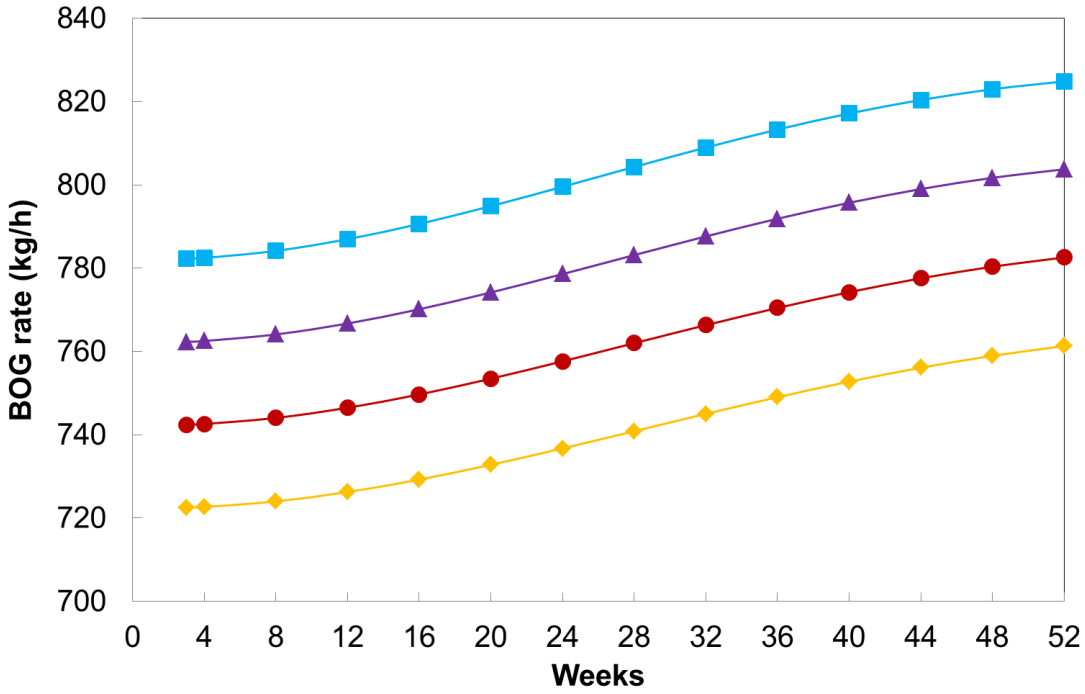

Figure 6.69 BOG rate due to variation of T air - superheated vapour model.
(-◆- T_{air}=5 °C; -●- T_{air}=15 °C ; -▲- T_{air}=25 °C; -■- T_{air}=35 °C)

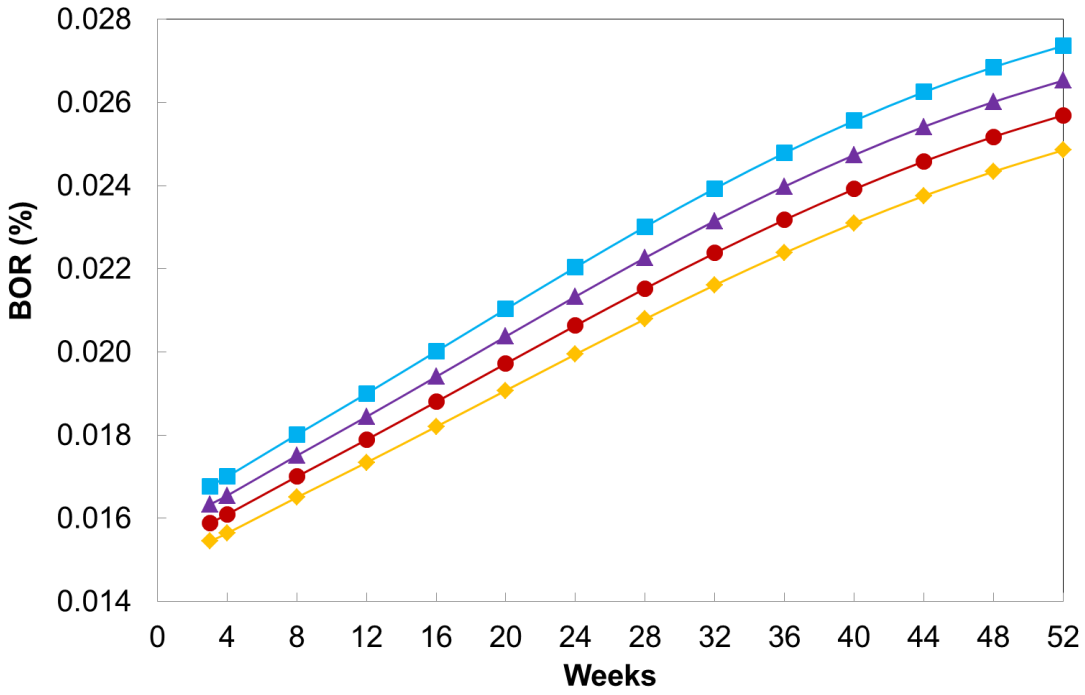

Figure 6.70 BOR due to variation of T air – superheated vapour model.
(-◆- T_{air}=5 °C; -●- T_{air}=15 °C; -▲- T_{air}=25 °C; -■- T_{air}=35 °C)

It is shown that on average the BOG rate increases by approximately 3% for every 10 ºC increase in the outside temperature, which is 1% higher when compared to the isothermal model approach. That is because the ratio of heat coming through the lateral wall compared to total amount of heat is higher. Same as in the isothermal model case, the change in BOG is primarily driven by the temperature differential between the tank and the surroundings. When considering the superheated vapour approach, it can be assumed that 1 ºC change in the outside temperature will change the BOG by approximately 0.3%.

6.2.5 INFLUENCE OF TIME STEP SIZE

The influence of time step size has been investigated for the superheated vapour model, using the LNG with N_2 mixture shown in Table 6.2. Figures 6.71, 6.72 and 6.73 respectively show the results of predicted BOG generation rate, boiling temperature and LNG methane content, for time step sizes of one day, one week and one month.

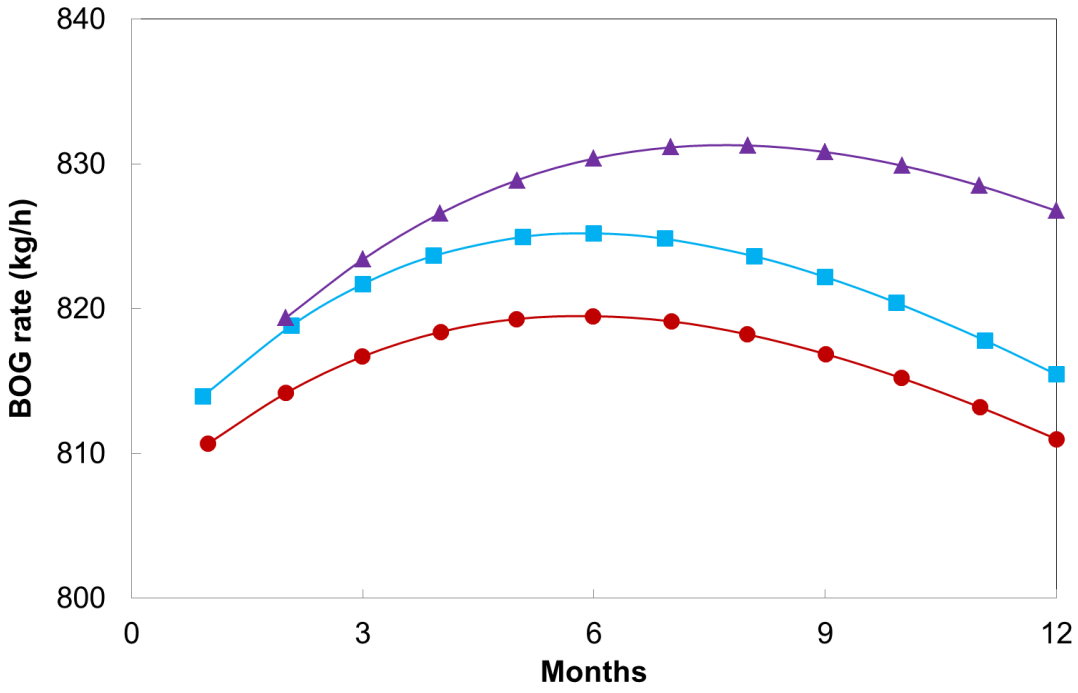

Figure 6.71 BOG rate for different time step sizes – superheated vapour model.
(-●- t_s: 1 day; -■- t_s: 1 week; -▲- t_s: 1 month)

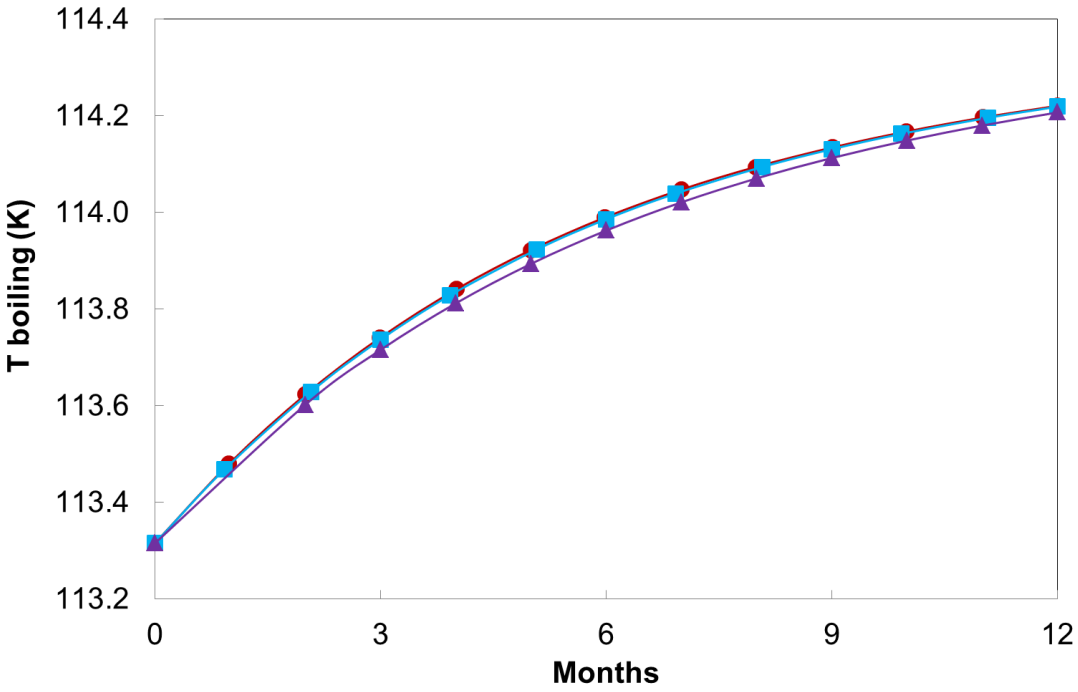

Figure 6.72 T boiling for different time step sizes – superheated vapour model.
(-●- t_s: 1 day; -■- t_s: 1 week; -▲- t_s: 1 month)

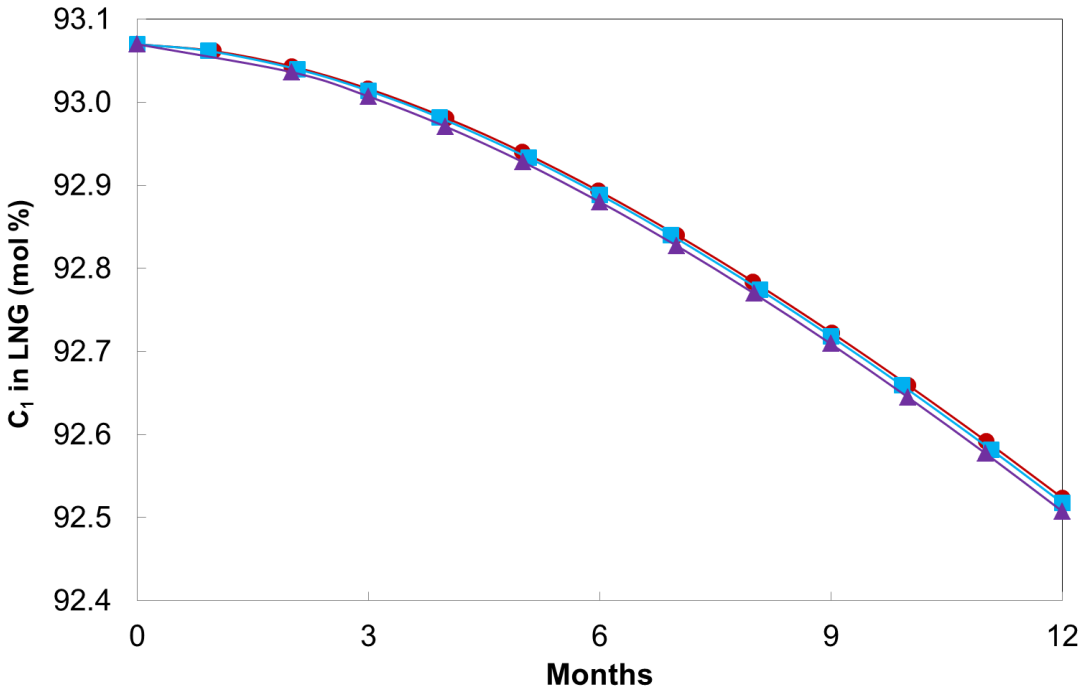

Figure 6.73 CH_4 in LNG for different time step sizes – superheated vapour model.
(-●- t_s: 1 day; -■- t_s: 1 week; -▲- t_s: 1 month)

Figure 6.71 shows that the maximum error in the predicted BOG generation rate between one day and one week time step sizes is 0.5%. In the same way the error between one day and one month time step sizes is within 0.6% at the early stage of weathering and progressively increases up to 1.9% by the end. In respect to boiling temperature and LNG methane content evolution, the errors are within 0.1% and 0.02% respectively.

Regardless the time step size the superheated vapour model produces the same results in the boiling temperature and methane content in LNG. For the BOG generation rate the agreement between the three time step sizes is within current industry requirements.

For the superheated vapour model case, the prediction of the vapour temperature was also assessed in regard to the use of different time step sizes. Figure 6.74 shows the predicted vapour temperature for the LNG with N_2 mixture, using time step sizes of one day, one week and one month, over one year weathering.

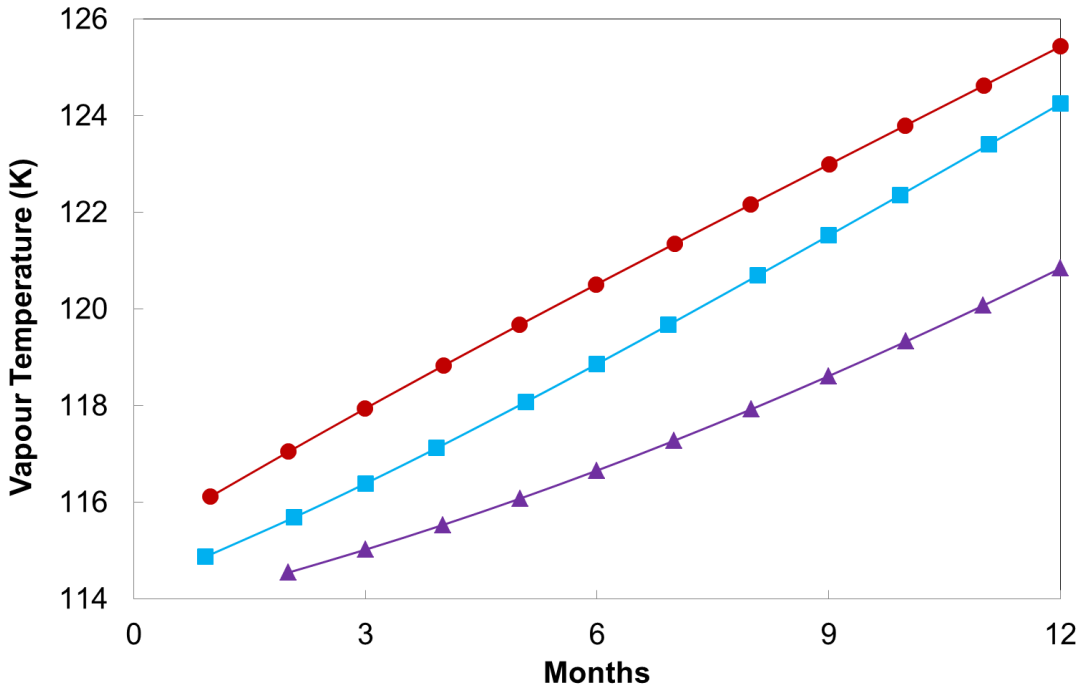

Figure 6.74 T vapour for different time step sizes – superheated vapour model.
(-●- t_s: 1 day; -■- t_s: 1 week; -▲- t_s: 1 month)

Therefore, the difference in the predicted vapour temperature between the one day and one week is around 1%, and ranges from near 2% up to 3% when comparing one day and one month time step sizes. Also in this case, the agreement between the three time step sizes, over the assessed weathering period, is within current industry requirements.

As mentioned earlier, the simulations and sensitivity analysis within this research project were run using one week as the time step size.

6.3 REFERENCES

[1] Anco Products (2006) *Resilient blanket product information – System 9000*. USA, Anco Products Inc.

[2] Arkema Group (2006) *Expanded perlite product information – CECA*. France, Arkema, S. A.

[3] Perry, H., Green, D. (1985) *Perry's chemical engineers' handbook 50th anniversary edition*. USA, McGraw-Hill.

[4] Operations supervisor, LNG regasification facility. (Personal communication, 28th March 2014).

[5] Aspen Technology (2007) *Aspen Hysys process simulator* (version 2006.5) [Software] USA. Aspen Technology, Inc.

[6] Conrado, C., Vesovic, V. (2000) The influence of chemical composition on vaporisation of LNG and LPG on unconfined water surfaces. *Chemical Engineering Science*, 55, 4549−4562

[7] Natural Gas Council (2005) *White paper on natural gas interchangeability and non-combustion end use*. NGC+, Interchangeability Work Group, USA.

7 CONCLUSIONS AND FUTURE WORK

7.1 CONCLUSIONS

The research conducted in this thesis has led to the following conclusions:

- Liquefied natural gas weathering is of great interest for the LNG industry since unlike other energy carriers, LNG quality may vary throughout the supply chain. LNG weathering is a complex phenomenon to analyse and model accurately, since there are a number of system parameters that determine the BOG generated and the extent of change of the LNG composition remaining in the storage container.

- A stand-alone model for rigorous prediction of LNG weathering in containment storage tanks, typically used in regasification terminals, has been developed. It fills an important gap in LNG regasification industry, as accurate prediction of LNG weathering can make a significant contribution to optimizing normal operations, as enables to accurately evaluate the compatibility of the stored LNG with the supplied gas system, as well as to capturing upside opportunities in long term LNG storage. The model builds on previously developed weathering models and provides a number of advances in so far as: (*i*) heat ingress is calculated based on the outside temperature and LNG composition, that allows for daily or seasonal variations; (*ii*) boil-off-ratio is not an input parameter, but is calculated as part of the simulations; and (*iii*) the LNG density is estimated using an accurate experimentally based correlation. Furthermore, the model incorporates the flexibility to choose the preferred approach to predict weathering, whether to consider the system in thermodynamic equilibrium or not. The non-equilibrium thermodynamic approach to allow uncoupling the vapour temperature over the weathering process, as the heat influx influence is separated into the vapour and liquid sides. The model has been coded using MS Visual Basic 6.0.

- The model was tested using measured data and in particular it was used to predict the LNG properties following marine transport ranging from 98h to 390h duration. The agreement with measured data that consisted of composition, volume reduction,

density and boiling temperature of transported LNG was deemed very satisfactory and within the current industry requirements. Concerning the quality measures, the predicted values of HHV and WI by both model approaches are better than 0.3%.

- When comparing the vaporization pattern between two tanks with different initial filling amounts of LNG, the tank with a bigger initial LNG volume will exhibit an earlier decrease in BOG generation than the tank with the smaller initial amount of LNG. That is a direct consequence of the indirect differential latent heat. As the LNG gets richer in heavier hydrocarbons its boiling temperature increases, and hence some of the heat ingress will go towards heating up the remaining LNG. For a given amount of LNG evaporated the storage tank with initially more LNG will have more liquid remaining. Hence more heat will be required to increase its temperature to a new boiling point, thus reducing the amount of heat available for evaporating the LNG.

- The BOG generation rate is 25% less when considering separating the heat influx influence into the vapour and liquid sides of the tank (superheated vapour model approach). This demonstrates that sometimes simple approaches such as the thermodynamic equilibrium (isothermal model) could take to rather conservative results; relying on them may lead to pricey designs and costly operations, as the decrease in BOG generation rate is indeed beneficial for the industry.

- Contact area in the tank plays an important part in the heat transfer calculation when considering rigorous modelling of LNG weathering (superheated vapour model). Initially the tank is full and as LNG evaporates (tank begins to empty) the contact area progressively reduces, thus less heat is going into the LNG. By the end of the weathering period the estimated LNG heat input for the superheated vapour model drops by 1.8%.

- Regardless of the LNG composition stored the BOR increases as the LNG inventory decreases in the tank. When considering the non-equilibrium thermodynamic approach (superheated vapour model), the heat input from the lateral wall significantly contributes to the BOG generation rate for the nearly full tank. Hence, as LNG is

vaporized from the tank the BOG generation rate progressively decreases, following the reduction of the wet heat transfer area. In contrast, when the tank has a low LNG inventory, the vaporization rate of LNG hardly changes, as it is mainly dominated by the constant heat ingress from the bottom slab Q_{slab}.

- The initial amount of nitrogen in LNG has a significant effect on BOG in the initial stages of weathering. The presence of nitrogen leads to a marked decrease of BOG generation. Even the presence of 0.5% mol of nitrogen will lead to nearly a 7% decrease in BOG, making the initial BOG unmarketable. That can be explained by the preferential evaporation of nitrogen and the resulting increase in the direct differential latent heat. As the initial BOG generated is very rich in nitrogen the resulting gas mixture falls out of spec by any regulatory measures.

- The increase of the amount of N_2 in the LNG mixtures leads to two thermodynamic effects, namely lowering the boiling point of the mixture and increasing the latent heat needed to vaporize an LNG drop. As LNG starts to weather, N_2, being the most volatile component in the mixture, will vaporize preferentially.

- The decrease in the boiling temperature, as the N_2 content in the mixture increases, leads to a larger temperature difference between the LNG and the surroundings, at least in the initial stages of the process. As a consequence the heat flux into the tank will increase. However, the effect is only minor and the heat flux will increase by at most 1.0 %, for an initial N_2 content of up to 1.5% mol. Therefore, the determining factor in the reduction of BOG for N_2 rich mixtures is due to the increase in the direct latent heat required to vaporize a drop of LNG.

- Although BOG expressed in molar terms will continue to decrease with increasing amount of nitrogen, the standard BOG expressed in mass terms will exhibit a minimum at around 1.5 % mol nitrogen. The analysis carried out, in terms of influence of nitrogen on the latent heat and the boiling temperature of the LNG mixture, concluded that the observed minimum is a direct consequence of the increase in the molecular weight of the generated BOG vapour, which is rich in nitrogen. The

existence of a minimum in BOG offers an intriguing possibility of operating LNG storage tanks by using nitrogen to minimize the BOG generation during the storage stage, providing the generated BOG vapour is not transferred to the outside gas network.

- For current LNG tanks used in storage and regasification facilities, one can, based on the analysis carried out in this work, devise a simple rule of thumb that 1 ^{o}C change in the ambient temperature will lead to a change in BOG of 0.2 % and 0.3% for the equilibrium and non-equilibrium thermodynamic modelling approaches respectively, irrespective of the size of the tank and initial LNG composition.

7.2 SUGGESTIONS FOR FUTURE WORK

The work conducted under this research could be extended further in the following areas:

1. Test and validate the model with actual LNG storage tank data

   Both modelling approaches developed under this research project were tested and validated with actual measurements from LNG shipping, by adjusting the overall heat transfer coefficient. It would be convenient to have real operating data from an actual LNG storage tank. By doing that the accuracy of both modelling approaches could be further assessed.

   From the industry perspective no special measurement devices are required to install in the tank to collect the actual operating data, as the basic instrumentation design for LNG tanks will work. Instead, special operating procedures should be put in place by leaving a loaded LNG tank to operate under long term storage mode and isolated, thus no LNG loading or unloading.

2. Improving the model by coding a different equation of state

   The Peng Robinson equation of state (PR-EOS) has been selected for the development of the LNG weathering model under this research project, to describe phase equilibrium and predict most of the associated thermodynamic and physical properties. The PR-EOS is a reasonable choice due to its prediction power, and has long

demonstrated to be a suitable method to describe hydrocarbon fluid behaviour mixtures, over a wide range of temperatures and pressures. However the new GERG 2008 equation could be a very good choice for the development of the more accurate LNG weathering model, as it has been developed specifically for natural gas. By the time of the selection was made for this research project, the GERG 2008 equation was not tested enough to be considered as a reliable candidate.

3. Improving the heat transfer model from vapour to liquid

   The heat transfer model from vapour to liquid can be upgraded by taking into account convection.

   In this respect, a simple approach to the problem could be to assume that the heat transfer through the vapour is by conduction, but using an effective vapour thermal conductivity k to act as a proxy for convection. Therefore, the equation that governs the heat contribution from the vapour to the liquid can be derived from Fourier's law and the conservation of energy equation.

   A more rigorous approach to estimate the convection heat transfer contribution would require implementing a full numerical computational fluid dynamics (CFD) solution.

4. Nitrogen content design study

   The existence of a minimum in BOG generation as the initial N_2 content increases, suggests that nitrogen content design is an interesting and non intuitive topic to study, either for long trips in LNG shipping, and for long term LNG storage in production and receiving facilities.

5. Study the effect of rollover

   Study the effect of rollover by relaxing the assumption of compositionally homogenous liquid and first allowing diffusion to govern the weathering in different layers and convection to set in.

6. Develop an LNG supply model

To explore the feasibility to develop a full LNG supply solution by integrating the modelling of LNG weathering from shipping to storage at the receiving terminal. Such a modelling tool will help the industry to optimize the scheduling and allocation of LNG cargoes, depending on the initial LNG quality, storage duration, whether it is short or long term, and gas market specifications.

APPENDICES

A. APPENDIX I – CARDANO'S METHOD TO SOLVE CUBIC EQUATIONS

To solve the Peng-Robinson cubic equation, the Cardano method has been used to develop the weathering model.

The method starts with the general cubic equation in the following form:

$$x^3 + jx^2 + kx + l = 0 \tag{A.1}$$

Notice that the expression above has the same form as the Peng-Robinson EOS written in its cubic version:

$$Z^3 - (1 - B)Z^2 + (A - 3B^2 - 2B)Z - (AB - B^2 - B^3) = 0 \tag{A.2}$$

Therefore, parameters (*j*), (*k*) and (*l*), are calculated as follows:

$$j = -(1 - B) \tag{A.3}$$

$$k = A - 3B^2 - 2B \tag{A.4}$$

$$l = -(AB - B^2 - B^3) \tag{A.5}$$

Following Cardano's method, a variable change is implemented:

$$x = z - \frac{j}{3} \tag{A.6}$$

This removes the second order term of the equation producing:

$$z^3 + pz + q = 0 \tag{A.7}$$

where:

$$p = -\frac{j^2}{3} + k \tag{A.8}$$

$$q = \frac{2}{27}j^3 - \frac{kj}{3} + l \tag{A.9}$$

To calculate the number of real roots of the cubic equation, a further parameter is calculated:

$$roots = \frac{q^2}{4} + \frac{p^3}{27} \tag{A.10}$$

If $roots < 0$, the cubic equation has three real roots:

$$Z_1 = m - \frac{j}{3} \tag{A.11}$$

$$Z_2 = -\frac{m}{2} + \sqrt{\left(\frac{m}{2}\right)^2 + \frac{q}{m}} \tag{A.12}$$

$$Z_2 = -\frac{m}{2} - \sqrt{\left(\frac{m}{2}\right)^2 + \frac{q}{m}} \tag{A.13}$$

where:

$$m = 2\sqrt{-\frac{q}{3}}\cos\left(\frac{\phi}{3}\right) \tag{A.14}$$

$$\phi = \cos^{-1}\left(-\frac{q}{2\sqrt{-\frac{q^3}{27}}}\right) \tag{A.15}$$

The PR cubic equation is solved twice to get Z^V and Z^L:

- once considering vapour phase composition y_i for A and B calculation and producing Z_1 as Z^V
- once considering liquid phase composition x_i for A and B calculation and producing Z_3 as Z^L

If *roots* > 0, there is only one real root. If this is the case, then no vapour-liquid equilibrium is expected at those calculation conditions.

B. APPENDIX II – NEWTON-RAPHSON NUMERICAL METHOD

As part of the VLE calculation procedure, to solve the PR-EOS, it is necessary to find the equilibrium temperature. For this purpose the Newton-Raphson numerical method was used.

The Newton-Raphson method is utilized to solve equations of the form *f(x) = 0*. It uses an iterative process where the function is approximated by its tangent line to approach one root of the function. The method starts with an initial guess and in an iterative approach, by means of the tangent, estimates the x-axis intersection point that usually is a better approximation to the real solution than the original guess. After few trials the method usually converges to the solution in *x*. Figure B.1 shows a sketch of the Newton-Raphson method.

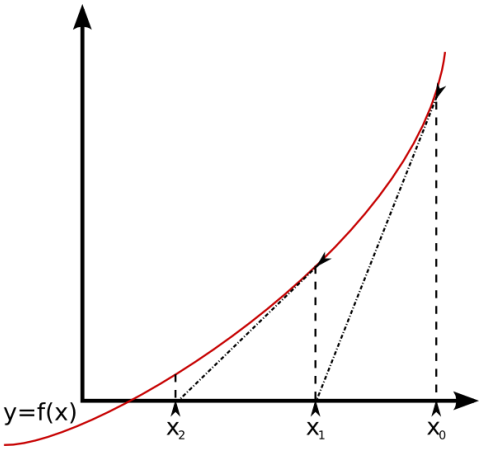

Figure B.1 Newton-Raphson numerical method

The iteration follows the equation below to calculate the new *x*:

$$x_{n+1} = x_n - \frac{f(x_n)}{f'(x_n)} \quad \text{(B.1)}$$

where *f'(x)* is calculated as follows:

$$f'(x_n) = \frac{f(x_n+\Delta x)-f(x_n)}{\Delta x} \quad \text{(B.2)}$$

where Δx is the incremental step (in the order of 1.10^{-5}).

To check whether the solution has been achieved, the following equation is verified within a tolerance ε of the order of 1.10^{-10}:

$$f(x_n) \leq \varepsilon \qquad \text{(B.3)}$$

C. APPENDIX III – TRAPEZOIDAL RULE NUMERICAL METHOD

The trapezoidal rule is a numerical method that approximates the value of a definite integral, by using the linear approximations of the integrated function.

Let´s take the following equation with a definite function:

$$Integral = I = \int_{x_i}^{x_{i+1}} y(x)dx \qquad \text{(C.1)}$$

Consider the area of a trapezium between two points of function *y*(*x*), as shown in Figure (C.1).

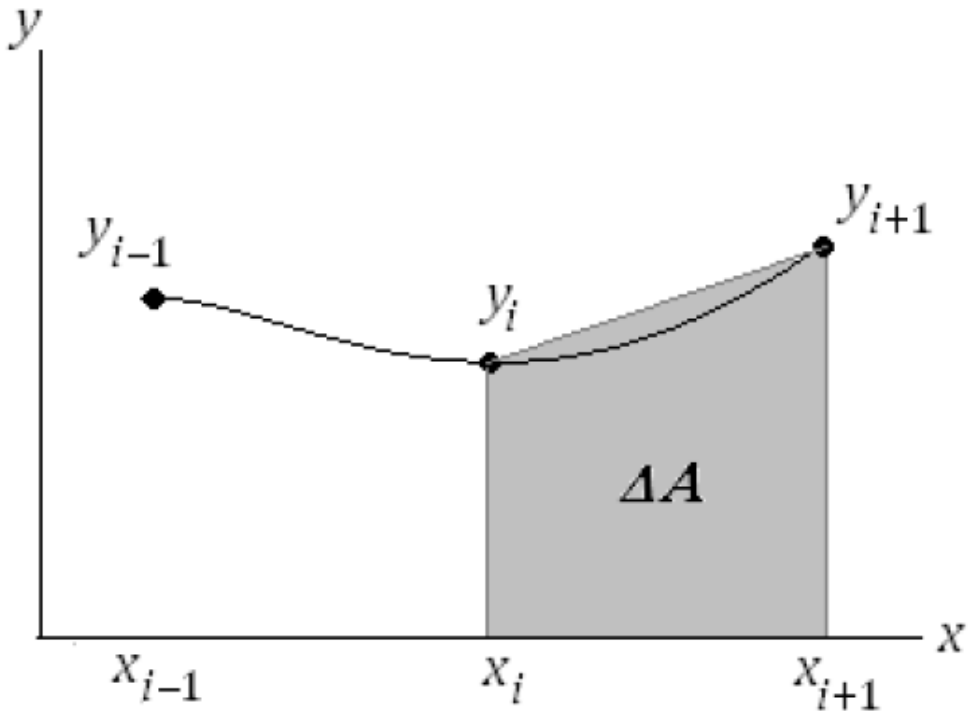

Figure C.1 Trapezium area between two points of function *y(x)*

The trapezoidal rule works by approximating the region under the graph of the function $y(x)$ as a trapezoid and calculating its area. The area of the trapezium is defined as follows:

$$\Delta A_{i+1} = \frac{1}{2}(x_{i+1} - x_i)(y_{i+1} + y_i) \quad \text{(C.2)}$$

The value of integral I within an interval with n+1 points is then the summation of the different areas of the sub-intervals as follows:

$$I = \int_{x_0}^{x_n} y(x)dx \approx \sum_{i=0}^{n-1} \Delta A_i \quad \text{(C.3)}$$

Considering that $\Delta x = x_{i+1} - x_i$ is constant, then the solution of eq. (C.3) is written as follows:

$$I = \int_{x_0}^{x_n} y(x)dx \approx \frac{1}{2}\Delta x(y_0 + y_n) + \Delta x \sum_{i=1}^{n-1} y_i \quad \text{(C.4)}$$